Electrically Connecting Bacteria to Nanoparticles for Biotechnological Applications.

Anna Maria Wróblewska-Wolna

Submitted in accordance with requirements for the degree of

Doctor of Philosophy

The University of Leeds

School of Biomedical Sciences

October 2019

The candidate confirms that the work submitted is their own, except where work which has formed part of jointly authored publications has been included. The contribution of the candidate and the other authors to this work has been explicitly indicated below. The candidate confirms that appropriate credit has been given within the thesis where reference has been made to the work of others.

The work in Chapter 4-7 of the thesis has been submitted to a review in Nanotechnology as follows:

Wroblewska-Wolna A. M., Harvie A. J., Rowe S. F., Critchley K., Butt J. N. , Jeuken L. J. C. (2019). Quantum dot interactions with and toxicity to *Shewanella oneidensis* MR-1, Nanotechnology.

A. M. Wroblewska-Wolna was responsible for the synthesis of QDs, nanotoxicology assessment, the microscopic investigation, photoreduction capabilities of QDs, data analysis, and writing of the manuscript. A. J. Harvie together with K. Critchley supervised QDs syntheses. S. F. Rowe and J. N. Butt oversaw the photoreduction experiments. L. J. C. Jeuken provided guidance regarding the design of experiments, data analysis, and contributed to the discussion and the writing of the manuscript.

Acknowledgements

I would like to thank my Supervisors Professor Lars J. C. Jeuken and Professor (!) Kevin Critchley for their guidance and support. Professor Jeuken supervised the biological part of my laboratory work while Professor Critchley introduced me to the mysterious nanoscience world. I am very grateful for showing me all the directions which my research could achieve. At the same time, I want to thank Professor Julea N. Butt for supervising me during the experiments which were conducted at the University of East Anglia. Additionally, most bacteria strains which I was working with were kindly gifted by Prof. Butt's group. Without these bacteria, I would not be able to act upon my experiments.

For their moral and technical support, I would like to thank Dr Vlad Vasilca and Dr Valentin Radu. We started together, we should have finished together, but life decided to go slightly different.

Additional thank you to Dr Joseph Oram, Dr Theodoros Laftsoglou, Dr Hope Adamson, Dr Andrew J. Harvie, Dr Mattias Gantner, Dr Kelly Koffyn, Dr Matthew Booth, Dr Mengqiu Li, Dr Ee Taek Hwang, Riitta Partanen, Honglin Rong, Dr Sam F. Row. Dr Sunjie Ye and Mr Martin Fuller performed most of the electron microscopy in this project and their help is greatly appreciated.

And lastly, thank you to all my family! To my Husband for being always for me during my happy and crisis times. To pick me up, when I had fallen and did not wish to go further. Thank you! I love you!

To my Son, Jasiu, who continually brightens my life. I love you!

To my parents for their mental support and for being always ready for greatly appreciated help. For consistently delivering a smile and encouragement. Thank you and love you.

Abstract

Combining abiotic photosensitisers such as semiconductor fluorescence emitting nanoparticles – quantum dots (QDs), with non-photosynthetic bacteria 'in vivo' presents an intriguing concept into the design of artificial photosynthetic organisms and solar-driven fuel production. *Shewanella oneidensis* MR-1 (MR-1) is a versatile bacterium concerning respiration, metabolism and biocatalysis, and is a very promising organism for artificial photosynthesis. The bacteria's synthetic and catalytic abilities, together with their longevity, provide a promising system for bacterial biohydrogen production. MR-1's hydrogenases are present in the periplasmatic space, and it follows QDs or their electrons will need to enter the periplasm via the Mtr pathway that is responsible for the extracellular electron-transfer ability of MR-1. Firstly, various QDs were tested for their nanotoxicology and further for interaction with MR-1 by fluorescence and electron microscopy. CdTe/CdS/TGA, CdTe/CdS/Cysteamine, commercial negatively charged CdTe and $CuIn_2S$/ZnS/PMAL QD were examined, and it was found that the latter two showed no toxicity for MR-1 as evaluated by a colony-forming units method and a fluorescence viability assay. Only commercial negatively charged CdTe QDs showed good interaction with MR-1. Detailed investigation of the above interaction by transmission electron microscopy showed QDs were placed both inside the cell and close to the membrane. Subsequently, the photoreduction power of QDs was evaluated by the methyl viologen assays with different sacrificial electron donors. It was indeed found that QDs have reduction potential sufficiently low to perform MV photoreduction. As assessed by gas chromatography, CdTe/CdS/TGA and negatively charged CdTe QDs supported hydrogen evolution in *Shewanella putrefaciens* CN-32. The above results establish a proof of concept for photosynthetic production of biohydrogen by CN-32. Further research should be invested in the use of biocompatible sacrificial electron donors and the development of appropriate bacteria mutants that would help to understand the assisted by QDs hydrogen evolution in this bacterium.

Contents

List of Tables

Table 7.1. A short history of documented microscopy evolution. Used abbreviations include: TEM – transmission electron microscopy, STED – stimulated emission depletion.

Table 8.1. Table 8.1. Genomic comparison of Shewanellaceae showing the presence (✔) or absence (-) of genes encoding the indicated proteins.

Table 8.2. The concentrations of different quantum dots used in the methyl viologen photoreduction assays. Abbreviation used: CIS/PMAL – CuInS2/ZnS/PMAL QDs, Comm. CdTe – commercial negatively charged CdTe QDs, CdTe/CdS/Cyst. – CdTe/CdS/Cysteamine QD, PL - photoluminescence. Extinction coefficients (ε) were measured at the absorbance maxima (Abs. λmax) of the sample of interest.

Table 8.3. Choice of SED for all QDs used in MV photoreduction assays. Although EDTA also supported MV reduction by CdTe/CdS/TGA QDs, TEOA was chosen for subsequent experiments. Abbreviation used: CdTe/CdS/Cyst. – CdTe/CdS/Cysteamine QDs, CIS/PML – CuInS2/ZnS/PMAL, CDTe comm. – commercial, negatively charged CdTe QDs, TEOA – triethanolamine, EDTA – ethylenediaminetetraacetic acid,SED – sacrificial electron donor.

List of Figures

Fig.5.3.1.1. Molecular structures of two thiols used in the ligand exchange experiments. LADPA stands for the lipoic acid derivative of dipicolylamine.

Fig. 5.3.1.2 Photoluminescence intensity (measured at the wavelength of 600 nm, normalised to ctrl) over the time of the experiment. Ctrl is a PL of CdTe/CdS/TGA QD before the addition of the thiol. Number of repetitions was n=2. Error bars were standard deviations and are 0.03, 0.05, 0.1, 0.1, 0.1, 0.09, 0.04, 0.02, 0.07, 0.03 for samples from 10, 20, 30, 40, 50, 60, 70, 80, 90, 100 min, respectively.

Fig.5.3.1.3. The precipitation of CdTe/CdS/TGA QDs was instantly visible upon addition of excess cysteine in the citric buffer pH 3. A. CdTe/CdS/TGA, B. CdTe/CdS/TGA with an excess of cysteine.

Fig. 5.3.2.1. Photoluminescence intensity (measured at the wavelength of 600 nm, normalised to ctrl) over the time of the experiment. Ctrl is a PL of CdTe/CdS/TGA QD before the addition of the thiol. Time 0 is the first PL spectrum taken after addition of LADPA. SD were 0.08, 0.02, 0.04, 0.02, 0.02, 0.4 for samples 10, 20, 30, 40, 50, respectively.

Fig.5.4.1.1. Overlaid absorbance and photoluminescence of negatively charged commercial CdTe QDs. The colour of the PL graph corresponds to the visible colour of the solution. The number of commercial negatively charged CdTe QDs ordered was n=3.

Fig. 5.4.3.1. Representative transmission electron microscopy pictures of negatively-charged commercial CdTe QDs. The insets represent a digital zoom of chosen QDs. The diameter of the zoomed nanoparticles are about 3 nm. The scale bars are top picture a 100 nm and bottom 10 nm. The micrographs were kindly obtained by Dr Sunyie Ye.

Fig. 5.4.3.2. Size frequency distribution of negatively charged commercial CdTe QDs. The mean value of commercial QD equals 2.7 nm with a standard deviation of 0.42 nm. A Gaussian curve was fitted to the frequency distribution measurements.

Fig. 5.4.4.1. Scheme of the amide bond formation from CdTe(COOH) QD (red circles) and amine derivative of dipicolyl amine (ADPA), catalysed by EDC and Sulfo-NHS. Small red circles represent protons, blue – oxygen, light green – carbon, dark green - nitrogen.

Fig.5.4.4.2. PL spectra of commercial QDs taken after cross-linking with ADPA at different ADPA to QD ratios, as indicated, and after addition of 10 mM $ZnSO_4$. Control samples (ctrl) were subjected to the same EDC/sulfo-NHS treatment but without ADPA. A. Commercial CdTe QDs before and after crosslinking to ADPA in ratio 1:10. B. 1:100 ratio of QDs to ADPA, C. 1:200 ratio. D. The different fluorescence intensity maxima were recorded. Number of repetitions was n=2. SD on Fig. 5.4.4.2 D were 0.7, 23.5, 13.5, 15.5, 17.5, 26.1, 36.4, 44.5 for samples Ctrl, Ctrl+Zn^{2+}, 1:10, 1:10+Zn^{2+}, 1:100, 1:100+Zn^{2+}, 1:200, 1:200+^{Zn2} + respectively.

Fig. 5.4.4.3. A dynamic light scattering of commercial CdTe QDs after coupling to ADPA (ratio 1:10) and the addition of 10 mM Zn2+ suggests three populations of agglomerating nanoparticles are present in the solution. The majority of them have a hydrodynamic size of ~ 10 nm. However, many larger particles are present too.

Fig. 5.5.1. The UV-Vis and PL spectra of CIS QDs suspended in chloroform. The number of CIS syntheses was n=5. Anna Wroblewska-Wolna performed 2 syntheses. The other 3 were gifts from either Dr Booth or Dr Harvie. The average size of QDs was 2.54 ± 0.15 nm.

Fig. 5.5.2.1. A dynamic light scattering of the solution of CIS/PMAL - d QDs in M9 bacterial growth media. The hydrodynamic size of this nanoparticle was measured as 11.75 nm, with a standard deviation of 3.4 nm.

Fig.5.6.1. Representative graph of UV-Vis and PL spectra obtained from CdTe/CdS/Cysteamine QDs. The number of performed syntheses was n=2, one of which was done by Dr A. Harvie while the other by the author of the thesis.

Fig. 5.7. A. TEM image of ultrathin gold nanowires in hexane. Scale bar is 100 nm. **B.** UV-Vis spectrum of the as-synthesised Au-NWs, displaying a characteristic absorbance peak at 520 nm. The number of AuNWs syntheses was n=4 with 3 performed by Anna Wroblewska-Wolna. One synthesis was performed by Dr Kellye Coffyn. Number of repetitions on the graph B is n=2. SD equals 0.03. **Fig. 5.7.1.1.** The polymerisation of dopamine in an oxidising solvent. The reaction scheme was taken from Valsabehagh et al. (2014).

Fig. 5.7.1.2. A. The spectrum of Au-NW-PDA after the 2-hour incubation in PDA solution presented a broad peak at wavelengths below 300 nm and a distinctive peak at 400 nm. The blue graph represents a control UV-Vis spectrum of dopamine

dissolved in 10 mM Tris, pH 8.5 without Au-NWs. The number of repetitions in graph A is n=2 and SD = 0.5 and 1.4 for PDA and Au-NW-PDA, respectively. **B.** The blue spectrum illustrates the absorbance spectrum of freshly synthesised Au-NWs in hexane. The Au-NW reconstituted in hexane (red spectrum) is confirmed by the high absorbance peak at the wavelength of 530 nm. The number of repetitions equals n=2 and SD equals 0.05 and 0.03 for reconstituted Au-NW and freshly synthesised wires, respectively.

Fig. 5.7.1.3. A and **B.** Transmission electron microscopy images of dopamine treated gold nanowires. **C.** Control image of Au-NWs in hexane. **D.** A control of unmodified Au-NWs reconstituted in water. Scale bars at figures A is 2 μm, C is 50 nm, B and D is 500 nm. The micrographs were taken by the author of thesis.

Fig. 5.7.2.1. The molecular structure of diethylene glycol aminothiol - DEGAT.

Fig. 5.7.2.2. A. Samples of ligand exchange experiments performed with Au-NW and DEGAT in chloroform and PBS pH 7.4, with varying molar ratios. From left to right: Au:sulfur molar ratios were: 1:1; 1:1.5; 1:2. **B.** UV-Vis spectra of the ligand replacement trials conducted in ethanol with a 1:1 molar ratio and in chloroform with a 2:1 ratio. Number of repetitions was n=2.

Fig. 5.7.2.3. Transmission electron microscopy pictures revealed break down of Au-NWs treated with a 1:2 Au : sulfur in DEGAT molar ratio in chloroform. Scale bars on Fig. A and B are 50 nm.

Fig.5.8.1. QDs, described in Chapter 5, presented a wide range of surface ζ - potentials. Both CdTe/CdS/TGA and the commercial CdTe QD had a negative surface charge. In contrast, CdTe/CdS/Cysteamine showed strong positive potential. Encapsulated in zwitterionic polymer $CuInS_2$/ZnS/PMAL QD (CIS/PMAL) had a pH-dependent surface potential (in the graph is shown when resuspended in buffer with pH 7.4).

Fig. 6.2. A. Effect of CdTe/CdS/TGA QDs on the viability of MR-1. Please note that the data on graph A is presented on the logarithmic scale. **B.** Viability data normalised against NC, plotted on a linear scale. NC = negative control (addition of an equal volume of 0.15 M NaCl, 20 mM HEPES, pH 7.2); PC = positive control (50 μg/ml kanamycin).

Fig. 6.3.1. A. The colony-forming units assay exposed no toxicity of commercial negatively-charged CdTe QDs to MR-1. **B.** The normalised values of nanotoxicity are presented on chart B. NC = negative control (addition of an equal volume of 20 mM HEPES, 0.15 M NaCl, pH 7.2); PC = positive control (50 µg/ml kanamycin).

Fig. 6.3.2. A. The normalised fluorescence of live-dead assay of MR-1 after overnight incubation with commercial negatively charged CdTe QDs. **B.** Percentage of viable MR-1 interacting with commercial QDs (n=3). The unit for A and B graphs are the percentage of NC control. The dead cells were stained with propidium iodide (PI) that is a nucleic acid stain which cannot penetrate the lipid bilayer. The positive control of this experiment included MR-1 incubation with 70 % isopropanol for 1 hour. In consequence, all bacteria were dead.

Fig. 6.4. A. The use of the colony-forming units technique revealed the severe toxicity of positively charged CdTe/CdS/Cysteamine QDs to MR-1. **B.** Data are presented normalised to the negative control. NC = negative control (addition of an equal volume of 20 mM HEPES, 0.15 M NaCl, pH 7.4); PC = positive control (50 µg/ml kanamycin).

Fig. 6.5.1. A. $CuInS_2$/ZnS/PMAL QDs incubated with MR-1 in M-1 media for three hours displayed no toxicity (n=4). QDs concentrations were 0.034, 0.34 and 3.4 µM. **B.** Normalised data portrayed the lack of toxicity of CIS/PMAL to MR-1. NC = negative control (addition of an equal volume of 20 mM HEPES, 0.15 M NaCl, pH 7.4); PC = positive control (50 µg/ml kanamycin).

Fig. 6.5.2. The nanotoxicity of PMAL to MR-1 results (n=3). **A** describes the toxicity in the CFU/ml units, and **B** depicts the normalised data versus NC. NC = negative control (addition of an equal volume of 20 mM HEPES, 0.15 M NaCl, pH 7.4); PC = positive control (50 µg/ml kanamycin).

Fig. 6.5.3. A. and **B.** CIS/PMAL QDs at tested concentrations were not toxic to *E. coli* (n=3)**. C.** and **D.** *E. coli* growth was stimulated by 85 mM PMAL. A and C present the data in CFU/ml, while B and D, show the data normalised to the negative control experiment. NC = negative control (addition of an equal volume of 20 mM HEPES, 0.15 M NaCl, pH 7.4); PC = positive control (50 µg/ml kanamycin).

Fig.7.1.1. Schematic of confocal microscopy with the designed by Minsky pinhole apparatus (redrawn from Jordan et al., 1998). Focused on the pinhole, illuminating

light source (laser) that runs through a dichroic mirror (DM), is imaged onto the object focal plane of the microscope objective (MO). The in-focus specimen leads to a maximum emission of light that is firstly reflected by DM and further focused by the detector pinhole. The light from the out of focus is partially blocked. Abbreviations used here: DM – dichroic mirror, MO – microscope objective.

Fig. 7.2.1.1. The interaction of MR-1 with two concentrations of CdTe/CdS/TGA QDs was investigated. Columns present concentrations of CdTe/CdS/TGA QDs. Row A shows the bright field images, B fluorescence and C merged A and B. Filter setting used included excitation at 410 ± 15 nm, dichroic mirror 500 nm and the emission filter 580 ± 25 nm. Scale bars are 10 μm.

Fig.7.2.1.2. The evaluation of heat shock procedure on MR-1 and 0.5 μM CdTe/CdS/TGA QDs was performed with the epifluorescence microscope. The columns present 30 s and 60 s of MR-1 incubation time in the temperature of 42 °C. A. bright field, B. fluorescence, C. merged A and B. The microscope filters used here were 410 ±15 nm for excitation and a 580 ± 25 nm for emission. Scale bars are 10 μm.

Fig. 7.2.1.3. Obtained by the epifluorescent microscope images of CN-32 incubated with 0.5 μM CdTe/CdS/TGA QDs for overnight. **A** – bright field, **B** – fluorescence, **C** – A and B merged. The used filter setting was the same as in Fig. 6.2.1.2. Scale bars are 10 μm.

Fig. 7.3.1. Overnight incubation of MR-1 with 50 nM CdTe/CdS/Cysteamine QD revealed no interplay as inspected by epifluorescent microscope. A - bright field, B – fluorescence and C – merged A and B. The filter settings employed here were excitation 410 ±15 nm, dichroic mirror 500 nm, emission 580 ± 12.5. Scale bars are 15 μm.

Fig. 7.3.2. The epifluorescence pictures of MR-1 after 1 h, 3 h and overnight incubation with 0.5 μM CdTe/CdS/Cysteamine QDs. The columns show incubation time and rows present A. bright field, B. fluorescence, C. A and B merged. The filters settings used here were the same as in Fig. 6.2.2.1. All scale bars are 20 μm.

Fig. 7.4.1. After overnight incubation, the commercial negatively charged CdTe QDs (5μM) presented a significant level of interaction with MR-1. A – bright field,

B – fluorescence, C – merged pictures. The filter settings in the microscope included: excitation 410 ±10 nm, dichroic mirror 500 nm, emission 535 ±24 nm. All scale bars are 25 μm.

Fig. 7.4.2. The negative and positive controls of MR-1 investigated with the bacterial fluorescence viability assay. The micrographs are overlays of bright field, and fluorescence Picture A portrays the negative control to which an equal volume of 20 mM HEPES, 0.15 M NaCl, pH 7.4 was added. 88 % of bacteria is viable in representative samples (n=3). B shows the MR-1 after 30 min incubation with prop-2-ol. Bacteria were stained with propidium iodide (PI) that is marked red. The filter settings used here include PI excitation at 560 ±27.5 nm, emission 650 ±37.5 nm with a dichroic mirror at 595 nm. Scale bars are 10 μm.

Fig. 7.4.3. The representative pictures of three concentration of commercial negatively charged CdTe QDs incubated overnight with MR-1 and stained with propidium iodide (PI). In columns marked are the QDs concentrations and in rows, the BF – bright field, PL – photoluminescence, PI – propidium iodide, M – merged channels. The green colour was used for PL and red for PI, thus dead and interacting with QDs MR-1 present yellow. The filter settings used here were for PI excitation at 560 ±27.5 nm, emission 650 ±37.5 nm with a dichroic mirror at 595 nm, and for commercial negatively charged CdTe QD excitation at 410 ± 10 nm, emission at 535 ± 24 nm with the dichroic mirror that reflects the light of the wavelength shorter than 500 nm. All scale bars are 10 μm.

Fig.7.4.1.1. Thin-section unstained transmission electron microscopy images of MR-1 after overnight incubation with 5 μM commercial negatively charged CdTe QDs. **A** and **B** show the control, **C - H** show the experimental samples. Red arrows indicate the electron-dense places where it is believed cadmium containing QDs are present. The orange arrows show the commercial CdTe QDs agglomerates. The red rectangles show some examples of membrane disruption and cell lysis. The scale bars of pictures A, B, E, F, G, H are 0.5 μm and on C and D are 100 nm.

Fig. 7.4.1.2. Analysis of transmission electron microscopy (TEM) images of MR-1 after overnight incubation with 5 μM of negatively charged CdTe QDs. Percentage of live (red) and dead (green) MR-1 are given, split to whether they interacted or

not with QDs (bars +QD and -QD). . The Ctrl bar corresponds to control (Ctrl) MR-1 grown without QDs.

Fig.7.4.2.1. Commercial negatively charged CdTe QDs coupled with an amine derivative of dipicolylamine incubated with MR-1 for 15 min as examined by the epifluorescence microscopy. The picture presented here shows an overlay of fluorescence and bright-field images. At the picture, green marks the precipitated QDs that are overlaid with bacteria (grey). The filter settings in the microscope included: excitation 410 ± 10 nm, dichroic mirror 500 nm, emission 535 ± 24 nm. The error bar is 10 μm.

Fig.7.4.3.1. The representative fluorescence micrographs of MR-1 incubated with CdTe/LADPA/Zn QDs. A – bright field, B – fluorescence, C – merged channels. Microscopy filters used here were: excitation – 470 nm ±10 nm, dichroic mirror – 500 nm, emission 580 nm ± 12.5 nm. The scale bars are 10 μm.

Fig. 8.1. The cartoon depicts the structure of light-harvesting biohybrids designed in this Thesis. Light irradiated photosensitizer – quantum dots – stimulated S. oneidensis MR-1 hydrogen evolution. Light irradiated QD's electrons are transferred to hydrogenases by outer membrane decaheame protein complex MtrCAB. Subsequently, the electron holes were created in QDs that had been sealed by electrons from sacrificial donors – triethanolamine (TEOA). Inset depicts [FeFe]HydA and [NiFe]HyaB hydrogenases that anaerobically produce hydrogen and are present in the MR-1 periplasm (PS). Abbreviations used: OM – outer membrane, IM – inner membrane, PS – periplasmatic space. Modified from Shi et al (2011).

Fig. 8.2.1. 0.3 mM MV was not reduced when the samples containing different QDs (CdTe/CdS/TGA, CdTe/CdS/Cysteamine, commercial negatively charged CdTe and CuInS2/ZnS/PMAL), 50 mM TEOA or 50 mM EDTA (for CIS/PMAL) in 50 mM HEPES, 50 mM NaCl were not irradiated. The control samples kept in the dark with 150 mM MES did not reduce MV; they are not present at the figure. The solid lines show absorbance at time zero, and dashed lines present absorption at 30 min of incubation in the dark.

Fig. 8.2.2. Photoreduction of methyl viologen (0.3 mM) using different QDs and SEDs. MV^+ concentration in μM after irradiation with a cold lamp with a power of

700 W m^{-2} for times in minutes stated on the X-axes. Graph **A** depicts the results of photoreduction by CdTe/CdS/TGA, **B** by CdTe/CdS/Cysteamine, **C** by commercial negatively charged CdTe QDs and **D** by $CuInS_2$/ZnS/PMAL QDs. In B and C, EDTA was disregarded as the photoreduction rate did not differ from the non-irradiated controls. MV, photosensitisers (QDs) and SEDs were resuspended in 50 mM HEPES, 50 mM NaCl, pH 7. SEDs used include 50 mM TEOA, 50 mM EDTA. MES (150 mM) was used both as a buffering agent and a sacrificial electron donor. MV^+ concentrations were calculated from the absorbance peak at 606 nm as the peak present at 396 nm interfere with QDs absorption. Error bars represent the standard deviation for results from at least two independent experiments. Abbreviations used include TEOA – triethanolamine, EDTA – ethylenediaminetetraacetic acid, MES – 2-ethanesulfonic acid

Fig.8.3.1. Gas chromatography calibration curve obtained using hydrogen/nitrogen calibration standard. The equation displayed on the graph was used to calculate the quantity of hydrogen produced by bacteria.

Fig. 8.3.2. Anaerobic production of hydrogen by four strains of *Shewanellaceae: S. oneidensis* MR-1, *S. spp. strain* MR-4, *S. putrefaciens* CN-32 and LS473 upon overnight growth in M72 media. No QDs were used in these experiments. Bacteria were grown in electron-acceptor limited conditions. Error bars represent the standard deviations that equal 82, 61, 82 for MR-1, MR-4, CN-32, respectively. The number of samples examined equals 4 (n = 4). As expected, LS473 did not produce any hydrogen.

Fig. 8.3.3. Anaerobic production of H_2 by CN-32. QD concentrations used in these experiments were: 0.6 and 1.2 μM of negatively charged commercial CdTe and 0.5 μM of CdTe/CdS/TGA (CdTe(-)) QDs. All samples were irradiated for 24 h with a photosynthetic growth lamp. Bacteria were incubated in 50 mM HEPES and 50 mM NaCl, pH 7, 50 mM TEOA, and the chosen QD. The average and standard deviation were calculated from the average H_2 production by irradiated CN-32 grown with cadmium-containing QD. The left and middle bars are coloured green as they present the commercial CdTe QDs but in different concentrations. Number of repetitions was 1.

List of Abbreviations

Abbreviation	Explanation
ADPA	Amine Derivative of dipicolylamine
AFM	Atomic Force Microscopy
ATP	Adenosine triphosphate
Au-NW	Gold nanowires
Au-NW-PDA	Gold Nanowires Modified by Polydopamine
BFC	Biological Fuel Cell
CD	Carbon dots
c. f.	(Latin) confer/conferatur, (English) compare
CFU/ml	Colony Forming Units in 1 millilitre of bacteria culture
CHES	N-Cyclohexyl-2-aminoethanesulfonic acid
CIS/PMAL	$CuInS_2$/ZnS/PMAL
CN-32	*Shewanella putrefaciens* CN-32
Cryo-EM	Cryogenic Electron Microscopy
Ctrl,	Control
Cy	Cyanine
CymA	Tetraheme Membrane-bound Menaquinol Dehydrogenase
d	Diameter
D	Diffusion Coefficient
DAPI	4′,6-diamidine-2′-phenylindole dihydrochloride
DDT	Dodecanethiol
DDT	Disk Diffussion Test
DEGAT	Diethylene glycol aminothiol
d_H	Hydrodynamic Size

DM	Dichroic Mirror
DMRB	Dissimilatory Metal Reducing Bacteria
DMS	Dimethyl Sulfite
DmsEFAB	Outer Membrane heme-containing Proteins Complex
DMSO	Dimethyl Sulfoxide
DTT	Dithiothreitol
E. coli	OMINMAX *E. coli*
EDC	1-ethyl-3-(3-dimethylaminopropyl) carbodiimide
EDTA	Ethylenediaminetetraacetic acid
EET	Extracellular Electron Transfer
e.g.	Latin ‘exempli gratia’
EM	Electron Microscopy
FACS	Fluorescence Activated Cell Sorting
FAD	Flavin Adenine Dinucleotide
FccA	Flavocytochrome Fumarate Reductase
FM	Fluorescence Microscopy
FRET	Forster Resonance Energy Transfer
G6PD	Glucose 6-phosphate dehydrogenase
GC	Gas Chromatography
GFP	Green Fluorescent Protein
HaCat	Cultured Human Keratinocyte Cell Line
HEPES	(4-(2-hydroxyethyl)-1-piperazineethanesulfonic acid)
HRTEM	High Resolution Transmission Electron Microscopy
HyaB	MR-1 Periplasmic [Fe-Ni] Hydorgenase
HydA	MR-1 Periplasmic [Fe-Fe] Hydorgenase
IM	Inner Membrane

ISO	International Organization of Standarization
ITO	Indium Tin Oxide
k	Boltzmann Constant, $1.38 \times 10^{-23}\ m^2 \times kg \times s^{-2} \times K^{-1}$
LADPA	Lipoic Acid Derivative of Dipicolylamine
LB	Luria Bertani Bacterial Growth Medium
LCA	Life Cycle Assessment
LE	Ligand Exchange
LED	Light Emitting Diode
LS473	*Shewanella oneidensis* MR-1 mutant strain without functional hydrogenase
M1	Modified M-1 Minimal Media for Bacteria Growth
MES	Microbial Electrochemical Systems
MES $_{buffer}$	2-morpholin-4-ylethanesulfonic acid
MFC	Microbial Fuel Cell
min	Minutes
MMC	Microbial Methanogenesis Cell
MQ	Menaquinon
MR-1	*Shewanella oneidensis* MR-1
MR-4	*Shewanella spp. strain* MR-4
MtrCAB	MR-1 Outer Membrane Proteins Complex That Reduces e. x. Iron Oxide Minerals
MTT	3-(4,5-Dimethylthiazol-2-yl)-2, 5-diphenyltetrazolium bromide
MV	Methyl Viologen
n	Number of repetitions with one sample
NAD^+	Nicotinamide Adenine Dinucleotide
NADPH	Nicotinamide Adenine Dinucleotide Phosphate

NC	Negative Control
NP	Nanoparticle
OD_{600}	Optical Density at 600 nm
OM	Outer Membrane
OmcA	Outer Membrane Cytochrome A from MR-1
OmcS	Outer Membrane Cytochrome S from *Geobacter sulfurreducens*
PALM	Photo Activated Localisation Microscopy
PBS	Phosphate Buffer Saline
PC	Positive Control
PC12	Pheochromocytoma Cell Line
PCR	Polymerase Chain Reaction
PDA	Polydopamine
PEM	Proton Exchange Membrane
PI	Propidium Iodide
PilA	*Geobacter sulfurreducens* protein
PL	Photoluminescence
PMAL-d	Poly(maleic anhydride-alt-1-tetradecene), 3-(dimethylamino)-1-propylamine derivative
PS II and I	Photosystem II and I
QD	Quantum Dot
qPCR	Quantitative real time polymerase chain reaction
r	The minimum distance between resolvable points
R-COOH	Organic carboxylic acid
RF	Riboflavin
$R\text{-}NH_2$	Organic amine

ROS	Reductive Oxygen Species
RPM	Revolutions per minute
rRNA	Ribosomal Ribonucleic Acid
RuP	$[Ru_2(bipy)_3]^{2+}$
Saline	20 mM HEPES, 0.15 M NaCl. pH 7.4
SD	Standard Deviation
SED	Sacrificial Electron Donor
SEM	Scanning Electron Microscopy
SHE	Standard Hydrogen Electrode
sMFC	Sediment Microbial Fuel Cell
SPEEK	Sulfonated Poly (Ether Ether Keton)
STC	Small Tetraheme Cytochrome
STED	Stimulated Emission Depletion Microscopy
STORM	Stochastic Optical Reconstruction Microscopy
TEOA	Triethanolamine
TGA	Thioglycolic Acid
TIPS	Triisopropylsilane, $C_6H_{22}Si$
TMAO	Trimethylamine-N-oxide
Tris	2-Amino-2-(hydroxymethyl)propane-1,3-dio
WST-1	tetrazolium salt, Colourimetric Mammalian Cell Viability Assay that measures mitochondrial dehydrogenases activity which cleaves WST-1 to formazan
ΔE	Transmission Energy Corresponding to the First Absorption Peak
λ	UV-Vis Absorbance Maximum
λ_{PL}	Photoluminescence Maximum

ε	Extinction Coefficient
η	Viscosity

Chapter 1. Microbial Electrochemical Systems. Introduction.

1. Microbial Electrochemical Systems.

Historical fuel supply emergencies, superseded now by the effects of global warming and ever-growing environmental pollution, have stimulated researchers to find alternatives to carbon-based fuels. The production of fuels and chemicals in the carbon-free way are investigated for the sake of global society (Nocera, 2017). Solar, wind and water-based energy sources, and systems that utilise engineered bacteria for value-added chemical and biofuel production are a few examples of substitutes to carbon energy that are now being explored (Chu and Majumdar, 2012). Here, examples of microbial electrochemical systems (MES) are described.

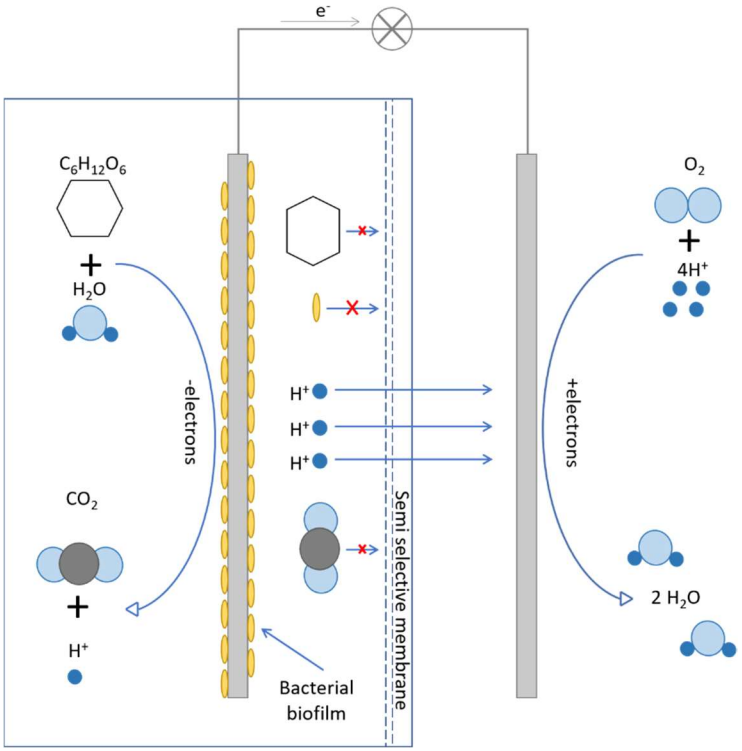

Fig. 1.1. Schematic diagram of an MFC device. Exoelectrogens in the anode chamber utilise available carbon sources (here, glucose) and harvest CO_2 and electrons as the products. The semi-selective membrane blocks the biotic and organic molecules from entering the air cathode where oxygen is reduced in a direct 4 electron reaction, producing water. Image modified from (Logan and Rabaey, 2012)

One of the best-characterised and most frequently used microbial electrochemical systems are microbial fuel cells (MFCs) (Fig. 1.1). MFCs drive metabolic electrons from exoelectrogenic bacteria that are further transported by an electric circuit to the cathode chamber where oxygen is reduced to water (Logan et al., 2006). Exoelectrogens are the bacteria that live on the surface of minerals and possess a specialised protein network that transfers metabolic

electrons through the outer-membrane to outside the cell (White et al., 2016). Both Gram-negative and Gram-positive bacteria in anaerobic conditions export their electron pool to the environment when reducing extracellular final electron acceptors. It is thought that exoelectrogenic bacteria export electrons to prevent the build-up of charge inside the cell, and this does not contribute to proton motive force (White et al., 2016).

Over the past few decades, MFCs that utilise exoelectrogens have captured significant scientific attention for the possibility of transforming organic waste directly into electricity (Lovley, 2006b). Microbially catalysed anodic current and microbial/enzymatic/abiotic cathodic electrochemical reactions were thoroughly investigated not only in the lab benches of academic institutions but also in an industrial setting. Throughout the years, many MES- and MFC-based devices have been engineered, with examples including the sediment MFC (sMFC) where the anode is immersed in nutrient-rich aquatic deposits and connected to an oxygen reducing cathode, microbial desalination cells, microbial methanogenesis cells (MMCs), and finally microbial electrochemical systems that use bacteria to produce highly valued chemical feedstocks (Logan et al., 2015). Collectively, MES are devices that use bacterial metabolism, in the form of whole cells or purified enzymes, often accompanied by inorganic nanoparticles, to produce either electricity or organic compounds (Logan et al., 2015; Kornienko et al., 2018).

Bacteria use energy from a variety of carbon sources and non-organic electron donors such as sulfur or iron minerals. The reduction of ambient materials by microbes creates not only an interesting area for fundamental studies but also far-reaching industrial applications. Used in MFCs, exoelectrogens improve wastewater treatment and simultaneously generate electricity. There are already several MFCs in industrial use, for instance: Foster's brewery in Yatala, Queensland (Australia) (Wang et al., 2008) and self-fed robots: EcoBot II and III (Melhuish et al., 2006). The use of MFCs in space has gained the interest of NASA, and now scientists are running tests to evaluate the scalability and efficiency of a system for production of electricity out of human excrement. Currently, astronauts’ excrement is

shipped back to earth, costing not only energy for transport but also loses the opportunity to produce electricity.

Microbial electrochemical systems possess many advantages over conventional fuel cells. These include: 1) longevity through using a biotic anodic electrocatalyst; 2) operation in the ambient temperature range from 15–45 °C; 3) a neutral working pH; 4) utilization of complex biomass (different types of waste and sludge); 5) moderate environmental impact judged by life cycle assessment (LCA) (Santoro et al., 2017). An LCA of three independent fuel cells performed by Foley (2010) compared (i) conventional anaerobic treatment with biogas generation, (ii) an MFC, and (iii) microbial electrolysis cell with hydrogen peroxide production. In a multi-categorical LCA approach, the impact on human health, ecosystem quality, climate change and resources used in the design of cells were combined to obtain the final numbers. Unavoidable post-treatment costs delivered a negative impact for all investigated systems, although biogas, electricity and hydrogen peroxide generated during the inspected treatments improved the overall score of the systems. For instance, the MFC performed better than an anaerobic system in all the assessed features but costly components in the structure of the MFC, like the expensive carbon cloth electrode and stainless steel parts, played a significant role in the global outcome (Foley et al., 2010).

Given the many benefits of MFCs, challenges also exist that must be met through research to make these devices profitable and fully industrialised. The following section will describe the pros and cons of MFCs and what can potentially be done to improve their performance. In the next subchapter, most frequently used exoelectrogen in MFC research are described in details.

1.1. *S. oneidensis* MR-1 and Extracellular Electron Transfer.

Shewanella oneidensis MR-1 (MR-1) is a Gram-negative, facultative bacterium that is able to dissimilatory reduce extracellular electron acceptors. It uses a variety of carbon sources for metabolism (lactate, pyruvate, sole carbon, DNA) and lives in diverse environments ranging from freshwater to industrial sewage. The unparalleled array of respiratory electron acceptors used by MR-1 can be attributed to the variation in the environment it lives in.

The significance of *Shewanella* species is emphasised by the ecological importance of these bacteria taking part in biogeochemical metal cycling, corrosion, subsurface bioremediation, food spoilage and opportunistic pathogenicity (Breuer et al., 2015). MR-1 was employed in fundamental studies of extracellular electron transfer and biotechnological applications. In contrast to another metal-reducing bacteria, *Geobacter,* MR-1 is a facultative bacterium (can live in aerobic or anaerobic conditions) and thus is easier to work with. Since its discovery in 1988, *Shewanella oneidensis* MR-1 is a strain of particular notability and became a model organism (Hau and Gralnick, 2007). MR-1 extracellular electron transfer (EET) is the best characterised from all exoelectrogens and will be described in depth in the following section.

1.1.1. Short History of *S. oneidensis* MR-1.

Due to limitations in the scientific tools available, the name for genus *Shewanella* has been frequently altered. Firstly, *Shewanella* was discovered in 1931 and recognised as responsible for butter putrefaction, and thus named *Achronobacter putrefaciens* (Derby and Hammer, 1931). A decade later, Long et al. (1941) reclassified the taxon as *Pseudomonas* and renamed it to *Pseudomonas putrefaciens*. Nonfermentative marine bacteria were again reclassified as *Alteromonas putrefacient* based on the molar per cent of guanine plus cytosine in its DNA (Baumann et al., 1972). The analysis of 5s rRNA sequence data pushed the reformed again name to *Shewanella* to honour Dr James M. Shewan for his work in fisheries microbiology (MacDonell and Colwell, 1985). To date, there exist at least 50 species of *Shewanella*, and it is postulated that more are yet to be discovered (Janda and Abbott, 2012).

MR-1 is the best characterised and explored bacterium from the genus *Shewanella*. The species name (*oneidensis*) comes from the name of the lake where MR-1 was first isolated – Oneida Lake in New York State, USA (Venkateswaran et al., 1999). MR abbreviation stands for **m**etal **r**educer and comes from the ability of MR-1 to reduce insoluble electron acceptors such as manganese(IV) to manganese(II) oxides (Myers et al., 1988). The optimum temperature of growth for MR-1 is 30 °C; however, this bacterium can sustain life in sub-zero temperatures (Abboud et al., 2005). The ability to live in such

an extreme environment is not often observed as at low temperatures the biomembrane lipids phase changes from liquid to gel. This transition should affect the membrane quinone pool and membrane enzymes, thus severely impacting bacterial respiration. It has been postulated that many *Shewanella* distract the gel transition by incorporating short, highly branched lipids together with the integrating of eicosapentaenoic acid in the lipid bilayer (Valentine and Valentine, 2004).

MR-1 performs anaerobic respiration utilising not only metals as terminal electron acceptors but also a variety of other acceptors: converting trimethylamine-N-oxide (TMAO) to trimethylamine, Fe(III) chelate and Fe(III) oxide to soluble Fe(II), sulfur/polysulfide/sulfite/thiosulfate to H_2S, Mn(III) and (IV) reduces to Mn(II) oxide, dimethyl sulfoxide (DMSO) to dimethylsulfide (DMS), arsenate to arsenite, but also reduces fumarate to succinate (Nealson and Scott, 2006). This versatility of electron acceptors used by MR-1 is characterised in-depth and discussed in the following sections.

1.1.2. Extracellular Electron Transport in *S. oneidensis* MR-1.

Microbial electrochemical synthetic systems utilise bacteria that traffic metabolic electrons extracellularly either to an insoluble electron acceptors or to an relectrode . As mentioned above, MR-1 can utilise a variety of electron acceptors in anaerobic conditions and possesses a complex network of proteins responsible for anoxic electron transport (Breuer et al., 2015; White et al., 2016). The MR-1 metabolic electrons travel through NADH–menaquinone oxidoreductase CymA (c-type cytochrome), that is an inner membrane electron distribution hub. C-type heame-binding proteins such as CymA contain a characteristic motif of CysXXCysHis in their primary sequence; this sequence is frequently used to screen bacterial and mammalian genomes to find potential heame-binding proteins (Heidelberg et al., 2002; Clarke et al., 2008). The hemes in c-type cytochromes are covalently attached to the cysteine residues while the iron atom is coordinated by the histidine. From CymA, electrons are further transported to either small tetraheame cytochrome, STC, and/or flavocytochrome fumarate reductase, FccA in the periplasm. STC is highly conserved among *Shewanella* species and is one of the most abundant cytochromes in the periplasmic space and

distributes electrons received from CymA to a variety of final electron acceptors in the periplasm (Coursolle and Gralnick, 2010; Alves et al., 2015). FccA not only catalyses the reduction of fumarate to succinate in a two-electron two-proton reaction but also reduces selenite to Se(0) nanoparticles (Li et al., 2014). Electrons received from CymA are further trafficked through FccA and STC to porin-cytochrome complexes like DmsEFAB and MtrCAB. DmsEFAB is responsible for the extracellular reduction of DMSO to DMS (Dos Santos et al., 1998; Bewley et al., 2012). A molybdenum-containing DmsA and an iron sulfur holding DmsB are outer membrane proteins as proved by immunogold stained MR-1 (Bewley et al., 2012). MtrA and its paralogue DmsE are decaheame cytochromes located within trans-outer membrane β-barrel proteins, MtrB and DmsF, respectively (Gralnick et al., 2006; Mcmillan et al., 2013; Edwards et al., 2018). MtrA protrudes into the periplasm, where it collects electrons from STC or FccA and traffics them to the extracellular lipoprotein and decaheame MtrC (Schicklberger et al., 2011; Sturm et al., 2015). The two to one protein complex of dodecaheame proteins OmcA and MtrC was shown to play a critical role in the EET and reduction of iron and manganese ions (Ross et al., 2007; Zhang et al., 2008). In the anaerobic stationary growth phase of MR-1 and under external acceptor limited conditions, CymA traffic electrons to the hydrogenases, HydA and HyaB, that evolve hydrogen or metabolise hydrogen in case of HyaB (Meshulam-Simon et al., 2007). Meshulam-Simon et al. (2007) postulated that hydrogen production with MR-1 plays a role in providing hydrogen to mixed microbial communities. There are also other terminal electron acceptors present in the periplasm. The prominent examples include NapE/NapA that reduces nitric to nitrous ions and NrfA that reduces nitrous ions to ammonium cations (Myers and Myers, 1997; Kern et al., 2008; Breuer et al., 2015). A schematic of proteins expressed and utilised by MR-1 is presented in Fig. 1.2.

It was initially unknown that MR-1 secretes flavins until Lies et al. (2005) used porous glass beads with the deposited ferric (hydr)oxide [Fe(III) (hydr)oxide] on their surface to observe the reduction of insoluble iron oxide at a distance larger than 50 µm from the bacterial membrane by colorimetric ferrozine assay. In further experiments the poised electrode as the terminal electron acceptor for MR-1 biofilm revealed that water-soluble electron shuttles like

riboflavin or flavin mononucleotide were responsible for electron shuttling in MR-1 (Marsili et al., 2008). The removal of flavins from the MR-1 biofilm growth medium decreased the electron transfer rate to the electrode by more than 70 %, suggesting electron shuttles are the dominant species in EET of MR-1.

Another method of electron transport in MR-1 and *Geobacter* by so-called nanowires was argued by Lovley and colleagues (Reguera et al., 2005). It was first postulated that electron transfer in nanowires was due to the presence of aromatic amino acids in the structure of *Geobacter* PilA proteins that transferred electrons in metallic-like conductivity (Lovley, 2012). However, Pirbadian et al. (2014) showed the MR-1 nanowires are outer membrane and periplasmic extensions of the extracellular components. The development of MR-1 nanowires as membrane appendages was confirmed by fluorescence microscopy footage; thus, the proof was visible and undeniably convincing (Lovley and Malvankar, 2015).

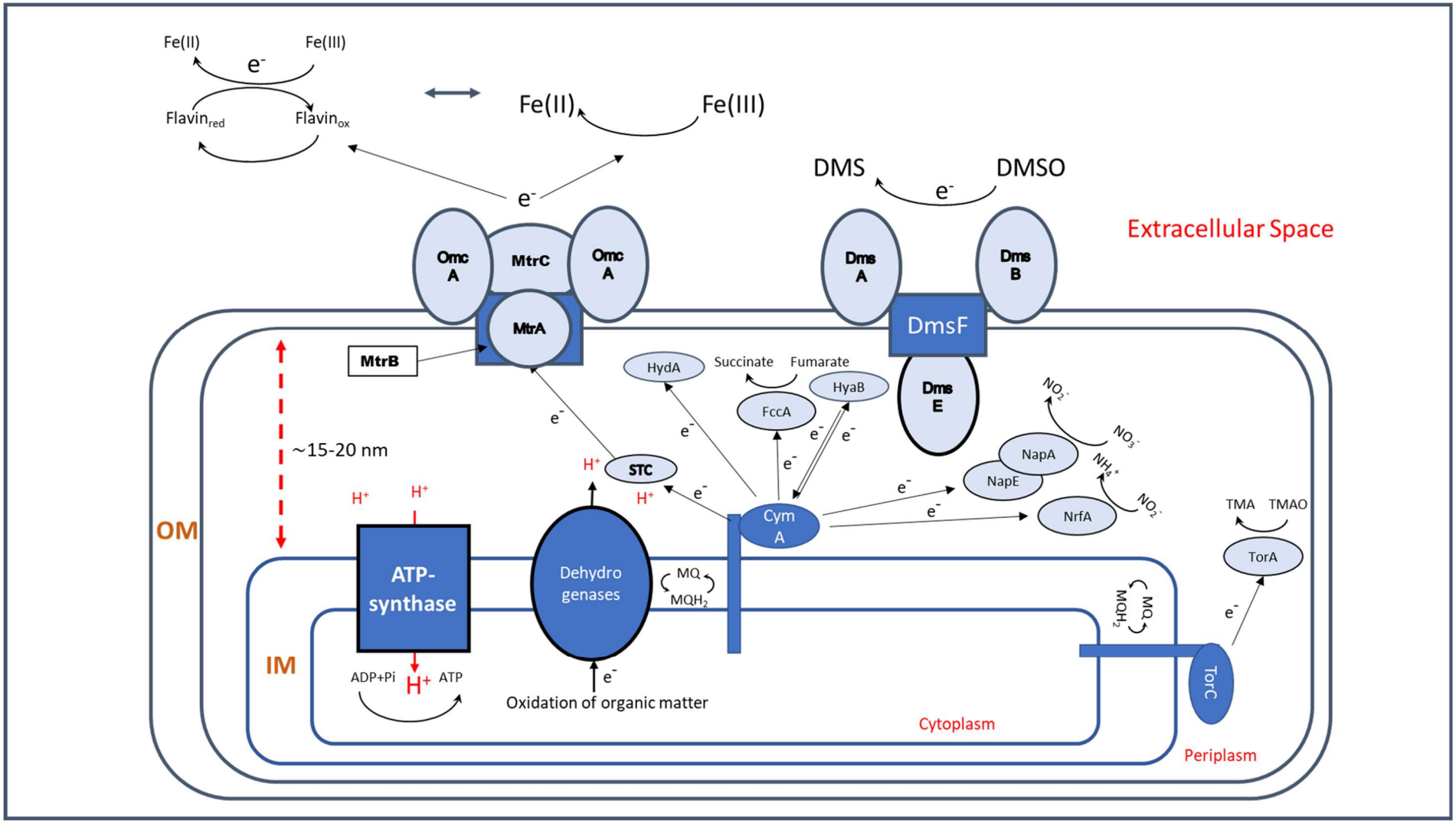
Fe(II)
Fe(III)
e-
Flavin red
Flavin ox
Fe(II)
Fe(III)
e-
DMS
DMSO
e-
Extracellular Space
Omc A
MtrC
Omc A
MtrA
Dms A
Dms B
DmsF
Dms E
MtrB
HydA
Succinate
Fumarate
HyaB
FccA
~15-20 nm
STC
Cym A
NapA
NapE
NrfA
NO2-
NO3-
NH4+
TMA
TMAO
TorA
TorC
OM
IM
ATP-synthase
Dehydro genases
MQ
MQH2
ADP+Pi
H+
ATP
Oxidation of organic matter
Cytoplasm
Periplasm

Fig. 1.2. Schematic of proteins anaerobically expressed by S. oneidensis MR-1. Metabolic electrons from the oxidation of carbon sources in the cytoplasm arem directed to the menaquinone pool in the inner membrane (IM) by inner membrane NADH or formate dehydrogenases. Dehydrogenases simultaneously reduce quinones and transfer protons to the periplasm creating a protonmotive force (PMF). ATP-synthase uses the PMF to catalyse the synthesis of ATP. The PMF is preserved by reoxidation of quinols by the homologues CymA or TorC. CymA distributes electrons for periplasmatic terminal reductases like the reduction of fumarate to succinate by FccA or through the extracellular reduction of metal oxides or dimethylsulfoxide by outer membrane (OM) proteins. TorC transfers electrons to TorA that reduces TMAO. Black arrows indicate electron flow, red arrows depict proton transport, and protons are marked in red. Image modified from (Laftsoglou, 2017).

Only recently, *Geobacter sulfurreducens* nanowires that perform electron transfer over distances longer than 10 µm were shown to be composed of micrometre-long polymerisation of the hexaheame cytochrome OmcS, with heames packed within 3.5–6 Å of each other rather than PilA proteins (Wang et al., 2019). ΔOmcS mutant nanowires showed lower conductivity and were half the height of the wild type OmcS as confirmed by direct current conductivity measurement and atomic force microscopy (AFM). The correlations found between PilA and biofilm conductivity as shown before (Malvankar et al., 2011) was argued as incorrect, and Wang showed overexpression of PilA accompanies the overproduction of OmcS; thus PilA is involved in secretion of this cytochrome (Wang et al., 2019). Nevertheless, Lovley still claims that the aromatic residue-rich PilA expressed in *Geobacter* thick biofilms is necessary for EET in conditions required for MFC work (Vargas et al., 2013; Lovley and Walker, 2019).

1.2. Microbial Fuel Cells.

MFCs grant the opportunity for the development of electricity production by bacteria. The exoelectrogens transfer their metabolic electrons to the anode. In a simple assembly, the anode chamber is separated using a proton exchange membrane (PEM) from the cathode chamber where reduction reactions occur, and anodic electrons are utilised either for reduction of chemicals like oxygen to water or harvested as electrical power (Fig.1.1).

However, the low power output and current densities still limit the scaling up of MFCs. Disadvantages hindering the further development of MFCs include the significant resistance that directly depends on the electrode material and the ion-selective membrane. Most of the total resistance of an operational

MFC is contributed by the internal resistance, which consists of the resistances of the anode, the cathode, the electrolyte and the membrane. High resistance PEMs impact the performance of MFCs; the low ion exchange capacity of the membrane reduces proton diffusion from the anode to the cathode, leading to low current and power densities (Leong et al., 2013). Initially, the cathode in an MFC was separated from the anode by a costly PEM. PEMs were later replaced by, again expensive, Nafion polymer membranes that also suffered from several issues. Both PEMs and Nafion have the same disadvantages that include oxygen leakage to the anode chamber, non-selective cation transferability as any cations were transferred to cathode chamber, cation accumulation in the Nafion membrane, substrate loss and biofouling of the membrane (Chae et al., 2008). The sustainable work of MFCs was increased when the PEMs were removed from the system. Although, when compared to an MFC with a PEM, five times higher power densities were achieved, the Faraday efficiency – the percentage of electrons recovered from the organic matter versus the theoretical maximum of all electrons taking part in current generation – was only about 70 % of the MFC with the PEM (Liu and Logan, 2004). This system suffered from a lower electron transfer rate from bacteria to anode due to the presence of oxygen. The PEM also contributes to the acidification of the anode electrolyte, and the cathode solvent becomes more alkaline due to the process of pH splitting. The degree of pH splitting depends on the choice of cation exchange membrane; a higher concentration of cations (Na^+, K^+, Ca^{2+} and NH_4^+) compared to protons in the anolyte, which then compete with protons for attachment to negatively charged functional groups in the Nafion membranes (Chae et al., 2008). The drastic drop in pH in the proximity of the bacteria anode interface results in the reduction of bacterial oxidation activity followed by limited proton production. A partial solution was found by removing any membranes in the MFC, thus reducing the resistivity substantially, and using ammonium as a sustainable proton shuttle (Cord-Ruwisch et al., 2011). Membrane-less MFCs also have their minuses that include fouling of the cathode surface, high electrolyte cross-over that impacts electrode work, and low electron transport from bacteria to the anode due to the presence of oxygen (Chae et al., 2008). PEMs are still used in MFCs; however, some modifications were investigated

and included the use of e.g. glass wool in a granular activated carbon-based MFC for dye water decolouration, detoxification and simultaneous electric power production (Kalathil et al., 2011). After 48 h of operation, the Kalathil MFC – without any PEM or platinum constituents – removed 73 % of colour dye from the anode and 77 % from the cathode, leaving the efflux non-toxic to mixed bacteria culture as assessed by the colourimetric resazurin reduction method. Simultaneously, the system produced a power output of 1.7 W/m^3 with an open-circuit voltage of 0.45 V. To compare, MFCs for wastewater remediation typically obtain power densities of 0.1–0.5 W/m^2 (Vologni et al., 2013). Innovative, less expensive sulfonated polymer membranes such as SPEEK (sulfonated poly(ether ether ketone)) membranes are robust and biocompatible; however they still possess similar problems to Nafion membranes (Mikhailenko et al., 2000).

The most efficient cathodes in MFCs are built from costly platinum, which limits the profitability of these cells. Consisting of a layer of catalysts, electrode and a membrane with the continuous influx of oxygen, the air cathode has been suggested as a solution (Santoro et al., 2017). Furthermore, the use of stainless steel brushes as a cathode has proved economically beneficial in microbial electrolysis cells as they give high current densities and high energy recoveries similar to those of the platinum electrode (Call et al., 2009). Additionally, biocathodes have also attracted scientific attention. MR-1, valued for their extracellular electron transport to the anode, was used as the electron acceptor in the cathode compartment. When a MR-1 biofilm in the cathode compartment was stained with a fluorescent redox sensor and acquired energy from the cathodic electron influx, a stable signal was recorded; energy obtained in this way might be of potential use for microbially synthesised products (Rowe et al., 2018).

Another part of MFC that alteration might be beneficial for the system is the exoelectrogens. Although single colony-inoculated MFCs are most frequently studied as they are more controllable, Logan and Regan (2006) postulate that mixed bacterial communities perform better in MFCs in terms of higher power output and more efficient waste degradation. At practical scales, energy output from MFCs is too low to meet energy-neutral operations. Domestic

wastewater contains plenty of feedstock chemicals with about 66 % of organics that can be used in MFC-based electricity production but also a multitude of indigestible pollutants (Ting and Lee, 2007). Equally, agricultural animal manure is high-strength wastewater and contains many volatile amino acids, lipids, and proteins that can be utilised in MFCs for power production. Application of single-chamber MFCs in agricultural water treatment was shown to reduce ten chemicals associated with swine farm odours by almost 80 % and simultaneously produces electricity at 228 mW/m^2 (Jung et al., 2008). The high carbohydrate content in food processing wastewater is beneficial for microbes in MFCs; for example, beer-brewing companies benefit from electricity production in single-chamber MFCs, still using costly platinum cathodes, with the power output of 483 mW/m^2 (Wang et al., 2008).

The anode surface is another MFC component that requires improvement to achieve better power output and current density (Kumar et al., 2013). The anode material in all MES must support bacterial growth, and thus must be biocompatible, stable and durable. At the same time, good electrical conductivity and high surface-to-volume ratios are crucial to obtain good performance MFCs. Unfortunately, high surface-to-volume ratio of porous anode materials frequently clogs up due to the dense bacterial biofilm formation (Wei et al., 2011). Clogging might be prevented by using nanoparticles passivated anodes with hole sizes larger than 10 µm (Min and Logan, 2004). Continued bacterial growth on the restricted electrode surface leads to poisoning and fouling that again limits the energy output. The enlarged spacing of the electrodes, their increased void and stacking are considered to be solutions to the fouling issues (Ghangrekar and Shinde, 2007).

More recently designed, 12 stacked, one chamber, membrane-less MFCs were used to generate electricity from neat urine, collected during the UK Glastonbury Festival in 2016 (Walter et al., 2018). Walter et al. (2018) modified the fuel cell system to store the MFC-obtained electric energy in 8 lithium iron phosphate cylindrical cells (each 3.2/5 V/Ah). Batteries were deployed to light 6 LED strips (consumed 424 W/day) for 9 h 30 min per day. The carbon-neutral pre-treatment system used in the Glastonbury trial

showed that MFC technology is satisfactorily mature to positively impact liquid waste management in urban, as well as rural areas (Walter et al., 2018).

Future perspectives of MFCs are brought forward by the expansion of nanotechnology. Chitosan-covered carbon nanotubes showed increased MFC efficiency at a power density of 4.75 W/m^3 and a current density of 16 A/m^3 (c.f. carbon cloth electrode 3.5 W/m^3 and 7 A/m^3) (Higgins et al., 2011). Additionally, the use of gold constituents such as grass-like nanostructures on the silicon anode was shown to increase power output nearly 3 times compared to a conventional carbon cloth electrode (Alatraktchi et al., 2012). A more recent study showed that a three-dimensional graphene aerogel anode decorated with costly Pt nanoparticles (NPs) and inoculated with MR-1 generated a power density of 1460 mW/m^2, which is over six times larger than a carbon cloth electrode (Zhao et al., 2015). Additional use of NPs in MES will be discussed further in section 2.2.2. Bionanotechnology in MES.

2. Bionanotechnology

2.1. Bionanotechnology – Definition and Examples.

Bionanotechnology is a discipline of science that merges the tools of nano- and biotechnology. Nanotechnology is a powerful engine for innovation that operates on the nanoscale, that has at least one dimension in the 1 – 100 nm range, and it is hoped that it can be used to create breakthrough solutions for emerging world problems such as climate warming, and ever-increasing pollution of the environment. The 'bio' part frequently includes the incorporation of purified enzymes or other biomolecules in biosensors or recently, the entire bacteria for sun-fuel conversion. Although combining bio and nano seems exciting, and many attempts have been performed, the outcome is often far from ideal. In the following sections, the advantages and drawbacks of nanobiodevices will be discussed in depth. This section introduces the topic only briefly.

One of many examples of bionanotechnological devices is biofuel cells (BFCs), which utilise biocatalysts (proteins) to produce electricity or chemicals. Yan and co-workers (2006) employed carbon nanotubes, which have both excellent electrical conductivity and electrochemical activity, to perform glucose oxidation with NAD^+–dependent glucose dehydrogenase as the anode biocatalyst and oxygen reduction on the cathode passivated with laccase. Unlike BFC, microbial fuel cells harvest the electrical energy present in wastewater, and that may contribute to an economical solution to the environmental pollution and energy crisis (Lovley, 2006a; Pant et al., 2010; Choudhury et al., 2017). MFCs were discussed in detail in section 1.2.

Recently developed biohybrid systems often use sunlight as a source of energy and harvest different metabolites from living organisms (Holzmeister et al., 2018). Bacteria, algae and yeast are utilised in biohybrids to harvest light and produce specific chemicals (Chisti, 2007; Oliveira et al., 2013; Nangle et al., 2017). A recent example used aquatic Acetobacterium *Moorella thermoacetica* for light-induced production of acetate (Sakimoto et al., 2016). Additionally, the production of shikimic acid, the precursor of many medicines, was reinforced by a eukaryotic genetically-modified model organism *Saccharomyces cerevisiae* and indium sulfite quantum dots (Guo et al., 2018).

There are many examples of bionanotechnological devices devoted to the production of valuable chemicals, electricity generation and sustainable, non-polluting waste remediation; nevertheless, the room for innovation, optimisation, improvements and research is always present (Blankenship et al., 2011).

2.2. Nanotechnology in MES.

Although gold nanoparticles (NP) have been used throughout the history for example when putting glitter onto pottery (4th century) or by cave dwellers in palaeolithic ages, only more recently in the 19th century were the unusual features of colloid gold particles described by Michael Faraday (Faraday, 1857). While cleaning thin sheets of gold with water, Faraday noticed the liquid became ruby in colour. After that, he investigated the behaviour of light shone on the liquid and concluded that the liquid contained particles too small to observe with the methods available for him (Thompson, 2008). Faraday was the first scientist to observe that some features of gold colloids were different from those of bulk gold. He is now recognised as a father of modern colloidal chemistry. Subsequently, scientists developed many techniques to enable the investigation and visualisation of nanoparticles. Following Faraday's observations, it is now known that in comparison to bulk materials, submicron dimensions give metals new and unusual features. As an example, gold nanoparticles melt at a significantly lower temperature and have higher resistivity than bulk gold (Buffat and Borel, 1976; Batista et al., 2015). Many organisations, such as the International Organization of Standardization (ISO), define NPs as entities having at least one dimension in the range of 1–100 nm.

Why did nanoparticles become popular? The most prominent advantage of nanoscale materials is their high surface to volume ratio. This relation amplifies their interface to interact with the biological, chemical and physical environment (Daniel and Astruc, 2004; Fadeel and Garcia-Bennett, 2010; Saha et al., 2012; Batista et al., 2015; Sakimoto et al., 2018). In the past three decades, many nanoparticles have been developed and characterised. Prominent examples of NPs include carbon nanotubes, a variety of gold

nanostructures and fluorescence semiconductor nanocrystals or quantum dots (QD) (Bera et al., 2010; Zeng et al., 2011; Lawal, 2016). Nowadays, nanoparticles and their unusual features are used not only in cosmetics and electronics but also in the nanoparticle-modified electrochemical cells or medicines. Some of the NPs applications are further discussed in the following sections.

Exemplifying the above, state-of-the-art television screens have been equipped with luminescence-producing quantum dots between the light-emitting diodes (LEDs) and filters to improve colour (Luo et al., 2018). Additionally, ultralight bicycles with a frame made of carbon nanotubes have been legalised in the Tour the France race and enable the riders to achieve significantly higher speeds (Kanellos, 2006).

Due to the worldwide emerging fossil fuel crisis and the need to develop and deliver alternative energy source, electrical properties of nano-sized materials are being examined in energy harvesting or generating systems. One example is microbial fuel cells (MFCs), which are bioelectrochemical systems that harvest bacterial metabolic electrons in an anode chamber. Water (from oxygen) or other value-added products are synthesised in the cathode compartment (Logan, 2008; Oliveira et al., 2013; He et al., 2017; Santoro et al., 2017; Lovley and Nevin, 2018). Bacteria in the MFCs often use nutrients from wastewater and in such instances contribute to sustainable and renewable electric power production. It is estimated that the efficient application of MFCs in the industry could trigger the production of 600 GW of renewable power (based on the availability of cellulose biomass energy/year) (Logan and Elimelech, 2012). However, MFCs suffer from low power output due to low bacteria yield and difficulties in the electron transfer process from the bacteria to the anode (Logan et al., 2015). The introduction of nanoparticles into the system might prove beneficial. An MFC constructed with a three-dimensional graphene aerogel decorated with platinum nanoparticles on the anode surface generated a power density of 1460 mW/m^2, which is over 6 times more than with a carbon cloth electrode (Zhao et al., 2015). This aerogel electrode has a macroporous structure which enhances bacteria attachment and electron transfer. Nanoparticles enlarge the anode surface

area, providing additional space for bacteria growth in MFC or enzymes immobilisation in the biofuel cell (BFC). The latter uses purified enzymes to produce electricity. Carbon nanotubes have good electronic and electrochemical properties when used in BFCs, were shown to efficiently oxidise glucose to gluconolactone while oxygen is reduced to water by laccase in a biocatalytic reaction (Yan et al., 2006).

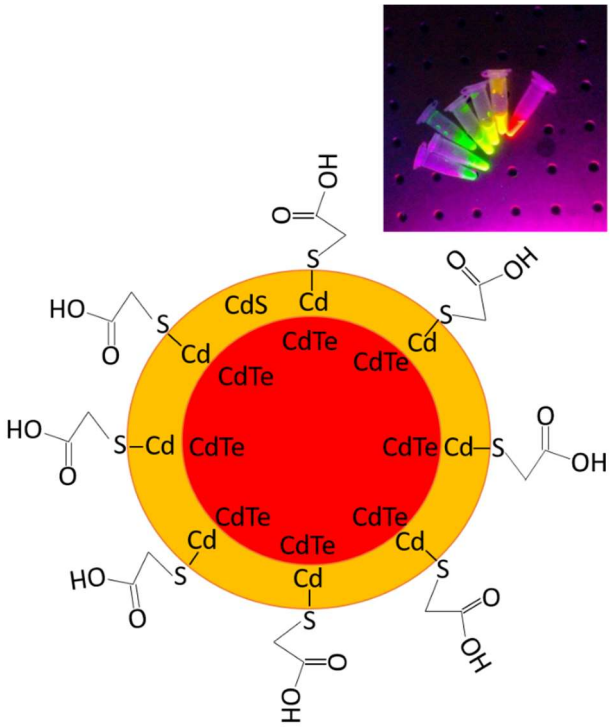

Fig.2.2. Semiconductor nanocrystals are composed of a CdTe core (red), a CdS shell (orange) and thioglycolic acid which results in a negative surface charge. The inset digital picture portrays the shift of the fluorescence wavelength upon the growth of the NPs core. The green colour emitted corresponds to a small QD's core, and red corresponds to a large core. QDs in the inset were CdTe/TGA QDs Modified from Holzinger et al (2014).

Nanosized sunlight harvesters, which aid charge transfer in electrochemical cells, have been employed in biological-inorganic hybrid systems producing simple fuel compounds (Sakimoto et al., 2016; Liu et al., 2017; Kundu and Patra, 2017). The biotic-abiotic hybrids use the naturally evolved bacteria power to produce a variety of carbon compounds. Indium phosphide QDs have been shown to support biomanufacturing work in genetically modified *Saccharomyces cerevisiae* (Guo et al., 2018). The sunlight-excited electrons from QDs took part in the regeneration of NADPH (nicotinamide adenine dinucleotide phosphate). Consequently, the synthesis of shikimic acid – the precursor for a number of medicines – was reinforced. Furthermore, the

introduction of cadmium ions and cysteine to *Moorella thermoacetica* growth media, induced bacterial self-photosensitization and encouraged solar-powered chemical production (Sakimoto et al., 2016). Not only were CdS QDs formed on the surface of *Moorella* bacteria, but these nanocrystals also collected light for a photosynthesis-like reaction, synthesising acetic acid. These nanosystems represent a novel approach to chemical synthesis driven by sunlight.

QDs surface can be altered by ligand exchange reactions (LE), which include replacement of the outermost functional groups with new ones (Sun et al., 2013) or by the chemical attachment of other molecules. After modification in such a way, QDs can work as nanosensors or the fluorescent nanoprobes (Jamieson et al., 2007; Ruedas-Rama et al., 2011; Williams et al., 2018). Carboxylic groups on the QD's surface can be coupled with the primary amines by the cross-linking method (Wang et al., 2002). These methods enable visualisation and targeted interaction of QDs with other species.

2.3. Coupling of QDs to Microbes in Solar Fuel and High-value Product Synthesis.

Plants with their astonishing sustainability and resistance to environmental changes have always amazed and inspired people, particularly scientists. Increased understanding of photosynthesis in plants, bacteria and algae has stimulated research on the design of hybrid devices that harvest sunlight for the synthesis of chemicals. Hybrid systems of non-photosynthetic bacteria and semiconductor nanoparticles (quantum dots) for sustainable CO_2 conversion through the utilisation of sun-power harvested by the QDs have been given the name artificial photosynthetic systems (Sakimoto et al., 2016). The creation of stable inorganic–biological platforms that integrate the synthetic potential of bacteria and light-harvesting abilities of semiconductor nanoparticles have generated a great deal of interest recently (Nangle et al., 2017; Kornienko et al., 2018).

A couple of crucial light-harvesting biohybrid systems have been reported in the literature. A photobioelectrochemical system has been created with the electrochemically active protein decaheme MtrC from MR-1 linked to dye-

functionalised TiO_2 nanoparticles. Photoexcited electrons from TiO_2/Ru(II)(bipyridine)$_3$ (RuP) were efficiently transferred to MtrC through a self-assembled lipid monolayer and finally to a gold electrode confirming that a redox protein can mimic the efficient charge separation found in natural photosynthesis (Hwang et al., 2015). Another group used Fe-Fe hydrogenases purified from *Clostridium acetobutylicum* that self-assembled on the surface of CdS/mercaptopropionic acid nanorods and photo-reduced protons to hydrogen; an outstanding H_2 generation quantum yield of 20% was achieved (Brown et al., 2012). Additionally, whole, non-photosynthetic bacterial cells were used to produce hydrogen and other valuable chemicals in photocatalytic reactions. Rowe et al. (2017) employed a membrane-permeable electron shuttle, methyl viologen (MV), which supported electron transfer from photoexcited water-soluble photosensitizers to MR-1 enzymes to perform H_2 evolution and for the reduction of pyruvate, fumarate and CO_2. Also, as mentioned previously, Sakimoto and colleagues (2016) added cadmium and cysteine to the growth media *of Moorella thermoacetica* that in turn, photosynthesise acetic acid. Kornienko et al. (2016) pushed the invention even further by characterising the metabolic pathways involved in the self-synthesis of CdS QDs by *M. thermoacetica* and the subsequent synthesis of acetic acid.

Electron influx into MR-1 has been recently exploited by Tefft and TerAvest for the synthesis of 2,3-butanediol from acetoin (2019). These authors genetically modified MR-1 by introducing proteorhodopsin and butanol dehydrogenase to the bacterium. When illuminated by green-emitting LEDs, proteorhodopsin acted as a photosensitiser that produced a proton-motive force, driving the reverse reaction of NADH reduction by quinol. The lipophilic quinone was reduced by an extracellular electrode via the Mtr pathway. Finally, NADH was exploited by butanediol dehydrogenase to catalyse the acetoin to butanediol reaction (Tefft and TerAvest, 2019). The production of 2,3-butanediol in modified MR-1 cells provides proof of concept that electrons can be introduced from the electrode to not only the periplasm, but also the cytoplasm of MR-1.

The concept of QD use as photosensitisers coupled with the MR-1 metabolic machinery for biohydrogen production were exploited here, and the obtained results can be found in Chapter 6.

2.4. Nanotoxicology.

Worldwide production and accumulation of NPs is increasing rapidly. Therefore, it is certain that nanoparticles are being widely released into the environment. The effects of NP release into natural habitats of bacteria, animals, and plants are not fully understood despite more than thirty years of nanotoxicology research. For instance, cadmium containing QDs are easy to synthesise and have desirable fluorescence properties; however, the pollution caused by their degradation and the release of cadmium ions into the water is sometimes out of control, accumulating in fish and aquatic microorganisms (Mueller and Nowack, 2008; Dhas et al., 2014).

Nanoparticles are characterised by several features that are significant for their toxicology. The size of QDs determines the fluorescence they emit; small nanocrystals emit at wavelengths close to the ultraviolet range, which is harmful to nearby proteins, lipids and nucleic acids (Suresh et al., 2013). Free cadmium ions released from the core trigger an increase in reactive oxygen species (ROS) production that stimulates biochemical degradation (Gomes et al., 2011). Unmodified and modified quantum dot surface properties such as ζ-potential also modify the toxicity of the nanoparticles (Derfus et al., 2004; Schneider et al., 2009). Lovrić et al. (2005) and later Pelletier et al. (2010), the more negative ζ-potential of QDs and cerium oxide nanoparticles the larger toxicity they present to the PC12 mammalian cell line and Gram-negative and positive bacteria, respectively. Both positively charged and smaller green-emitting QDs were more toxic to PC12 than larger red emitters as assessed by measuring metabolic activity of cells after the contact with QDs by colourimetric MTT assays. On the other hand, Pelletier et al. (2010) observed that Gram-negative bacteria respond to cerium oxide nanoparticles exposure differently to Gram-positive bacteria; bacterial morphology was taken into account to explain the above differences. Another critical argument in the assessment of nanoparticle toxicity is their shape. The presence of edges and

corners in the NP structure makes the structural chemicals more reactive than those in the core (Das et al., 2012).

Many techniques for NP toxicity assessment have been established. Bacterial nanotoxicology often employs counting of colony-forming units (CFU) developed by bacteria after contact with NP; this method measures the number of viable bacteria in 1 ml of the sample by spreading the sample on an agar plate followed by incubation until the countable colonies are present. A similar method, the disk diffusion test (DDT) measures the growth inhibition zone around a filter paper soaked with the tested chemical (Pelletier et al., 2010).

Molecular biochemistry assays, involving the real-time polymerase chain reaction (quantitative PCR – qPCR) monitor changes in the transcriptome induced by exposure to NPs, and provide substantial insight (Keer and Birch, 2003). The enzymatic activity of proteins in cells can be correlated to cell viability after contact with the toxin (Qiu et al., 2017). The frequently elevated ROS levels due to bacterial contact with NPs can be monitored by a colourimetric method that detects the presence of hydrogen peroxide (Foley et al., 2010; Qiu et al., 2017). Microscopy can be of use in live–dead assays, utilising fluorescence dyes that stain dead and live cells differently (Leuko et al., 2004).

Nevertheless, many viability techniques have their drawbacks. For instance, numerous enzymes, and nucleic acids might still be detected even if the host cell is dead. Also, some bacteria when present in a hostile environment can maintain their biochemical performance but not be able to divide; consequently the undividable bacteria diminish the accuracy of the CFU method (Xu et al., 1982; Zhao et al., 2017).

In conclusion, only through using a combination of techniques (CFU, live–dead fluorescence assays, qPCR, enzymatic assays and ROS level monitoring techniques) can a fuller understanding of what impact the NPs may have on living organisms be achieved. The colony-forming unit method and live–dead fluorescence assay used in this thesis, and the obtained results, are presented in Chapter 4.

2.5. Microbial Electrochemical Systems and Bionanotechnology – Summary.

Substantial development in MFC technologies has been achieved since their original inception. Currently, MFCs are employed not only in bioremediation, biosensors, and toxic metals recovery but also to generate electricity, for instance, the previously mentioned 'EcoBots' that harvest energy from insect digestion using built-in MFCs (Melhuish et al., 2006). NPs are now frequently being designed and investigated for use as anode structures providing enhanced power generation compared to standard metal electrodes (Alatraktchi et al., 2012). Nevertheless, the low power output prohibits the full industrialisation of bacterial fuel cells, and much research must be dedicated to overcoming the complications with scalability, low current production and high internal resistance. Crucially, the power output becomes lower with increasing reactor volume (Logan and Rabaey, 2012; Santoro et al., 2012); thus small versions of MFCs like prosthetic MFC-powered devices or lab-on-chip technologies are under constant investigation (Kumar et al., 2013). Also critical is the price of materials used in the MFCs; for instance, precious metals required for efficient cathode work.

On the other hand, solar fuel production has gained significant interest when living bacteria started to be utilised for photochemical production. Interfacing nature's photocatalytic machinery with synthetic materials aims to overcome the limitations of natural and artificial photosynthesis. Photosynthetic systems I and II (PS I and PS II, respectively) efficiently harvest visiblelight by the use of chlorophylls and another photosynthetic pigments like β-carotene and phycoerythrin, however, little light is absorbed in the red and infrared spectrum. The use of size-tailored CdTe QDs for visible light absorption improved the absorption in the purple bacterium *Rhodobacter sphaeroides* photosynthetic centres (Nabiev et al., 2010). The limitations of the Nabiev system are the costly protein purification and nanoparticle syntheses followed by the limited longevity of the system (McCormick et al., 2015; Kornienko et al., 2018). Consequently, modification of extracellular electron transfer in exoelectrogens such as MR-1, as described in detail in section 1.1.2, was

used for intracellular CdSe QD synthesis, which might be of use in light-harvesting systems that synthesise valued chemicals (Tian et al., 2017).

3. Thesis Aims.

Inorganic–biological hybrid systems have the potential to be sustainable and versatile chemical platforms through integrating the synthetic potential of bacteria and light-harvesting abilities of semiconductor nanoparticles (Nocera, 2017; Kornienko et al., 2018).

The work described here endeavoured undertake the construction of a biohybrid system for the production of hydrogen. For this purpose, the interactions between a model bacterium capable of hydrogen evolution - *S. oneidensis* MR-1 - and photosensitisers was selected for study. A range of photosensitisers semiconductor nanoparticles QDs with different physicochemical features were chosen and examined.

Firstly, a set of QDs, including negatively charged CdTe/CdS/TGA, zwitterionic $CuInS_2$/ZnS/PMAL, positively charged CdTe/CdS/Cysteamine and finally commercial negatively charged CdTe QDs were synthesised or purchased. The QDs absorbance, photoluminescence, the surface ζ potential and the hydrodynamic size will be described.

Subsequently, the nanotoxicity of these QDs towards MR-1 and a control bacterium, *E.coli,* using a colony-forming units method will be evaluated and QDs that showed mild toxicity, were further tested with viability assays.

The interaction of the QDs with MR-1 by epifluorescence and transmission electron microscopy will be described. Bacteria grown anaerobically and aerobically can be used to study if outer membrane protein compositions affects the interaction pattern with QDs.

Finally, hydrogen production supported by photosensitisers of selected species of *Shewanellaceae* genus, including *Shewanella oneidensis* MR-1, *Shewanella spp. strain* MR-4, *Shewanella putrefaciens* CN-32 will be described as well as the selection of sacrificial electron donors.

Chapter 4. Materials and methods.

4.1. Materials used.

Unless otherwise stated all the materials were purchased from Sigma-Aldrich or Fisher Scientific (UK). All chemicals were used as received. Analytical grade reagents were prepared using MiliQ^{TM} water (resistivity 18.2 MΩ·cm, Millipore). “Commercial” CdTe QDs were purchased from PlasmaChem GmbH (Rudower Chaussee 29, D-12489 Berlin, Germany). Propidium iodide (PI) was obtained from Thermo Fisher. Malvern Zeta Sizer-Nano Series- Zen 3600 was used for the ζ potential and hydrodynamic size measurements. Electronic absorbance and photoluminescence spectra were recorded on a Perkin−Elmer Model Lambda35 and Perkin−Elmer Model LS55 spectrometer, respectively.

Ultrafiltration columns (Centrisart I, with a molecular weight cut off 20,000 kDa) used in the filtration of $CuInS_2$/ZnS QDs encapsulated in PMAL-d from free-floating polymer were purchased from Sartorius AG, company.

4.2. Statistical analysis

Values are expressed as mean ± standard deviation (SD). Paired and unpaired two-tailed Student’s t-tests and ANOVA were performed using GraphPad Prism v6 (GraphPad Software, USA). Significance was defined as $p \leq 0.05$, 0.01, 0.001 and graphically presented as one, two or three stars, respectively.

4.3. Bacteria strains and their growth conditions.

Shewanella oneidensis MR-1 (ATCC 700550 MR-1), *spp*. strain MR-4 (MR-4), *putrefaciens* CN-32 (ATCC BAA-453, CN-32) and LS 473 were a kind gift from Prof. Julea N. Butt from the University of East Anglia in Norwich. The Omnimax *Escherichia coli* (*E. coli*) strain was a kind gift from Prof. Stephen Baldwin from the University of Leeds. Corresponding names in brackets will be used onwards.

Bacterial strains were stored at -80 ˚C in 25 % glycerol, 25 % distilled water, 50 % Luria Bertani medium. Aliquots of the frozen strains were streaked on to

LB-agar plates and incubated for ~24-48 hr at 30 °C or 37 °C for *Shewanellaceae,* and *E. coli* strains, respectively. Single colonies were used to inoculate typically 10 ml of a chosen medium which was then shaken aerobically at 200 RPM for ~20 hr.

4.3.1. Bacterial media used

Luria-Bertani media often referred to as a rich media or LB-media, contained: yeast extract 10 g/l, tryptone 5 g/l, sodium chloride 10 g/l dissolved in MilliQ water. The solid plate media (referred to as LB-agar) contained all the ingredients used for LB-media formulation, with the additional 15 g/l of agar. All rich bacterial media underwent autoclaving at a temperature of 121 ºC for 20 minutes. All other buffers used in the experiments were autoclaved in the described conditions unless otherwise stated.

Minimal Media were filter sterilised through a 0.22 µm pore size filter containing mixed cellulose ester membranes. Two different minimal media were used for different species of bacteria. M9 minimal media**,** used for *E. coli* growth, contained: 6 g/L Na_2HPO_4, 3 g/L KH_2PO_4, 1 g/l NH_4Cl, 0.5 g/l NaCl, 3 mg/l $CaCl_2$ and 120 mg/l $MgSO_4$, 20 % (w/v) of D-glucose, 40 µg/ml of L-leucine and 40 µg/ml L-threonine. Modified M1 media (abbreviated as M1), used for MR-1 and CN-32, contained: 28 mM NH_4Cl, 1.34 mM KCl, 4.4 mM Na_2HPO_4, 1.5 mM Na_2SO_4, 0.7 mM $CaCl_2$, 1 mM $MgCl_2$, 5 mM PIPES (piperazine-N, N′-bis(2-ethanesulfonic acid)), pH 7.4. A 100 times concentrated vitamin mixture (1 l of vitamin medium contains 0.08 µM (0.02 mg) biotin, 0.045 µM (0.02 mg) folic acid, 0.5 µM (0.1 mg) pyridoxine hydrochloride, 0.15 µM (0.05 mg) thiamine hydrochloride, 0.13 µM (0.05 mg) riboflavin, 0.4 µM (0.05 mg) nicotinic acid, 0.2 µM (0.05 mg) DL-pantothenic acid, 0.3 µM (0.05 mg) p-aminobenzoic acid, 0.2 µM (0.05 mg) lipoic acid, 14.3 µM (2 mg) choline chloride, 7 nM (0.01 mg) vitamin B_{12} (cobalamin)), and a hundred times concentrated trace elements mixture (1 l of trace elements medium contains 5 µM (10 mg) of $FeCl_2 \cdot 4H_2O$, 25 µM (5 mg) of $MnCl_2 \cdot 4H_2O$, 14.4 µM (3 mg) of $CoCl_2 \cdot 4H_2O$, 14.6 µM (2 mg) of $ZnCl_2$, 1.8 µM (0.5 mg) of $Na_2MoO_4 \cdot 4H_2O$, 3.2 µM (0.2 mg) of H_3BO_3, 3.8 µM (1 mg) of $NiSO_4 \cdot 6H_2O$, 15.8 µM (0.02 mg) of $CuCl_2 \cdot 2H_2O$, 40 µM (0.06 mg) $Na_2SeO_3 \cdot 5H_2O$, 71 µM

(0.08 mg) $Na_2WO_4 \cdot 2H_2O$) were added to the M1 medium (Myers & Nealson, 1988). As a carbon sources 50 mM sodium D, L-lactate was used for MR-1 and other *Shewanellaceae*.

For the incubation of MR-1 with QDs after ligand exchange experiments, the M1 without trace elements and vitamins were used. The altered M-1 medium contained 28 mM NH_4Cl, 1.34 mM KCl, 4.4 mM Na_2HPO_4, 1.5 mM Na_2SO_4, 0.7 mM $CaCl_2$, 1 mM $MgCl_2$, 5 mM PIPES, pH 7.4.

4.4. Bacterial Viability Assays

4.4.1. Colony-forming unit viability assays (CFU assay).

CFU assays were used to determine the number of viable bacterial cells present in the medium. One colony in the colony-forming units test is assumed to be generated by a single live bacterium.

Bacteria were grown in sterile 50 ml Falcon tubes. The large volume of test tubes aimed to achieve good aeration of samples. After MR-1 entered the mid-logarithmic growth phase (as assessed by the light dispersion of a sample recorded by optical density at the wavelength of 600 nm (OD_{600}), experimental samples were created by the addition of different concentrations of QDs.

Quantum dots at three or two concentrations were mixed with MR-1 or *E. coli* in the test tubes. Kanamycin (50 µg/ml – working concentration) and 20 mM HEPES, 0.15 M sodium chloride, pH 7.4 (saline) were used as positive (PC) and negative controls (NC), respectively. Subsequently, samples were put into the bacterial incubator with shaking velocity of 200 RPM, for 3 or 20 hours, at a temperature of 30 °C or 37 °C for MR-1 or *E. coli*, respectively. The viability experiments times and temperature depended on the tested QDs and microorganisms. After incubation, a serial dilution technique was used to determine the CFU. A cartoon with the principle of the technique is presented in Fig. 3.4.1. Dilution steps are repeated until bacteria are diluted enough to give “countable” colonies when plated on the LB - agar plates; these plates were put into the plate incubator, at a temperature of 30 °C for about 48 hours for MR-1 or 37 °C for ~20 h for *E. coli*. Bacterial colonies were counted manually. The number of counted colonies was corrected for the dilution used,

and the results are expressed in colony-forming units per 1 ml of solution (CFU/ml).

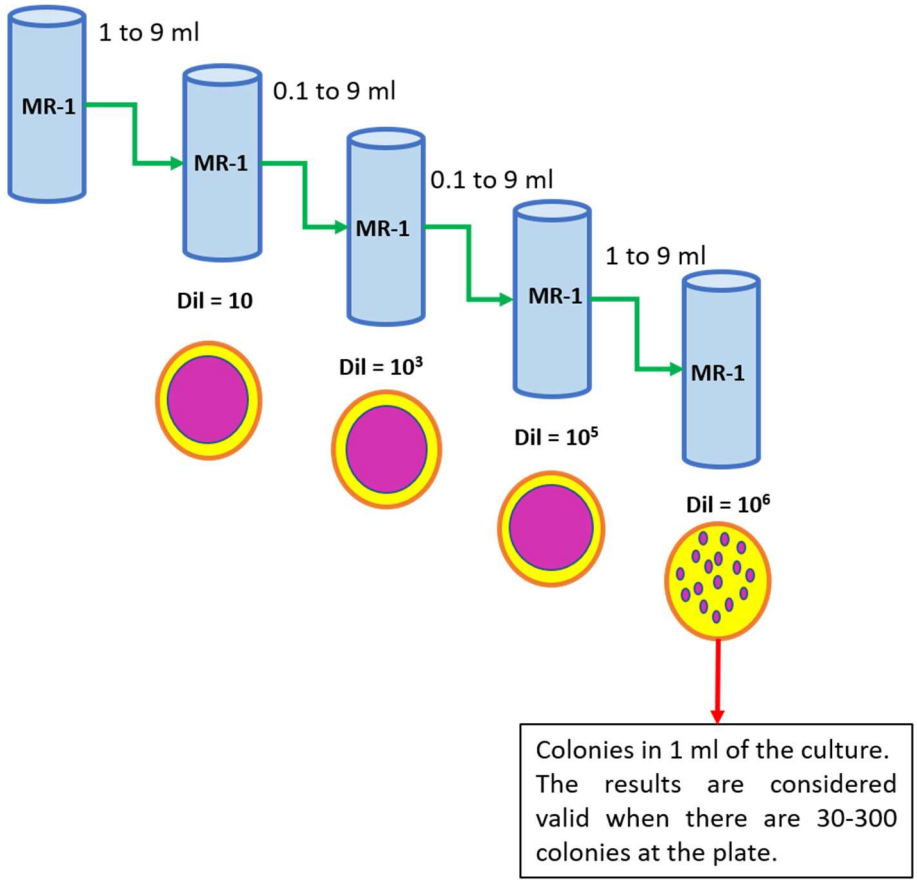

Fig.4.4.1. Assessing nanoparticle toxicity to bacteria by the serial dilution method. Each vial contains the separate culture of the same species of bacteria. From the first vial, the small volume of the sample is transferred to the fresh medium. The steps are repeated until bacteria are diluted enough to give the countable colonies when plated and grown on the agar plates. Cartoon redrawn from Rice et al (2015).

4.4.2. Fluorescence bacterial viability assay

Bacteria were grown as described in Section 4.4.1 until OD_{600} reached 0.4. A 60 μM stock solution of propidium iodide (PI, a red fluorescence nucleic acid intercalating stain that only stains cells with impaired membranes, Fig. 3.4.2.1) was used as received from the manufacturer - ThermoFisher and stored at -20 °C until use. PI is excited by light of the wavelength 535 nm that result with the broad peak of photoluminescence between 550-700 nm with the maximum at 617 nm. The PI stock solution was mixed with bacteria in 1:1 [volume:volume] ratio and incubated for 15 min. Afterwards, the sample of bacteria was placed on poly-L-lysine coated glass slides for 15 min at 20 °C.

Unbound bacteria were washed away using a 20 mM HEPES, 0.15 M NaCl solution, pH 7.4. The slides were analysed with an epi-fluorescent microscope using both bright light and fluorescence using filters 560/40 (excitation), 595 (dichroic mirror), 630/60 (emission). Stained and unstained bacteria were counted manually. Poly-L-lysine (MW≤30000 g/mol) covered glass slides were prepared by 20 min incubation of glass slides with 100 µg/ml water solution of poly-L-lysine at 20°C. The unbound polymer was washed away with 20 mM HEPES, 0.15 M NaCl, pH 7.4.

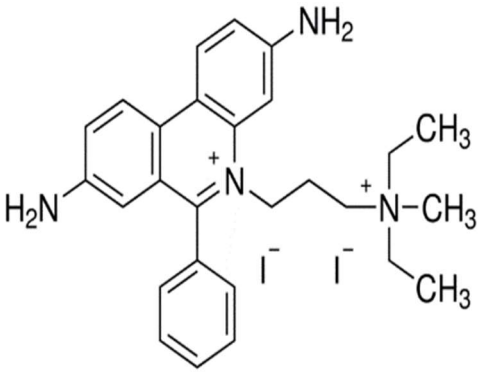

Fig. 4.4.2.1. Molecular structure of phenanthridinium, 3,8-diamino-5-[3-(diethylmethylammonio) propyl]-6-phenyl-, diiodide which is widely known as propidium iodide - PI.

4.5. Nanoparticle syntheses.

4.5.1. CdTe/CdS Quantum Dots Syntheses.

CdTe core was synthesised according to a procedure by N. Gaponik et al. (2002). In a typical synthesis 0.985 g (2.35 mmol) of$Cd(ClO_4)_2$ $6H_2O$ is dissolved in 125 mL of water, and 5.7 mmol of the thiol stabilizer (see Table 4.5.1 for details) are added under stirring, followed by adjusting the pH to the appropriate values by 10 µl dropwise addition of 1 M solution of NaOH. The solution is placed in a three-necked flask fitted with a septum and valves and is deaerated by N_2 bubbling for ~30 min. Under stirring, H_2Te gas (generated by the reaction of 0.2 g (0.46 mmol) of solid Al_2Te_3 with 15-20 ml of 0.5 M H_2SO_4 under N_2 atmosphere) is passed through the solution together with a slow nitrogen flow for ~15 min. CdTe precursors are formed at this stage which is accompanied by a change of the solution color, depending on the thiols used, to dark red (2-mercapto- ethylamine) or orange (2-mercaptoacetic

acid). The precursors are converted to CdTe nanocrystals by refluxing the reaction mixture at 100 °C under open-air conditions with condenser attached.

To reduce CdTe QDs nanotoxicity and to elevate their photoluminescence, 2.35 mmol (178.9 mg) of thiourea puriss in 2 ml of water was added to freshly synthesised CdTe core and incubated for an hour in boiling conditions (Green et al., 2009). After the shell was built, QDs were cooled by immersion of the reaction vessel into cold water until the temperature of the solution was around 25 °C. The solution was stored in the reaction vessel at 4 °C in the dark.

Before further experiments, CdTe QDs were cleansed by triple precipitation by propan–2-ol (volume ratio of QDs to alcohol was 1:3) and centrifuged at the speed of 10000×g for 5 minutes. Supernatants were discarded and pellets resuspended in the appropriate buffer. Thioglycolic acid capped CdTe/CdS QDs were dissolved in 20 mM HEPES, pH 7.4, and 20 mM MES, pH 5.6 was used for CdTe/CdS/Cysteamine QDs.

Synth. Con. / QD Type	Capping agent	pH	λ_{PL} [nm]	Surface charge (pH=7)	t [min]	Stability
CdTe/CdS/TGA	2-mercaptoacetic acid	11.2-11.8	550	Negative	45-60	Stable
CdTe/CdS/Cysteamine	2-Aminoethane-1-thiol	5.6-5.9	580-600	Positive	60-80	Moderate

Table 4.5.1. The reagents and the reaction conditions of the CdTe quantum dots syntheses. Thioglycolic acid (TGA) capped CdTe/CdS QDs were synthesised in the ultra-clean water of pH between 11.2-11.8, and standard photoluminescence maxima peaks were at the wavelength 550 nm. The post-synthesis product had a negative surface charge and was stable for months. In contrary, cysteamine capped CdTe/CdS QDs were synthesised in the pH 5.6-5.9 solution, produced positively charged QDs of photoluminescence maxima at 580-600 nm. CdTe/CdS/Cysteamine QDs were moderately stable. Abbreviations used: TGA – thioglycolic acid, λ_{PL} – photoluminescence maximum, min – minute, Synth. – Synthesis, Con. – Conditions.

4.5.2. Ligand Exchange Experiments.

The ligands used in the ligand exchange (LE) experiments discussed here included cysteine - Cys and lipoic acid derivative of dipicolylamine - LADPA. While Cys aimed to allow pH dependant charge to be present on the QD's surface, LADPA was used as a molecule that specifically binds to Gram-negative bacteria (Ngo et al., 2012).

Before LE, the TGA stabilised CdTe/CdS QDs were subjected to an additional purification procedure that included precipitation of QD with propan-2-ol -

propanol (see section 4.5.1.) and further solvent exchange to the buffer solution of choice. Buffers used for Cys or LADPA LE were citric acid pH 3 and 50 mM HEPES pH 8.5, respectively. A 200 molar excess of the ligand was added to the LE reaction mixtures containing CdTe/CdS/TGA QDs. To remove oxygen, which might be disadvantageous to the LE reaction, reaction tubes were prepared and then sealed with rubber septa in a MBraun glove box (< 1 ppm O_2). To monitor reaction progress, vials were monitored with spectrofluorimeter (excitation 400 nm and the photoluminescence spectra were recorded every 5 minutes at the range of wavelengths 450 nm – 750 nm). More details on LE optimisation are discussed in the results Sections 5.3.1 and 5.3.2.

4.5.3. Crosslinking of Commercial Negatively Charged CdTe QDs with Amine Derivative of Dipicolylamine.

An amine derivative of dipicolylamine (abbreviated as ADPA) was dissolved in water (0.35 mM) and cross-linked to commercial QDs (7.2 μM) resuspended in phosphate buffer saline (PBS, pH 7). 50 μM 1-ethyl-3-(3-dimethylaminopropyl) carbodiimide (EDC) and 5 mM 3-sulfo-succinimidyl benzoate sodium salt (sulfo-NHS) were used as crosslinking agents. The crosslinking reactions were kept in the dark for 3 hours, with no shaking. Different molar ratios of QD to ADPA were tested and included 1, 10, 100, 200 of the ADPA molar excess. Biologically relevant metals such as Na^+,K^+ are discriminated when binding to picolylamines. Only zinc binds to a tridentate ligand with three nitrogen donors that afford good selectivity for Zn^{2+} and leaves coordination sites free for anion binding (Ngo et al., 2012). After modification of the QDs, $ZnSO_4$ was injected into the samples, and the concentration range tested was from 1 μM to 10 mM. The reaction progress was monitored by spectrofluorimeter and epifluorescence microscopy. Photoluminescence spectra of commercial QDs were taken before and after the cross-linking and with or without zinc ions. The commercial CdTe QDs were excited at 400 nm, and the PL was recorded at a wavelength range from 450 nm to 650 nm. The results of crosslinking are presented in Section 5.4.4.

4.5.4. Copper Indium Sulfide with Zinc Sulfide Shell Quantum Dots Synthesis

The $CuInS_2/ZnS$ (abbreviated as CIS) quantum dots were synthesised as described by Booth et al. (2012).

Briefly, a three-neck glass flask was placed in the fume hood and purged with argon for 30 minutes. 0.25 mmol (47.5 mg) copper(I) iodide, and 0.25 mmol (73 mg) of indium(III) acetatewere placed in the flask and degassed for 20 min with argon. Subsequently, 4 ml of 1-dodecanethiol (DDT) was added to the reaction flask. In CIS synthesis, DDT served as a stabilising agent, solvent and sulfur donor. The transparent yellow reaction mixture was vigorously stirred, and the temperature was rapidly raised from 25 °C to 100 – 150 °C and the colour became orange. Upon further heating to 220 °C, the colour became red to very dark red after which the reaction was quenched by immersing the flask (still connected to argon flow) in the water bath (t=20 °C). The next step focused on the synthesis of the shell: 0.2 mmol of zinc stearate, dissolved in 4 ml of octadecene, was added to the previously synthesized QDs. The temperature was again raised to 180 °C with stirring for a further one hour. After the reaction was accomplished, the $CuInS_2/ZnS$ QDs were removed from the flask with the Pasteur pipette, and slightly diluted with chloroform to encourage stable colloidal suspension. Before the use in further experiments, CIS QDs were washed to remove any unbound solvents. The washing procedure included mixing of QDs with a the mixture of chloroform, methanol and acetone (1: 1: 10 volume ratio) followed by centrifugation at 4000 RPM for 5 min at 20 °C was used to wash freshly synthesised CIS QDs. The washing procedure was repeated at least three times, and supernatants were discarded while pellets were suspended in chloroform. The synthesised QDs were kept in the dark at 4 °C.

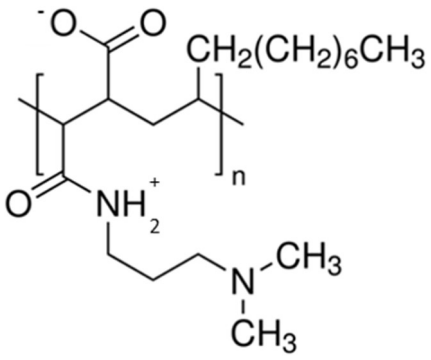

Fig.4.5.4.1. Structure of poly(maleic anhydride-alt-1-tetradecene), 3-(dimethylamino)-1-propylamine derivative (PMAL-d).

Before use in biological experiments, the hydrophobic CIS QDs were encapsulated in zwitterionic polymer PMAL-d (Fig. 4.5.4.1.). 10 mg/ml of PMAL-d in chloroform was mixed with CIS QDs in a 20 or 25 to 1 molar ratio of polymer to QD. The resulting mixture was vigorously stirred for 2 hours, and left overnight in a desiccator under vacuum, in the dark, at 20°C for the chloroform to evaporate. The following day, the dried CIS/PMAL sample was mixed with Milli-Q water, and the pH was adjusted by the drop-wise addition of NaOH until pH = 10. The PMAL-d coated QDs were filtered (pore size 0.2 mm) to remove large agglomerates. The free polymer was removed by four cycles of dilution each followed by ultrafiltration using Centrisart I at 4000×g for 30 min, 4 °C (cut off 20 kDa supplied by Generon) centrifuge tubes. As prepared CIS/PMAL QDs were further used in the experiments.

4.5.5. Gold Nanowires Synthesis.

Prior to AuNWs synthesis, all glassware was carefully cleaned in aqua regia. CAUTION: Aqua Regia is a corrosive solution of 3 parts of hydrochloric acid and 1 part of nitric acid. The procedure of gold nanowires synthesis (AuNW) was published before (Feng et al., 2009). Glass tubes were filled with 3 mg (7.6 µmol) of hydrogen tetrachloroaurate(III) trihydrate ($HAuCl_4 \cdot 3H_2O$, M_W = 292.88 g/mol), also known as chloroauric acid, 2.5 ml of hexane and 100 µl oleyamine (OA, M_W = 267.5 g/mol). OA was used here as a source of sulfur, stabiliser and one-dimensional growth template. The solution mentioned above had a bright yellow colour. Next, 150 µl of the reducing agent, triisopropylsilane (TIPS, M_W = 158.4 g/mol), was added to the mixture that was kept at 30 °C for 4-5 hours. After that time, the solution became very dark red

and was stable for months. The AuNWs was desiccated under vacuum until no solvent was present.

4.5.5.1. Polydopamine Functionalisation of Gold Nanowires.

The two separate approaches of making AuNWs dispersible in aqueous solvents included use of polydopamine (PDA) and diethylene glycol aminothiol (Hasan et al., 2002; Lee et al., 2007).

Before nanowires functionalisation, 2 ml of Au-NWs (C_{Au} = 2.9 μM) in an organic solvent (hexane) was evaporated overnight in a desiccator. Dried Au-NWs were subsequently immersed in a 2 mg/ml solution of dopamine in 10 mM TRIS pH 8.5. The sample was placed on the roller for 2 hours, during which the solution obtained a dark brown appearance. The reaction was stopped by five sequential centrifugations for 5 minutes at the speed of 10000 RPM. The supernatants were discarded, and the resulting product was resuspended in water. The centrifugation aimed to discontinue the polymerisation of dopamine and remove unreacted species. PDA functionalised AuNWs were further investigated by UV-Vis spectroscopy and transmission electron microscopy. These results are discussed in Chapter 5.7.1.

4.5.5.2. Diethylene Glycol Aminothiol Transfer Au-NWs into Aqueous Solution.

Diethylene glycol aminothiol was a kind gift received from Dr James Murray, Department of Chemistry, the University of Leeds, and will be referred to as DEGAT (molecular structure of DEGAT is presented in Fig. 4.5.5.2.). DEGAT was received as a powder and is a polar zwitterionic molecule that contains one of each: thiol and amine groups. The thiol group is connected by the long chain of alkyls (9 carbons) with two glycol groups, and at the end is the ethylamine. DEGAT is readily dispersible in the polar organic solvents. The solvents investigated here included ethanol, methanol and chloroform.

The ligand exchange experiment involved the use of a two-phase liquid–liquid system, as described previously by Brust and Walker (Brust et al., 1994; Hostetler et al., 1999). Preparation of Au-NWs dissolved in hexanol for LE purpose is described in the section 4.5.5. The dried Au-NWs were dispersed

in hexanol and DEGAT was added in the tested solvent (i.e. ethanol, methanol or chloroform). Different molar ratios of Au atoms in Au-NW to DEGAT were tested (1:1, 1:1.5, 1:2, 2:1). The samples were mixed by vortexing for 30 - 60 min, until the well-dispersed mixtures of solvents was observed. Samples in the organic solvents were mixed with phosphate buffer saline (PBS, pH 7.4) and a suspension was created by energetical vortexing for 15-30 min. The samples were further incubated overnight with shaking at 200 RPM. After that, the trials were centrifuged for 90 min, at 17000×g, and the coloured top layer (aqueous phase) was loaded to an Eppendorf tube by the glass pipette. Overnight desiccation of the sample aimed at the total withdrawal of organic solvents that might remain in the aqueous phase. Electronic absorbance spectroscopy and transmission electron microscopy (TEM) results of DEGAT functionalised Au-NWs are outlined in Chapter 5.7.2.

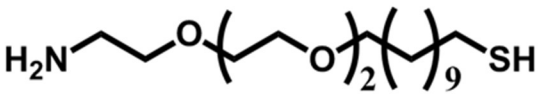

Fig. 4.5.5.2. The molecular structure of diethylene glycol aminothiol.

4.6. Interaction of Bacteria with Quantum Dots - Microscopic Investigation.

4.6.1 Epifluorescence Microscopy

MR-1 were grown in M-1 as described in Section 3.4.1. After the desired optical density was obtained, 2 ml of the bacteria were harvested by 10 min centrifugation at 8000 RPM. Supernatants were discharged and pellets resuspended in 5 ml of 0.15 M NaCl, 20 mM HEPES, pH 7.4 in a 15 ml vials and mixed with given concentrations of QDs and incubated at 30 °C with 200 RPM shaking. The negatively charged custom-made and commercial CdTe QDs incubated with MR-1 and CN-32 were incubated 16 h, 200 RPM shaking.

CdTe/CdS/Cysteamine QDs were incubated with MR-1 for 1, 3, or 18 h. CIS/PMAL QDs were incubated with MR-1 for 3 or 18 h, 200 RPM shaking.

For CIS/PMAL, also longer times (18 h) and incubation under anaerobic conditions were tested (for anaerobic growth details, please, see section 3.6). The MR-1/QD mixtures were washed by centrifuging 3 times for 10 min at 8000×g in an Eppendorf tube centrifuge and resuspended with the plastic Pasteur pipette in 2 ml of 0.15 M NaCl, 20 mM HEPES, pH 7.4. A small volume of the samples (5-10 µl) was placed on glass slides treated with poly-L-lysine (see Chapter 3.5.2 for more details). Lastly, the samples were covered with the glass cover slides and were rested for 10 min. Fluorescence and bright field microscopy were performed on an Inverted Epifluorescent Microscope (Nikon Eclipse Ti-U), and images were analysed with NIS elements software. Table 3.6.1 describes all the filter settings used for visualisation of MR-1 interaction with QDs.

QD / Filters	Excitation	Dichroic Mirror	Emission
CdTe/CdS/TGA	410 ± 15 nm	500 nm	580 ± 25 nm
Commercial CdTe	410 ± 15 nm	500 nm	535 ± 24 nm
CdTe/CdS/Cysteamine	410 ± 15 nm	500 nm	580 ± 25 nm
CIS/PMAL	335 ± 20 nm	500 nm	650 ± 37.5 nm
Propidium Iodide	560 ± 27.5 nm	595 nm	650 ± 37.5 nm

Table .4.6.1. The filters settings used to visualise the interaction of QDs with MR-1.

4.6.1.1. Heat Shock of *S. oneidensis* MR-1 with 0.5 µM CdTe/CdS/TGA QDs.

To encourage uptake or binding of CdTe/CdS/TGA QD by MR-1 heat shock procedures, commonly employed for DNA uptake, were attempted.

MR-1 was grown as described in Section 4.4.1. CdTe/CdS/TGA QDs were added to give the final concentration of 0.5 µM and incubated for 30 minutes on ice. Samples were subjected to a heat shock for either 30 or 60 seconds

at 42 °C and subsequently cooled down on the ice for 2 minutes. MR-1 was harvested and washed by centrifugation at 5000 RPM for 10 min three times to remove any unbound QD. Next, 10 µl of each sample was put on poly-lysine covered glass slides and examined with epi-fluorescent microscopy, as described above. The results obtained are discussed in Chapter 6.

4.6.2. Transmission Electron microscopy – TEM.

4.6.2.1. TEM of Gold Nanowires.

Gold nanowires were synthesised as discussed in section 4.5.5. Although as prepared Au-NWs are stable in hexane, they need to undergo ligand exchange procedure to make them resuspend in aqueous solvents and biocompatible. The results of the two LE procedures are discussed in Chapter 4. Described here is only the TEM procedure to visualise AuNWs.

Before TEM procedure was executed, AuNWs were thoroughly washed by 3 successive centrifugations (10000 RPM for 10-90 min) and resuspended in either hexanol (for untreated AuNWs), or phosphate buffer saline for DEGAT and DPA modified AuNW. Single drops of AuNWs solution was placed on a carbon-coated 400 mesh copper grids (Agar Scientific) that were glow discharged to be made hydrophilic, and the solvent was evaporated. Subsequently, the AuNWs deposited on the grids were visualised by TEM (JEOL 1400, tungsten filament and Gatan UltraScan 1000 XP CCD camera). The results of these investigations are presented in Chapters 5.7.1 and 5.7.2.

4.6.2.2. Electron Microscopy of *Shewanella oneidensis* MR-1 Incubated with 5 µM Commercial CdTe Quantum Dots.

For transmission electron microscopy experiments, MR-1 after the 18 h incubation with either 5 µM of commercial CdTe QDs (as described in Section 4.5.1), or an equal volume of 20 mM HEPES, 0.15 M NaCl, was harvested by centrifugation 5000 RPM, 10 min, and fixed by 2.5 % glutaraldehyde in 0.1 M phosphate buffer for 2.5 hours. The fixed MR-1 samples were washed twice for 30 minutes each change with 0.1 M phosphate buffer pH 7.2. Further, the fixed samples were dehydrated using an ascending alcohol series: 20 %, 40 %, 60 %, 80 %, 2x100 % for 20 minutes. The embedding in resin was performed by the two exchanges into propylene oxide 20 minutes each

change, followed by transfer to embedding moulds in fresh 100 % agar for overnight incubation with shaking at temperature 60 °C. An ultramicrotome was employed to obtain the thin sections of the samples. The transmission electron microscope (JOEL-1400) was used to examine prepared sections.

4.7. Light-driven H_2 Evolution by *Shewanellaceae* with Quantum Dots as Photosensitisers (in the absence of methyl viologen).

4.7.1. Selection of Sacrificial Electron Donors for Methyl Viologen Photoreduction by Quantum Dots

Methyl viologen assays were performed inside an N_2-filled chamber (glovebox, MBraun) at < 1 ppm O_2. Buffers and QD solutions were purged with nitrogen for at least 1.5 hours before transferring them into the glovebox. A KL5125 Cold 150 W light source with high-quality UV filter quartz glass (Krüss) fitted with a 150 W (15 V) halogen lamp (Osram) was used in all experiments unless otherwise stated. Non-irradiated samples (controls) were kept in the same conditions as specified below but were covered in dark cloth. The volume of samples was 1 ml. Reagents were suspended in 50 mM HEPES and 50 mM NaCl, pH 7, unless otherwise stated (e.g., when MES buffer was used as sacrificial electron donor - SED).

4.7.2. H_2 Evolution by *Shewanellaceae* with Quantum Dots as Photosensitisers.

In these experiments, four strains of *Shewanellaceae* were investigated: MR-1, *Shewanella spp.* strain MR-4 (MR-4), CN-32 and LS473. LS473 is a double knock-out strain of MR-1 (Δ*hydA, hyaB*) missing the hydrogenases. Bacterial strains were handled as in section 4.3. The resultant cultures were used to inoculate (2 % (v/v)) 10 ml M72 medium (comprised of 15 g/l casein digest peptone, 5 g/l papaic digest of soybean meal, 5 g/l NaCl, pH 7.8) with 37.5 mM sodium D,L-lactate (electron donor), 18.8 mM sodium fumarate (electron acceptor), 1.88 mM $NiCl_2$ and 37.5 mM HEPES in glass Hungate tubes (17 ml total volume). The tubes were sealed, the headspaces (7 ml) were purged

with N_2 for 5 min, and the cultures were incubated without shaking at 30 °C for 24 hr to induce expression of hydrogenase (except for LS473). Headspace H_2 was quantified after 24 hr using gas chromatography to confirm expression of hydrogenase.

After quantifying headspace H_2, Hungate tubes were taken into a glovebox and the culture transferred to Eppendorf tubes. The tubes were removed from the chamber and bacteria were harvested by centrifugation (5 min, 13000 RPM, 5 °C). The tubes were then returned to the glovebox, the supernatants were removed, and the cell pellets were gently re-suspended in anaerobic 50 mM HEPES, 50 mM NaCl, pH 7 buffer. Suspensions were centrifuged as before, and the cell pellets returned to Glovebox were gently re-suspended to OD_{590nm} ≈0.25 in anaerobic 50 mM HEPES, 50 mM NaCl, pH 7 in the presence of a given concentration of QDs and a sacrificial electron donor (SED). Samples containing QDs CdTe/CdS/TGA or commercial negatively charged CdTe were supplemented with 50 mM TEOA as SED. CIS/PMAL QDs photoreduction was supported with 50 mM EDTA. Experimental solutions were then transferred to clear, colourless glass vials with PTFA/silicon septum caps and incubated for a further 24 hr at 25 °C with or without irradiation from a photosynthetic growth lamp (power = 0.02 kW m^{-2}). After this time, headspace H_2 was quantified using gas chromatography. LS473 was used as a negative control of the experiments.

Chapter 5. Characterisation of Nanoparticles.

5.1. Nanoparticles – From Fundamentals to Some Applications.

One of the most prominent advantages of nanoscale materials (over, for instance, macroscopic electrode materials) is their high surface-to-volume ratio. The amplified interface of nanoparticles triggers an increase in their interaction with biological, chemical and physical environments (Sakimoto et al., 2018). Carbon nanotubes, a variety of gold nanostructures and fluorescent semiconductor NPs, known as quantum dots, are prime examples of nanoparticles (Daniel and Astruc, 2004; Batista et al., 2015). Multiple semiconductor QD systems have been utilised as promising photosensitisers for harvesting solar energy (Nabiev et al., 2010; Kundu and Patra, 2017).

Quantum dots are semiconductor nanoparticles that when irradiated produce fluorescence (Reiss et al., 2009). The colour of the emitted light depends on the size of the QD and thus can be tuned depending on the requirements. The smaller the QDs, the higher the energy of the fluorescence they emit; therefore, the emitted light shifts from blue to red with increasing QD size. A wide fluorescence excitation spectrum, narrow emission, ease of synthesis and resistance to photobleaching makes QDs valuable fluorescent probes that are beneficial over organic dyes (e.g., Cy2, 3 or 5, DAPI) (Uyeda and Dot, 2005).

Structurally, QDs consist of two elements: the core and the shell (Loukanov et al., 2004). The core of QDs is formulated by the semiconductor elements that with the diminished size start to experience quantum confinement effects that alter their physical and chemical features that differ from the bulk material. Quantum confinement effects are observed when the size is sufficiently small that the energy level spacing of a nanocrystal exceeds kT (where k is Boltzmann's constant and T is temperature) (Bera et al., 2010). The shell, on the other hand, enhances the fluorescence intensity by decreasing the number of exciton recombination events via non-radiative pathways; in this way, the quantum yield, brightness, photo-stability, and resistance to photobleaching is enhanced (Derfus et al., 2004). Photo-oxidative

degradation and release of toxic heavy metals from the QD core are also mitigated by the introduction of the shell (Yong et al., 2013).

The surface chemistry determines the interaction of QDs with other species (Medintz et al., 2005). Many QD synthesis routes produce dots with a hydrophobic, and thus non-biocompatible, surface. The introduction of specific chemical compounds such as zwitterionic polymers, amino acids, antibodies, proteins or chemicals that precisely bind to the desired components alter the QD surface (Ngo et al., 2012; Booth et al., 2013; Holzinger et al., 2014). QD surface functionalisation by carbodiimide chemistry is frequently used to reinforce the specific binding to other chemicals (Ruedas-Rama et al., 2011). Overall, the chemical elements introduced by ligand exchange (LE) processes – the modification of the outer-most layer of QDs or encapsulation of QDs in the polymers – impact the nanotoxicology of the QDs.

The high surface-to-volume ratio of nanoparticles is frequently exploited in MFCs that suffer from low power output due to truncated electron transfer on the microbe–anode interface (Logan et al., 2015). The introduction of biotic or abiotic nanoparticles enhances electron flow by increasing the electrode surface available to bacteria to respire on (Alatraktchi et al., 2012). The utilisation of gold nanowires, with a conductivity almost of bulk gold for enhanced electron transfer between microbes and electrode, is feasible, however, it requires the employment of ligand exchange procedures that are challenging and not trivial (Critchley et al., 2010; Tamang et al., 2011; Gross et al., 2014). The wide excitation spectrum of QDs was utilised in biohybrid systems that harvest sunlight to enable chemical production by bacteria or eukaryotic organisms (Sakimoto et al., 2016; Sakimoto et al., 2017; Nangle et al., 2017; Kornienko et al., 2018). In the ‘methods’ Chapter 3, synthesis of QDs and one nanowire was described. In this chapter, short, general descriptions of syntheses are given, followed by a characterisation of different QDs and one Au nanowire. These QDs are subsequently used in Chapter 5, 6 and 7. General techniques used in the assessment of nanoparticles will also be discussed in this chapter.

5.2. Negatively Charged CdTe/CdS/TGA QDs

Cadmium-based QDs with negative surface charge have been extensively used in research (Rogach et al., 2007; Wang and Jiang, 2013). CdTe/CdS/TGA QDs (see Fig. 4.1), and were synthesised as described in Chapter Material and Methods 4.5.1 (Gaponik et al., 2002). Briefly, the reaction employed thioglycolic acid (TGA, IUPAC name: sulfanylacetic acid) as a stabilising agent (Fig. 4.1). After completion of CdTe core growth, thiourea puriss was added to build the QD's shell (CdS). CdTe/CdS/TGA nanocrystals were stored in the post-synthesis aqueous mixture. The conditions outlined above help to stabilise the QDs in solution and prevent them from precipitation. The nanoparticles were washed to remove unreacted thiols or cadmium/tellurium ions before subsequent experiments. This procedure is also described in detail in Chapter 4.5.1.

Immediately after the synthesis of CdTe/CdS/TGA QDs, ultraviolet and visible light (UV-Vis) absorbance and photoluminescence (PL) spectra maxima were recorded and used to determine the concentration and size of nanocrystals (Yu et al., 2003). Eq. 4.2.1 was used to calculate the diameter of all CdTe nanocrystals.

Eq. 5.2.1.

$$d = (9.8127 \cdot 10^{-7}) \cdot \lambda^3 - (1.7147 \cdot 10^{-3}) \cdot \lambda^2 + (1.0064) \cdot \lambda - (194.84)$$

In Eq. 5.2.1. d is the diameter of CdTe QDs, expressed in nm, and λ is the wavelength of the first excitonic absorption peak. It should be noted that Yu et al. (2003) obtained Eq. 5.2.1 by fitting experimental data to a polynomial function.

The same group correlated the CdTe QDs extinction coefficient, the diameter and the value of transition energy corresponding to the first absorption peak (Yu et al., 2003). Eq. 5.2.1.1 is the mathematical relationship of these values and that was used to calculate the concentration of the CdTe/CdS/TGA.

$$\epsilon = 3450 \cdot \Delta E \cdot (d)^{2.4} \qquad \textit{Eq. 5.2.1.1.}$$

where ε is the extinction coefficient expressed in $M^{-1} \cdot cm^{-1}$, while ΔE is transition energy corresponding to the first absorption peak expressed in electronvolts (eV) and d is the QD diameter (nm).

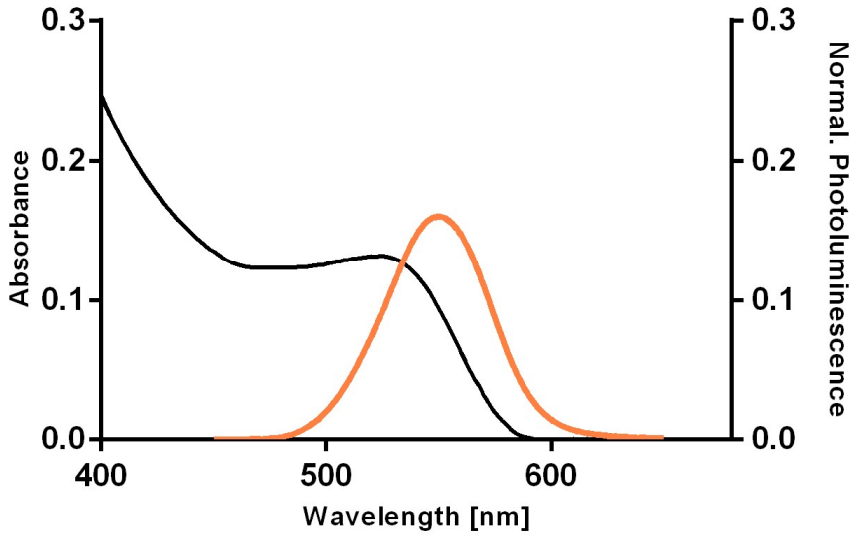

Fig.5.2.1. One of the characteristic UV-Vis absorbance (black) and photoluminescence (orange) spectra of negatively charged CdTe/CdS/TGA. The number of CdTe/CdS/TGA syntheses (*n*) was 8 (4 of which were done by Anna Wroblewska-Wolna and 4 by Dr Andrew Harvie). The average size of QDs was 3.23±0.48 nm.

The maxima of UV-Vis and PL spectra in Fig.4.2.1 are 525 nm and 550 nm, respectively (Fig.5.2.1). These values were used to calculate the diameter and extinction coefficient at 530 nm and results equalled, d = 3 nm and ε_{525} = 113 $mM^{-1} \cdot cm^{-1}$.

5.2.1. CdTe/CdS/TGA QDs ζ-potential

The ζ - potential is an electrostatic charge on the surface of colloids in a dispersion. Electrophoretic mobility of the colloid determines whether the charge is positive or negative. Such mobility is proportional to the electrophoretic velocity. Thus electrophoresis measures the applied potential at which particles move to one of the poles at a certain speed. Fig.5.2.1.1. illustrates the ionic layers that surround and contribute to the ζ - potential value of nanoparticle in the solvent.

Both Stern and slipping plane (Fig. 5.2.1.1.) are often called an electric double layer (EDL) of the particles in the solution. The ζ - potential reflects the

potential difference between the EDL of electrophoretically mobile particles and the layer of dispersant around them at the slipping plane (Bhattacharjee, 2016). As it is impossible to measure ζ - potential directly, it must be deducted from electrophoretic mobility of a charged particle in the applied electric potential.

The mathematical description of the ζ - potential is presented below (Bhattacharjee, 2016).

$$\mu_e = \frac{V}{E} \qquad \textit{Eq.5.2.1.1.}$$

In Eq. 4.3. μ_e is the electrophoretic mobility, V is a particle velocity, and E is the electric field strength applied in the system (V/cm).

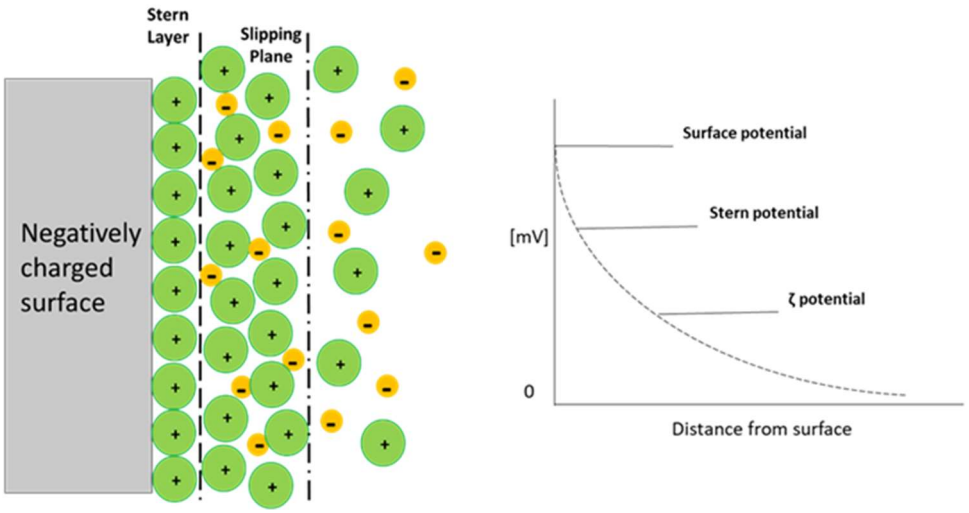

Fig.5.2.1.1. The negatively charged surface in solution (grey rectangle) is surrounded by positively charged ions present in the solvent (green circles). The first layer of ions is known as the Stern layer. The next layer of ions includes a mixture of positive and negative (yellow circles) particles and forms a slipping plane. Slipping plane defines the ζ-potential. The inset graph illustrates the theoretical electric potential of each layer discussed above. Modified from Bhattacharjee et al (2016).

When the particle mobility has been established, the ζ - potential can be calculated with Helmholtz-Smoluchowski Eq. 5.2.1.2 (Smoluchowski, 1906; Bhattacharjee, 2016).

$$\mu_e = \frac{\varepsilon_r \varepsilon_0 \zeta}{\eta} \qquad \textit{Eq. 5.2.1.2.}$$

In Eq. 5.2.1.2, ε_r is the relative permittivity/dielectric constant of the medium, ε_0 is the permittivity of vacuum and η is a viscosity of the solvent.

The decisive factors in the stability of colloidal suspensions are the attraction and repulsion forces. Attraction can induce flocculation and agglomeration, while repulsion between particles stabilises the suspension. The attraction is brought about through the van der Waals forces, while repulsion is dependent on electrostatic forces. Stable suspensions of particles typically have strong ζ-potentials (of the same charge). Besides electrostatic interactions, suspensions can be stabilised by steric repulsion when polymer coatings on nanoparticles physically prevent particles from direct interaction. The surface ζ potential strongly depends on the environmental conditions, such as pH, ionic strength and chemical composition of the employed buffers (Leroy et al., 2015). In the technique measuring ζ - potential, the laser beam light is split and create an incident and a reference beam. When the small electric field is applied to the charged sample, and the particles move at a certain velocity and the direction, the laser beam is scattered, and the detector positioned at the appropriate angle records the data. Further, all data is combined and the difference in frequency of light (Doppler shift) between each datasets are mathematically analysed by the software (Bhattacharjee, 2016).

The ζ - potentials of CdTe/CdS/TGA QDs were recorded. Firstly, debris and aggregates in QDs samples were removed by filtering samples through a 0.2 μm membrane. If not removed, these fragments cause a significant error in the results, as aggregates scatter light significantly more than the small particles.

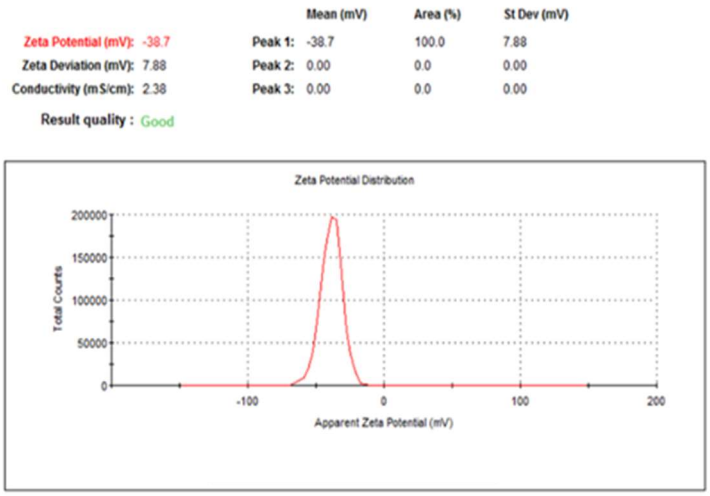

Fig.5.2.1.2. CdTe/CdS/TGA surface ζ-potential measurement showed a negative potential of -38.7 mV.

A representative result of ζ - potential measurement is presented in Fig. 5.2.1.2. All performed measurements of CdTe/CdS/TGA QD ζ - potential were averaged (-32.3 mV), the standard deviation was calculated at 3.72 mV, and the number of repetitions (*n*) equalled 20. These results indicate that all CdTe/CdS/TGA QDs had a strong negative surface charge.

These negatively charged CdTe/CdS/TGA QDs were further used in ligand exchange (LE) reactions (Chapter 5.3.).

5.2.2. Hydrodynamic Size of CdTe/CdS/TGA QDs by Dynamic Light Scattering

Nanoparticles in aqueous solutions can interact with a variety of available chemical entities, such as lipids, proteins, and vitamins, which impact the physical properties of QDs and often cause them to agglomerate, and/or precipitate (Roiter et al., 2008; Barroso, 2011; Dubavik et al., 2012; Maffre et al., 2014). To further characterise the aggregation state, Dynamic Light Scattering (DLS), which may also be known as Photon Correlation Spectroscopy (PCS) or Quasi-Elastic Light Scattering, is frequently used in the nanoparticle science. DLS empowers researchers to measure the hydrodynamic diameter (d_H) of nanoparticles down to the size of 1 nm. d_H of a particle represents the size of a particle itself but includes the Stern Layer and slipping plane created by ions present in the solution (see Fig. 5.2.1.1.).

DLS measures the Brownian motion of the particle and relates it to its size (Ipe et al., 2006; Wang and Jiang, 2013; Sun et al., 2013). Brownian motions are random movements, which all molecules experience. The hydrodynamic size obtained by DLS depends on the solution viscosity (η), the absolute temperature in Kelvin (T), the translation diffusion coefficient (D) and the Boltzmann constant (k). The mathematical relationship between these values for the spherical particle is given in the Stokes-Einstein calculation and presented in Eq. 5.2.2.1.

$$d_H = \frac{k \cdot T}{3 \cdot \pi \cdot \eta \cdot D} \qquad \text{Eq. 5.2.2.1.}$$

The crucial features of stable NPs suspension include pH and ionic strength, both of which are controlled by the buffer used in the experiment. Together they determine the conductivity of the solution, hence have a significant impact on both the diffusion speed and electric double-layer known as Debye length. Furthermore, the temperature determines the solution's viscosity, and thus both must be accurately controlled. DLS measures the speed at which the particle diffuses within a solution. In DLS experiment, laser light is shone at the cuvette containing the sample of interest and the fluctuation of the scattered light is recorded. Next, the obtained data is acquired in a correlator (digital processing board). Finally, the information is passed to the computer where the software analyses the data and correlates it to the hydrodynamic size.

The example of dynamic light scattering of CdTe/CdS/TGA is presented in Fig. 5.2.2.

The relatively large hydrodynamic size of CdTe/CdS/TGA QDs and a significant standard deviation (41.11 +/- 13.21 nm) of the measurement implies QDs agglomeration. As documented in the literature, the hydrodynamic size of stable yellow emitting and Cd-containing QDs should be of about 10 nm in diameter (Reiss et al., 2009; Tamang et al., 2011; Mattera et al., 2016).

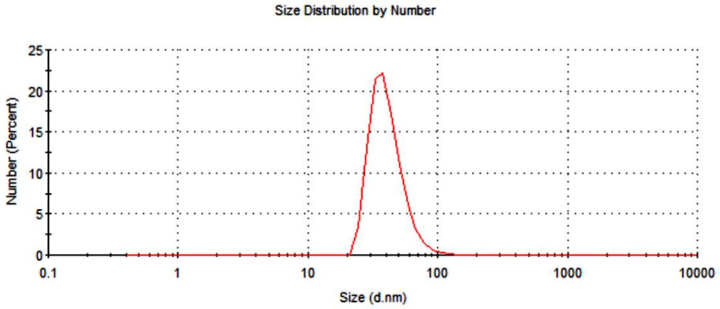

Fig.5.2.2.1. Dynamic light scattering showed CdTe/CdS/TGA QDs suspended in 20 mM HEPES, pH 7.2, present a hydrodynamic size of 41.11 ± 13.21 nm (*n*=3).

5.2.3. High Resolution Transmission Electron Microscopy of CdTe/CdS/TGA QDs

Negatively charged CdTe/CdS/TGA QDs were characterised by high resolution transmission electron microscopy (HRTEM). The purpose of this work was to inspect the quality and shape of the nanocrystals.

Representative images of CdTe/CdS/TGA are presented in Fig. 5.2.3.1. HRTEM showed that the CdTe/CdS/TGA QDs have a circular shape, are well dispersed on the EM grid and do not create many large agglomerates. To obtain a good quality size distribution, 270 QDs were measured by the ImageJ software. Fig. 5.2.3.2. presents fitting of a Gaussian curve to the results obtained from micrographs.

The Eq. 5.2.3.1. was used for Gaussian curve calculation.

$$Y = A \cdot \exp\left\{-0.5 \cdot \left(\frac{X - X_0}{SD}\right)^2\right\} \qquad \text{Eq. 5.2.3.1.}$$

In Eq. 5.2.3.1, *A* is the amplitude which is the height of the centre of NPs size distribution (see Fig. 5.2.3.2.), *X* – size particle, X_0 – centre of median, SD – standard deviation.

Both the median and SD determined from the histogram might deviate from the mean and standard deviation computed directly from the raw data. There are two reasons for the inconsistency. The first is that creating the frequency distribution requires a subjective decision about the bin width. That influences the best-fit values of mean and standard deviation. The second reason is that nonlinear regression assumes that the residuals (the distances of the points from the curve) follow a Gaussian distribution.

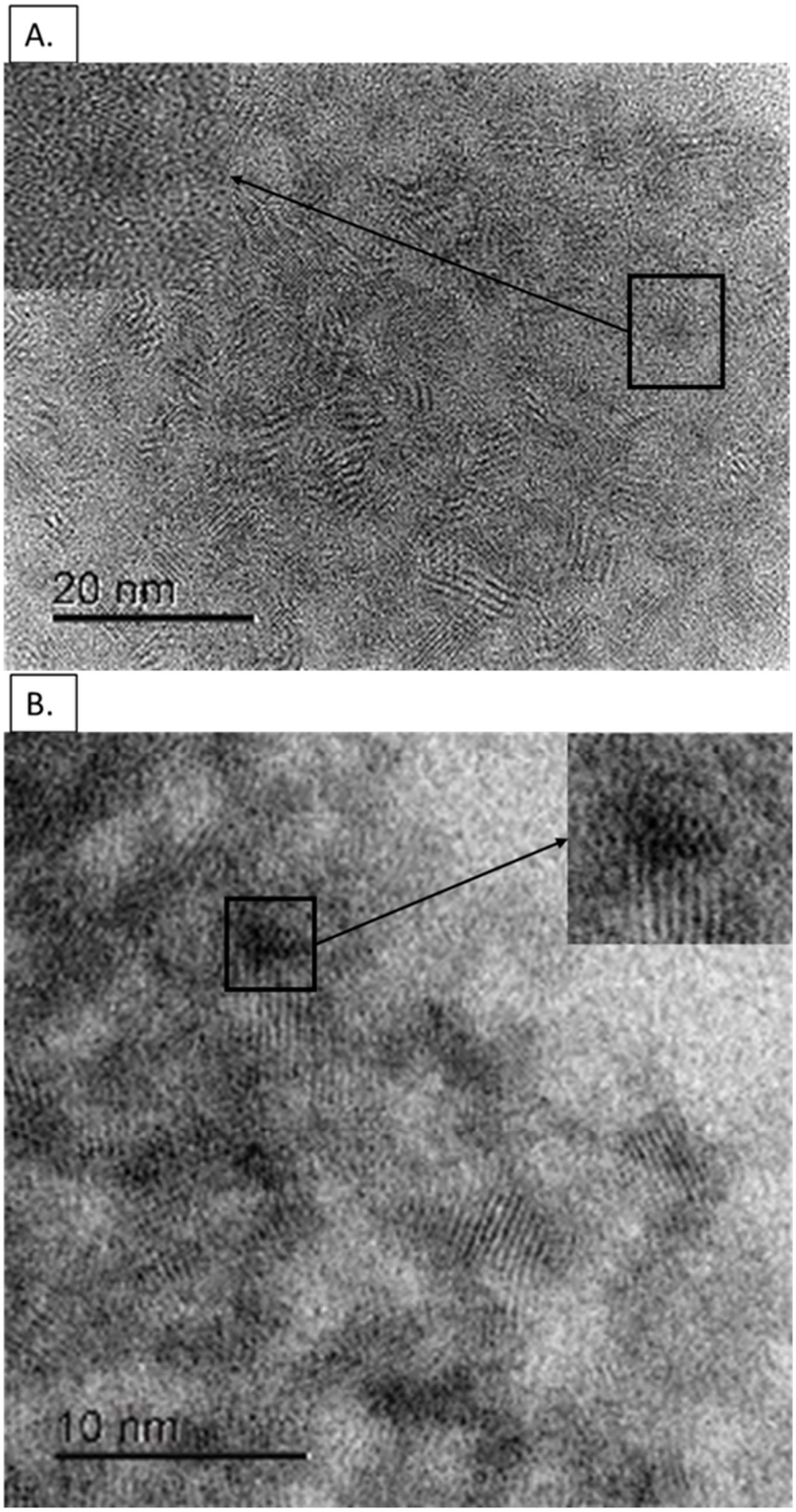

Fig.5.2.3.1. **A, B.** The representative transmission electron microscopy images of CdTe/CdS/TGA QDs. The insets represent an additional digital zoom of chosen QDs.. The scale bars at pictures A and B are 20 nm and 10 nm, respectively. HRTEM pictures were obtained by Dr Harvie.

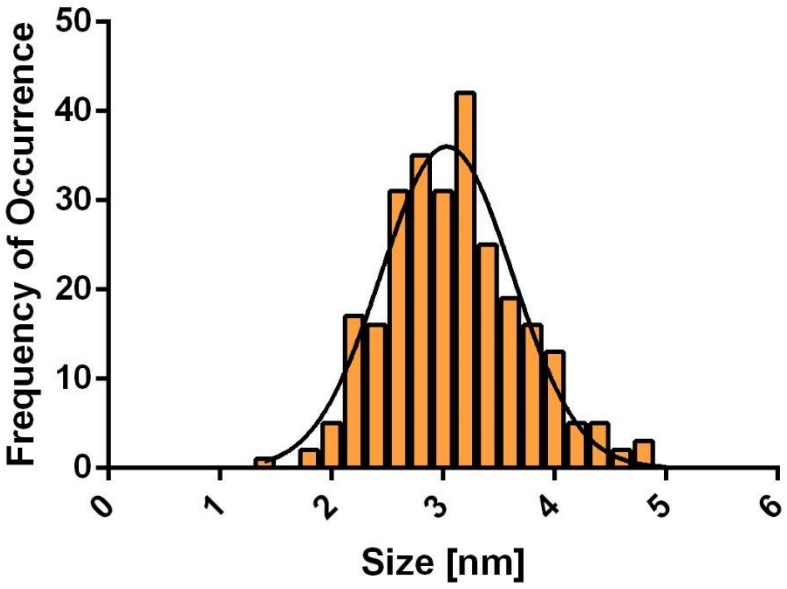

Fig.5.2.3.2. Size frequency distribution of custom made CdTe QDs. The mean size of CdTe QDs was 3.1 nm with the standard deviation of ±0.6 nm.

The Gaussian curve was fitted to CdTe/CdS/TGA QDs of size between 1.5 nm to 5.2 nm. The above analysis revealed that analysed QDs had a mean size of 3.1 nm with a standard deviation of ±0.6 nm. In the agreement with HRTEM results, calculations from UV-Vis, and PL spectra presented the QDs average diameter was 3 nm.

5.3. Ligand Exchange with CdTe/CdS/TGA.

5.3.1. CdTe/CdS/TGA to CdTe/CdS/Cysteine Ligand Exchange.

Here, zwitterionic CdTe/cysteine QDs were prepared using ligand exchange – LE - from the CdTe/CdS/TGA particles described in the previous section.

For successful QD LE, the reaction environment must be optimised (Niidome et al., 2007; Hatakeyama et al., 2011). Variation in the pH, ionic strength and the excess molar ratio of desired molecules should be tested in the reaction system. Such excess will shift the equilibrium towards the decomposition of the initial substrate, followed by the thiols substituents and product creation (Gaponik et al., 2002; Sun et al., 2013a). The LE reaction is given in Fig. 5.3.1.

QDs are typically stored in the reaction solution which, among other, contains 'free' TGA molecules. Those need to be removed before LE reactions.

The unreacted thiols and cadmium ions might alter the accuracy and efficiency of the reaction. Furthermore, various organic solvents with different hydrophobicity might also be employed for different nanoparticles, as described later in Chapter 5.6.

$$CdTe/CdS/TGA+Cys_{ex} \rightleftharpoons CdTe/CdS/Cys+TGA$$

Fig. 5.3.1. Example of a ligand exchange reaction scheme. Depicted is the scheme for LE with CdTe/CdS/TGA using an excess of cysteine. The resulting product is CdTe/CdS QDs capped with cysteine and released TGA.

The solution of CdTe/CdS/TGA was evenly divided into the test tubes. Subsequently, further reagents were added that included concentrated thiols and buffers and Milli-Q water. The progress of ligand exchange reactions was monitored by PL. Red - shifts in the fluorescence emission maxima were taken to indicate aggregation, while a substantial reduction in fluorescence intensity might indicate break down or dissolution of the QDs.

A zwitterionic amino acid, cysteine was used to substitute thioglycolic acid in the QDs. Cysteine contains three functional groups: thiol, amine and carboxyl. Each has different protonation constants: amine, $pK_a = 10.7$; carboxylic acid, $pK_a = 1.92$; side-chain thiol, $pK_a = 6.04$. After ligand exchange, the thiol group will create a coordinate bond with cadmium in the QDs core and therefore should not contribute to the pH dependence of the QDs charge. The experimental pH performed in citric acid buffer, pH 3 and a 200 molar excess of cysteine was used (compared to CdTe/CdS/TGA particles).

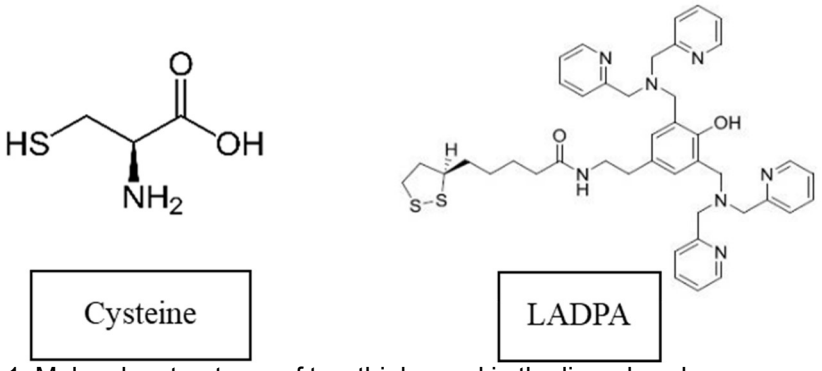

Fig.5.3.1.1. Molecular structures of two thiols used in the ligand exchange experiments. LADPA stands for the lipoic acid derivative of dipicolylamine.

When the cysteine solution was added, the reaction sample instantly suffered from a high degree of agglomeration as is portrayed in Figs. 5.3.3 and 5.3.4. Addition of cysteine suspended in citric acid pH 3 triggered the instant and sharp increase in the PL intensity as the emitted light was scattered by the coagulating nanocrystals (Fig. 5.3.3). Furthermore, the PL spectra shifted towards the longer wavelength (from PL maximum at ctrl sample 600 nm to 610 nm at sample recorded after 10 minutes from the start of reaction), indicating the nanocrystals agglomerated. The shift in PL maxima remained constant through the experiment. The number of repetitions were n=2 and both attempts resulted in nanoparticles agglomeration. Moreover, the PL intensity increased immediately when the cysteine was added to reaction mixture indicating QDs coagulated (Fig5.3.1.3). In summary, the ligand exchange reaction discussed above was ineffective.

Domingos et al. investigated the influence pH had on the stability of CdTe/CdS/poly(acrylic)acid carboxyl-terminated, commercial QDs (Domingos et al., 2013). Their finding indicated that pH lower than 5 triggered substantial degradation of CdTe/CdS. Additionally, citric acid is a chelating agent; as such, it dissolves cadmium, thus reduces CdTe/CdS/TGA QDs stability. This reaction might be more successful if it was performed with a non-chelating buffer at higher pH. Cysteine at this state would electrostatically repel the carboxylic group of thioglycolic acid; consequently the QD agglomeration would be avoided.

L-Cysteine capped CdTe resuspended in phosphate buffer pH 9 has previously been shown to have a zeta potential of -14.6 mV with a hydrodynamic diameter of 7.1 nm (Xu et al., 2015). In the available literature,

cysteine stabilised CdTe QDs charge is described as pH-dependent (Li et al., 2010; Xu et al., 2015). However, no pH and surface charge profiles were reported.

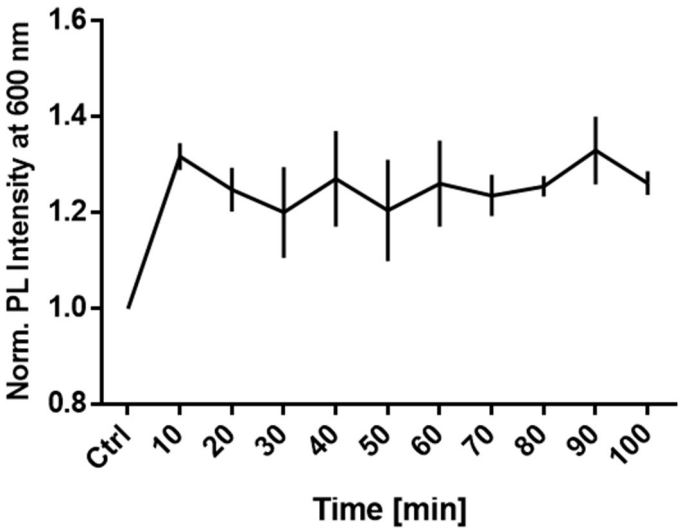

Fig. 5.3.1.2. Photoluminescence intensity (measured at the wavelength of 600 nm, normalised to ctrl) over the time of the experiment. Ctrl is a PL of CdTe/CdS/TGA QD before the addition of cysteine. Number of repetitions was n=2. Error bars were standard deviations and are 0.03, 0.05, 0.1, 0.1, 0.1, 0.09, 0.04, 0.02, 0.07, 0.03 for samples from 10, 20, 30, 40, 50, 60, 70, 80, 90, 100 min, respectively.

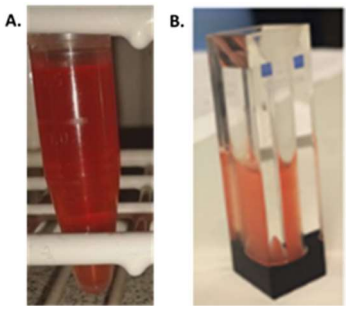

Fig.5.3.1.3. The precipitation of CdTe/CdS/TGA QDs was instantly visible upon addition of excess cysteine in the citric buffer pH 3. A. CdTe/CdS/TGA, B. CdTe/CdS/TGA with an excess of cysteine.

5.3.2. CdTe/CdS/TGA to CdTe/CdS/LADPA Ligand Exchange.

A lipoic acid derivative of dipicolylamine has two reactive thiol groups, which makes it feasible for thiol replacement reactions (Fig. 4.3.1.). The LE reaction set up was similar to when the cysteine was used. The molar ratio of QDs to ligand was 1:200 and the selected buffer was 50 mM HEPES with pH 8.5. Structurally, dipicolylamine consists of two pyridines with a pK_a ~ 5.5 and a tertiary amine with pK_a ~ 10.5; the neutral charge was then estimated at pH 12. Therefore, LADPA at pH 8.5 is positively charged. The results of the ligand exchange reaction are presented in Fig. 5.3.2.1 and show fast agglomeration

of nanoparticles upon addition of LADPA to the QDs, as documented by the rapid increase of fluorescence intensity followed by the observed rise in turbidity. The multiple optimisation approaches were executed in different reaction conditions. The molar ratios of QDs to LADPA were differentiated and included from 1:2, 1:20 and 1:200. The LE conditions were investigated in depth and variations included: reagents incubation at 4 °C, and 30 °C, with or without shaking, and incubation times used for 30 min - 20h were tested. Furthermore, in some tests, zinc ions were added to LE mixtures. The only test that used 20 time molar excess of LADPA to CdTe/CdS/TGA QDs was successful and created a short-lived conjugated with LADPA QDs solution with an enlarged hydrodynamic size of 34 nm that might have suggested the forthcoming agglomeration of QDs. The CdTe/LADPA QDs were stable only for about 20 h. Fortunately, the CdTe/LADPA QDs were examined for the interaction with bacteria, before the nanoparticles coagulated (see Section 6.2.3.3). Nevertheless, similar to the LE with cysteine, the PL spectra of dTe/CdS QDs were red-shifted, indicating nanoparticle agglomeration. Upon the addition of LADPA, the solution of QDs flocculated indicating immediate coagulation of QDs.

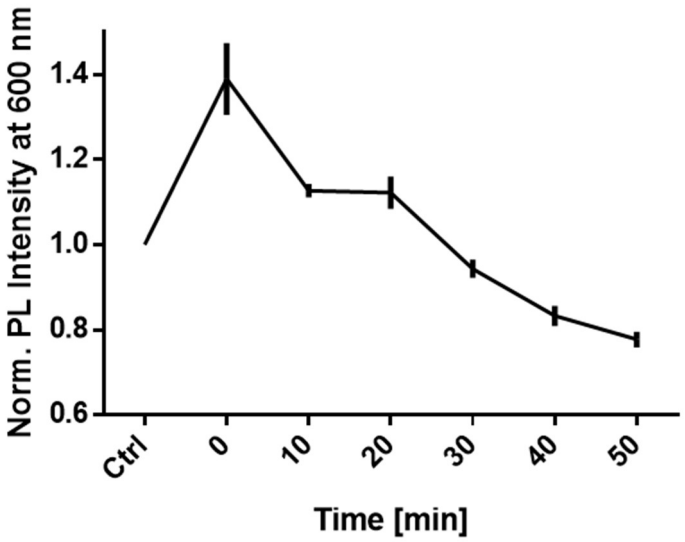

Fig. 5.3.2. Photoluminescence intensity (measured at the wavelength of 600 nm, normalised to ctrl) over the time of the experiment. Ctrl is a PL of CdTe/CdS/TGA QD before the addition of the thiol. Time 0 is the first PL spectrum taken after addition of LADPA. Number of repetitions is n=2. Error bars were SD and are 0.08, 0.02, 0.04, 0.02, 0.02, 0.4 for samples 10, 20, 30, 40, 50, respectively.

As the ligand exchange process with both LADPA and cysteine did not work, commercially-available negatively charged CdTe QDs were purchased. Such nanocrystals are frequently used for surface modification and specific binding to other species (Ruedas-Rama et al., 2011).

5.4. Commercial Negatively Charged CdTe Quantum Dots – A Tool for the Surface Adaptations

Negatively-charged commercial CdTe QDs were received as a yellow powder. For biological applications, nanoparticles were suspended in ultraclean water as advised by the manufacturer. The supplier also indicates that these nanocrystals do not have a shell in their structure, although the nanoparticles are stabilised with carboxylic groups. In the available literature, commercial QDs are frequently used for comparison to custom-made QDs (Maffre et al., 2014). Studies have employed commercial QDs functionalising their surfaces by coupling methods (Kelf et al., 2010; Mattera et al., 2016), cross-linking (Wu et al., 2003) or stabilising them with different polymers (Maffre et al., 2014).

5.4.1. UV-Vis and PL of Commercial CdTe QDs

The UV-Vis and PL spectra were recorded, as described in Chapter 4.2. Representative graphs are shown in Fig. 5.4.1.1. The results obtained here were used to determine the size and concentration of commercial QDs. The Eq. 5.2.1 and 5.2.2 were used for this purpose.

The diameter of the core of the QD, which absorbs light at 500 nm and emits PL at 530 nm, equals 3.0 nm. The extinction coefficient at the wavelength of 530 nm of these QDs is 106 $mM^{-1} \cdot cm^{-1}$.

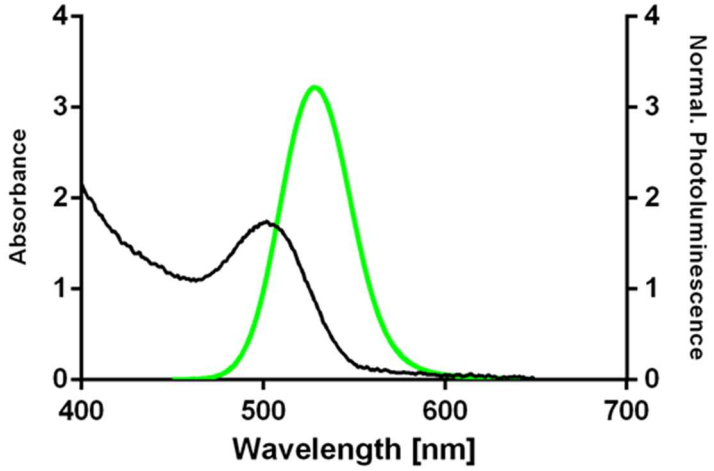

Fig.5.4.1. Overlaid absorbance and photoluminescence of negatively charged commercial CdTe QDs. The colour of the PL graph corresponds to the visible colour of the solution. The number of comercial negatively charged CdTe QDs ordered was n=3.

5.4.2. The Surface ζ - Potential of Commercial CdTe QDs

The quality of the nanoparticles was assessed by the ζ potential measurements. The commercial QDs showed a strong negative potential at the surface. The 17 repetitions (n) of the zeta potential measurements of these QDs in water gave an average of -24.1 mV potential with a standard deviation of 5.9 mV.

5.4.3. Transmission Electron Microscopy of Commercial CdTe QDs

Negatively-charged CdTe commercial QDs were characterised by high resolution transmission electron microscopy (abbreviation HRTEM). The purpose of this work was to visualise the quality and the shape of nanocrystals.

The pictures of negatively charged commercial CdTe QDs are presented in Fig. 5.4.3.1. Two hundred nanocrystals were measured and analysed with the use of ImageJ software.

The results show that commercial nanocrystals have an approximately circular shape and do not create many large agglomerates. The nanoparticles are monodispersed with a median size of 2.7 nm, in line with the size based on PL. There were many smaller (0.5-1.5 nm) particles visible, however, these were not QDs. The Gaussian Curve was fitted to the frequency distribution chart (Fig. 5.4.3.2, Eq. 5.2.3.1.).

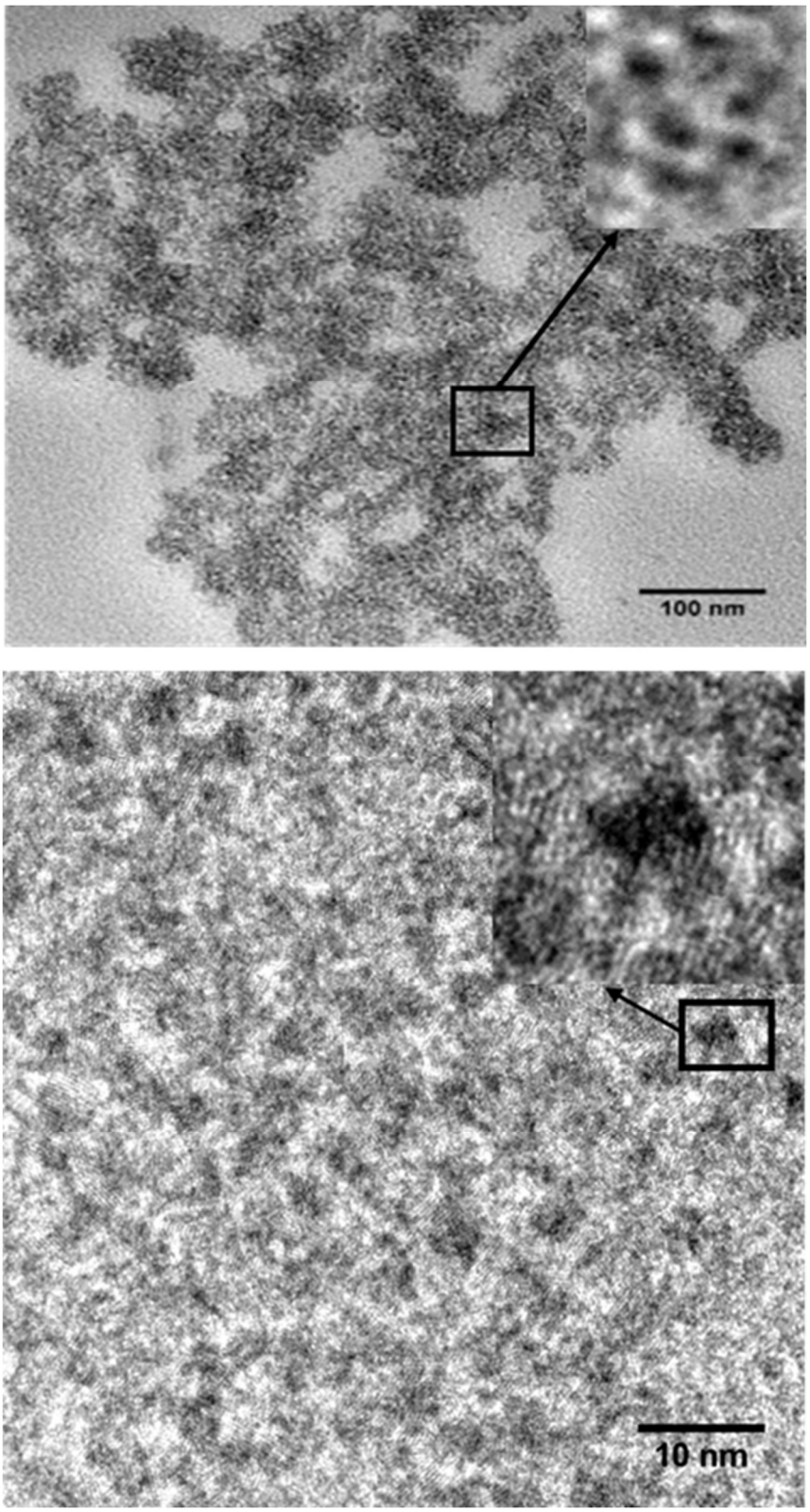

Fig. 5.4.3.1. Representative transmission electron microscopy pictures of negatively-charged commercial CdTe QDs. The insets represent a digital zoom of chosen QDs. The diameter of the zoomed nanoparticles are about 3 nm. The scale bars are top picture a 100 nm and bottom 10 nm. The micrographs were kindly obtained by Dr Sunyie Ye.

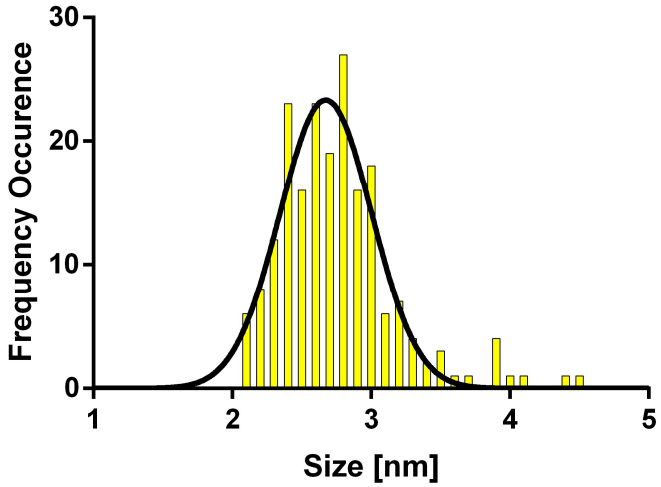

Fig. 5.4.3.2. Size frequency distribution of negatively charged commercial CdTe QDs. The mean value of commercial QD equals 2.7 nm with a standard deviation of 0.42 nm. A Gaussian curve was fitted to the frequency distribution measurements.

5.4.4. Cross-Linking of Commercial CdTe QDs with Dipicolylamine

Zinc dipicolyl amine (Zn(II)–DPA) - complexes and derivatives are versatile anion receptors with prominent selectivity for phosphates over most other anions in aqueous media (Lakshmi et al., 2004; Sakamoto et al., 2009; Ngo et al., 2012). This feature has been used to chemically or physically modify biomembranes (Lakshmi et al., 2004; Leevy et al., 2006; Sakamoto et al., 2009; Yuen and Jolliffe, 2013; Choi et al., 2014). The anion sensing of DPA was also used to detect Gram-negative bacteria such as *E. coli* (Leevy et al., 2006). DPA has been coupled to a diverse range of fluorophores and chromophores to enable sensing of anionic species and also determine physicochemical constants (Wong et al., 2009). DPA consists of two picolyl substiuentes each with a nitrogen atom through which to interact (Fig. 5.4.4.1.). The connection of these aromatic rings with another tertiary amine offers the valence electrons to create a cooridinate bond with zinc or other electrophiles. Other biologically abundant cations such as Na^{+}, K^{+}, Ca^{2+}, or Ni^{2+} bind to DPA with lower affinity than zinc ions (Madden et al., 1970; Xue et al., 2008).

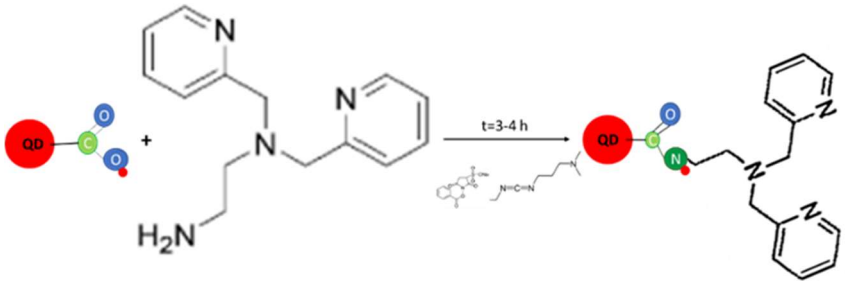

Fig. 5.4.4.1. Scheme of the amide bond formation from CdTe(COOH) QD (red circles) and amine derivative of dipicolyl amine (ADPA), catalysed by EDC and Sulfo-NHS. Small red circles represent protons, blue – oxygen, light green – carbon, dark green - nitrogen.

Cross-linking employs the reaction of carboxylic acid groups (R-COOH), present on the organic shell of the commercial QDs, with a primary amine (R-NH_2), creating an amide bond. 1-ethyl-3-(3-dimethylaminopropyl) carbodiimide (EDC) activates the carboxyl group, which generates an unstable by-product amine-reactive O-acylisourea intermediate. Further introduction of the primary amine species with the added support of 3-sulfo-succinimidyl benzoate sodium salt (abbreviated as sulfo-NHS), forms the sulfo-NHS ester. Such ester eagerly reacts with phosphate or carboxyl groups creating amidophosphates and amides, respectively (Fig. 5.4.4.1.). EDC crosslinking is most efficient in an acidic buffer such as MES pH 4-6 as the EDC-modified carboxylic acid intermediate (o-acylisourea) is unstable at neutral or alkaline pH. However, the use of sulfo-NHS compensates for this by creating a more stable sulfo-NHS ester intermediate, which still reacts with amines to create amide bonds.

The crosslinking reactions are frequently used in biochemical studies that include coupling of nanoparticles to proteins or acids and for protein modifications (Grabarek and Gergely, 1990; Conde et al., 2014). For instance, CdSe quantum dots with ZnS shell were conjugated to fullerenes using EDC chemistry. Different lengths of amino alkanethiols were investigated and attached to the carboxylated fullerenes by EDC. Subsequently, the thiolates interacted with CdSe/ZnS QDs creating the linkers enabling efficient electron transfer between both parties (Xu and Cotlet, 2011). It was postulated that the above findings could be used in small and large scale photovoltaic devices, for instance, solar cells.

An amine derivative of dipicolylamine (abbreviated as ADPA, Fig. 5.4.4.1) was dissolved in water (0.35 mM) and cross-linked to commercial QDs (7.2 μM) resuspended in phosphate buffer saline (PBS, pH 7). The choice of buffer is crucial in cross-linking experiments as the buffering molecules must not contain primary amines (e.g. Tris). Different molar ratios of QD to ADPA were tested.

Name:	M_W	C_S	C_W	CL 1QD:10ADPA
Commercial CdTe QDs	20000	100 μM	5 μM	50 μl
ADPA	242.3	350 μM	15 μM	42.9 μl
EDC	191.7	1000 μM	50 μM	50 μl
Sulfo-NHS	217.13	100000 μM	5000 μM	50 μl
PBS, pH 7.0	NA	10 x Stock	NA	100 μl
MilliQ	18	NA	NA	607.1 μl
Total volume	NA	NA	NA	1000 μl
$ZnSO_4$	161.47	10000 μM	1 μM	100 μl

Table 5.4.4.1. The representative ingredients used in the crosslinking of commercial negatively charged CdTe QD with the amine derivative of dipicolylamine in the molar ratio of QD to ADPA 1:10. Used abbreviations: MW – molecular weight, CS – stock concentration, CW – working concentration, CL – cross-linking, NA – not applicable, PBS – phosphate buffer saline, ADPA – amine derivative of dipicolylamine, EDC - 1-Ethyl-3-(3-dimethylaminopropyl)-carbodiimide, Sulfo-NHS - N-hydroxysuccinimide.

The experimental trials were kept in the dark for 3 hours. After modification of the QDs, $ZnSO_4$ was injected into the samples to a final concentration of 10 mM. The reaction progress was monitored by PL and epifluorescence microscopy (see Chapter 5). Spectra of commercial QDs were taken before and after the cross-linking as well as with or without zinc ions (Fig. 4.4.4.2). An example of negatively charged commercial CdTe QDs crosslinking reaction with amine derivative of dipicolylamine (ADPA) at the molar ratio 1:10 (QD:ADPA) is presented in Table 5.4.4.1.

All examined ADPA to QD ratios resulted in significant loss of fluorescence as compared to the control sample (ctrl, Fig.5.4.4.2). Addition of zinc ions (10

mM) caused further agglomeration of the nanocrystals as all samples maxima shifted to longer wavelength. The shifts in the fluorescence (Fig. 5.4.4.2) indicate aggregation of QDs as larger particles disperse light more efficiently.

Following these measurements, the ζ-potential of QDs before and after LE was obtained. The ADPA-modified commercial QD (ratio of QD:ADPA was 1:10) had a ζ potential of -29.8 mV which is higher (less negative) than commercial QD control zeta potential of -36 mV (n = 3) with standard deviation 0.68 and 3.4 mV, respectively.

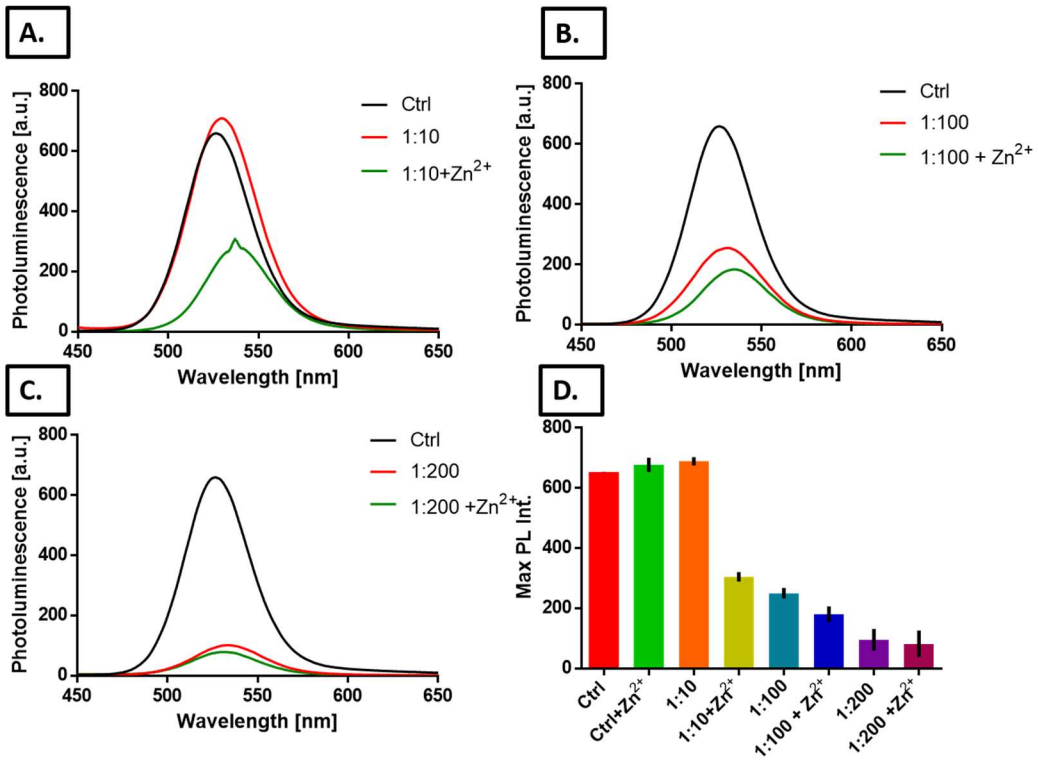

Fig.5.4.4.2. PL spectra of commercial QDs taken after cross-linking with ADPA at different ADPA to QD ratios, as indicated, and after addition of 10 mM $ZnSO_4$. Control samples (ctrl) were subjected to the same EDC/sulfo-NHS treatment but without ADPA. **A.** Commercial CdTe QDs before and after crosslinking to ADPA in ratio 1:10. **B.** 1:100 ratio of QDs to ADPA, **C.** 1:200 ratio. **D.** The different fluorescence intensity maxima were recorded. Number of repetitions was n=2. Error bars are SD. Fig. 5.4.4.2 D SD were 0.7, 23.5, 13.5, 15.5, 17.5, 26.1, 36.4, 44.5 for samples Ctrl, Ctrl+Zn^{2+}, 1:10, 1:10+Zn^{2+}, 1:100, 1:100+Zn^{2+}, 1:200, 1:200+Zn^{2+} respectively.

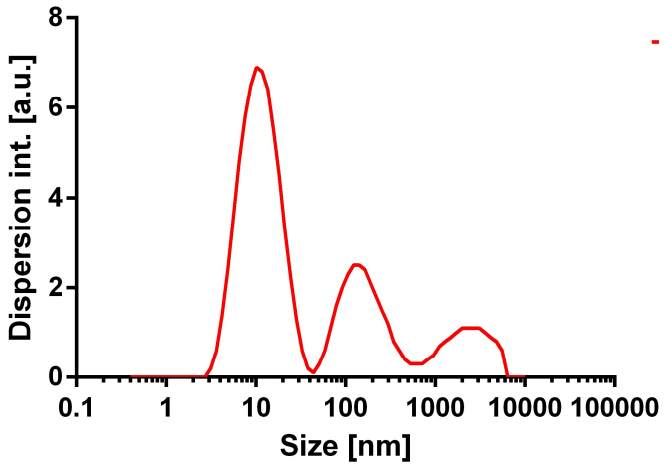

Fig. 5.4.4.3. A dynamic light scattering of commercial CdTe QDs after coupling to ADPA (ratio 1:10) and the addition of 10 mM Zn^{2+} suggests three populations of agglomerating nanoparticles are present in the solution. The majority of them have a hydrodynamic size of ~ 10 nm. However, many larger particles are present too.

5.5. $CuInS_2$/ZnS/PMAL – Zwitterionic Quantum Dots

The synthesis of $CuInS_2$/ZnS (CIS) QDs is described in the Methods Chapter, Section 4.5.4. The outcome of the CIS synthesis is a hydrophobic solution of highly fluorescent nanoparticles, which require further cleaning with chloroform-methanol-acetone mixture. The hydrophobicity of CIS QDs is a property that needs to be controlled for QDs biological application. Booth *et al.* 2013 encapsulated the particles with the zwitterionic polymer PMAL-d (Chapter 4, Fig. 4.5.4.1.) to enhance the water solubility of CIS QDs. The CIS QD encapsulation with PMAL-d procedure is described in the Methods Chapter 4.5.4.

The UV-Vis and photoluminescence spectra of CIS QDs are presented in Fig.5.5.1.. The PL maximum is at the wavelength of 620 nm. The diameter calculated by Eq. 5.5.1 was 3.0 nm, and the extinction coefficient at 400 nm was 42 $mM^{-1} \cdot cm^{-1}$ (Eq. 5.5.2.).

Fig. 5.5.1 presents UV-Vis and PL spectra of CIS QDs. The size and concentration of the nanoparticles is determined according to published procedures (Booth et al., 2012).

$$d = 68.952 - 0.213\lambda_{PL} + 1.717 \cdot 10^{-4}\lambda_{PL}^2 \qquad \textit{Eq. 5.5.1.}$$

The Eq. 5.5.1 was used to calculate the diameter (*d*) of the CIS nanoparticle from the wavelength of the PL peak (λ_{PL}). This equation was determined by Booth et al., 2012, by the fitting of data obtained by the luminescence spectra

to the size of CIS particles determined with high resolution TEM using a polynomial function (Booth et al., 2012). The same group determined the way to calculate the molar extinction coefficient at 400 nm (ε_{400nm}) using the knowledge of the diameter (d) of CIS particles (Eq. 5.5.2).

$$\varepsilon_{400\,nm} = 830d^{3.7} \qquad \textit{Eq. 5.5.2.}$$

In Eq. 5.5.2 ε_{400} – extinction coefficient [$mM^{-1}\cdot cm^{-1}$], d – dimeter of CIS QD [nm].

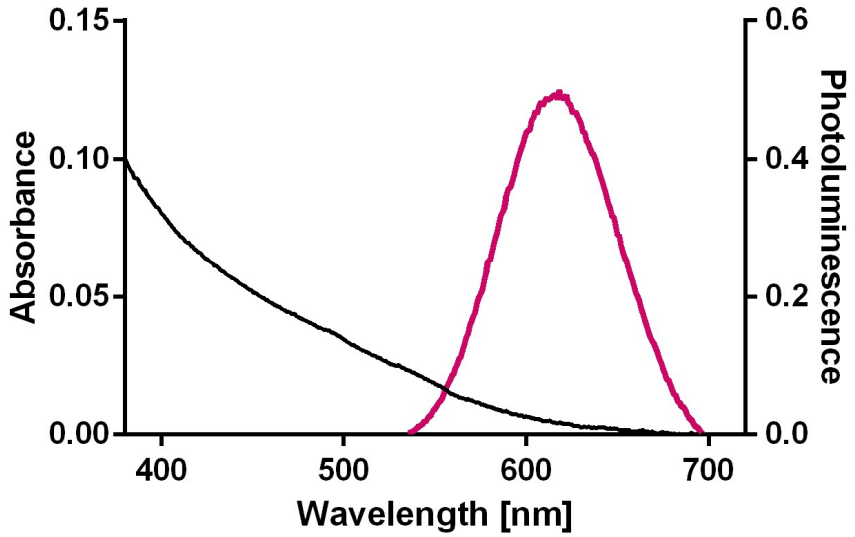

Fig. 5.5.1. The UV-Vis and PL spectra of CIS QDs suspended in chloroform. The number of CIS syntheses was n=5. Anna Wroblewska-Wolna performed 2 syntheses. The other 3 were gifts from either Dr Booth or Dr Harvie. The average size of QDs was 2.54 ± 0.15 nm.

5.5.1. ζ - potential of CIS/PMAL QDs

The ζ potential of the particles encapsulated in amphiphilic substances like PMAL-d have a pH-dependant value. When the pH becomes acidic, the tertiary amine groups protonate and QDs develop a positive surface charge, while in an alkaline solution the carboxylic acid group deprotonates in CIS/PMAL QD to give a negative surface potential (Booth et al., 2013). Similar behaviour of amphipol encapsulated QDs is presented in the literature for other nanoparticles (Kelf et al., 2010; Sun et al., 2013). ζ - potential measurements of CIS/PMAL QD suspended in 20 mM HEPES, pH 7.4

showed an average potential of + 1.6 mV with *n*=5 measurements, and a standard deviation of 0.27 mV.

5.5.2. Dynamic Light Scattering of $CuInS_2$/ZnS/PMAL QDs

The dynamic light scattering results of CIS\PMAL QDs suspended in M9 media (please see Materials 4.3.1) show a stable solution of the QDs with a hydrodynamic size of 11.75 ± 3.4 nm. The typical DLS result is presented in Fig. 5.5.2.1. The average size of CIS/PMAL in the M9 and 20 mM HEPES, pH 7.4 buffers was 12 ± 2 nm, *N* = 10. M9 media was also tested with a view of measuring the interaction between the NP and bacteria in the future (please see Chapter 6), for which a growth media is more appropriate than HEPES buffer. CIS/PMAL QD presented good stability in 20 mM HEPES buffer as well as in M9 bacteria media growth.

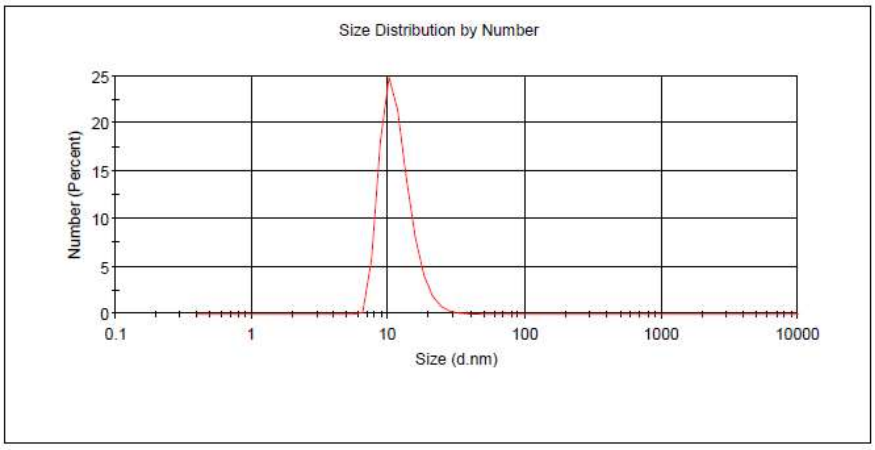

Fig. 5.5.2.1. A dynamic light scattering of the solution of CIS/PMAL - d QDs in M9 bacterial growth media. The hydrodynamic size of this nanoparticle was measured as 11.75 nm, with a standard deviation of 3.4 nm.

5.6. CdTe/CdS/Cysteamine Quantum Dots

The limited success in ligand exchange experiments (Sections: 5.3., 5.4., 5.5.4.) triggered an attempt to synthesise cadmium-based QDs capped with a cysteamine (IUPAC name: 2-aminoethanethiol) in an attempt to create pH-dependent charged QDs.

Based on the UV-Vis and PL spectra of CdTe/CdS/Cysteamine (Fig.5.2.1) the calculated by Eq. 5.5.1 diameter of QDs was 2.6 nm, and the extinction coefficient at 510 nm was 117 $mM^{-1} \cdot cm^{-1}$ (Eq. 5.2.2).

The full synthesis reaction was described in Chapter 4.5.1. The synthesis was similar to CdTe/CdS/TGA, except that cysteamine and different pH 5.4 of the solution were used. As with CdTe/CdS/TGA QDs, CdTe/CdS/Cysteamine QDs were kept in the post-synthesis solution, for the sake of nanoparticle stability. The number of CdTe/CdS/Cysteamine syntheses was n=4 and the average size of QDs was 3 ± 0.36 nm. The usual maximum photoluminescence maximum was from 580 – 600 nm.

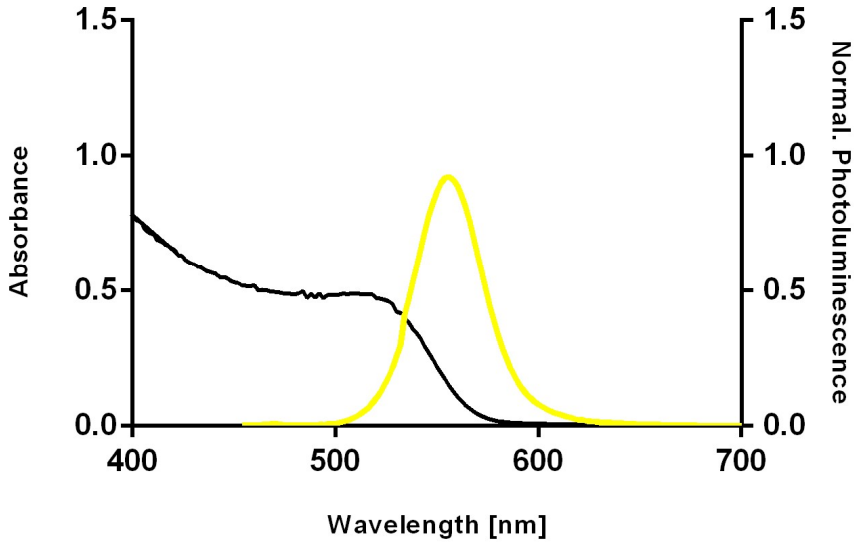

Fig.5.6.1. Representative graph of UV-Vis and PL spectra obtained from CdTe/CdS/Cysteamine QDs. The number of performed syntheses was n=2, one of which was done by Dr A. Harvie while the other by the author of the thesis.

5.7. Gold Nanowires

Gold nanowires were synthesised according to Feng et al., 2009. The full description of the synthesis is in Chapter 3.5.5. Here only brief description is provided. The chloroauric acid was reduced by triisopropylsilane (TIPS, $C_6H_{22}Si$). Oleyamine ($C_{18}H_{35}NH_2$) was used as a stabiliser and one-dimensional growth template, to create gold nanowires (Au NWs) resuspended in hexane (C_6H_{14}). TEM image of Au-NW and characteristic UV-Vis spectrum of freshly synthesised AuNWs are presented in Fig. 5.7.

Au-NWs are hydrophobic, thus not soluble in water. Hydrophilicity is a crucial property for biological experiments performed in this thesis. Consequently, ligand exchange reactions were attempted.

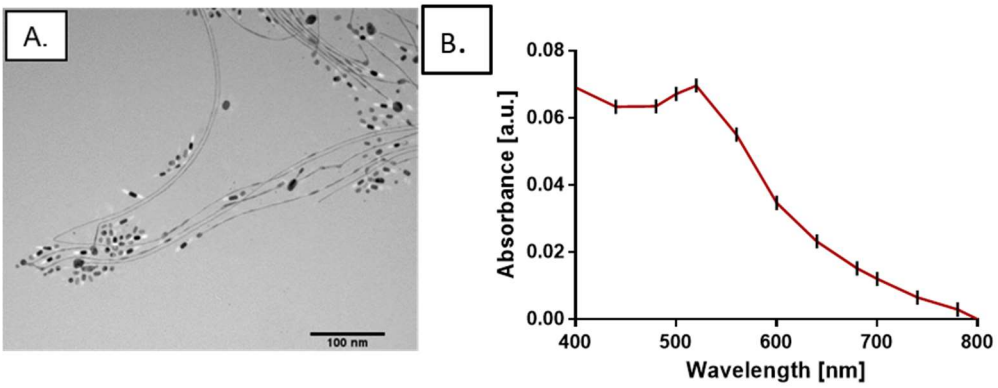

Fig. 5.7. **A.** TEM image of ultrathin gold nanowires in hexane. Scale bar is 100 nm. **B.** UV-Vis spectrum of the as-synthesised Au-NWs, displaying a characteristic absorbance peak at 520 nm. The number of AuNWs syntheses was n=4 with 3 performed by Anna Wroblewska-Wolna. One synthesis was performed by Dr Kellye Coffyn. Number of repetitions on the graph B is n=2 and SD equals 0.03.

5.7.1. Polydopamine Testing for Au-NWs Functionalisation

Frequently utilised by living organisms (like mussels for surface attachment and in humans as a neurotransmitter), the catecholamine - dopamine is known to polymerise in basic environments (Lee et al., 2007; Dreyer et al., 2013). When dopamine is dissolved in 10 mM Tris pH 8.5 buffer, a thin layer of a polydopamine (PDA) is formed on solid surfaces (Fig.5.7.1.1.). The polymeric structure of PDA was documented to adhere to any substance present in the reaction solution (Lee et al., 2007). Here, a polydopamine coating was tested for the functionalisation of Au-NWs.

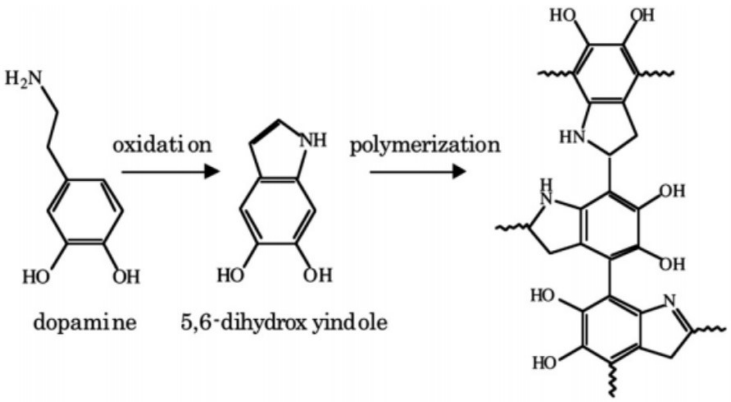

Fig. 5.7.1.1. The polymerisation of dopamine in an oxidising solvent. The reaction scheme was copied from Valsabehagh et al. (2014).

As synthesised Au-NW-PDA were inspected with UV-Vis absorbance. The obtained spectra of Au-NW-PDA and PDA without Au-NW are presented in Fig. 5.7.1.2. A. Fig. 5.7.1.2. B portrays the importance of Au-NW purification

before use in further experiments. The thoroughly purified Au-NWs present a sharp and of larger intensity peak at 530 nm.

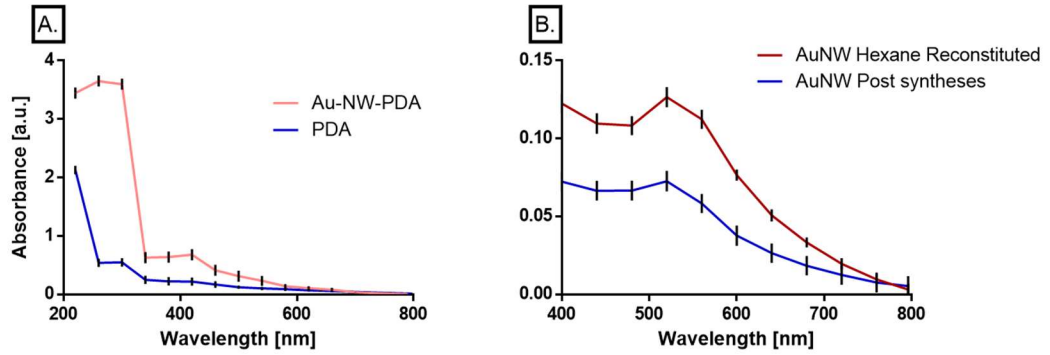

Fig. 5.7.1.2. **A**. The spectrum of Au-NW-PDA after the 2-hour incubation in PDA solution presented a broad peak at wavelengths below 300 nm and a distinctive peak at 400 nm. The blue graph represents a control UV-Vis spectrum of dopamine dissolved in 10 mM Tris, pH 8.5 without Au-NWs. Error bars are SD and are 1.4 and 0.5 for Au-NW-PDA and PDA, respectively. **B**. The blue spectrum illustrates the absorbance spectrum of freshly synthesised Au-NWs in hexane. The Au-NW reconstituted in hexane (red spectrum) is confirmed by the high absorbance peak at the wavelength of 530 nm. Error bars are SD and are 0.05 and 0.03 for AuNW Post synthesis and AuNW recosntitued, respectively.

As shown in Fig. 5.7.1.2 A, the blue spectrum is characteristic for catecholamines, with peaks at 280 and 400 nm (Vaselbehagh et al., 2014). The same elevated peaks are present also in the UV-Vis spectrum of Au-NW-PDA. The missing absorbance at wavelengths of 520–530 nm indicated the Au-NW changed their structure. The transmission electron microscopy was employed to evaluate the Au-NW-PDA structure after ligand exchange procedure (Fig.5.7.1.3.).

The samples containing Au-NW-PDA and control samples consisting of Au-NWs with a previously evaporated organic solvent followed by resuspending them in water (Fig.5.7.1.3. D) and hexane (Fig.5.7.1.3. C) were examined by transmission electron microscopy. The relevant electron microscopy images are presented in Fig. 5.7.1.3. The attained colloidal solution was stable and did not show signs of decomposition or aggregation for several months. This is confirmed by TEM (Fig. 5.7.1.3 A and B), which indicates that the PDA treatment of Au-NW resulted in the formation of Au nanoparticles.

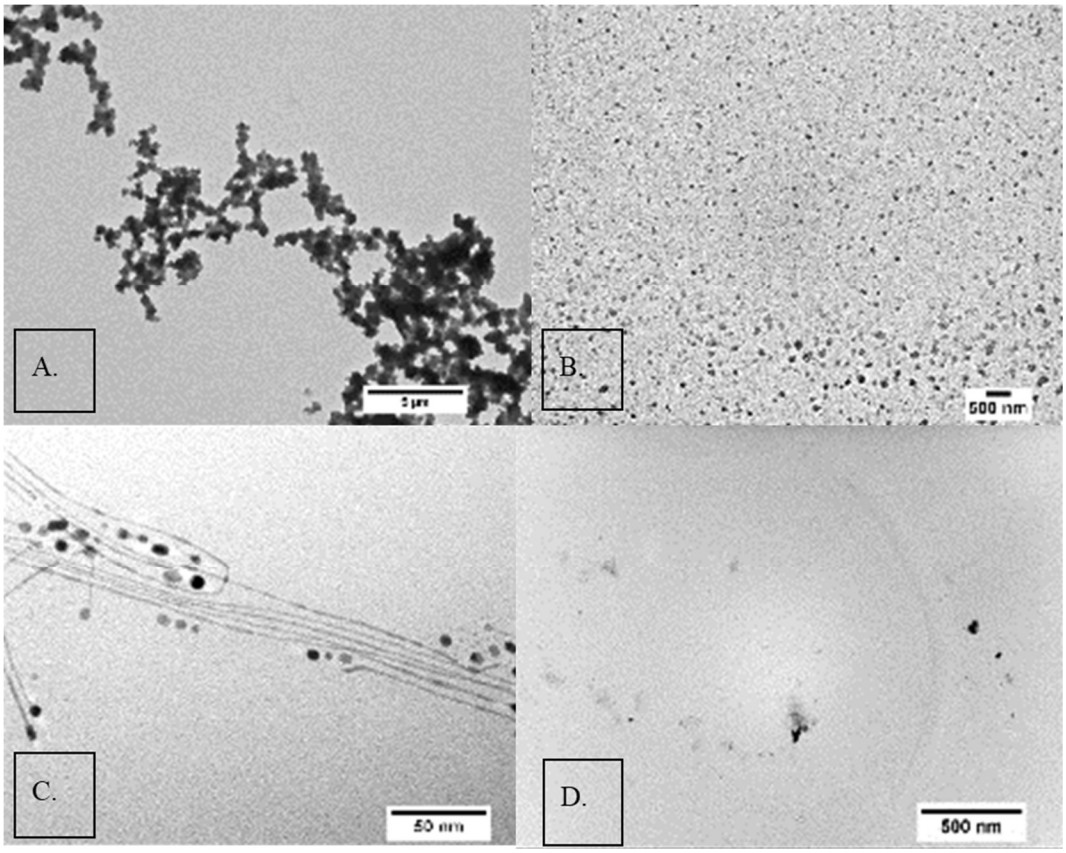

Fig. 5.7.1.3. A and **B.** Transmission electron microscopy images of dopamine treated gold nanowires. **C.** Control image of Au-NWs in hexane. **D.** A control of unmodified Au-NWs reconstituted in water. Scale bars at figures A is 2 μm, C is 50 nm, B and D is 500 nm. The micrographs were taken by the author of thesis.

The missing absorbance at wavelengths of 520–530 nm of Au-NW-PDA and TEM images that show the creation of gold nanoparticles after the Au-NW functionalisation with polydopamine indicated the breakdown of Au-NWs (Fig. 5.7.1.2 and 5.7.1.3).

5.7.2. Diethylene Glycol Aminothiol Test to Transfer Au-NWs into Aqueous Solution

As PDA modification was not successful, a different approach of ligand exchange was attempted. Diethylene glycol aminothiol (DEGAT, Fig. 5.7.2.1.), provided by Dr James Murray from the Department of Chemistry at the University of Leeds, was used in ligand exchange reactions. DEGAT is readily dispersed in polar organic solvents, such as ethanol, methanol and chloroform.

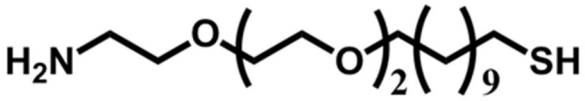

Fig. 5.7.2.1. The molecular structure of diethylene glycol aminothiol - DEGAT.

The ligand exchange experiment is described in Chapter 4.5.5.2. Au-NW and DEGAT were suspended/dissolved in an appropriate molar ratio of gold to sulfur atoms. Different molar ratios (1 to 0.5, 1, 1.5, 2. 2.5 and 3) were examined (Fig. 5.7.2.2 A). An Au : sulfur 1:2 ratio was selected based on trial experiments. Finally, the mixture in the organic solvent was combined with phosphate buffered saline pH 7.4.

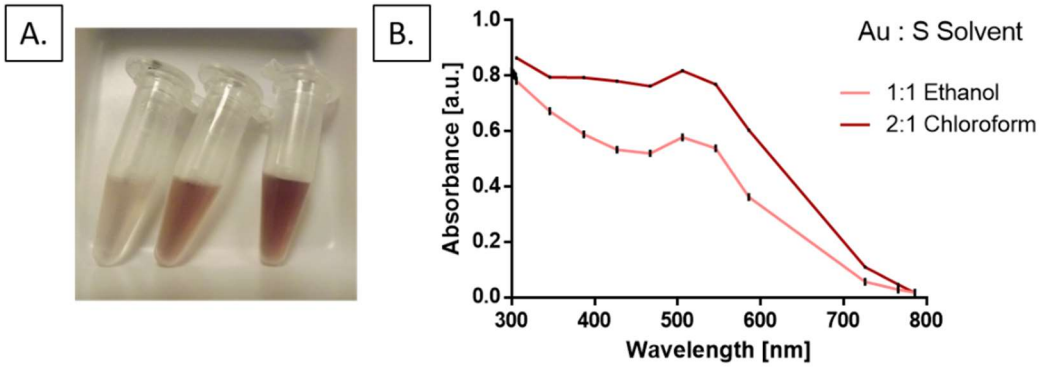

Fig. 5.7.2.2. **A.** Samples of ligand exchange experiments performed with Au-NW and DEGAT in chloroform and PBS pH 7.4, with varying molar ratios. From left to right: Au:sulfur molar ratios were: 1:1; 1:1.5; 1:2. **B.** UV-Vis spectra of the ligand replacement trials conducted in ethanol with a 1:1 molar ratio and in chloroform with a 2:1 ratio. Number of repetitions was n=2.The error bars are SD equal 0.02 and 0.05 with 2:1 chloroform and 1:1 ethanol, respectively.

As-prepared samples were vigorously mixed at room temperature and incubated overnight. Next, the samples were harvested by centrifugation at 17000 RPM for 90 min. The organic solvent was discarded and any remaining chloroform was removed by overnight desiccation of the samples. Visual absorption of the resulting samples (now in aqueous solution) showed a surface plasmon resonance peak at 520 nm, characteristic for gold nanowires (Fig. 5.7.2.2. B).

However, further investigation with transmission electron microscopy (TEM, Fig. 5.7.2.3.), clearly indicated that again the Au-NW were broken down to monodispersed Au nanoparticles (Fig. 5.7.2.3 B).

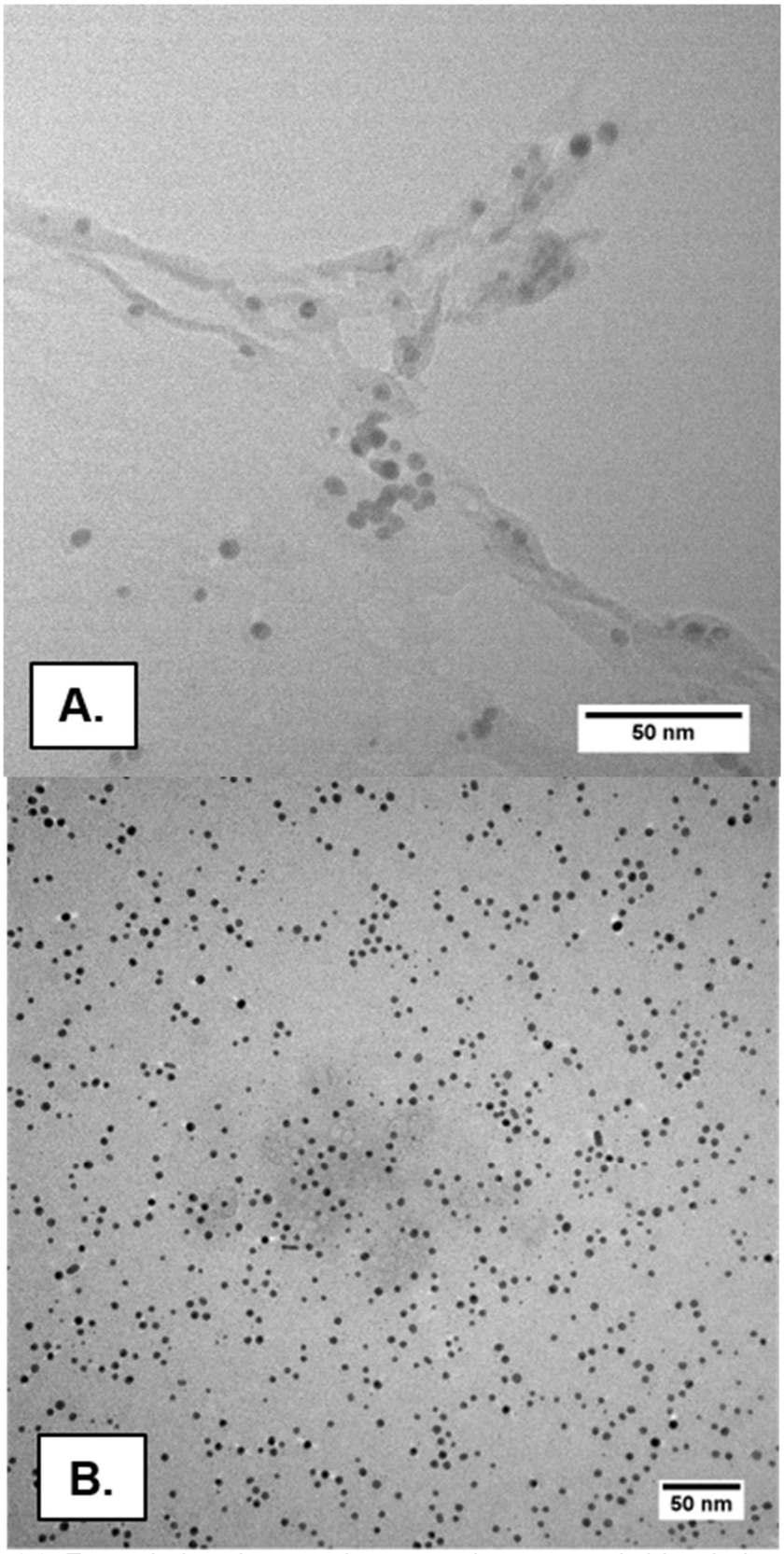

Fig. 5.7.2.3. Transmission electron microscopy pictures revealed break down of Au-NWs treated with a 1:2 Au : sulfur in DEGAT molar ratio in chloroform. Scale bars on Fig. A and B are 50 nm.

5.8. Syntheses and Characterisation of Nanoparticles – Summary

In this chapter, the synthesis of various water-dispersions of nanoparticles and nanowires are described. The most successful syntheses were those of quantum dots. The straightforward synthesis of CdTe/CdS/TGA QDs was described. Methods to calculate sizes and the excitation coefficients were also shown. Surface properties of all QDs were investigated by the use of dynamic light scattering and ζ - potential measurements. A summary of the zeta potentials of all QDs is presented in Fig. 5.8.1.

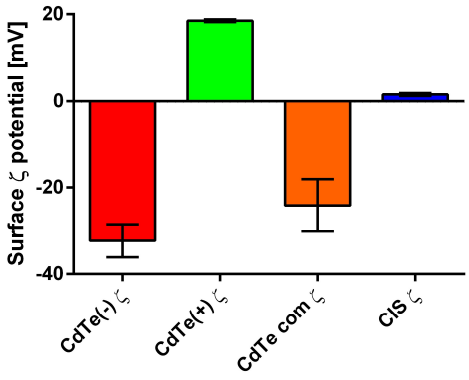

Fig.5.8.1. QDs, described in Chapter 4, presented a wide range of surface ζ - potentials. Both CdTe/CdS/TGA and the commercial CdTe QD had a negative surface charge. In contrast, CdTe/CdS/Cysteamine showed strong positive potential. Encapsulated in zwitterionic polymer $CuInS_2$/ZnS/PMAL QD (CIS/PMAL) had a pH-dependent surface potential (in the graph is shown when resuspended in buffer with pH 7.4).

High resolution transmission electron microscopy was employed for the precise size measurement of commercial and homemade cadmium - based QDs. Additionally, nanocrystals $CuInS_2$/ZnS/PMAL QDs, which lack the heavy metal Cd, were synthesised and characterised since Cd is known to be toxic in the biological experiments (Booth et al., 2013).

NPs / Action	CdTe(-)		CdTe(+)	CdTe com	CIS/PMAL	AuNWs	
Synthesis	✓		✓	–	✓	✓	
Type of NP. modification	Cysteine	LADPA	NP	ADPA	NA	DEGAT	PDA
LE Success	–	–	NA	–	NA	–	–

Table 5.8. The table shows the variety of nanoparticles characterised throughout Chapter 5. The different LE reactions and the rating of their success are presented in the table. Abbreviations used in the table include: CdTe(-) – CdTe/CdS/TGA QDs, CdTe(+) – CdTe/CdS/cysteamine QDs, CdTe com - negatively charged commercial CdTe QDs, CIS/PMAL – CuInS2/ZnS/PMAL QDs, AuNWs – gold nanowires, NA – not applicable, LADPA – lipoic acid derivative of dipicolylamine, ADPA – amine dipicolylamine, DEGAT - diethylene glycol aminothiol, PDA – polydopamine, LE – ligand exchange.

In Chapter 6, the toxicity of the nanocrystals to microorganisms will be described. Their interaction with bacteria will be investigated by light and electron microscopy in Chapter 7. Work towards a design of QD: bacteria hybrid system will be inspected in Chapter 8.

Chapter 6. **Nanotoxicology of Quantum Dots to *Shewanella oneidensis* MR-1.**

6.1. Nanotoxicology – Introduction.

Toxicology is a division of science concerned with the nature, effects and recognition of poisons. The toxins can be medicines, pollutants and new substances that are introduced into the environment. Because worldwide production and accumulation of NPs are increasing rapidly, it is certain that nanoparticles will be widely released into the environment. For instance, sunscreens that contain TiO_2 nanoparticles are not toxic to humans, although might be poisonous to other organisms such as fish and bacteria due to titanium dissolution (Mueller and Nowack, 2008; Das et al., 2012; Dhas et al., 2014). Despite three decades of research into nanoparticle (NP) toxicity, their effects are still not fully understood (Fadeel and Garcia-Bennett, 2010; Wick et al., 2010) and substantial research into the nanotoxicology assessment of NPs already released into the environment is still missing (Leigh et al., 2012; Suresh et al., 2013). Therefore, it is essential to understand and evaluate how nanoparticles might access living organisms and what effects their presence may trigger.

The establishment of nanoparticle toxicity, namely nanotoxicology, has been systematically investigated in a range of laboratory experiments as presented in the literature (Winterbourn, 2008; Suresh et al., 2013; Manke et al., 2013; Davies, 2016). Elemental analysis of NPs can suggest possible ways of toxicity induction. Many NPs are composed of heavy metals, such as iron, silver, cadmium, and gold, providing additional toxic effects. For example, although iron is a cofactor of many proteins, iron oxide NPs are documented to damage *E. coli* membranes and significantly increase the level of reactive oxygen species (ROS) (Li et al., 2018). The shape and size of NPs play an essential role in their interaction with microorganisms. Uneven, rough, irregular shapes contribute to the liberation of NP constituents (Das et al., 2012). The atoms on the corners or edges of the NPs are more biologically and chemically reactive than atoms present in the core. Another crucial feature in nanotoxicology is nanoparticle ζ potential. The more negative the NP ζ potential, the more toxic they are (Schneider et al., 2009; Q. Xiao et al., 2013). Equally, the NP size contributes to toxicity. For example, small QDs

emit light with higher energy, which may impose the destruction of biomolecules as well as enhance ROS generation (Suresh et al., 2013; Moos and Slaveykova, 2014). Additionally, surface functionalization plays a role in defining NP toxicity too. An added layer of atoms at the QD surface introduces new chemical elements (e.g. sulfur, silicon, phosphorus, zinc) as well as new physicochemical features (Karakoti et al., 2015). All these additions alter the potential toxicity of QDs, and their effects need to be examined in depth.

There are many techniques to monitor the impact of nanoparticles on organisms. Changes caused by NPs introduced to the microbial environment can be inspected by real-time polymerase chain reaction (quantitative PCR; qPCR) (Keer and Birch, 2003). qPCR enables scientists to examine changes to the bacterial transcriptome. These variations are linked to bacterial viability. Commonly used techniques in bacterial nanotoxicology are the colony-forming unit (CFU) method and, less frequently, the disk diffusion test. The colony-forming unit method determines the number of bacterial cells able to proliferate upon contact with the potentially toxic elements. The number of viable bacterial colonies is counted on Petri dishes filled with solidified media. The diffusion test is also performed on a Petri dish. However, the toxin is administrated on small filter paper disks which are positioned in the middle of a dish onto which bacteria were inoculated earlier. The diameter of the growth inhibition zone is measured which corresponds to bacterial viability in the acquired conditions (Pelletier et al., 2010). It is important to note that diffusion test cannot be performed on NPs that do not form stable suspensions, thus might not diffuse between filter paper and agar filled plate.

All of the above methods have their drawbacks. Nucleic acids, such as DNA, can still be present, and some enzymes can still be functional in bacteria even after the microorganism is unable to divide. A phenomenon like this describes bacteria that have lost their culturability. The metabolic activity of the undividable bacteria has been described in the literature and was shown to have a substantial impact on the reliability of bacterial viability assays (Xu et al., 1982; Zhao et al., 2017). The bacteria that lost their culturability might influence the performance on some bioelectrochemical devices, such as nanosensors. Nanosensors use the whole bacteria and other chemical

compounds, such as NPs, to record the presence of some chemicals (Holzinger et al., 2014; He et al., 2016). In such an instance, bacterial culturability is essential for the longevity of the system.

The ideal nanotoxicological assessment includes various techniques that characterise multiple aspects of NP toxicity on an organism. For instance, a holistic approach that included the evaluation of ROS production, bacterial gene profile changes, and the effects of applied radiation on TiO_2 mixed with *Shewanella oneidensis* MR-1 (MR-1) has been reported (Qiu et al., 2017). Besides the impact of TiO_2 NPs on the growth of MR-1, riboflavin concentration, which is naturally secreted under the anaerobic conditions by MR-1, was monitored and used as a viability indicator (Marsili et al., 2008; Coursolle et al., 2010; Qiu et al., 2017). Furthermore, MR-1 cells are known to release the cytosolic enzyme glucose-6-phosphate dehydrogenase (G6PD) upon cell damage (Qiu et al., 2017). Qiu and colleagues monitored this phenomenon with the fluorescent molecule resorufin, which is generated by G6PD and NADPH when reducing resazurin (Qiu et al., 2017). Changes in the resorufin photoluminescence levels in the G6PD extracted from MR-1 culture worked as an indicator of cell viability. The mechanistic studies of the Qiu group showed the irradiated TiO_2 NPs inhibited MR-1 growth only at the high concentration of 100 mg/ml (Suresh et al., 2013; Qiu et al., 2017).

Other conventional methods to determine viability include live/dead assays, often performed with fluorescence ‘kits’ that are commercially available, which stains live and dead cells with different, selective fluorescence dyes. An often-applied method uses SYTO 9 for all cell staining and propidium iodide (PI) for dead cell staining (Berney et al., 2007; Liu et al., 2018).

One of the aims of the research presented in this thesis is to determine whether nanoparticles described in Chapter 4 can produce solar fuels in a biotic/abiotic hybrid system. For solar fuel production, biohybrids must be sustainable and provide a long lifetime. Thus, the toxicity of the QDs towards the bacteria was determined in this chapter. The significance of the toxicity results is discussed concerning relevant publications.

S. oneidensis MR-1 (MR-1) and QDs were treated as described in Chapter 3.3. Methods used to study the viability of MR-1 are described in Section 3.4.1, but a brief description of the experiment is provided here. MR-1 was grown overnight at 30 °C in M-1 media. Bacteria were harvested by centrifugation and pellets were resuspended in 20 mM HEPES, 0.15 M NaCl, pH 7.4 to an optical density of ~0.4 at 600 nm after which selected QDs were added at various concentrations. Cultures with QDs of 1 ml were further grown and incubated in 15 ml flasks overnight (~ 18 h) at 30 ºC, with shaking at 200 RPM. The following day, bacteria were harvested by centrifugation (5000 RPM, 10 min). The supernatants were discarded and pellets resuspended in 1 ml of 20 mM HEPES, 0.15 M NaCl, pH 7.4. The final volume of the samples (bacteria, QDs, antibiotic or saline) never exceeded 2 ml. Fully aerobic growth was ensured by using large volume flasks, providing continuous aeration of bacteria. Bacteria were harvested and subjected to the serial dilution procedure. Upon completion of the above procedure, small volumes of diluted bacteria were spread on the surface of the LB-agar containing Petri dishes. Trials were put into a 30 °C incubator for about 20 hours or until the single colonies became visible. Colonies were manually counted and finally expressed as colony-forming units in one millilitre of the examined sample (unit: CFU/ml). All of the above was repeated at least three times to establish correct statistics.

6.2. CdTe/CdS/TGA Quantum Dot Toxicity to *S. oneidensis* MR-1.

A graph presenting the outcome of n = 4 independent bacterial viability assays for two concentrations of CdTe/CdS/TGA QDs is presented in Fig. 6.2.

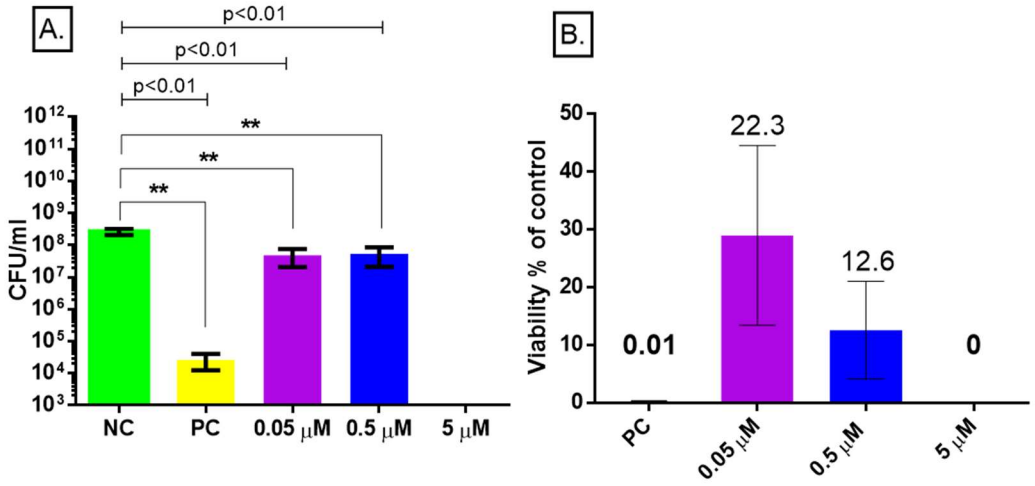

Fig. 6.2. **A.** Effect of CdTe/CdS/TGA QDs on the viability of MR-1 (n = 2). Please note that the data on graph A is presented on the logarithmic scale. **B.** Viability data normalised against NC, plotted on a linear scale. NC = negative control (addition of an equal volume of 0.15 M NaCl, 20 mM HEPES, pH 7.2); PC = positive control (50 μg/ml kanamycin).

Fig. 6.2 shows that 0.05 μM CdTe/CdS/TGA QD solutions leave only 22.3 % of viable bacteria. Incubation of the QDs at higher concentration - 0.5 μM - with MR-1 demonstrates that 12.6 % of them can grow in the applied conditions. CdTe/CdS/TGA QDs at concentration 5 μM in 20 mM HEPES, pH 7.4 were unstable and coagulated. In conclusion, negatively-charged cadmium telluride QD, capped with the thioglycolic acid, displays some toxicity up 0.5 μM, but a significant fraction of MR-1 can survive.

Schneider and colleagues investigated the viability of MR-1 after overnight exposure to CdTe/TGA QDs. Full growth inhibition was documented at 1 μM of QDs (Schneider et al., 2009). Importantly, the bacterial media employed by Schneider was Luria-Bertani media, which according to data discussed in this thesis, causes NP coagulation. Notably, this group used ‘core-only’ quantum dots. An addition of nanoparticle shell, as done in the research presented here, can reduce toxicity (Reiss et al., 2009). The shell of the QDs not only moves the photoluminescence maximum towards longer wavelength but also creates a barrier between the photooxidation sensitive core and the outside environment. The shell of the QD prevents the liberation of toxic cadmium ions and limits ROS generation. The former is documented to be the primary route for the toxicity of cadmium-containing QDs (Rzigalinski and Strobl, 2009; Chen et al., 2012).

6.3. Toxicity of Negatively-Charged CdTe Commercial Quantum Dots to *S. oneidensis MR-1*.

The tested concentrations of commercial NP were 0.05, 0.5 and 5 μM. The results of nanotoxicology studies revealed lower toxicity for negatively charged commercial CdTe QDs as compared to custom CdTe/CdS/TGA QDs. The obtained results from 3 independent experiments are presented in Fig. 6.3.1.

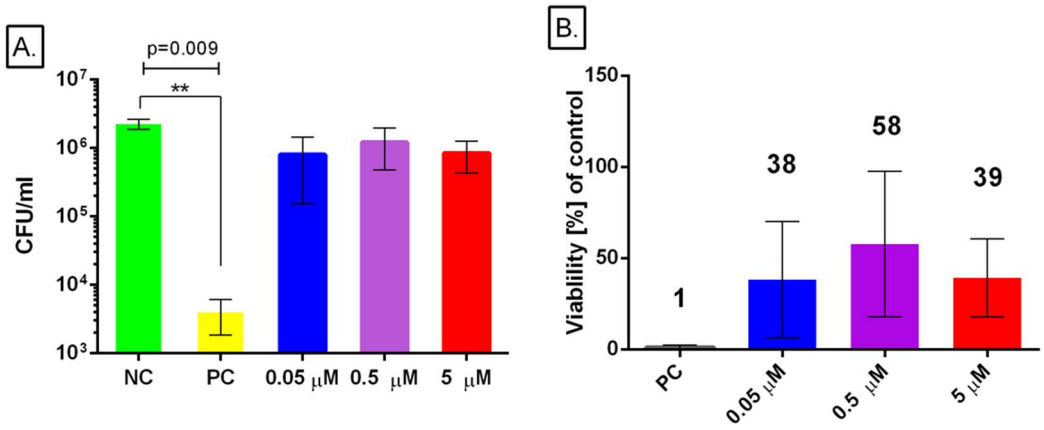

Fig. 6.3.1. A. The colony-forming units assay exposed no toxicity of commercial negatively-charged CdTe QDs to MR-1 (n = 3). B. The normalised values of nanotoxicity are presented on chart B. NC = negative control (addition of an equal volume of 20 mM HEPES, 0.15 M NaCl, pH 7.2); PC = positive control (50 μg/ml kanamycin).

The commercial negatively-charged CdTe QDs reduced bacterial viability to about 40 % after overnight incubation, although the results are not significant compared to the NC. To confirm these results, a live-dead fluorescence assay was performed. This enabled discrimination between live and dead bacteria, while at the same time correlate this to their interaction (or not) with commercial QDs. The epifluorescence microscopy was used to observe the interaction of commercial CdTe QD with MR-1. These results are presented in Chapter 6. Results of the nanotoxicity given by 3 independent investigations by the 'live-dead' fluorescence assay are presented here (Fig. 6.3.2).

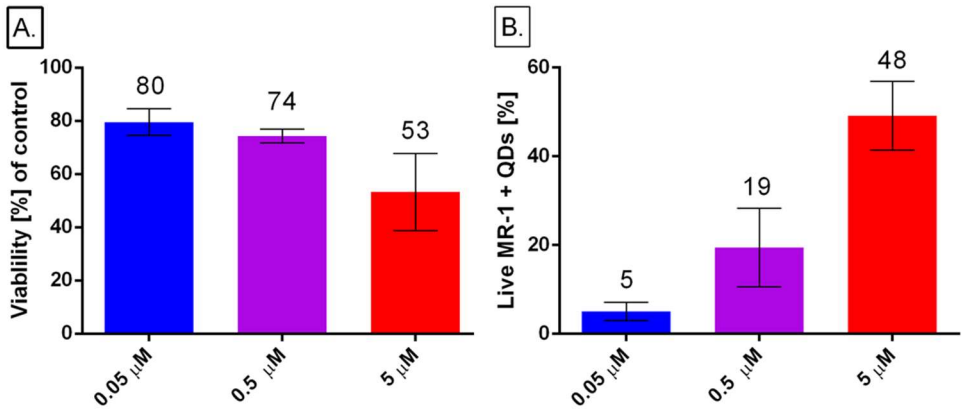

Fig. 6.3.2. **A**. The normalised fluorescence of live-dead assay of MR-1 after overnight incubation with commercial negatively charged CdTe QDs (n = 3). **B**. Percentage of viable MR-1 interacting with commercial QDs. The unit for A and B graphs are the percentage of NC control. The dead cells were stained with propidium iodide (PI) that is a nucleic acid stain which cannot penetrate the lipid bilayer. The positive control of this experiment included MR-1 incubation with 70 % isopropanol for 1 hour.

The percentage of live bacteria (as compared to negative control) after overnight incubation with commercial negatively charged CdTe QDs is presented in Fig. 6.3.2 A. The outcome demonstrates that more than 50 % of bacteria are viable after overnight incubation with all tested concentrations of commercial CdTe QDs. These results are in agreement with the CFU/ml method (Fig. 6.3.1). Fig. 6.3.2 B presents the level of live bacteria that also interact with commercial QDs. The results revealed that a significant population of live bacteria show an interaction with commercial negatively charged CdTe QDs at a concentration of 5 µM. These results indicate that interaction between MR-1 and QDs is heterogeneous; a fraction of MR-1 interacts with commercial QDs. The epifluorescence microscopy pictures of this experiment are presented in Chapter 6. Importantly, there is no indication that only dead bacteria interact with commercial negatively-charged QDs or, *vice versa*, that direct interaction between QDs and MR-1 results in a decrease of viability.

In summary, the nanotoxicity of the commercial, negatively-charged CdTe QDs present no or limited toxicity to MR-1 as shown by two independent methods (CFU and fluorescence viability assay). Those findings generated some confusion as it was shown previously that cadmium-containing QDs increase the ROS production thus generate oxidative stress to bacteria and mammal cell lines (Chen et al., 2012; Oh et al., 2016). The uncertainty was

addressed by employing fluorescence and electron microscopy to characterise the interaction between bacteria and commercial negatively-charged CdTe QDs (see Chapter 7). The possibility of using the the commercial negatively charged CdTe QD in the hybrid system to produce solar fuels (hydrogen) was investigated later (see Chapter 8).

6.4. Nanotoxicity of CdTe/CdS/Cysteamine QDs to *S. oneidensis* MR-1.

S. oneidensis MR-1 was grown and handled as described in Chapter 4.4.1 and 6.2. The same concentrations of 0.05, 0.5 and 5 μM were initially tested. However, useful results were not obtained as the bacteria incubated with 0.5 μM of CdTe/CdS/Cysteamine QDs did not grow. To further investigate the toxicity, nanoscale concentrations of QDs were selected: 0.5, 5 and 50 nM. The CdTe/CdS/Cysteamine nanotoxicity results from 3 independent trials are presented in Fig. 6.4. The concentration of 500 nM is present in Fig. 6.4 for the comparison purpose.

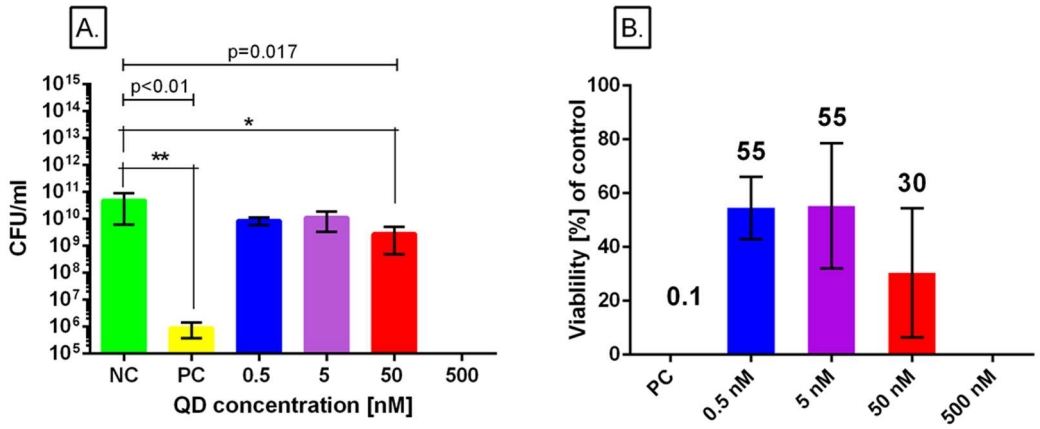

Fig. 6.4. **A.** The use of the colony-forming units technique revealed the severe toxicity of positively charged CdTe/CdS/Cysteamine QDs to MR-1 (n = 3). **B.** Data are presented normalised to the negative control. NC = negative control (addition of an equal volume of 20 mM HEPES, 0.15 M NaCl, pH 7.4); PC = positive control (50 μg/ml kanamycin).

Although only the highest concentration of QDs proved to be significantly toxic, we note that the tested QDs concentrations were in the nanomolar range rather than the micromolar range (compare Fig. 6.4 with Fig 6.2-5.3). The CdTe/CdS/Cysteamine QDs left only 30 % of MR-1 viable after incubation with

50 nM nanoparticles. Nevertheless, the lower concentrations of QDs gave promising results. 55 % of the MR-1 population was viable when incubated overnight with both 0.5 and 5 nM of CdTe/CdS/Cysteamine QDs.

Lovrić at al. investigated the cellular distribution of CdTe QDs with different surface properties in mammalian cell lines (Lovrić et al., 2005). QDs with small sizes and with positive charges on their surface triggered more significant toxicity for cells as documented by MTT assay. These data are in agreement with the results presented here. Firstly, as discussed in Chapter 5.6, cysteamine doped CdTe QDs were 2.5–3 nm in size and emitted yellow light fluorescence (thus higher energy than red emitters). Secondly, the positive charge might give rise to amplified toxicity too. Positively charged CdTe QDs were significantly more toxic to MR-1 than any QDs investigated here.

The above data is very informative and aids the better understanding of the toxicity caused by positively charged CdTe/CdS/Cysteamine QDs discussed in Chapter 5.4. Further, the interaction of these QDs with MR-1 will be studied through the use of fluorescence microscopy, and photoreduction abilities of CdTe/CdS/Cysteamine QDs was assessed; these results are discussed later (see Chapters 7 and 8, respectively).

6.5. Nanotoxicology of $CuInS_2$/ZnS/PMAL to *S. oneidensis* MR-1 and *Escherichia coli*.

The viability of MR-1 and *E. coli* in the presence of $CuInS_2$/ZnS/PMAL (CIS/PMAL) QDs was assessed slightly differently compared to the tests described above. The significant difference was the incubation time of QDs with bacteria. Instead of overnight incubation, three-hour cultures were examined by the colony-forming units method. Cultures of MR-1 in M-1 modified minimal media were incubated with CIS/PMAL QDs at three concentrations: 0.034, 0.34 and 3.4 μM. The obtained data from 5 independent trials are presented in Fig. 6.5.1.

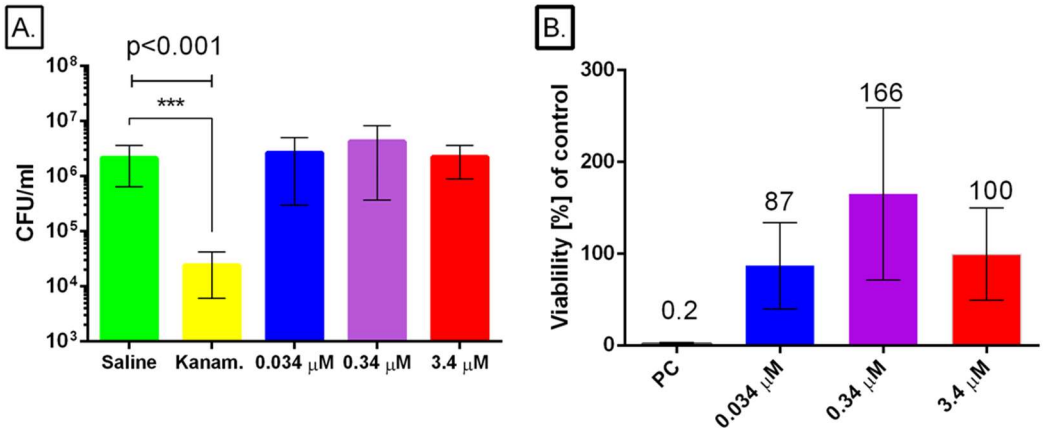

Fig. 6.5.1. **A.** $CuInS_2$/ZnS/PMAL QDs incubated with MR-1 in M-1 media for three hours displayed no toxicity (n = 5). QDs concentrations were 0.034, 0.34 and 3.4 μM. **B.** Normalised data portrayed the lack of toxicity of CIS/PMAL to MR-1. NC = negative control (addition of an equal volume of 20 mM HEPES, 0.15 M NaCl, pH 7.4); PC = positive control (50 μg/ml kanamycin).

Lower toxicity of CIS/PMAL QDs was aimed for, as CIS/PMAL QDs do not contain cadmium. Cadmium from QDs increased the production of reactive oxygen species has previously been shown to add to toxicity (Rzigalinski and Strobl, 2009; Schneider et al., 2009; Suresh et al., 2013). Indeed, CIS/PMAL QDs were documented by Booth and colleagues as particles which did not decrease the viability of HaCat cells until concentrations went above 10 μg/mL (equals 0.34 μM) in a WST-1 assay (Booth et al., 2013). The residual toxicity of CIS/PMAL QDs was postulated as mostly due to the polymer coating (Booth et al., 2013). In contrast, the change of the MR-1 growth dynamics such as the small increase in growth with 0.34 μM CIS/PMAL QDs (Fig. 6.5.1 B) was a surprise and inspired further investigation. For this reason, a control experiment was designed, employed and executed: the examination of PMAL toxicity to MR-1. The chemical structure of PMAL is presented in Fig. 3.5.4.1 in Chapter 3.5.4. The concentration of PMAL in the viability assay is 25 time that of the CIS/PMAL QDs. The obtained results from 3 independent trials are presented in Fig. 6.5.2.

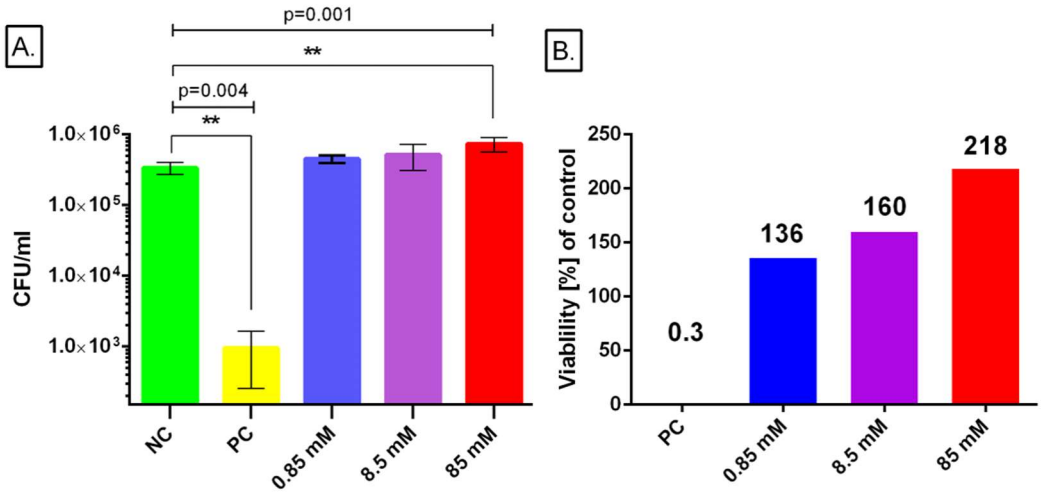

Fig. 6.5.2. The nanotoxicity of PMAL to MR-1 results (n = 3). **A** describes the toxicity in the CFU/ml units, and **B** depicts the normalised data versus NC. NC = negative control (addition of an equal volume of 20 mM HEPES, 0.15 M NaCl, pH 7.4); PC = positive control (50 µg/ml kanamycin).

The PMAL toxicity evaluation showed that MR-1 growth is stimulated at a PMAL concentration of 85 mM. These results inspired further examination of CIS/PMAL and PMAL nanotoxicity to a second bacterial species, namely *E. coli* (OMNIMAX). This experiment aimed to evaluate if MR-1 possesses a unique resistivity to PMAL or that it might be a more common feature in Gram-negative bacteria. Details of the *E. coli* viability experiment when incubated with CIS/PMAL and PMAL are presented in Chapter 4.4.1. The same QDs and PMAL concentrations as shown in Fig. 6.5.1 and 6.5.2 were applied in the described above experiment. The obtained results from toxiciy assessment of CIS/PMAL QDs n = 4 and PMAL n = 3 independent trials to *E. coli* are presented in Fig. 6.5.3.

The $CuInS_2$ core surrounded by a ZnS shell and encapsulated with PMAL molecules proved to be not toxic to MR-1 and control bacteria *E. coli*. PMAL not only makes these CIS QDs hydrophilic but also empowers the creation of a stable colloidal solution. However, the results presented in this chapter showed that 85 mM PMAL also promotes the growth of not only MR-1 but also *E. coli*.

MR-1 is known for its flexible respiratory chain but also for its outstanding ability to metabolise a variety of energy sources, like pyruvate, lactate, acetate and others (Serres and Riley, 2006; Driscoll et al., 2007; Pinchuk et al., 2011). Furthermore, metallic NPs of cerium oxide (CeO_2) when inspected for toxicity

to MR-1 left bacteria unaffected (Pelletier et al., 2010). The experiment mentioned in section 5.1, which focused on the TiO_2 toxicity of to MR-1 was investigated and also showed no severe effects on bacterial viability until the concentration of up to 100 mg/ml (Qiu et al., 2017). The $CuInS_2$/ZnS/PMAL QDs toxicity to MR-1 has never been examined before.

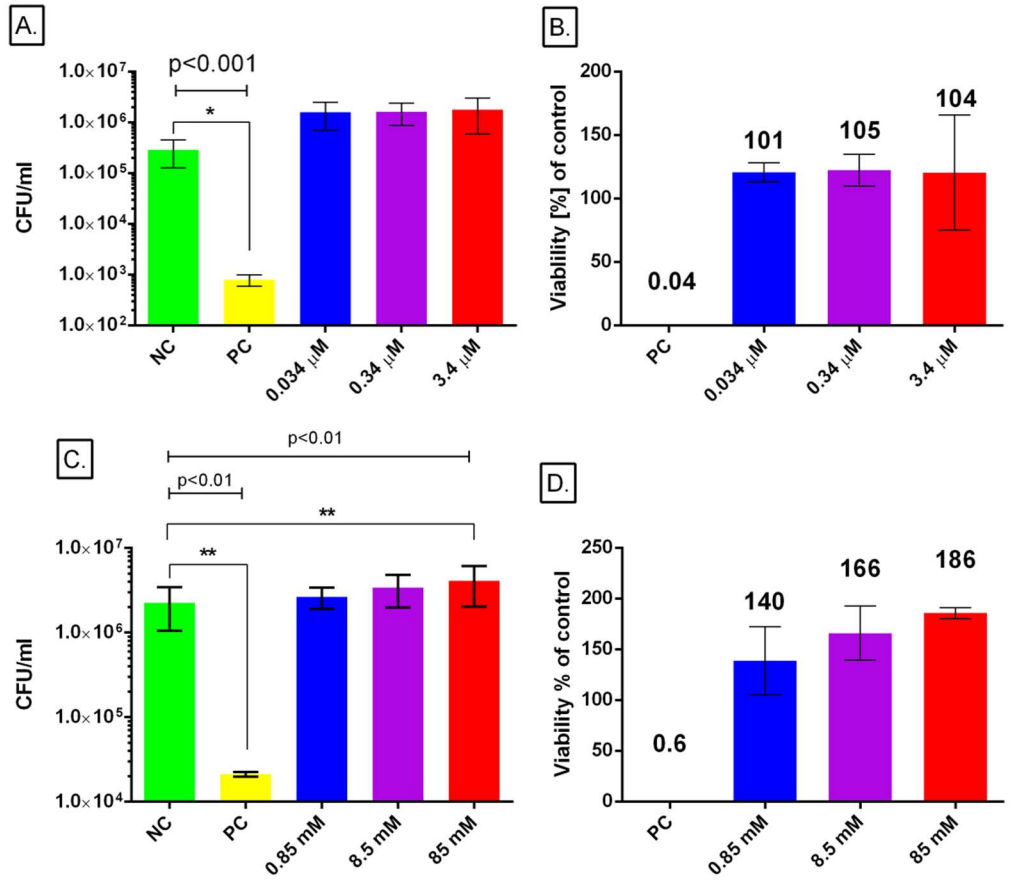

Fig. 6.5.3. **A**. and **B.** CIS/PMAL QDs at tested concentrations were not toxic to *E. coli* (n = 3). **C**. and **D.** *E. coli* growth was stimulated by 85 mM PMAL (n = 3). **A** and **C** present the data in CFU/ml, while **B** and **D**, show the data normalised to the negative control experiment. NC = negative control (addition of an equal volume of 20 mM HEPES, 0.15 M NaCl, pH 7.4); PC = positive control (50 µg/ml kanamycin).

The results presented here led to further investigations into the interaction of CIS/PMAL with MR-1 as well as the examination of QDs and different *Shewanellaceae* in the hydrogen-producing hybrid system. These results are presented in Chapter 6 and 7, respectively.

6.6. Nanotoxicology – Summary.

As a wide variety of nanoparticles continue to be developed and the quantity of nanoparticles introduced into the environment increases, nanotoxicology becomes a crucial task for scientists to develop and investigate. Ways of limiting NP toxicity to animals and humans should be established and introduced in nanoparticle production. The QDs employed in the research discussed here were to be used in biotic-abiotic hybrid systems that produce hydrogen. Those devices must not produce harmful pollutants that have a long lifetime in the environment.

Method / QDs/Chem.	Bacteria Tested	Concentration of QDs/Chemical	Nanotoxicity Results
CdTe/CdS/TGA	MR-1	0.05, 0.5 μM	Toxic
Commercial CdTe	MR-1	0.05, 0.5, 5 μM	Not Toxic
CdTe/CdS/Cysteamine	MR-1	0.5, 5, 50 nM	Toxic
$CuInS_2$/ZnS/PMAL	MR-1	0.034, 0.34, 3.4 μM	Not Toxic
	E. coli	0.034, 0.34, 3.4 μM	Not Toxic
PMAL	MR-1	0.85, 8.5, 85 mM	Stimulant
	E. coli	0.85, 8.5, 85 mM	Stimulant

Table 6.6. The table depicts the nanotoxicology results of diverse QDs at different concentrations to MR-1 and *E. coli*. The outcomes were classified as a stimulant (bacterial growth was stimulated), not toxic, and toxic. Abbreviation used: chem. – chemical.

The results presented in Chapter 6 allowed the QDs to be divided into three groups: not toxic, toxic, and stimulating bacteria growth. The colony-forming unit method and fluorescence dye staining using PI enabled the understanding of QD toxicity to MR-1 and the control *E. coli* strain. A summary of the QD nanotoxicology assessment is presented in Table 6.6. Encouraging results for CIS/PMAL QDs proved not toxic to MR-1 and *E. coli*. CIS/PMAL QDs present no toxicity to investigated bacteria at the concentrations used. Additionally, MR-1 and *E. coli* growth were stimulated by a zwitterionic polymer (PMAL) that encapsulated CIS QDs core.

Although, the toxicity of CdTe/TGA, note lack of the shell, was assessed before (Schneider et al., 2009), there is no data present in the available literature which has investigated the toxicity of the commercial negatively

charged CdTe and CdTe/CdS/Cysteamine QDs to MR-1. In contrast to CIS/PMAL toxicity, commercial negatively charged CdTe QDs also evidenced no statistically significant toxicity to MR-1, however, it relays in disagreement with the results available in the literature (Rzigalinski and Strobl, 2009). Certainly, the increased number of repetitions performed by CFU and fluorescence viability assay would help better understanding of the investigated system. The employment of fluorescence activated cell sorting (FACS) method would bring more confidence to results obtained.

The QDs discussed here will now be evaluated for interaction with MR-1 by fluorescence and electron microscopy. These results are presented and described in Chapter 7.

Chapter 7. Quantum Dot Interaction with *S. oneidensis* MR-1.

7.1. Microscopy History and Further Applications.

Quantum Dots have been heralded as a novel fluorescent probe for, among others, fluorescent microscopy, because they are bright, have high quantum yields and do not photobleach like organic fluorescent dyes (Bera et al., 2010). Before microscopy of QDs and their interaction with the bacterium *Shewanella oneidensis* is described, this chapter will give a brief historical overview of microscopy.

The first approach to microscopy was already recorded by Seneca almost 2000 years ago, who used spherically shaped glass filled with water to magnify small objects (Seneca, ca 62 AD). However, fluorescent microscopy did not develop until the 19th century**.** The most important discoveries, including electron microscopy, are summarised in chronological order Table 7.1.

In 1845, Sir F. W. Herschel observed that colourless tonic water, when illuminated by the UV lamp, becomes bright blue. Quinine in tonic water absorbs UV light and emits fluorescence at a longer wavelength. This fluorescence shift is known as the Stokes shift (Stokes, 1852).

Fig. 4.2 presented in Chapter 4.2 shows the example of Stoke's shift in the absorbance and fluorescence emission of CdTe/CdS/TGA QDs. After Stoke's findings, E. Abbe described the limits of optical resolution (Eq. 6.1) and concluded that the lateral resolution limit of a lens-based optical microscope is about half of the illuminating wavelength (Abbe, 1873).

$$r = \frac{\lambda}{2NA} \qquad \text{Eq. 7.1.}$$

In the Eq. 7.1 r is the minimum distance between resolvable points – the resolution [nm], λ – the wavelength [nm], NA– the numerical aperture, a dimensionless number that characterises the range of angles over which the system can accept or emit light.

In 1990, the green fluorescence protein (GFP) was discovered and isolated from the jellyfish Aequorea Victoria (Prasher et al., 1992). Simultaneously, confocal laser scanning microscopy (CLSM) became commercially available,

significantly advancing the field of fluorescence microscopy. In confocal scanning microscopy, originally built and patented by Minsky (1961), only a single point of a specimen is illuminated with a light source at a time. An entire image (in all three directions) is recorded by scanning the specimen; this reduces background and secondary fluorescence (i.e. signal-to-noise). Furthermore, a pinhole limits the detection of fluorescence out of a focal plane (Fig. 6.1.1.), increasing optical resolution, especially in the depth direction (Minsky, 1961).

Date	Name	Discovery	Ref.
62 AD	Seneca	Magnifying properties of water-filled bottle	Seneca, ca 62 AD
1266-67	R. Bacon	Telescope	Bacon, 1267
1650	C. Huygens	Light Microscope	Huygens, 1622
1845	F. W. Herschel	Fluorescence Microscope	Herschel, 1845
1852	G. G. Stokes	Distance between absorbance and emission maxima.	Stokes, 1852
1873	E. Abbe	Optical Resolution Limit	Abbe, 1873
1931	E. Ruska	Transmission Electron Microscope	Ruska, 1987
1937	M. Ardenne	Scanning Electron Microscope	Ardenne, 1938
1961	M. Minsky	Pihole Aparatus	Minsky, 1961
1988	J. C. H. Spence	High-resolution TEM	Spence, 1988
1992	D. C. Prasher	Green Fluorescence Protein	Prasher et al., 1992
1994	S. W. Hell	STED	Hell and Wichmann, 1994

Table 7.1. A short history of documented microscopy evolution. Used abbreviations include: TEM – transmission electron microscopy, STED – stimulated emission depletion.

Thus, CLSM enables the visualisation of thin sections of a specimen with excellent focus and selective excitation.

Although not used in the research discussed here, it would be an omission not to mention the various super-resolution confocal fluorescent microscopes, which inventions were honoured with the Nobel Prize in 2014. For instance, in 1994, Stefan Hell developed stimulated emission depletion – STED microscope. STED creates the image of the specimen by selective deactivation of fluorophores, producing a higher resolution image by recording single fluorescent molecules one at a time. The width of a single light spot,

produced by a single fluorescent dye that is temporarily 'activated', is still determined by the optical resolution as described by Abbe, but the centre of a single light spot can be determined with a higher resolution. By activating/deactivating one fluorescent dye at a time, a high resolution image can be built up over time. The altered light beam scans through the specimen and creates an image with an improved resolution of 90 – 100 nm (Klar et al., 2000).

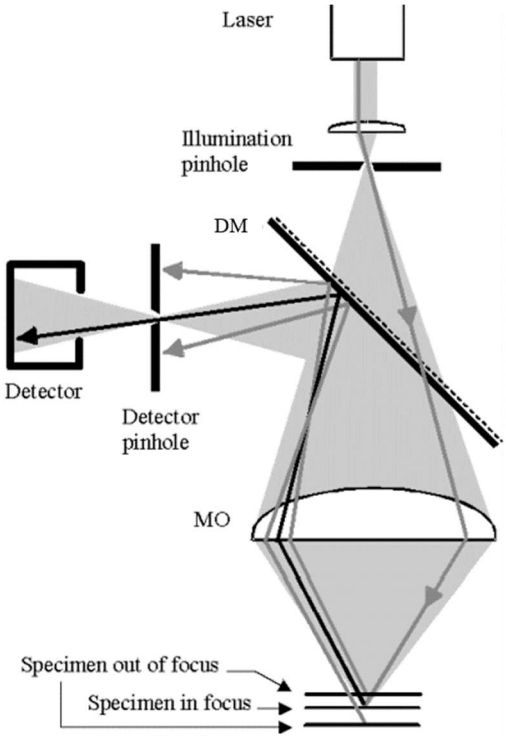

Fig.7.1.1. Schematic of confocal microscopy with the designed by Minsky pinhole apparatus (redrawn from Jordan et al., 1998). Focused on the pinhole, illuminating light source (laser) that runs through a dichroic mirror (DM), is imaged onto the object focal plane of the microscope objective (MO). The in-focus specimen leads to a maximum emission of light that is firstly reflected by DM and further focused by the detector pinhole. The light from the out of focus is partially blocked. Abbreviations used here: DM – dichroic mirror, MO – microscope objective. Figure redrawn from Abbe 1873.

In-depth visualisation of biological species can also be obtained by electron microscopy (EM). The first transmission electron microscope (TEM) was invented in 1931 by Ruska, who in 1986 was awarded a Nobel Prize (Ruska, 1987). TEM is valued for the increased resolution, which nowadays is of 0.2 nm and can visualise two atoms apart (Kisielowski et al., 2008; Erni et al., 2009). Nearly simultaneously to the development of TEM, in 1937 scanning electron microscopy (SEM) was pioneered by Manfred von Ardenne. Contrary to TEM, SEM visualises the topography of the specimen and is based on the detection of scattered electrons.

Fluorescence microscopy is of particular interest here as it is the primary tool to examine the interaction of bacteria with a variety of quantum dots. This

interaction is essential to encourage the hybrid system of bacteria and QDs to produce fuel. Therefore the interaction between bacteria and fluorescent quantum dots was investigated in depth. In the following sections, all QDs described in Chapter 4, and 5 are examined with inverted epifluorescent microscopy. When the interaction was observed, further characterisation was performed with transmission electron microscopy.

7.2. CdTe/CdS/TGA Quantum Dots Interplay with *S. oneidensis* MR-1.

The initial investigation studied whether electrostatic interactions could couple *S. oneidensis* MR-1 (MR-1) with negatively charged CdTe/CdS/TGA QDs. In the available literature, MR-1 is described to have either a negative or a positive surface charge (Dague et al., 2006; Korenevsky and Beveridge, 2007; Furukawa and Dale, 2013). Furukawa showed that MR-1 possesses a small negative surface charge due to the presence of lipopolysaccharide (LPS) in the outermost cell layer. Contrary, Korenevky and Beveridge argued that MR-1 has a small positive charge of about 7.6 mV in aerobic conditions (Korenevsky and Beveridge, 2007).

MR-1 was grown aerobically in M-1 media (see Section 4.4.1 for details) to an optical density of ~0.4 at 600 nm after which CdTe/CdS/TGA QDs (0.05 or 0.5 µM, Emission = 550 nm, see Section 5.2) was added. QDs at appropriate concentration added to 1 ml of bacterial cultures were further incubated in 15 ml flasks overnight (~18 h) at 30 °C, 200 RPM. The following day, bacteria were harvested by centrifugation (5000 RPM, t = 10 min). The supernatants were discarded and pellets suspended in 1 ml of 0.15 M NaCl, 20 mM HEPES pH 7.2. Centrifugation was repeated 3 times to ensure the removal of unbound QDs. Following these steps, 5 - 10 µl of samples were put onto poly-L-lysine coated glass slides and covered with a coverslip. Poly-L-lysine is a biocompatible cationic polypeptide that has been intensively studied and broadly used in a wide range of applications, providing one of the most commonly used substrate coatings to allow cell adhesion (Mazia et al., 1975; Heath et al., 2015). The prepared slides were rested for 10 min to minimise

the bacteria motility after which they were examined with the epifluorescent microscope. Appropriate filter settings used in the microscope are given in Fig. 7.2.1.1. Epifluorescence microscopy revealed that CdTe/CdS/TGA QDs interacted with only a minor subpopulation of MR-1. It is possible that this subpopulation represents bacteria with damaged membrane integrity. It was also observed that MR-1 cells became longer in the experimental conditions. The cells became elongated after the overnight QDs exposure to 0.5 μM CdTe/CdS/TGA QDs and presented the average length of 6.8 μm with an SD of 2.9 nm (n = 3). The measurement discriminated whether cells interacted or not with QD. MR-1 incubated with 0.5 μM CdTe/CdS/TGA QDs were 2.5 longer than control bacteria.

Bacteria cell elongation, known as filamentation, has been documented as a reaction to environmental stress (Kloepfer et al., 2005; Schneider et al., 2009; Dumas et al., 2010; Pramanik et al., 2018). For instance, Schneider et al. showed that more than 90 % of MR-1 grown in LB medium supplemented with 1 μM of CdTe/TGA QDs showed elongated cell size (at least twice longer than control). Oxidative stress experienced by bacteria is thought to inhibit cell division, while cell biomass increased (Schneider et al., 2009). Interruption of chromosome replication following DNA damage has also been proposed to induce bacteria filamentation (Huismant et al., 1984).

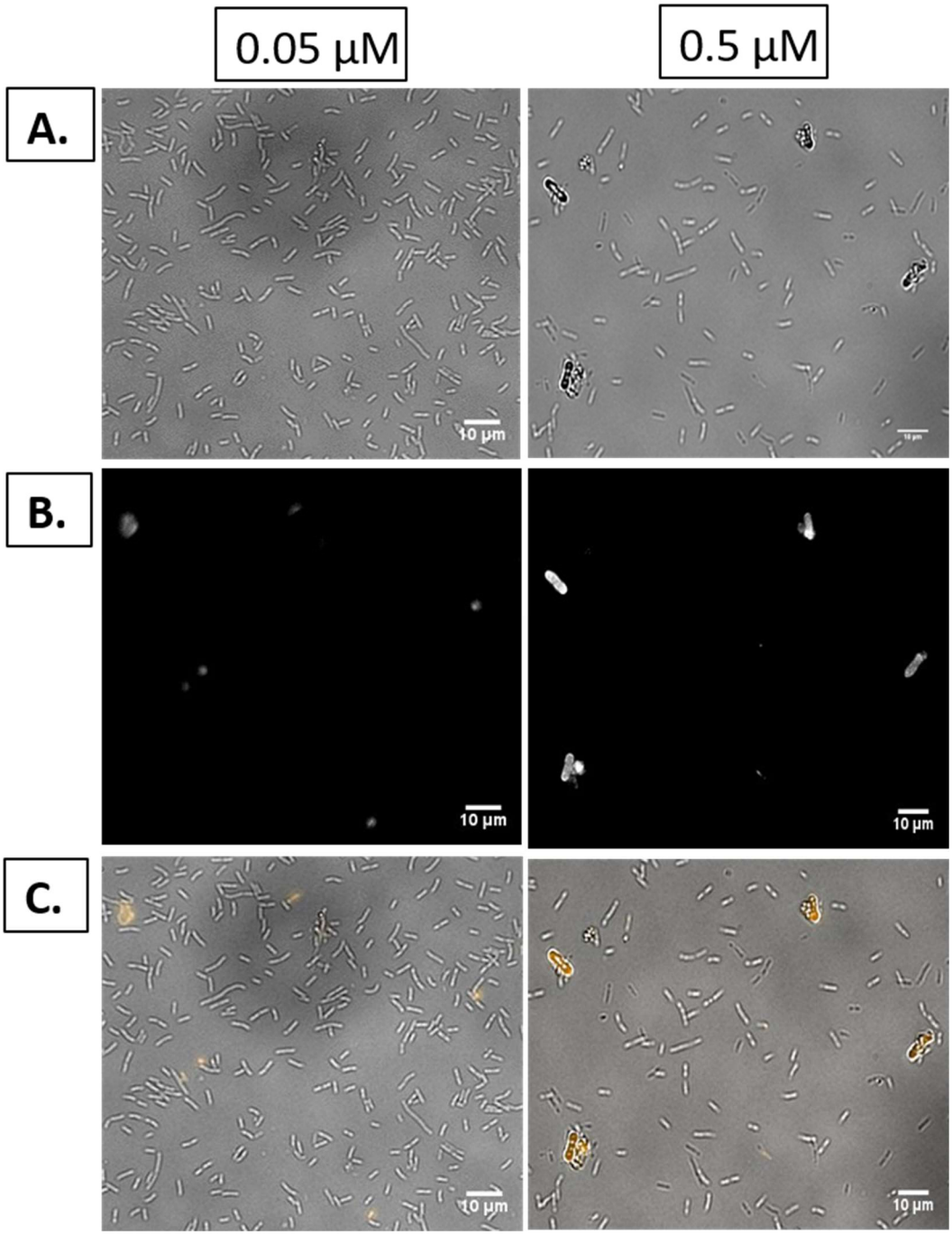

Fig. 7.2.1.1. The interaction of MR-1 with two concentrations of CdTe/CdS/TGA QDs was investigated. Columns present concentrations of CdTe/CdS/TGA QDs. Row A shows the bright field images, B fluorescence and C merged A and B. Filter setting used included excitation at 410 ± 15 nm, dichroic mirror 500 nm and the emission filter 580 ± 25 nm. Scale bars are 10 µm.

Further research was undertaken to establish whether a heat shock would facilitate the interaction or uptake of CdTe/CdS/TGA QDs to MR-1. Heat shock is commonly used to transform bacteria with (negatively charged) DNA, including plasmids. During this procedure, cells are exposed to the high

temperature (42 °C) for a short time (usually 30 - 60 s) to increase membrane permeability and create transient membrane pores.

MR-1 was grown as described in Section 4.4.1. Bacteria in the mid-logarithmic growth phase were put into an ice bath for 30 min. Subsequently, CdTe/CdS/TGA QDs (0.05 or 0.5 μM; emission = 550 nm, see Section 5.2) were added to bacteria. Next, samples were incubated at 42 °C for 30 or 60 s and afterwards placed on ice. Microscopy samples were prepared as discussed in Section 7.2 (Fig. 7.2.1.2).

S. oneidensis MR-1, which underwent heat shock procedure with 0.05 and 0.5 μM CdTe/CdS/TGA QDs, did not show any interaction. Although the heat shock procedure still lengthened the bacteria, the increase in size was much less compared to the over-night incubation (3.7 ± 1 nm and 3.6 ± 1.4 nm for heat shock with 0.05 and 0.5 μM CdTe/CdS/TGA QDs, respectively, compared to 2.7 ± 0.4 μm for the control). Visible were also some small aggregates which showed interaction with QDs. However, these were not bacterial cells (see Fig. 7.2.1.2 C).

As no interaction with MR-1 was observed, different *Shewanella* species were tried. In comparison to other tested bacteria*, Shewanella putrefaciens* CN-32 (CN-32) has the highest positive surface potential and hence the best chance to show electrostatic binding to the negatively charged CdTe/CdS/TGA QDs (Korenevsky and Beveridge, 2007). CN-32 was grown aerobically up to an optical density of 0.4 and then incubated overnight with 0.5 μM CdTe/CdS/TGA QDs. The CN-32 cells were treated the same as MR-1 described in Section 6.2 and visualised by epifluorescent microscope (Fig. 7.2.1.3).

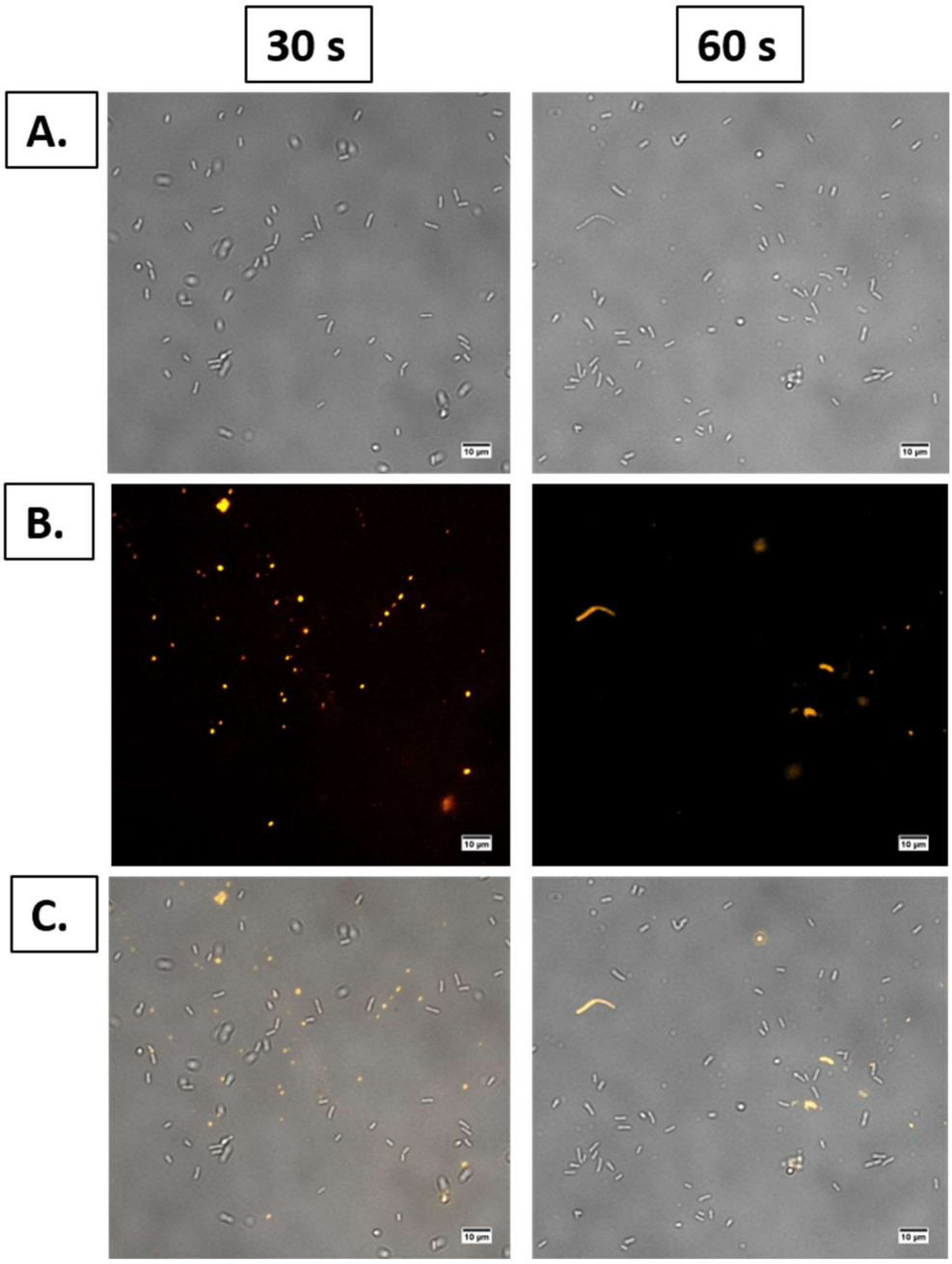

Fig.7.2.1.2. The evaluation of heat shock procedure on MR-1 and 0.5 μM CdTe/CdS/TGA QDs was performed with the epifluorescence microscope. The columns present 30 s and 60 s of MR-1 incubation time in the temperature of 42 °C. A – bright field, B. fluorescence, C. merged A and B. The microscope filters used here were 410 ±15 nm for excitation and a 580 ± 25 nm for emission. Scale bars are 10 μm.

Like MR-1, CN-32 did not show any interaction with CdTe/CdS/TGA QDs. Additionally and in contrast to MR-1, no size abnormalities were observed for CN-32 incubated with 0.5 μM CdTe/CdS/TGA QDs.

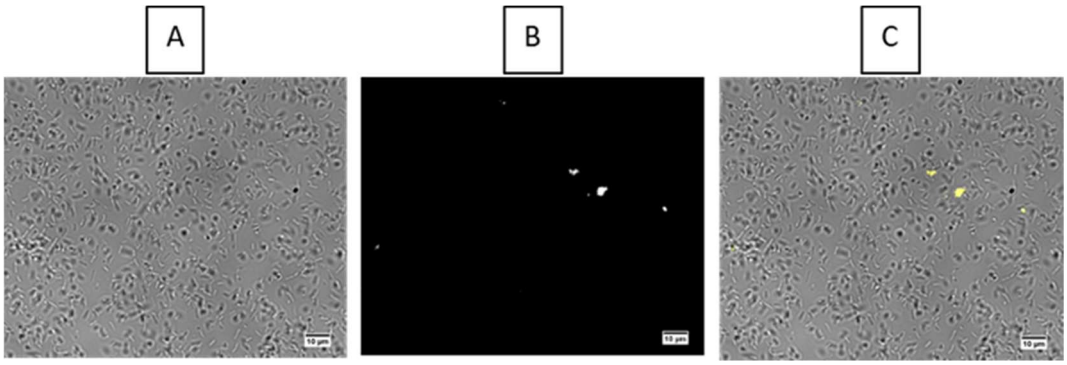

Fig. 7.2.1.3. Obtained by the epifluorescent microscope images of CN-32 incubated with 0.5 μM CdTe/CdS/TGA QDs for overnight. **A** – bright field, **B** – fluorescence, **C** – A and B merged. The used filter setting was the same as in Fig. 6.2.1.2. Scale bars are 10 μm.

In summary, CdTe/CdS/TGA QDs at two tested concentrations of 0.05 and 0.5 μM did not show any interaction with MR-1 or CN-32. Either simple incubation or heat shock treatments did not induce binding. Consequently, electrostatic interactions between aerobically cultured and potentially positively charged MR-1 and CN-32 with CdTe QDs capped with thioglycolic acid was not sufficient to induce binding.

7.3. Positively Charged CdTe/CdS/Cysteamine QDs Interaction with *S. oneidensis* MR-1.

As MR-1 did not bind with negatively charged CdTe/CdS/TGA QD, the further experiment aimed to investigate electrostatic interaction with positively charged CdTe/CdS/Cysteamine QDs (emission = 580 nm). Since Korenevsky and Beveridge, 2007 and Halder et al., 2013 describe contradicting results for the surface charge of MR-1, it could be that MR-1 has a mostly negative potential and thus bind to positively charged QDs.

MR-1 was grown and incubated with CdTe/CdS/Cysteamine QDs as in Section 7.2. Due to the severe toxicity of positively charged CdTe/CdS/Cysteamine QDs (see Chapter 6), only nanomolar concentrations of QDs were investigated at first.

Very little interaction was observed at 50 nM (Fig. 7.3.1), and thus, despite its toxicity, MR-1 was also aerobically incubated at a higher concentration of CdTe/CdS/Cysteamine QDs (0.5 μM) at various times. The experiment

included 1 h, 3 h, and overnight incubation. Representative pictures are shown in Fig. 7.3.2. Even at 0.5 μM, no interaction was observed.

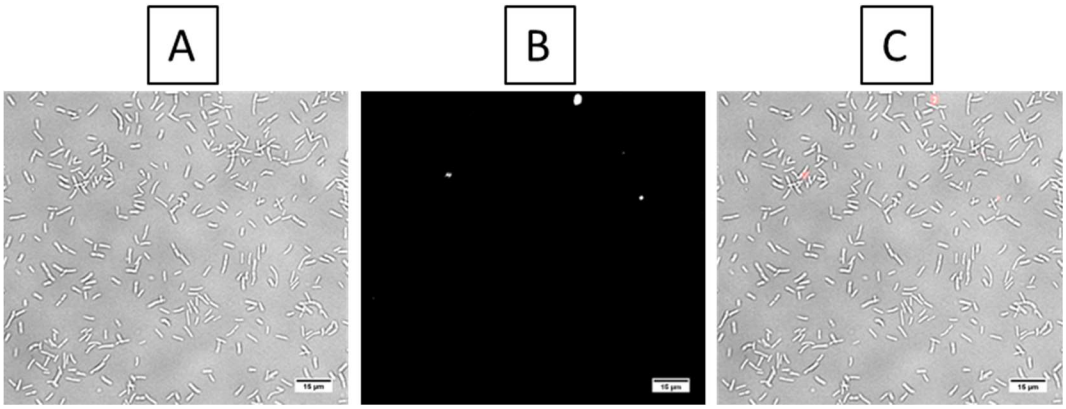

Fig. 7.3.1. Overnight incubation of MR-1 with 50 nM CdTe/CdS/Cysteamine QD revealed no interplay as inspected by epifluorescent microscope. A - bright field, B – fluorescence and C – merged A and B. The filter settings employed here were excitation 410 ±15 nm, dichroic mirror 500 nm, emission 580 ± 12.5. Scale bars are 15 μm.

Similarly to MR-1 incubated with CdTe/CdS/TGA QDs, the size of the MR-1 cell was increased after incubation with CdTe/CdS/Cysteamine**,** but to a smaller extent. MR-1 length after overnight incubation with both 50 nM and 0.5 μM CdTe/CdS/TGA QDs increased to an average of 4.0 ± 1.1 μm. Bacteria became about 1.5 times longer as compared to the control bacteria that were grown without QDs.

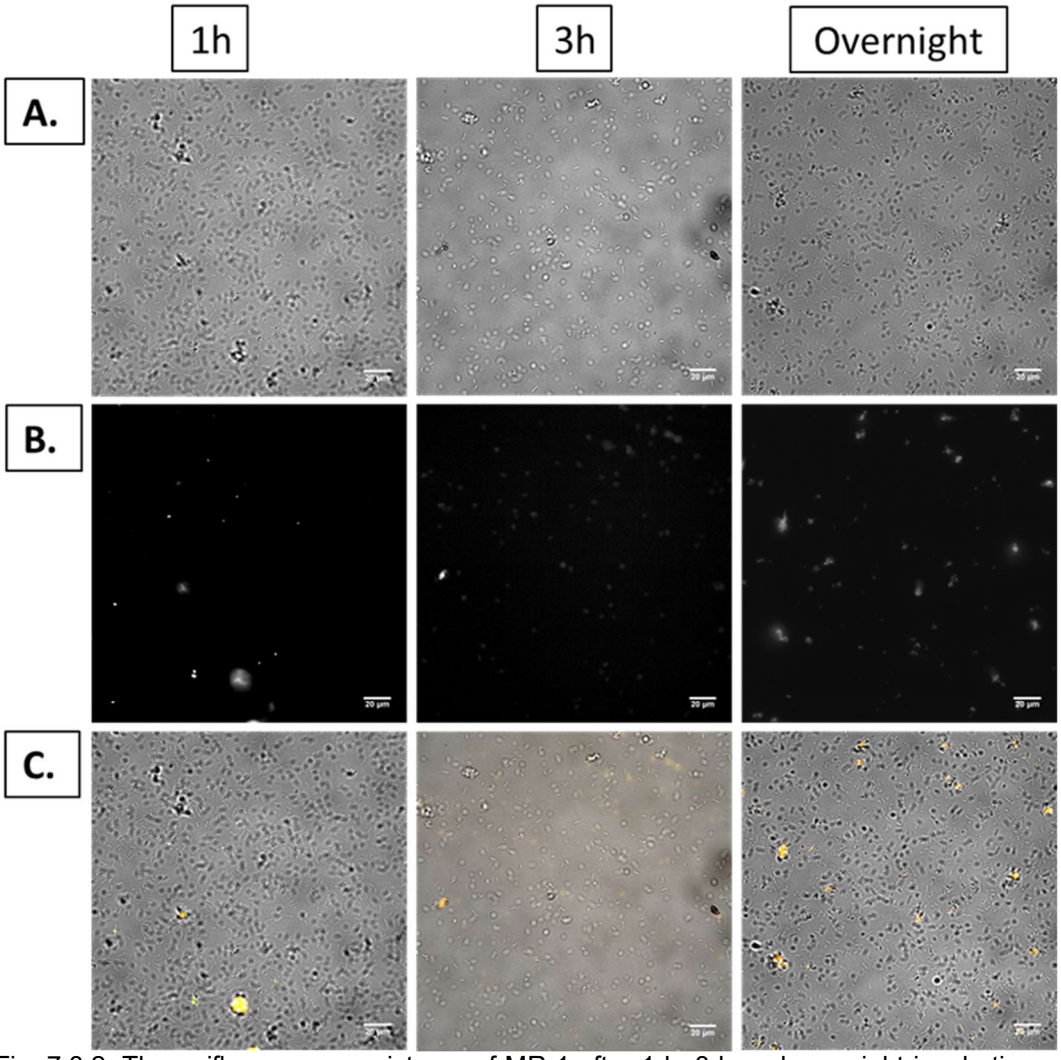

Fig. 7.3.2. The epifluorescence pictures of MR-1 after 1 h, 3 h and overnight incubation with 0.5 μM CdTe/CdS/Cysteamine QDs. The columns show incubation time and rows present A. bright field, B. fluorescence, C. A and B merged. The filters settings used here were the same as in Fig. 6.2.2.1. All scale bars are 20 μm.

7.4. Negatively Charged Commercial CdTe QDs Interaction with *S. oneidensis* MR-1.

Because no binding of QDs was observed based on electrostatic interactions, it was attempted to modify QDs with compounds that are known to tightly bind to Gram-negative bacteria (Rice et al., 2015). Dipicolylamine molecules are widely used as specific sensors to Gram-negative bacteria. Dipicolylamines selectively and preferentially bind zinc ions to create a positively charged binding pocket in the molecule, which creates coordination bonds with negatively charged species like lipopolysaccharides on Gram-negative bacteria surface (Lakshmi et al., 2004; Ngo et al., 2012; Yuen and Jolliffe,

2013; Rice et al., 2015). It was thus attempted to modify commercial QDs by cross-linking them with dipicolylamines.

However, upfront crosslinking, MR-1 was incubated with unmodified commercial, negatively charged CdTe QDs (emission at 530 nm) as described in Section 6.2. The tested concentrations of negatively charged commercial CdTe QDs were 0.05, 0.5 and 5 μM. Low concentrations (0.05 and 0.5 μM) only showed a small degree of interaction with commercial QDs. Interestingly, however, even without further modification, a significant number of bacteria were coated with commercial QDs when incubated at 5 μM (Fig. 7.4.1).

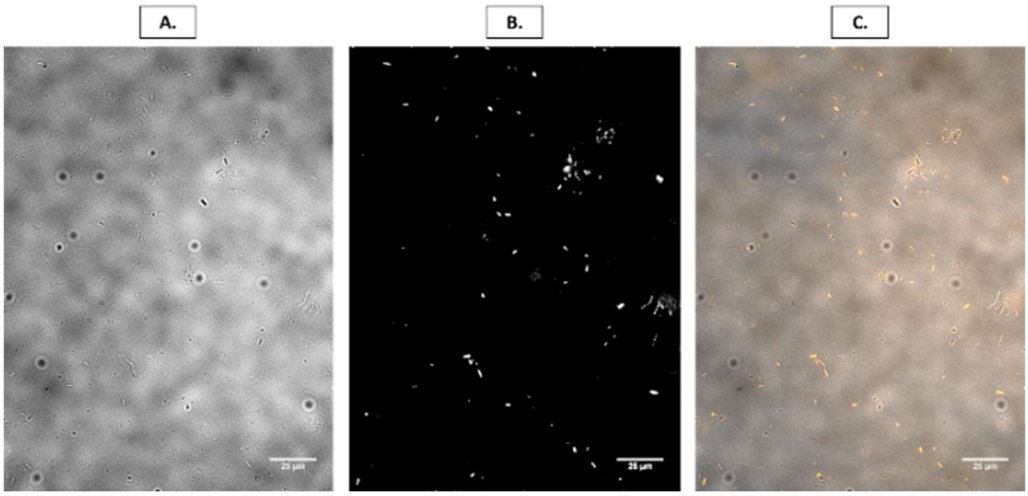

Fig. 7.4.1. After overnight incubation, the commercial negatively charged CdTe QDs (5μM) presented a significant level of interaction with MR-1. **A** – bright field, **B** – fluorescence, **C** – merged pictures. The filter settings in the microscope included: excitation 410 ±10 nm, dichroic mirror 500 nm, emission 535 ±24 nm. All scale bars are 25 μm.

A live-dead assay was performed to study if the observed interaction is related to the viability of this sub-population. General nanotoxicological effects of commercial negatively charged CdTe QDs to MR-1 was already discussed in Section 5.3 by monitoring colony forming units (CFU) and, here, MR-1 was treated as described in the previous section, but the fluorescence dye - propidium iodide (PI) – was used to determine whether a bacterium is viable. The non-permeable dye PI interacts with DNA of dead bacteria only as the dead bacteria have impaired membrane integrity. Fig. 7.4.2 shows the control experiments of untreated MR-1 (negative control) and incubated with prop-2-ol for 30 min (positive control). The fluorescent microscopy results of this investigation are presented in Fig. 7.4.3.

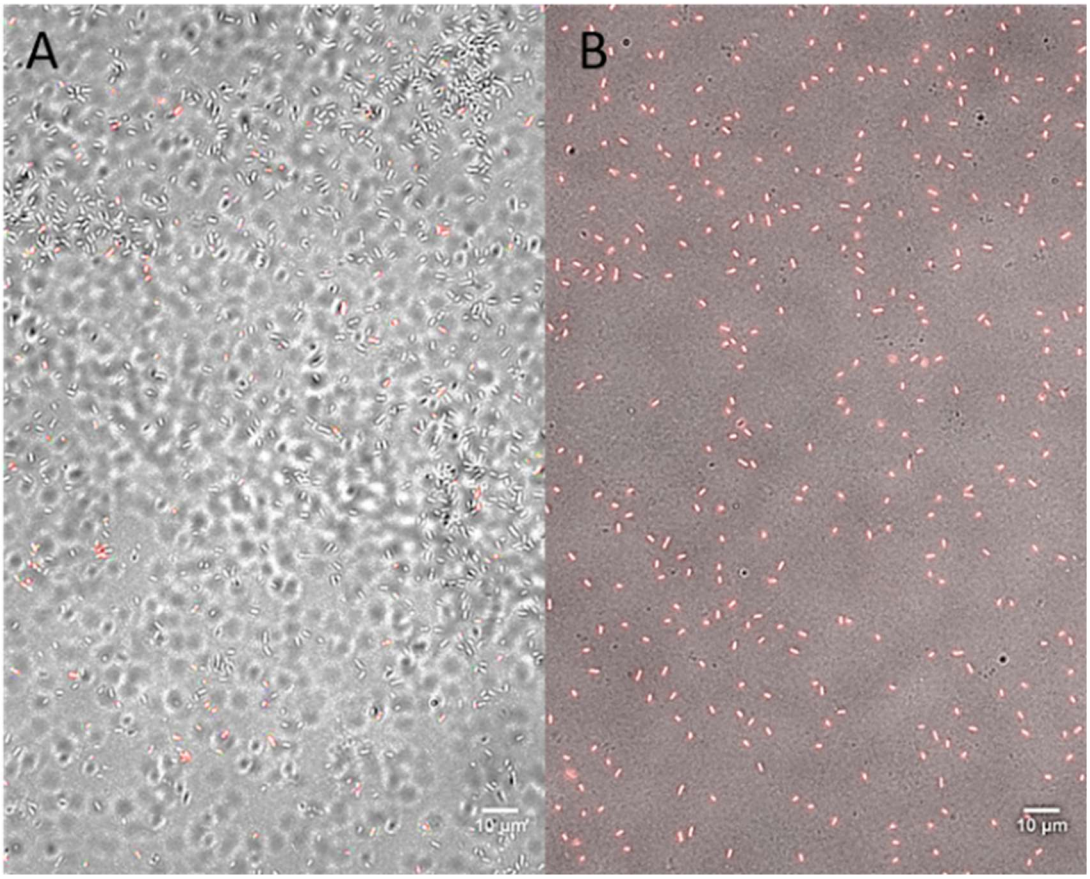

Fig. 7.4.2. The negative and positive controls of MR-1 investigated with the bacterial fluorescence viability assay. The micrographs are overlays of bright field, and fluorescence. Picture **A** portrays the negative control to which an equal volume of 20 mM HEPES, 0.15 M NaCl, pH 7.4 was added. 88 % of bacteria is viable in representative samples (n=3). **B** shows the MR-1 after 30 min incubation with prop-2-ol. Bacteria were stained (shown here in red) with propidium iodide (PI). The filter settings used here include PI excitation at 560 ±27.5 nm, emission 650 ±37.5 nm with a dichroic mirror at 595 nm. Scale bars are 10 µm.

Micrographs were analysed by manually counting PI stained and QD stained bacteria in the fluorescent micrographs. Three representative images of each concentration of QDs were analysed for each QD concentration. The findings were already discussed in Chapter 6, and the obtained results are shown in Fig. 6.3.2. The low number of PI-stained bacteria confirmed previous viability studies (CFU method, Section 6.3) that commercial CdTe QDs are not toxic to MR-1 after overnight incubation.

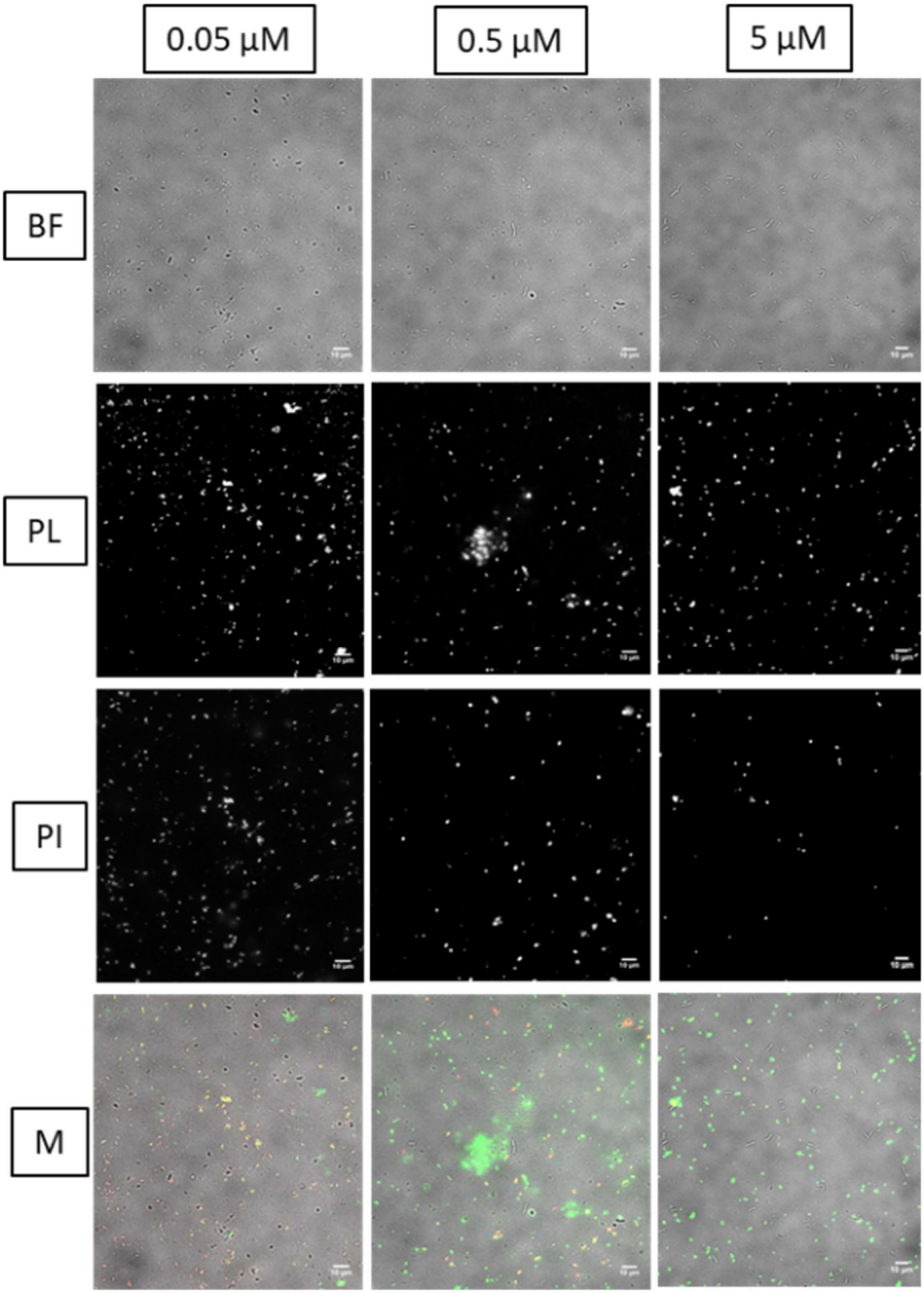

Fig. 7.4.3. The representative pictures of three concentrations of commercial negatively charged CdTe QDs incubated overnight with MR-1 and stained with propidium iodide (PI). In columns marked are the QDs concentrations and in rows, the BF – bright field, PL – photoluminescence, PI – propidium iodide, M – merged channels. The green channel was used for PL and red for P, thus dead and interacting with QDs MR-1 present as yellow. The filter settings used here were for PI excitation at 560 ±27.5 nm, emission 650 ±37.5 nm with a dichroic mirror at 595 nm, and for commercial negatively charged CdTe QD excitation at 410 ± 10 nm, emission at 535 ± 24 nm with the dichroic mirror that reflects the light of the wavelength shorter than 500 nm. All scale bars are 10 µm.

are importantly, however, analysis of interaction and viability of MR-1, incubated with commercial negatively charged QDs, shows that a significant number of bacteria are both viable (not PI stained) while interacting with commercial QDs (Figure 7.4.1). Such results encouraged further and more detailed study of the above interaction by transmission electron microscopy (TEM). TEM was used to identify the location of the commercial QDs concerning the bacterial cell and discussed in the next section (7.4.1).

7.4.1. Interaction of Commercial Negatively Charged CdTe QDs with *S. oneidensis* MR-1 Investigated by Transmission Electron Microscopy.

MR-1 was grown and treated with commercial negatively charged CdTe/QDs, as discussed in the previous section. The QDs concentration of 5 μM presented an excellent interaction with MR-1, as shown in Fig. 7.4.1 and 7.4.3 and thus was the concentration selected for transmission electron microscopy (TEM) examination. After the overnight incubation, the sample was centrifuged as described above, and fixed by 2.5 % glutaraldehyde in 0.1 M phosphate buffer for 2.5 hours. Details of sample preparations are described in Section 4.7.2.2. The representative pictures of control - untreated (A and B) and treated with 5 μM commercial CdTe QDs bacteria (C - F) are presented in Fig. 7.4.1.1.

Control samples show a healthy lipid bilayer structure, and cell division was visual too (Fig. 7.4.1.1 A and B). However, samples of MR-1 with commercial QD presented a significant number of bacteria with disrupted membranes. In some micrographs, QDs were visible in the cytoplasm (red arrows in Fig. 7.4.1.1 C, D, E) and also interacting with the membrane of, possibly, dead bacteria (red arrow at Fig. 7.4.1.1 C, E, F). QD agglomerates were also visible outside of bacteria (Fig.7.4.1.1 F). These results are much unexpected as these QDs were shown by fluorescence live/dead assay and by CFU method to have no significant toxicity to MR-1 (please see Chapter 6 for more details).

The obtained electron micrographs were reexamined, and bacteria were classified into four groups: viable and interacting with QD, viable and not interacting with QDs, dead and interacting with QDs, dead and not interacting

with QDs. Viable bacteria are defined as those with unimpaired membranes. The data were obtained by manual counting and is presented as the percentage of total bacteria counted (Fig. 7.4.1.2). The number of repetition of this experiment is n=1. Bacteria in the control sample (Ctrl) were grown aerobically in M-1 medium at 30 °C with 200 RPM shaking, and no QDs were added.

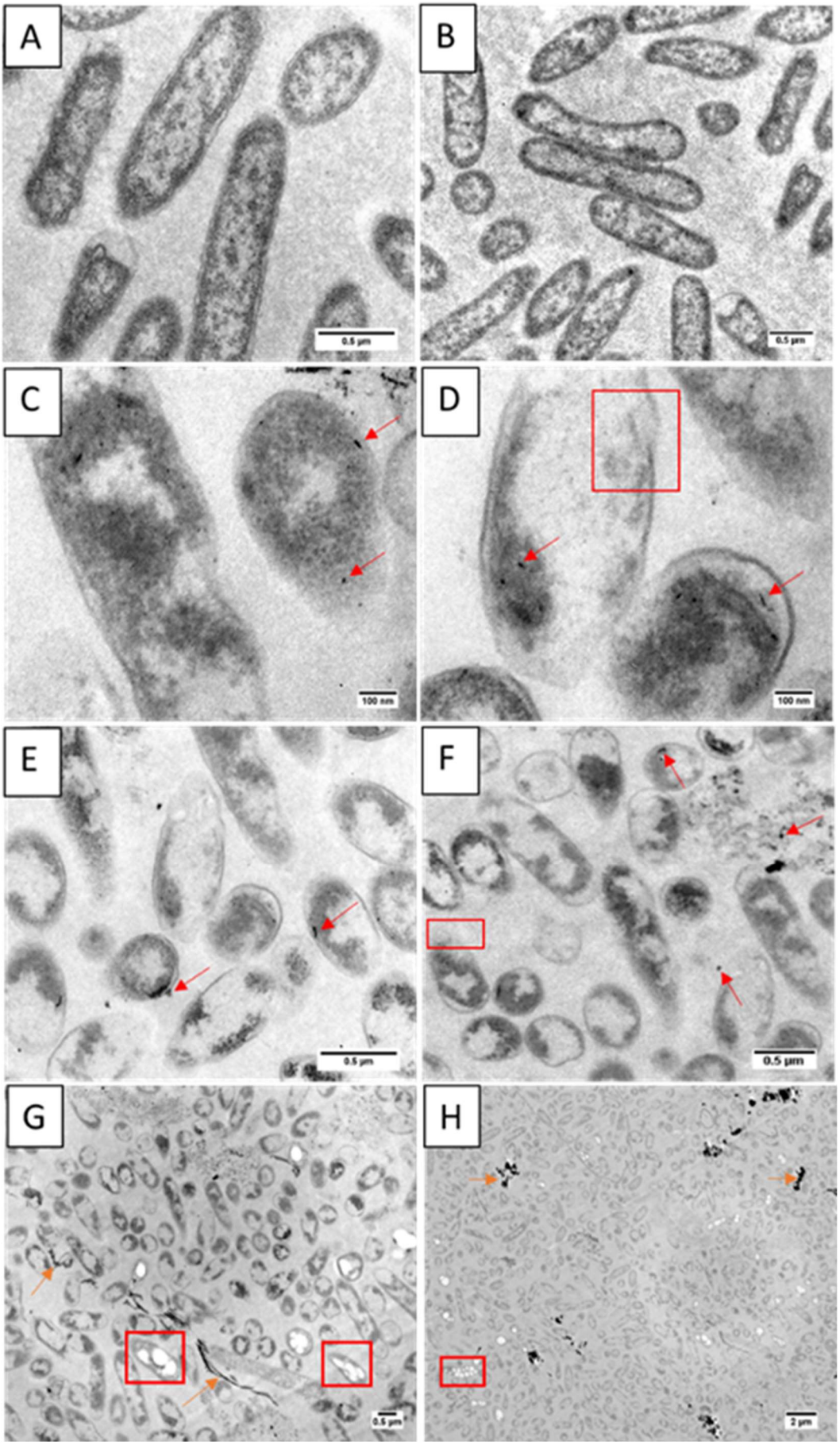
A
B
C
D
E
F
G
H

Fig.7.4.1.1. Thin-section unstained transmission electron microscopy images of MR-1 after overnight incubation with 5 μM commercial negatively charged CdTe QDs. **A** and **B** show the control, **C - H** show the experimental samples. Red arrows indicate the electron-dense places where it is believed cadmium containing QDs are present. The orange arrows show the commercial CdTe QDs agglomerates. The red rectangles show some examples of membrane disruption and cell lysis. The scale bars of pictures A, B, E, F, G, H are 0.5 μm and on C and D are 100 nm.

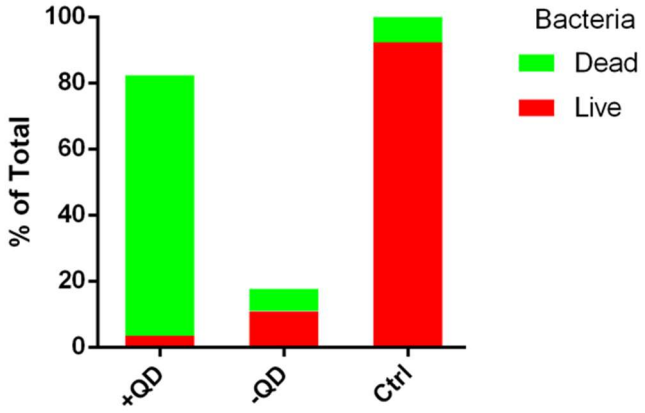

Fig. 7.4.1.2. Analysis of transmission electron microscopy (TEM) images of MR-1 after overnight incubation with 5 μM of negatively charged CdTe QDs. Percentage of live (red) and dead (green) MR-1 are given, split to whether they interacted or not with QDs (bars +QD and -QD). . The Ctrl bar corresponds to control (Ctrl) MR-1 grown without QDs.

Seven electron micrographs were analysed, and the number of investigated bacteria was 350 (Fig. 7.4.1.2.). The transmission electron microscopy investigation of MR-1 incubated overnight with 5 μM commercial CdTe QDs showed that 85.7 % of bacteria lost their membrane integrity. Many of bacteria cells showed signs of cell lysis (Fig. 7.4.1.1 red rectangles). Only 14.3 % of MR-1 was live and interacted with commercial CdTe QDs. The control sample of MR-1 grown overnight, in 30 °C, with shaking 200 RPM, and visualised by electron microscopy showed 92 % of live bacteria. The control sample evaluation excluded the possibility that chemicals applied in the fixation procedure triggered artefacts. It should also be noted the TEM was performed only once to visualise the interaction of MR-1 with negatively charged CdTe QDs. The above explains the lack of error bars in Fig. 7.4.1.2. The repetitions would increase the creditability of the experiment and shine some light on the further understanding of the system.

On the other hand, fluorescence live-dead assay and CFU method showed commercial, negatively charged CdTe QD at concentrations of 0.05, 0.5 and 5 μM were statistically not significantly toxic as compared to the control sample (see Section 6.3). Nevertheless, some toxicity was present, especially for the highest concentration of investigated QD (5μM) as only 39 % of

bacteria remained viable after the overnight incubation with commercial negatively charged CdTe QDs.

Fluorescence live-dead assays showed that 88 % for negative control (that did not contain QDs), 81 % for 0.05 μM, 87 % for 0.5 μM and 63 % for 5 μM of MR-1 were viable, hence would not stain with propidium iodide, after overnight incubation with 5 μM of commercial QDs (see Fig. 6.3.2.A). The above results were expressed as the percentage of control. Once more, the significantly lower viability of MR-1 (63 %) after overnight incubation with commercial negatively charged CdTe QDs comes in agreement with CFU method. Again, the increased number of repetitions in CFU and fluorescence viability assay would make the results explicit and the electron microscopy findings would become clearer.

The contradicting results (TEM versus CFU and fluorescence live-dead assay) can be investigated further by biochemical assays, such as the lactate dehydrogenase assay, which measures the release of the cytosolic lactate dehydrogenase enzymes. An assessment of changes in the oxygen consumption by MR-1 upon commercial CdTe QDs exposure, that can be measured by the respirometry would also provide more information. The most reliable results could be obtained with the fluorescence activated cell sorting (FACS) that would clearly rank cells into four groups as in Fig. 7.4.1.2.

7.4.2. Interaction of an Amine Derivative of Dipicolylamine Modified Commercial Negatively Charged CdTe QDs with *S. oneidensis* MR-1.

As mentioned previously, Zn(II)-dipicolylamines can specifically bind to Gram-negative bacteria. Here, amine derivative of dipicolylamine - ADPA (for structure see Fig. 5.4.4.1) are cross-linked to commercial negatively charged CdTe QDs. In a different strategy, ligands on CdTe/CdS/TGA QDs were exchanged with a lipoic acid derivative of dipicolylamine – LADPA (for structure see Fig. 4.3.2). Details of conjugation and synthesis are described in Sections 4.4.4 and 4.3.2, respectively. The following sections (7.4.2 and 7.4.3) present the interactions of dipicolylamine modified QDs with MR-1 revealed by the epifluorescent microscope.

Negatively charged commercial QDs were mixed with a 10 times molar excess of amine derivative of dipicolylamine - ADPA in phosphate saline buffer, pH 7.0. The coupling agents (EDC and sulfo-NHS) were added to the above mixture, followed by 4 hours incubation at room temperature, in the dark. The completion of the procedure included centrifugation of the sample at 10000 RPM for 10 min. The obtained pellet was resuspended in 20 mM HEPES, 0.15 M NaCl, pH 7.4. Simultaneously, samples of MR-1 were grown in M-1 media until the optical density reached 0.4. Subsequently, bacteria were transferred to M-1 media that did not have any zinc ions (see Chapter 4.3.1. for more details). Then bacteria were mixed with 0.5 μM ADPA modified commercial negatively charged CdTe QDs and incubated for 15 minutes, at 200 RPM at room temperature. 1 mM zinc ions ($ZnSO_4$) were administrated to CdTe/ADPA QDs 5 min before the samples were treated as described in section 6.2 and visualised by epifluorescence microscopy. A representative micrograph is presented in Fig. 7.4.2.1.

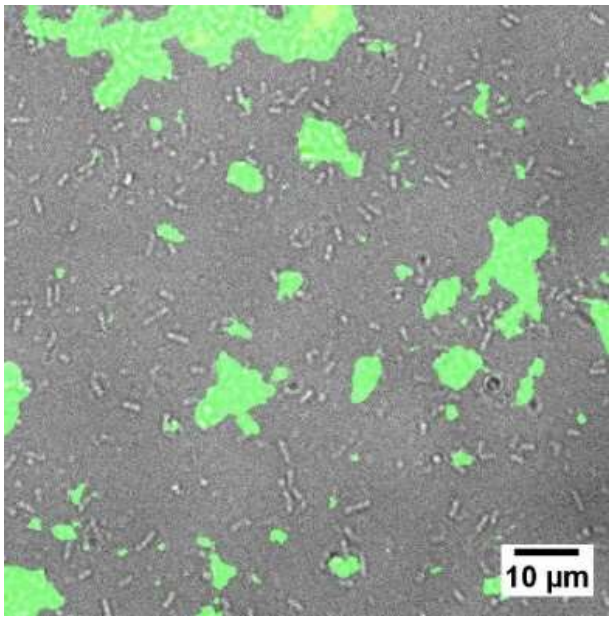

Fig.7.4.2.1. Commercial negatively charged CdTe QDs coupled with an amine derivative of dipicolylamine incubated with MR-1 for 15 min as examined by the epifluorescence microscopy. The picture presented here shows an overlay of fluorescence and bright-field images. At the picture, green marks the precipitated QDs that are overlayed with bacteria (grey). The filter settings in the microscope included: excitation 410 ± 10 nm, dichroic mirror 500 nm, emission 535 ± 24 nm. The error bar is 10 μm.

As is clear from Figure 7.4.2.1, commercial CdTe QDs coupled to ADPA exhibits significant agglomeration upon addition of 1 or 10 mM Zn^{2+}. These results are coherent with Fig. 5.4.4.3, which shows a dynamic light scattering of the ADPA modified QDs following the addition of 10 mM Zn^{2+}. Despite using a lower concentration of zinc ions (1 mM), CdTe/ADPA still proved to be unstable and coagulate rapidly.

7.4.3. Interaction of *S. oneidensis* MR-1 with CdTe/CdS/TGA QDs Modified with Lipoic Acid Derivative of Dipicolylamine.

CdTe/CdS/TGA QDs were modified with the lipoic acid derivative of dipicolyl amine (LADPA) in the way described in Chapter 5.3.2.1. Briefly, CdTe/CdS/TGA QDs (with maximum photoluminescence at λ_{PL} = 545 nm) were mixed with the 10 times excess of LADPA and incubated in 20 mM HEPES, pH 8.5, overnight at 20 °C with shaking at 200 RPM. Subsequently, the ζ potential of control QDs and ligand exchange samples was measured and showed -33.4 ± 2.2 mV and -44.8 ± 2.2 mV, respectively. The solution of modified QDs was stable for about 20 h, and its hydrodynamic size was measured to be 34 nm.

Inspired by work published by Gruenwedel (1968), which presented a low dissociation constant for zinc and dipicolylamine in the range of nanomoles, the decision was made to lower the zinc concentration in the investigated system. LADPA has two dipicolylamine groups in its structure and thus can bind two Zn^{2+} cations per LADPA molecule (see Fig. 5.3.2). Thus, 10 μM of Zn^{2+} ions were added to the experiment just after 0.5 μM of CdTe/CdS/LADPA QDs were mixed with bacteria. MR-1 was grown to OD_{600} of about 0.4 in M-1 media. Bacteria samples were centrifuged for 10 min, at 5000×g. Supernatants were discarded and pellets suspended in minimal media without trace elements and vitamins (see Section 4.3.1). The prepared sample was incubated with 0.5 μM CdTe/CdS/LADPA QDs for 3 or 20 h. The 3 h incubation time did not result in any visible interaction. However, the more prolonged incubation led to a substantial number of bacteria interacting with CdTe/LADPA QDs (Fig. 7.4.3.1).

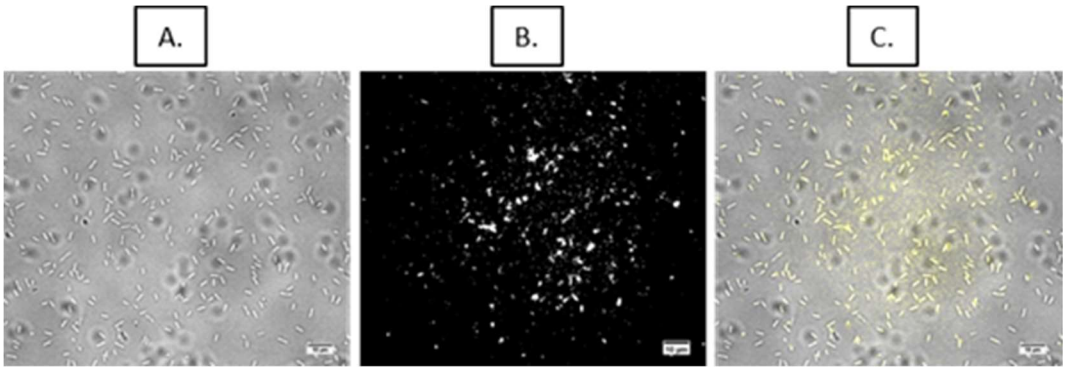

Fig.7.4.3.1. The representative fluorescence micrographs of MR-1 incubated with 0.5 μM of CdTe/LADPA/Zn QDs. A – bright field, B – fluorescence, C – merged channels. Microscopy filters used here were: excitation – 470 nm ±10 nm, dichroic mirror – 500 nm, emission 580 nm ± 12.5 nm. The scale bars are 10 μm.

No size abnormalities were observed as visualised bacteria were of 2.8 ± 0.5 μm in length.

The above experiment gave some promising results. However, the issues with the synthesis and the need for further optimisation of the ligand exchange with LADPA and CdTe/CdS/TGA QDs emerged as CdTe/CdS/LADPA were unstable in solution (see Chapter 5.3.2); this prevented further work with CdTe/CdS/LADPA.

7.5. CIS/PMAL QDs Interface with *S. oneidensis* MR-1.

CIS/PMAL QDs are encapsulated in zwitterionic polymer PMAL (see Fig. 4.5.4.1). The molecule has two amine groups one primary and one tertiary. At neutral or low pH, the latter is protonated, giving CIS/PMAL a positive charge (Booth et al., 2013). Besides amine groups, PMAL has a carboxyl group that is neutral or basic depending on solvent pH, providing the QDs with a negative surface charge at pH>7. It also has a long – 14 C – alkane chain, creating an amphiphilic polymer that can encapsulate the hydrophobic CIS quantum dots. The existing hydrophobic ligands – dodecanethiol - DDT on the CIS surface were coupled with the long hydrophobic chains of the amphipol through hydrophobic interactions, leaving the polar hydrophilic groups exposed.

MR-1 was treated as described in section 7.2. Three concentration of CIS/PMAL QDs (0.034, 0.34, 3.4 μM) were investigated. The applied incubation time was primarily 3 hours, although overnight incubations were also performed. Interaction of MR-1 with CIS/PMAL QDs was examined under

aerobic and anaerobic conditions. Unfortunately, no interaction of MR-1 with CIS/PMAL QDs in either of applied conditions was observed. Besides MR-1, interaction with *E. coli* was investigated. *E. coli* incubated for 3 h with CIS/PMAL QDs were examined with the epifluorescence microscope. Again, this study did not reveal any interaction between CIS/PMAL QD and *E. coli*.

7.6. Quantum Dots Interaction with *S. oneidensis* MR-1. A Summary.

In this Chapter, *S. oneidensis* MR-1 and variety of QDs with different physicochemical features were investigated by fluorescence and electron microscopy.

MR-1 is a Gram-negative bacterium and as such possesses two biomembranes decorated with lipopolysaccharide (LPS) on the outer membrane. The polymeric structure of LPS protects Gram-negative bacteria from bacteriocidal chemicals.

As mentioned in Section 7.2, the surface of MR-1 was postulated either negatively or positively charged (Dague et al., 2006; Korenevsky and Beveridge, 2007; Furukawa and Dale, 2013; Gao et al., 2019). However, no electrostatic interaction between MR-1 and either CdTe/CdS/TGA or CdTe/CdS/Cysteamine QDs was observed. A heat-shock procedure was attempted to induce binding or uptake of 0.5 μM CdTe/CdS/TGA, but this was unsuccessful too. Inspired by the work by Korenevsky, who showed that *Shewanella putrefaciens* CN-32 (CN-32) has a higher positive potential, CdTe/CdS/TGA was incubated with CN-32 (Dague et al., 2006; Korenevsky and Beveridge, 2007). As for MR-1, overnight aerobic incubation with 0.5 μM of the negatively charged CdTe/CdS/TGA QDs also failed to show any interaction with CN-32.

LPS is a dynamic layer that will reduce interaction with nanoparticles but does not prevent interplay. For instance, it has been described that MR-1 can interact directly with hematite, although the interaction is increased when LPS is removed (Gao et al., 2019). Furthermore, QDs modified with Zn^{2+} complexes of lipoic acid (LADPA) and amine derivatives of dipicolyl amine

(ADPA) were also studied, as these compounds have previously been shown to specifically bind to bacteria (Lakshmi et al., 2004; Ngo et al., 2012; S. Xiao et al., 2013). While some interaction with CdTe/LADPA was discovered, CdTe/ADPA QDs were unstable, thus presented no interaction with MR-1.

The unmodified commercial negatively charged CdTe QDs were examined for interaction with MR-1. While some interaction was visible for 0.05 and 0.5 μM, after overnight incubation, at high concentration (5 μM) a substantial number of bacteria cells were stained with the QDs. The above finding encouraged the use of fluorescence live-dead bacteria assay to evaluate both MR-1 viability and the interaction pattern. The finding was consistent with the CFU method presented in Chapter 5 and also indicated that the fraction of live bacteria interacted with 5 μM commercial QDs. However, the analysis of this interaction by transmission electron microscopy suggested that interaction with the commercial QDs impaired the structural integrity of the membranes of MR-1. This finding was unfortunate and indicated the need for further investigation. The increase of the repetition number would allow explicit understanding and the use of a range of biochemical assays would inmprove the quality of the obtained results.

Finally, QDs encapsulated with a zwitterionic polymer (PMAL) were tested for interaction with aerobically grown MR-1, but no interactions were observed.

Further research could focus on MR-1 grown in anaerobic conditions, as this alters the proteins expressed on the outer membrane (compared to microbes grown in aerobic conditions). Additionally, recent findings show that MR-1, which has its LPS layer removed, show better hematite reduction than the normal MR-1 (Gao et al., 2019). A similar approach might mitigate the finding of QDs that interact either with MR-1 that is missing LPS.

Despite the lack of interaction (or interaction causing membrane damage) between QDs and MR-1, all of the nanoparticles were further studied for their ability to create a biohybrid system for solar fuel production. In the biohybrid system, it is attempted to transfer light-excited electrons from QDs to the outer membrane MtrCAB protein complex. MtrCAB enables transmembrane electron transport to periplasmic proteins such as hydrogenase, which are

expressed in anaerobically grown MR-1 and produce biohydrogen. These results are further described in Chapter 8.

Chapter 8. An investigation of light-driven H_2 evolution by different strains of *Shewanellaceae* with quantum dots as photosensitisers (in the absence of methyl viologen).

8.1. Introduction.

In Chapters 5, 6 and 7, experiments were conducted to elucidate whether it is possible to create inorganic biological hybrid systems able to produce hydrogen. For this purpose, a set of semiconductor photosensitiser QDs was synthesised and characterised. Following this, nanotoxicology and interactions between QDs and bacteria were investigated by fluorescence and electron microscopy. The hybrid system consisting of MR-1, photosensitisers QDs, and chosen sacrificial electron donor that can deliver photo-energised electrons to bacterial enzymes in the absence of exogenous electron shuttles will be investigated here. The photoenergised electrons from QDs can, for instance, be transferred across the outer membrane via porin:cytochrome complexes thus enter the periplasmic space where the hydrogenases are located (Shi et al., 2011; Nangle et al., 2017; Kornienko et al., 2018) (please see Chapter 1 and 2 for more details).

Bacteria being the focus of this work possess significant phenotypic and genomic variation. For instance, *S. spp.* strain MR-4 and MR-1 have been studied in the phenotype microarray assays to determine the differences in their elements utilisation patterns (Rodrigues et al., 2011). Bacteria were grown in aerobic conditions on plates that contained nearly universal, defined medium with all the essential nutrients needed for bacteria growth (including C, N, P, S, K, Na, Mg, Ca, Fe, amino acids, purines, pyrimidines, and vitamins). When the sulfur catabolism pathways were examined, bacteria were grown on media that contained all the nutrients for the microbes growth except sulfur which was substituted with various sulfur sources of known concentration. The data obtained in this way revealed that MR-4 does not utilise any of the tested sulfur sources tested (L-cysteine, sulfinic acid, glutathione, and Glu-Met) while MR-1 exploit 19 of the verified S-containing compounds (Rodrigues et al., 2011). The same study suggested that MR-4 and MR-1 are likely to share enzymatic pathways in the degradation of glucose dimers (maltose) and polymers (starch). The genotypic relatedness of MR-4 and MR-1 was found to be 80 %.

For the hybrid system to work, a strain that is able to produce hydrogenase capable of producing hydrogen and possesses an extracellular electron transfer machinery that can exchange electrons between extracellular QDs and intracellular enzymes such as hydrogen is required.

For the hybrid system to work you need a strain that is able to produce hydrogenase capable of producing hydrogen and an extracellular electron transfer machinery that will be able to exchange electrons between extracellular QDs and intracellular enzymes such as hydrogenases. Hydrogen metabolism in MR-1 and MR-4 is similar, although bacteria reside in different ecosystems like freshwater sediments and the Black Sea, respectively. The metabolic assays followed by the genetic analysis of *Shewanella spp.* confirmed that most have encoded genes and produce active [NiFe] hydrogenases, but few have [FeFe] hydrogenases (Table 8.1.) (Marshall et al., 2008; Kreuzer et al., 2014).

For the hybrid system to work, *Shewanella* strain that is capable of hydrogenase production and has an extracellular electron transfer machinery that will be able to exchange electrons between extracellular QDs and intracellular enzymes such as hydrogenases is essential.

Despite the fact MR-4 is more similar to MR-7 (their relatedness was 93 % with regards to the other genome pairs), *Shewanella spp.* strain MR-7 does not have the genes encoding for *hydA*, which is present in MR-1 and MR-4. The drastically different natural environments occupied by MR-1 and MR-4, combined with the presence of the *hydA*, inspired the selection of these organisms to establish if they would be able to produce biohydrogen upon the photoreduction of enzymes by QDs.

Correspondingly to MR-1 and MR-4, *Shewanella putrefaciens* CN-32 is a Gram-negative, facultative anaerobe, and displays dissimilatory metal-reducing behaviour (Cheng et al., 2019). The mutant cells of CN-32 that had their entire MtrCAB complex deleted were recently shown to be able to reduce methyl orange (Min et al., 2020). Anaerobic regulators (e.g., Fur and EtrA) and periplasmic c-type cytochromes (Sputcn32_2333) were identified as a potent chemical reduction agents of methyl orange in CN-32 (Min et al., 2020). The

outer membrane protein complexes in CN-32, together with the presence and activity of HydA and HyaB hydrogenases stimulated the selection of this bacterium into the hydrogen-producing biohybrid system inspected in this Thesis.

Shewanella strain	*mtrCAB*	*mtrDEF*	*omcA*	*hydA* [FeFe] hydrogenase	*hyaB* [NiFe] hydrogenase
oneidensis MR-1	✓	✓	✓	✓	✓
spp. strain MR-4	✓	✓	✓	✓	✓
spp. strain MR-7	✓	✓	✓	-	✓
ANA-3	✓	✓	✓	-	✓
baltica OS185	✓	✓	✓	-	✓
loihica PV-4	✓	✓	✓	-	✓
putrefaciens CN-32	✓	-	-	-	✓
putrefaciens 200	✓	-	-	-	✓
putrefaciens W3-18-1	✓	-	-	-	✓
amazonensis SB2B	✓	✓	✓	-	✓

Table 8.1. Genomic comparison of Shewanellaceae showing the presence (✔) or absence (**-**) of genes encoding the indicated proteins.

The Mtr membrane proteins complex in *Shewanella* spp. establishes the respiratory electrons' pathway for the respiratory electrons in- and outflux (Breuer et al., 2015). The proteins involved in the electron transport in MR-1 were described in Chapter 1.1.2 and portrayed in the Fig. 1.2. Many *Shewanella* spp. have MtrCAB complexes accompanied by OmcA, however, only few show the presence of MtrDEF genes. As compared to MR-1, CN-32 lost the genes encoding for MtrDEF and OmcA proteins but gained *undA* gene. *MtrC* and *undA* deletion mutants in CN-32 were shown to present

respectively severe and slight negative impact on the electron transfer from bacteria to electrode (Wu et al., 2018).

Not only membrane proteins are responsible for *Shewanella spp*. interaction with the environment. *Shewanella* are the Gram-negative bacteria and as such, possess a complex outer membrane biochemical dressing. The surface of bacteria is altered by the structure of lipopolysaccharides and peptidoglycan (a polymer consisting of sugars and amino acids). All the constituents of at the surface of Gram-negative bacteria have a varied thickness and supplementary modifications (phosphorylation, acetylation and creation of disulfide bonds) (Halder et al., 2015). As stated previously, Korenevsky et al. (2002) found that the cell surface of anaerobically grown CN-32 lacks both fibrous materials (i.e. does not possess extensive arrays of long-branched lipopolysaccharide) and a capsule that facilitate cell adhesion to iron oxide rocks like in the case of MR-1, MR-4 and *S. amazonensis* SB2B. It was also shown that aerobically grown CN-32 is more hydrophobic than MR-1 and MR-4. Consequently, CN-32 has almost equal positive potential on the cell surface to *S. baltica* 63, however, it is significantly larger than the one which MR-1 surface has (Korenevsky and Beveridge, 2007). Moreover, it is likely that *Shewanella spp.* also differ in the production of the natural electron shuttles (i.e. flavins), and soluble periplasmic cytochromes (i.e. small tetraheame cytochrome – STC) which may hinder or aid the electron transport to hydrogenases (Brutinel and Gralnick, 2011).

The crucial chemical in the hydrogen-producing biohybrid system are molecules capable of donating electrons to the other parties. Although considered as a cumbersome component in artificial photosynthesis, these molecules are the reduction power in photo-induced reactions aiming at producing value-added molecules by photo-induced reduction of low energy value substrates (Pellegrin and Odobel, 2017). These molecules are called the sacrificial electron donors (SED) and support the photoelectrochemical reactions. The most frequently used and abundant SED in nature is water molecule fuelling the natural photosynthesis with electrons. The water molecule in plants is firstly oxidised to oxygen molecule and electrons, and

both generate the biological reductant NADPH molecules that ultimately supports CO_2 reduction into biomass (Barber, 2006).

In our biohybrid system, SEDs donate the electrons to the photoexcited QDs, providing them to gain the reduction power. However, the electron donation by SEDs is irreversible and creates the partially reduced species that are extremely eager to react with the surroundings. The good SED must have two essential features: firstly it must be thermodynamically compatible with the photosensitiser, thus able to reduce QDs and secondly, must be capable of irreversible transformation upon single-electron oxidation into an inert molecule. Many SEDs were tested for the artificial photosynthesis systems and include amphipathic amines, aromatic amines, carboxylic acids, biological compounds like ascorbic acid and other (Pal et al., 2012; Pellegrin and Odobel, 2017). In the system discussed here, the tested SEDs involved frequently used elsewhere triethanolamine, a potent dimethyl sulfoxide and environmentally mild, zwitterionic sulfonic acid buffering agent HEPES (4- (2-hydroxyethyl)-1-piperazineethanesulfonic acid).

The research executed here is divided into small sections; firstly the sacrificial electron donors that would efficiently give their electrons to QDs will be examined; following the above findings, the hydrogen production by different species of *Shewanella* in the electron acceptor limiting conditions will be measured by the gas chromatography; in the end, the same species accompanied by photosensitiser QDs and chosen SED will be examined to evaluate if QDs support biohydrogen production.

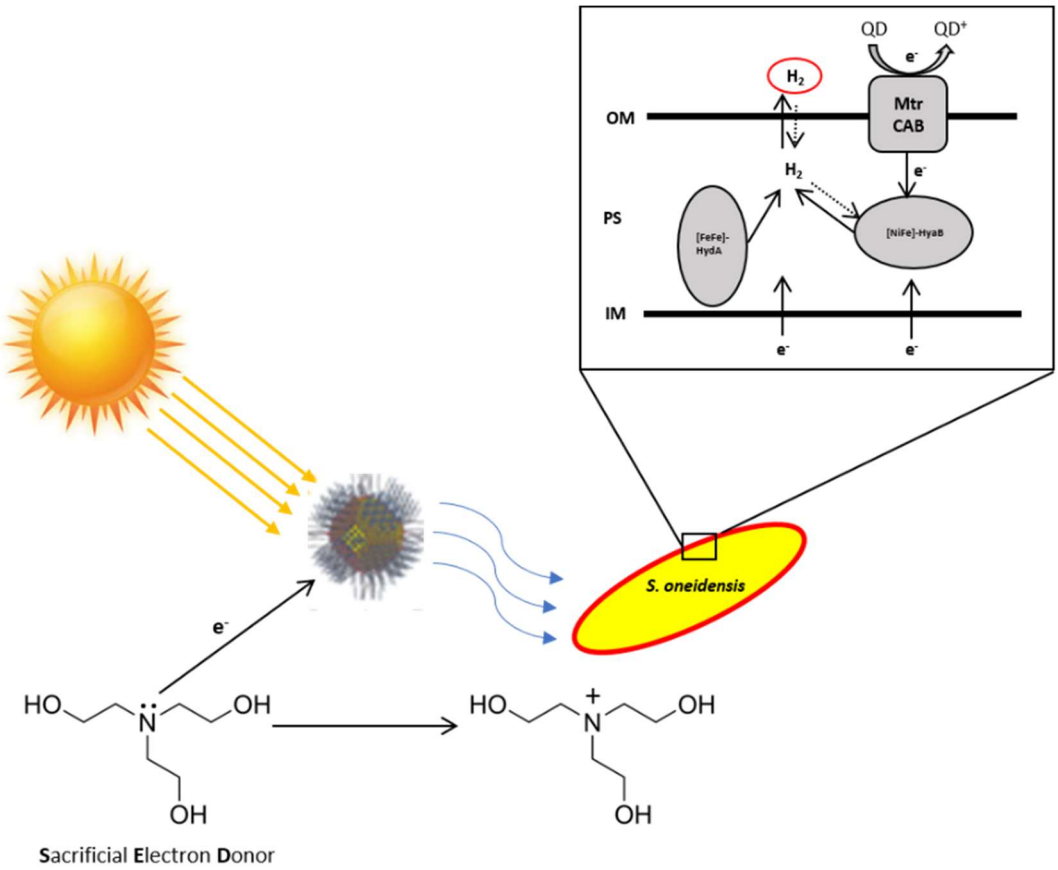

Fig. 8.1. The cartoon depicts the structure of light-harvesting biohybrids designed in this Thesis. Light irradiated photosensitizer – quantum dots – stimulated *S. oneidensis* MR-1 hydrogen evolution. Light irradiated QD's electrons are transferred to hydrogenases by outer membrane decaheame protein complex MtrCAB. Subsequently, the electron holes were created in QDs that had been sealed by electrons from sacrificial donors – triethanolamine (TEOA). Inset depicts [FeFe]HydA and [NiFe]HyaB hydrogenases that anaerobically produce hydrogen and are present in the MR-1 periplasm (PS). Abbreviations used: OM – outer membrane, IM – inner membrane, PS – periplasmatic space. Modified from Shi et al (2011).

8.2. Photoreduction of Methyl Viologen by QDs under Conditions Compatible with *S. oneidensis* MR-1 Enzyme Activity.

Methyl viologen, also known as paraquat, is often used as a herbicides and consists of redox-active heterocycles. MV, as an oxidant, has a reduction potential of -0.45 V versus the standard hydrogen electrode (Watanabe and Honda, 1982).

The work executed here aimed to evaluate whether light-irradiated QDs can reduce methyl viologen (MV) under the anaerobic conditions where relevant MR-1's proteins and enzymes (e.g. MtrCAB and hydrogenase) are expressed.

The [NiFe] HyaB hydrogenase in MR-1 is able to either synthesise hydrogen or to catabolise it, depending on the bacteria metabolism (Meshulam-Simon et al., 2007). The catabolism of hydrogen is supported by the presence of [FeFe] HydA hydrogenase, however, this enzyme is incapable of hydrogen production.

QD Type	CIS/PMAL	CdTe/CdS/TGA	CdTe Comm.	CdTe/CdS/Cyst.
Concentration [μM]	2.6	0.5	1.2	0.5
ε [$M^{-1}\cdot cm^{-1}$]	24600	747600	16647	97732
PL λ_{max} [nm]	620	550	542	610
Abs. λ_{max} [nm]	400	524	500	520

Table 8.1. The concentrations of different quantum dots used in the methyl viologen photoreduction assays. Abbreviation used: CIS/PMAL – $CuInS_2$/ZnS/PMAL QDs, Comm. CdTe – commercial negatively charged CdTe QDs, CdTe/CdS/Cyst. – CdTe/CdS/Cysteamine QD, PL - photoluminescence. Extinction coefficients (ε) were measured at the absorbance maxima (Abs. λ_{max}) of the sample of interest.

If irradiated QDs have a reduction potential that can reduce MV^{2+} to MV^{+}, it follows they also have enough driving force to reduce protons to hydrogen by [NiFe]HyaB in MR-1. The reactions 8.2.1-8.2.3 depict the redox reactions investigated here.

$$MV^{2+} + e^{-} \rightarrow MV^{+} \quad E_m = -440\ mV \qquad \text{Eq.8.2.1.}$$

$$MV^{2+} + QD + TEOA + h\nu \rightarrow MV^{+} + QD + TEOA^{+} \qquad \text{Eq. 8.2.2}$$

$$2H^{+} + 2e^{-} \rightarrow H_2 \quad E_m = -420\ mV \qquad \text{Eq.8.2.3.}$$

Firstly, sacrificial electron donors (SED) that support MV reduction most efficiently were assessed. The examined SEDs include triethanolamine (TEOA, 50 mM), ethylenediaminetetraacetic acid (EDTA, 50 mM), and 2-(N-morpholino), ethanesulfonic acid (MES, 150 mM), pH 7 buffer. All the experiments described below were performed inside an N_2-filled chamber (glovebox) at < 1 ppm O_2. Buffers and QD solutions were purged with nitrogen for at least 1.5 h before transferring them to the glovebox. A KL5125 Cold 150 W light source with high-quality UV filter quartz glass (Krüss) fitted with a 150 W (15 V) halogen lamp (Osram) was used in all experiments. Non-irradiated samples were treated as specified above but were covered in dark cloth, and

the lamp was off. Only very little quantity of reduced MV^+ was present in samples that were not irradiated (Fig. 8.2.1).

The volume of all samples was 1 ml. The reagents were suspended in 50 mM HEPES and 50 mM NaCl, pH 7, unless otherwise stated (e.g., when MES buffer was tested for the ability to work as SED). The working concentration of MV was 0.3 mM. The concentrations, extinction coefficients, photoluminescence and absorbance maxima of examined quantum dots are given in Table 8.1.

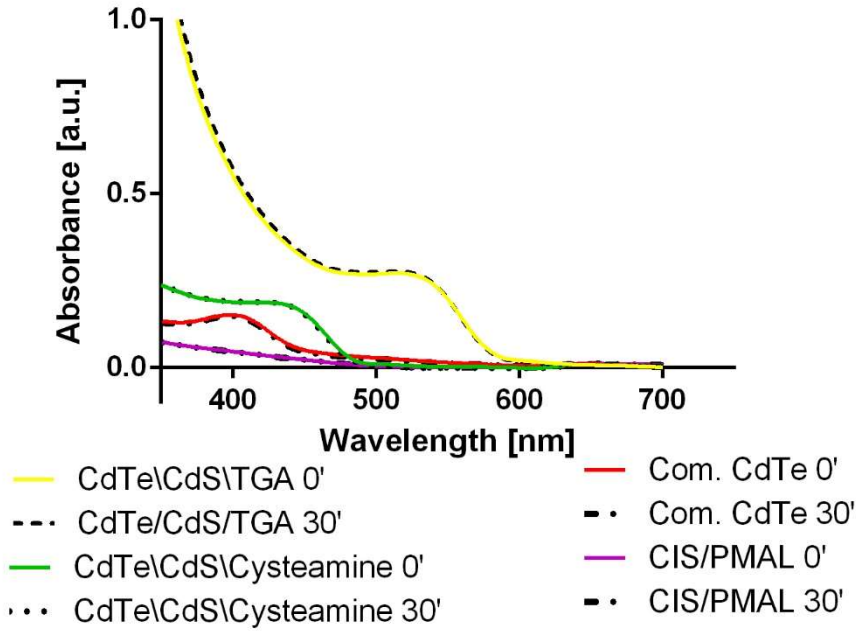

Fig. 8.2.1. 0.3 mM MV was not reduced when the samples containing different QDs (CdTe/CdS/TGA, CdTe/CdS/Cysteamine, commercial negatively charged CdTe and $CuInS_2$/ZnS/PMAL), 50 mM TEOA or 50 mM EDTA (for CIS/PMAL) in 50 mM HEPES, 50 mM NaCl were not irradiated. The control samples kept in the dark with 150 mM MES did not reduce MV; they are not present at the figure. The solid lines show absorbance at time zero, and dashed lines present absorption at 30 min of incubation in the dark.

Preliminary data showed that the QDs tested are photoelectrochemically active, and consequently photoreduce methyl viologen (Fig. 8.2.2). The results differ for each examined SED and QD system. For instance, for CdTe/CdS/TGA or commercial CdTe QD samples, the reduced MV concentrations with MES as SED were less than half those with TEOA. In contrast, MES showed comparable levels of MV^+ to TEOA in samples containing CdTe/CdS/Cysteamine QDs as photosensitisers, and far higher

levels for CIS/PMAL QDs. EDTA worked well for CdTe/CdS/TGA and CIS/PMAL QDs with MV^+ concentration of up to 5.2 μM and 2 μM, respectively. When CdTe/CdS/Cysteamine or commercial negatively charged CdTe QDs were mixed with EDTA and irradiated, MV^+ concentrations were not significantly different from control samples that were held in the dark (for these reasons the EDTA data was omitted in Fig.8.2.2 B and C). It was also observed that the longer irradiation did not bring about the higher MV^+ concentration (*e.g.* Fig. 8.2.2 A, B and D), suggesting an equilibrium was formed.

The highest MV^+ concentration of 5.2 μM presented here was achieved using CdTe/CdS/TGA QDs as photosensitiser supported by 50 mM EDTA and 30 min irradiation with the cold lamp. Similarly, commercial negatively charged CdTe QDs with 50 mM TEOA as SED photoreduced MV^{2+} to give an MV^+ concentration of 4.3 μM after 30 min irradiation. Additionally, 5 μM of MV^+ was delivered when CdTe/CdS/TGA QDs with 50 mM TEOA were irradiated for 10 min. However, in this case, prolonged irradiation caused the concentration of reduced MV to drop. Subsequently, the need for further optimisation of reaction conditions is required.

Based on the MV reduction assays, the best SEDs for each QD are specified in Table 8.2. TEOA became the working SED for most QDs, as it does not influence bacterial viability as much as EDTA. EDTA as a chelating agent may also impact the activity of enzymes and their divalent metal-containing cofactors (e.g. for Fe^{2+}, Ni^{2+}). However, TEOA did not support photoreduction of MV by CIS/PMAL QDs, and thus EDTA was used in further experiments that contained CIS/PMAL as photosensitiser.

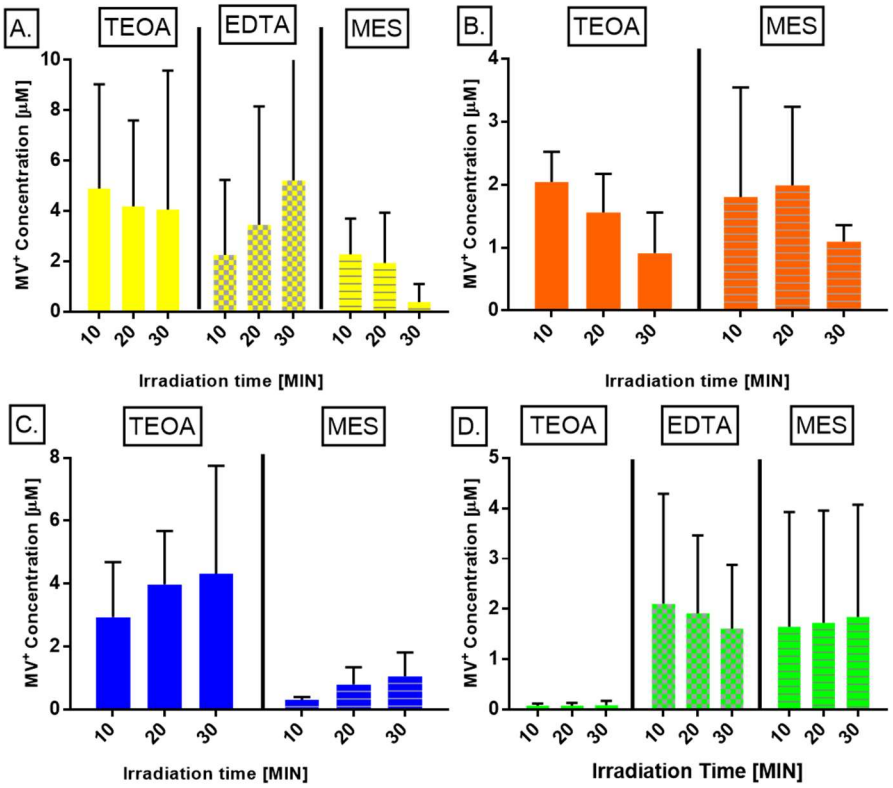

Fig. 8.2.2. Photoreduction of methyl viologen (0.3 mM) using different QDs and SEDs. MV^+ concentration in µM after irradiation with a cold lamp with a power of 700 W m^{-2} for times in minutes stated on the X-axes. Graph **A** depicts the results of photoreduction by CdTe/CdS/TGA, **B** by CdTe/CdS/Cysteamine, **C** by commercial negatively charged CdTe QDs and **D** by $CuInS_2$/ZnS/PMAL QDs. In B and C, EDTA was disregarded as the photoreduction rate did not differ from the non-irradiated controls. MV, photosensitisers (QDs) and SEDs were resuspended in 50 mM HEPES, 50 mM NaCl, pH 7. SEDs used include 50 mM TEOA, 50 mM EDTA. MES (150 mM) was used both as a buffering agent and a sacrificial electron donor. MV^+ concentrations were calculated from the absorbance peak at 606 nm as the peak present at 396 nm interfere with QDs absorption. Error bars represent the standard deviation for results from at least two independent experiments. Abbreviations used include TEOA – triethanolamine, EDTA – ethylenediaminetetraacetic acid, MES – 2-ethanesulfonic acid.

QD name	CIS/PMAL	CdTe/CdS/TGA	CdTe/CdS/Cyst.	CdTe comm.
SED	EDTA	TEOA	TEOA	TEOA

Table 8.2. Choice of SED for all QDs used in MV photoreduction assays. Although EDTA also supported MV reduction by CdTe/CdS/TGA QDs, TEOA was chosen for subsequent experiments. Abbreviation used: CdTe/CdS/Cyst. – CdTe/CdS/Cysteamine QDs, CIS/PML – $CuInS_2$/ZnS/PMAL, CDTe comm. – commercial, negatively charged CdTe QDs, TEOA – triethanolamine, EDTA – ethylenediaminetetraacetic acid,SED – sacrificial electron donor.

The above experimental results suggest that further optimisation of the MV photoreduction essay is required. Nevertheless, only a small number of experimental routes for photoreduction have been exploited so far; for most studies, TEOA or EDTA have been used as electron donors. More typically

biological, and thus more abundant and less harmful to the environment, SEDs like lactic acid, oxalate, thiols, thiolates, phenols, tertiary amines should be investigated in future photoreduction experiments (Pellegrin and Odobel, 2017).

8.3. Preliminary Assessment of Light-driven H_2 Evolution by *Shewanellaceae* with Quantum Dots as Photosensitisers.

In this section, gas chromatography (GC) has been exploited to inspect hydrogen evolution in *Shewanellaceae* grown under electron-acceptor limited anaerobic conditions. To stimulate *hydA* and *hyaB* hydrogenases expression in anoxic conditions, lactate was used at twice the concentration compared to the terminal electron acceptor, fumarate, requiring *Shewanella* to use protons as terminal electron acceptor after fumarate runs out. Bacteria with electron donor and acceptor were dissolved in M72 growth media and supplemented with 37.5 mM HEPES and 1.88 mM $NiCl_2$ (Meshulam-Simon et al., 2007; Shi et al., 2011; Rowe et al., 2017). As introduced in section 8.1, four strains of bacteria were investigated: MR-1, MR-4, CN-32, and LS473. LS473 is a mutant strain of *Shewanella oneidensis* MR-1 in which the genes encoding the large subunits of the [FeFe]- and [NiFe]-hydrogenases were deleted. This hydrogenase deletion mutant of MR-1 was used as a negative control (bacteria that do not produce any hydrogen) to all experiments conducted in Chapter 7. The standard curve used to quantify hydrogen concentration was obtained and is presented in Fig.8.3.1.

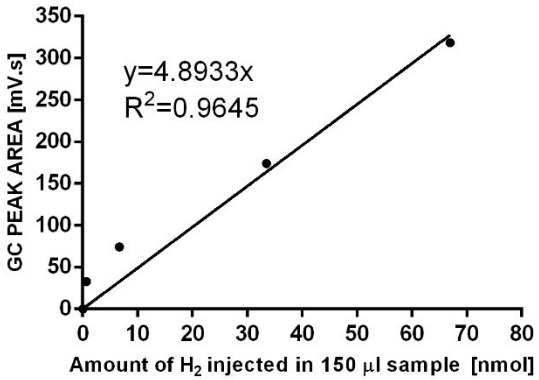

Fig.8.3.1. Gas chromatography calibration curve obtained using hydrogen/nitrogen calibration standard. The equation displayed on the graph was used to calculate the quantity of hydrogen produced by bacteria.

Further details of these experiments are presented in Chapter 4.3 and 4.8.2. Glass Hungate tubes (17 ml total volume) contained 10 ml M72 medium with 37.5 mM sodium DL-lactate (electron donor), 18.8 mM sodium fumarate (electron acceptor), 1.88 mM $NiCl_2$ and 37.5 mM HEPES for hydrogenase production in *Shewanellaceae*. The tubes were sealed, the headspaces (7 mL) were purged with N_2 for 5 min, inoculated and the cultures were incubated with no shaking at 30 °C for 24 h. Headspace H_2 was quantified after 24 h using gas chromatography (Fig. 8.3.2).

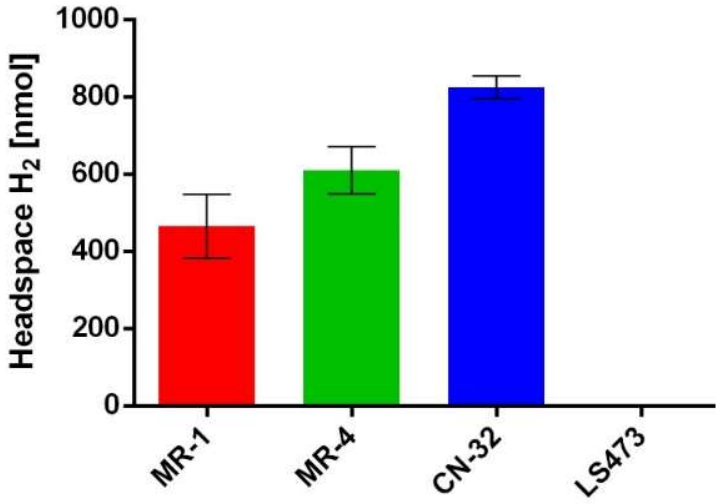

Fig. 8.3.2. Anaerobic production of hydrogen by four strains of *Shewanellaceae: S. oneidensis* MR-1, *S. spp. strain* MR-4, *S. putrefaciens* CN-32 and LS473 upon overnight growth in M72 media. No QDs were used in these experiments. Bacteria were grown in electron-acceptor limited conditions. Error bars represent the standard deviations that equal 82, 61, 82 for MR-1, MR-4, CN-32, respectively. The number of samples examined equals 4 (n = 4). As expected, LS473 did not produce any hydrogen.

It is worth noting that MR-1 hydrogen production recorded by GC and presented here is in agreement with data obtained by others (Meshulam-Simon et al., 2007; Rowe et al., 2017) but is lower than results presented by Kreuzer *et al.*, 2014.

After quantifying headspace H_2, Hungate tubes were taken into an N_2-filled chamber and the contents transferred to Eppendorf tubes. The tubes were removed from the chamber and bacteria were harvested by two subsequent centrifugations (5 min, 13,000 RPM, 4 °C). Trials were moved again to the glovebox, supernatants were removed, and pellets were resuspended in

anaerobic 50 mM HEPES, 50 mM NaCl, pH 7. Samples were then supplemented with 50 mM TEOA and either 0.5 µM CdTe/CdS/TGA or commercial CdTe QDs at 0.6 µM or 1.2 µM concentrations. Alternatively, 50 mM EDTA and 2.6 µM CIS/PMAL QDs were added. The QD working concentrations and their brief characteristics are specified in Table 7.1. To avoid light interference, the samples were then transferred to gas sealed, colourless glass vials with PTFA/silicon septum caps and incubated for 24 h at 25 °C with or without irradiation from a photosynthetic growth lamp (power = 0.02 kW m^{-2}). After this time, headspace H_2 was quantified using GC (Fig. 8.3.3).

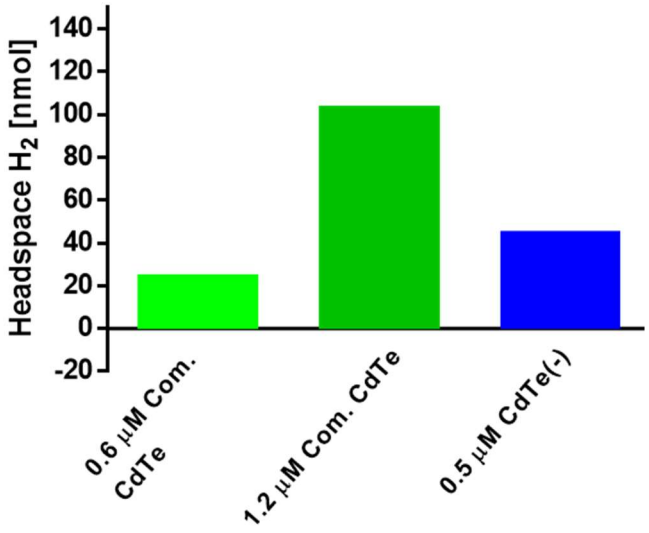

Fig. 8.3.3. Anaerobic production of H_2 by CN-32. QD concentrations used in these experiments were: 0.6 and 1.2 µM of negatively charged commercial CdTe and 0.5 µM of CdTe/CdS/TGA (CdTe(-)) QDs. All samples were irradiated for 24 h with a photosynthetic growth lamp. Bacteria were incubated in 50 mM HEPES and 50 mM NaCl, pH 7, 50 mM TEOA, and the chosen QD. The average and standard deviation were calculated from the average H_2 production by irradiated CN-32 grown with cadmium-containing QD. The left and middle bars are coloured green as they present the commercial CdTe QDs but in different concentrations. Number of repetitions was 1.

The obtained results showed that MR-1 and MR-4 did not produce any hydrogen with any QDs as photosensitisers and any SED. As predicted, also LS473 proved not to produce any hydrogen with all investigated QDs. Likewise, samples that were not irradiated did not generate hydrogen. Additionally, 2.6 µM CIS/PMAL QDs supplemented with 0.5 mM EDTA and incubated with MR-1, MR-4, CN-32 and LS473 (in the presence or absence of irradiation) were also examined in above-described experiments, and the

results showed that no hydrogen was produced. The use of a potent chelating agent EDTA played a crucial role in inhibiting hydrogen evolution in all examined bacterial strains. Many enzymes, for instance, hydrogenases expressed by MR-1, use divalent metal cations as a cofactors; thus, their activity was inhibited by EDTA. In contrast to MR-1 and MR-4, CN-32 produced hydrogen when incubated with 0.5 μM CdTe/CdS/TGA, and commercial negatively charged CdTe QDs at two concentration of 0.6 μM and 1.2 μM (Fig. 8.3.3).

Please bear in mind that data that are shown in Fig. 8.3.3 are from one experiment only. Further replicates were not possible to obtain as access to GC was unavailable. Due to the same reason, data on light-driven hydrogen evolution by *Shewanellaceae* using CdTe/Cds/Cysteamine QDs as photosynthesisers were not obtained.

8.4. Discussion.

All examined quantum dots demonstrated the ability to photoreduce MV in anaerobic conditions. However, none of the experimental setups succeeded to reduce more than 2 % of MV^{2+}. The highest MV^{+} concentration obtained for CdTe/CdS/TGA QDs with 50 mM EDTA as SED was 5.2 μM (after 30 min irradiation). This finding is a proof of concept, however, the need for further optimisation of experimental conditions is clear. For example, it would be interesting to see if MV photoreduction is dependent on the photosensitiser QD concentration or see how altered concentrations of SEDs influence the system. A biocompatible SED like ascorbate, although possessing a high reduction potential, has been shown to damage metallic nanoparticles in one study (Pal et al., 2012). Guttentag et al. showed that dehydroascorbate inhibits the electron donor ability of ascorbic acid (Guttentag et al., 2012). Upfront irradiation for 1 h of a solution that contained ascorbic acid as SED and carbon-doped TiO_2 nanoparticles did not produce any hydrogen and the reaction mixture darkened. Aiming to restore the photoreduction potential of TiO_2 nanoparticles, TEOA was added but failed to induce hydrogen evolution. However, glycerol was shown to be a good electron donor that allowed

hydrogen evolution by copper-passivated titanium dioxide (Maldonado et al., 2018).

In future experiments, investigations are needed into the impact of prolonged irradiation on QDs fluorescence on the electron transfer might have in the understanding of system longevity. The photodegradation triggered by light and MV might impact QD's structure and toxicity therefore QD irradiated samples with MV but without SED should be inspected to investigate SED's impact on QD's fluorescence. Finally, the structure of the quantum dots used might be altered since Dworak et al. found that the electron transfer rate from CdS QDs to MV^{2+} is proportional to the QD shell thickness (Dworak et al., 2011). Addition of an extra layer of QD shell might achieve a higher reduction rate while also lower nanotoxicity.

The inspection of four strains of *Shewanellaceae*, irradiated and not, in the presence and absence of photosensitisers for light-driven H_2 production. in was the focus of Chapter 8 (see Eq. 8.2.3). Notably, only CN-32 evolved biohydrogen after overnight irradiation, using 50 mM TEOA, and only with cadmium-containing QDs. This strain of *Shewanella*ceae might have produced H_2 when incubated with CdTe QDs because of its beneficial surface zeta potential (Korenevsky and Beveridge, 2007). Korenevsky et al. argued that CN-32 kept in 0.01 M NaCl and in anaerobic conditions, has a positive potential of 33.5 ± 1.1 mV; this was the highest surface zeta potential of investigated *Shewanellaceae* by Korenevsky. In such an instance, electrostatic forces might be responsible for CN-32 hydrogen production when incubated with Cd-containing QDs as these nanocrystals have a negative surface charge. If hydrogen production were only driven through electrostatic interactions between the QD and bacteria, then, as observed, CN-32 would not be expected to produce hydrogen when incubated with CIS/PMAL QD. A zwitterionic polymer encapsulating CIS QDs prohibits the electrostatic interaction of CIS/PMAL with CN-32 as its zeta potential is close to 0 at pH 7. To test for electrostatic interactions, the working pH of the solution could be varied, to alter the zeta potential of CIS/PMAL to become negative at pH>7 (Booth et al., 2013). Intriguingly, however, our fluorescence microscopy

experiments did not show any direct interaction of CdTe/CdS/TGA or CIS/PMAL QDs with CN-32 (see Chapter 7).

To investigate further whether the interaction depends on outer membrane cytochromes (e.g. MtrCAB), mutant cells that had the above cytochromes deleted would have to be examined by GC and microscopy. To my knowledge, such mutants of CN-32 are not available.

Even though the results obtained for *Shewanellaceae* H_2 production without nanoparticles were researched extensively, the incubation of CN-32 with QDs needs further investigation. Similarly, for MV assays, the concentration of QDs and SEDs might require adjustment, and control tests must be executed. For instance, control experiments should be completed and may include: use of anaerobically grown bacteria with different SEDs but without QD. Another control option could be an abiotic control – measurements of QD PL with SEDs but without bacteria or MV. Additionally, GC hydrogen quantification with or without QDs should have been normalised by assessing the protein content in the experimental samples. The discussion given above shows that the results presented here are only preliminary; however, it is hoped that further investigation could produce a promising outcome.

Chapter 9. Summary and Conclusions.

9.1. Introduction.

Application of *Shewanella oneidensis* MR-1 in microbial electrochemical synthetic systems was the primary concern of the study described here. Knowledge of its genome sequence and extracellular electron transfer (EET) pathways, ease of growth either in anaerobic and aerobic conditions, the variety of terminal electron acceptors utilised by MR-1 in nature and the laboratory setting, made this bacterium a useful model organism that is of particular interest for scientists. The exoelectrogenicity of MR-1 initiated the development of microbial fuel cells that possess the potential for environmentally-friendly electric power production and simultaneous waste remediation (Min and Logan, 2004). Unfortunately, the theoretical maximum power output from MFCs is limited by many issues with regard to construction costs, high internal resistivity, and low power output, that prohibit its scalability (Oliveira et al., 2013). The niche application of MFCs requiring only low power output but working over long periods have gained noticeable attention (Finneran et al., 2002). MFC systems have been pushed further towards the production of high-value chemicals using bacteria, and even eukaryotic cells, controlled by QD-harvested irradiation (Kornienko et al., 2018; Guo et al., 2018).

9.2. Results Summary.

The study presented in this thesis aims to generate a background for understanding research into the assembly of hybrid MR-1/QDs systems for biohydrogen production. The intention was to find the least toxic nanoparticles that would interact with MR-1. For this purpose, the nanotoxicology was tested for selected quantum dots with different surface features, and their interaction with MR-1 was investigated by fluorescence and electron microscopy. The photoreduction activity of all tested QDs was examined, and their potential to support biohydrogen production in three strains of *Shewanella* was also studied.

Nanoparticles were selected based on their possible interaction with MR-1, and included custom-made CdTe/CdS/TGA, CdTe/CdS/Cysteamine and

CuInS2/ZnS/PMAL (CIS/PMAL) QDs and commercially available negatively charged CdTe QDs. The ζ potential and hydrodynamic size of the employed QDs was established. The high resolution TEM confirmed the size of CdTe/CdS/TGA and commercial QDs. Commercial QDs and CdTe/CdS/TGA were further employed in the multiple surface modifications that included respectively crosslinking to the amine derivative of dipicolylamine and ligand exchange with LADPA (Chapter 5). LE procedures were also tested to make gold nanowires of conductivity similar to bulk gold, hydrophilic (Chapter 4). Finally, the crosslinking of commercial QDs with amine derivative of dipicolylamine and LE that created CdTe/CdS/LADPA QDs gave the anticipated result, and together with the rest of QDs were further investigated in the following chapters.

The toxicity of prepared QD–MR-1 hybrid systems was evaluated by nanotoxicology techniques. The colony-forming unit method was used to establish the fraction of bacteria able to live after contact with QD for 3–18 h. While CdTe/CdS/TGA QDs at concentrations of 0.05–0.5 μM showed moderate toxicity to MR-1, positively charged CdTe/CdS/Cysteamine QDs at concentrations 0.5–50 nM presented severe toxicity; bacteria were unable to survive at concentrations higher than 50 nM. The colony-forming method also showed that CIS/PMAL and commercial QDs were not significantly toxic to MR-1 at concentrations of 0.034–3.4 μM, and 0.05–5 μM respectively. The lack of CIS/PMAL QD toxicity was not a surprise as they were previously shown not to be toxic to mammal cell line HaCat until the concentration of 0.34 μM that is low compared to CdTe/TGA QDs (Booth et al., 2013). However, comparable results for commercial cadmium-containing QDs seemed unreliable as heavy metals in the nanoparticle structure were shown to trigger an increase in ROS generation, thus inducing cell structure damage (Dumas et al., 2009). Finally, the fluorescent live–dead assay confirmed the colony-forming method results that commercial CdTe QDs are not toxic to MR-1. Next, the nature of the interaction of QDs with bacteria was visualised by inverted epi-fluorescence microscopy and TEM (Chapter 7).

The epifluorescent microscopy revealed that only interaction of MR-1 with CdTe/CdS/TGA and CdTe/CdS/Cysteamine was with dead bacteria that had

impaired membrane integrity. However, morphological signs of stress were evident, as MR-1 incubated with positively and negatively charged CdTe/CdS QDs suffered from filamentation. Bacterial filamentation is a sign of severe toxicity that inhibits cell division, and others have also shown similar findings (Huismant et al., 1984; Schneider et al., 2009; Pramanik et al., 2018). No interaction or signs of filamentation were found with CIS/PMAL QDs after 3 h, 20 h, aerobic or anaerobic incubation with MR-1. A significant fraction (48 %) of MR-1 was alive and interacted with commercial CdTe QDs as inspected by PI staining of dead cells. MR-1's hydrogenases, [FeFe]-Hyd A and [NiFe]-HyaB, are present in the periplasmatic space (Shi et al., 2011). It follows that for photoenergised electrons to reach these enzymes, QDs will need to be able to enter the periplasm, or electrons need to be transported to the periplasm via the Mtr pathway, which is responsible for MR-1's extracellular electron transfer. The localisation of the commercial QDs incubated for 20 h with MR-1 was inspected by TEM, and indeed electron-dense CdTe spots were visible in the cytoplasm and periplasmatic space. Also, and to our surprise, the majority of bacteria had biomembranes integrity broken and presumably were dead; this finding is in contradiction with the data obtained using the colony-forming unit and fluorescence live–dead assays. The above underlines the importance of the complexity of nanotoxicology evaluation. Thus, biochemical viability assays should have been employed to gain a more detailed picture of the system (Qiu et al., 2017). Firstly, biochemical assays inspecting the changes in the level of ROS generated or riboflavin secreted by MR-1 after contact with QDs (see Chapter 4 and 5 for details) should be executed. The data obtained in this way could help comprehend the unexpected conflicting results obtained by live–dead assay and CFU method versus the membrane disruption in MR-1 observed with TEM assessment.

As a step towards the assembly of hydrogen-producing biotic/abiotic biohybrids, various QDs were tested for their photo-reducing potential. The photoreduction potential of CdTe/CdS/TGA, CdTe/CdS/Cysteamine, a commercially-available, negatively charged CdTe and $CuInS_2$/ZnS/PMAL QDs was confirmed by measuring their ability to photoreduce methyl viologen with different sacrificial electron donors (SEDs). Three SEDs (50 mM TEOA, 50 mM EDTA or 150 mM MES) that most efficiently support MV reduction

were assessed. The findings proved that the most effective SED was QD-specific and included 50 mM TEOA productively photoreduced MV with CdTe/CdS/TGA, CdTe/CdS/Cysteamine and commercial CdTe QD, but for photoirradiation CIS/PMAL QDs MV reduction 50 mM EDTA gave the best results.

In acceptor-limited conditions, selected hybrids of anaerobically grown MR-1 and other *Shewanellaceae*, including CN-32, MR-4 and the mutant bacteria LS473, supported by selected SEDs and QDs, were inspected for hydrogen production. Anaerobically grown CN-32 supported by 50 mM TEOA and either commercial or custom made CdTe QDs were shown to evolve hydrogen. Further research should be carried out to understand why only CN-32 evolved hydrogen with cadmium-containing QDs. Additional results from a QD toxicology assessment for CN-32 and MR-4 would give some better understanding. Furthermore, the methodical examination of hybrids containing CdTe QDs supported by TEOA and CN-32, testing the design of CN-32 mutant cells and some additional controls for the system itself, are required. Firstly, replication of the experiments already undertaken must be performed followed by control experiments to check that hydrogen evolution recorded by gas chromatography was not due to cell lysis. Also, identification of more environmentally-friendly SEDs like ascorbic acid or glycerol could potentially provide better longevity to the system. Testing other QDs such as those based on carbon or silica would decrease the pollution factor of the system.

9.3. Future perspectives.

The design of the microbial fuel cell that uses MR-1 in both anodic and cathodic chambers would be intriguing. The chosen QDs would be added to a previously anaerobically grown thin biofilm of MR-1 in the buffer containing only essential ingredients like sugars, salts, and amino acids. Both MFC chambers with added QDs and bacteria would be inspected to determine the QDs influence on the produced both the electric charge and the potential achieved. The both electrodes in MFC would be of a carbon source depending on the budget. The inexpensive option would be a graphite rods as they are

easily available, not toxic, conducting and biologically stable. Contrary to the low-cost solutions, the carbon granules, providing high surface to volume ratio for the enhanced bacterial growth would be an option too. Moreover, the tested variables will be limited only to the QDs added to allow the conclusions drawing.

The system would be monitored by the cyclic voltammetry and chronoamperometry to control the electrochemical changes triggered by introduction of the electroactive QDs. Additionally, results obtained by the potentiostat measurements of the built MFC would provide some insight into the electrical power changes compared to the system without QDs.

The captivating aspect of MFC research accompanied by QDs, could be taken further if the QDs are replaced with carbon dots (CD) (Yang et al., 2020). Many times CD have been shown as an alternative to semiconductor QDs as they are inexpensive, have low toxicity and were shown to work well as photosensitizers, electron acceptors and donors; in the MFC system, all benefits of CDs would be an advantageous over the QDs associated MFC (Wang and Hu, 2014; Luo et al., 2020). Recently the carbon cloth anode decorated with nitrogen-doped CDs was able to accommodate twice as thick bacteria biofilm due to the increased hydrophilicity of anode (Guan et al., 2019). Guan (2019) system produced electricity with increased power output that was 1.1 higher than with the row carbon paper anode. The system with anaerobically grown MR-1 biofilm with added CD could be explored for the production of electrical charges.

Finally, the synthesis of the modified QDs with the added layers in their shell structure would also be intriguing to explore. The addition of bovine serum albumin on the surface of CdTe/TGA QDs was shown to increase their biocompatibility and longevity as compared to sensitive to irradiation prior modifications CdTe/TGA QDs (Tsipotan et al., 2017). Similarly, embedding CdSe QDs into the onion-like silica shells was found to result in monodispersed, photostable and stable across different pH values QDs (Serrano et al., 2011). Corresponding approach would certainly contribute the solar to chemical conversion by MR-1 accompanied by silica modified CdTe/CdS QDs.

In summary, combining abiotic photosensitisers with non-photosynthetic bacteria ‘in vivo’ presents an intriguing concept in the design of artificial photosynthetic organisms for solar-driven fuel production. MR-1 is a versatile bacterium with respect to respiration, metabolism and biocatalysis, and is a very promising organism for artificial photosynthesis. Taken together these results inform on the possibilities and bottlenecks when developing bionanotechnological systems for the photosynthetic production of biohydrogen by MR-1.

Bibliography

Abbe, E. 1873. Beiträge zur Theorie des Mikroskops und der mikroskopischen Wahrnehmung. *Archiv f. mikrosk. Anatomie*. **9**(1), pp.413–418.

Abboud, R., Popa, R., Souza-Egipsy, V., Giometti, C.S., Tollaksen, S., Mosher, J.J., Findlay, R.H. and Nealson, K.H. 2005. Low-temperature growth of *Shewanella oneidensis* MR-1. *Applied and environmental microbiology*. **71**(2), pp.811–816.

Alatraktchi, F.A.Z. a., Zhang, Y., Noori, J.S. and Angelidaki, I. 2012. Surface area expansion of electrodes with grass-like nanostructures and gold nanoparticles to enhance electricity generation in microbial fuel cells. *Bioresource Technology*. **123**, pp.177–183.

Alves, M.N., Neto, S.E., Alves, A.S., Fonseca, B.M., Carrêlo, A., Pacheco, I., Paquete, C.M., Soares, C.M. and Louro, R.O. 2015. Characterization of the periplasmic redox network that sustains the versatile anaerobic metabolism of Shewanella oneidensis MR-1. *Frontiers in Microbiology*. **6**(JUN), pp.1–10.

Ardenne, von M. 1938. Das Elektronen-Rastermikroskop. Theoretische Grundlagen. *Z. Physik*. **109**(9–10), pp.553–572.

Bacon, R. 1267. Handwritten manuscript. *Royal MS, British Library London*. **7 F**(VIII).

Barber, J. 2006. Photosystem II: An enzyme of global significance. *Biochemical Society Transactions*. **34**(5), pp.619–631.

Barroso, M.M. 2011. Quantum dots in cell biology. *Journal of Histochemistry and Cytochemistry*. **59**(3), pp.237–251.

Batista, C.A.S., Larson, R.G. and Kotov, N.A. 2015. Nonadditivity of nanoparticle interactions. *Science*. **350**(6257), p.1242477.

Baumann, L., Baumann, P., Mandel, M. and Allen, Richard, D. 1972. Taxonomy of aerobic marine eubacteria. *Journal of Bacteriology*. **110**(1),

pp.402–429.

Bera, D., Qian, L., Tseng, T.K. and Holloway, P.H. 2010. Quantum dots and their multimodal applications: A review. *Materials*. **3**(4), pp.2260–2345.

Berney, M., Hammes, F., Bosshard, F., Weilenmann, H.U. and Egli, T. 2007. Assessment and interpretation of bacterial viability by using the LIVE/DEAD BacLight kit in combination with flow cytometry. *Applied and Environmental Microbiology*. **73**(10), pp.3283–3290.

Bewley, K.D., Firer-Sherwood, M.A., Mock, J.-Y., Ando, N., Drennan, C.L. and Elliott, S.J. 2012. Mind the gap: diversity and reactivity relationships among multihaem cytochromes of the MtrA/DmsE family. *Biochemical Society Transactions*. **40**(6), pp.1268–1273.

Bhattacharjee, S. 2016. DLS and zeta potential - What they are and what they are not? *Journal of Controlled Release*. **235**, pp.337–351.

Blankenship, R.E., Tiede, D.M., Barber, J., Brudvig, G.W., Fleming, G., Ghirardi, M., Gunner, M.R., Junge, W., Kramer, D.M., Melis, A., Moore, T.A., Moser, C.C., Nocera, D.G., Nozik, A.J., Ort, D.R., Parson, W.W., Prince, R.C. and Sayre, R.T. 2011. Comparing photosynthetic and photovoltaic efficiencies and recognizing the potential for improvement. *Science*. **332**(6031), pp.805–809.

Booth, M., Brown, A.P., Evans, S.D. and Critchley, K. 2012. Determining the Concentration of CuInS2 Quantum Dots from the Size Dependent Molar Extinction Coefficient. *Chem. Mater.* **24**, pp.2064–2070.

Booth, M., Peel, R., Partanen, R., Hondow, N., Vasilca, V., Jeuken, L.J.C. and Critchley, K. 2013. Amphipol-encapsulated CuInS2/ZnS quantum dots with excellent colloidal stability. *RSC Advances*. **3**(43), p.20559.

Breuer, M., Rosso, K.M., Blumberger, J. and Butt, J.N. 2015. Multi-haem cytochromes in Shewanella oneidensis MR-1: structures, functions and opportunities. *Journal of The Royal Society Interface*. **12**(102), pp.20141117–20141117.

Brown, K.A., Wilker, M.B., Boehm, M., Dukovic, G. and King, P.W. 2012. Characterization of photochemical processes for H 2 production by CdS

nanorod-[FeFe] hydrogenase complexes. *Journal of the American Chemical Society*. **134**(12), pp.5627–5636.

Brust, M., Walker, M., Bethell, D., Schiffrin, D.J. and Whyman, R. 1994. Synthesis of Thiol-derivatised Gold Nanoparticles in. *Journal of the Chemical Society, Chemical Communications*., pp.801–802.

Brutinel, E.D. and Gralnick, J.A. 2011. Shuttling happens: soluble flavin mediators of extracellular electron transfer in Shewanella. *Applied Microbiology and Biotechnology*. **93**(January 2012), pp.41–48.

Buffat, P. and Borel, J.P. 1976. Size effect on the melting temperature of gold particles. *Physical Review A*. **13**(6), pp.2287–2298.

Call, D.F., Merrill, M.D. and Logan, B.E. 2009. High surface area stainless steel brushes as cathodes in microbial electrolysis cells. *Environmental Science and Technology*. **43**(6), pp.2179–2183.

Chae, K.J., Choi, M., Ajayi, F.F., Chang, S.I., Park, W. and Kim, I.S. 2008. Mass Transport through a Proton Exchange Membrane (Nafion) in Microbial Fuel Cells †. *Energy & Fuels*. (22), pp.169–176.

Chen, N., He, Y., Su, Y., Li, X., Huang, Q., Wang, H., Zhang, X., Tai, R. and Fan, C. 2012. The cytotoxicity of cadmium-based quantum dots. *Biomaterials*. **33**(5), pp.1238–1244.

Cheng, L., Min, D., Liu, D.F., Li, W.W. and Yu, H.Q. 2019. Sensing an Approaching Toxic Arsenate by Shewanella putrefaciens CN-32. *Environmental Science and Technology*. **53**(24), pp.14604–14611.

Chisti, Y. 2007. Biodiesel from microalgae. *Biotechnology Advances*. **25**, pp.294–306.

Choi, K.Y., Silvestre, O.F., Huang, X., Hida, N., Liu, G., Ho, D.N., Lee, S., Lee, S.W., Hong, J.I. and Chen, X. 2014. A nanoparticle formula for delivering siRNA or miRNAs to tumor cells in cell culture and in vivo. *Nature Protocols*. **9**(8), pp.1900–1915.

Choudhury, P., Uday, U.S.P., Mahata, N., Nath Tiwari, O., Narayan Ray, R., Kanti Bandyopadhyay, T. and Bhunia, B. 2017. Performance improvement of microbial fuel cells for waste water treatment along with

value addition: A review on past achievements and recent perspectives. *Renewable and Sustainable Energy Reviews*. **79**(April 2016), pp.372–389.

Chu, S. and Majumdar, A. 2012. Opportunities and challenges for a sustainable energy future. *Nature*. **488**(7411), pp.294–303.

Clarke, T.A., Holley, T., Hartshorne, R.S., Fredrickson, J.K., Zachara, J.M., Shi, L. and Richardson, D.J. 2008. The role of multihaem cytochromes in the respiration of nitrite in *Escherichia coli* and Fe(III) in *Shewanella oneidensis*. *Biochemical Society Transactions*. **36**(5), pp.1005–1010.

Conde, J., Dias, J.T., Grazú, V., Moros, M., Baptista, P. V and de la Fuente, J.M. 2014. Revisiting 30 years of biofunctionalization and surface chemistry of inorganic nanoparticles for nanomedicine. *Frontiers in chemistry*. **2**(July), p.48.

Cord-Ruwisch, R., Law, Y. and Cheng, K.Y. 2011. Ammonium as a sustainable proton shuttle in bioelectrochemical systems. *Bioresource Technology*. **102**(20), pp.9691–9696.

Coursolle, D., Baron, D.B., Bond, D.R. and Gralnick, J.A. 2010. The Mtr Respiratory Pathway Is Essential for Reducing Flavins and Electrodes in Shewanella oneidensis. *Journal of Bacteriology*. **192**(2), pp.467–474.

Coursolle, D. and Gralnick, J.A. 2010. Modularity of the mtr respiratory pathway of Shewanella oneidensis strain MR-1. *Molecular Microbiology*. **77**(4), pp.995–1008.

Critchley, K., Khanal, B.P., Górzny, M.L., Vigderman, L., Evans, S.D., Zubarev, E.R. and Kotov, N.A. 2010. Near-bulk conductivity of gold nanowires as nanoscale interconnects and the role of atomically smooth interface. *Advanced Materials*. **22**(21), pp.2338–2342.

Dague, E., Duval, J., Jorand, F., Thomas, F. and Gaboriaud, F. 2006. Probing surface structures of Shewanella spp. by microelectrophoresis. *Biophysical Journal*. **90**(7), pp.2612–2621.

Daniel, M.C.M. and Astruc, D. 2004. Gold Nanoparticles: Assembly, Supramolecular Chemistry, Quantum-Size Related Properties and

Applications toward Biology, Catalysis and Nanotechnology. *Chemical Reviews*. **104**, pp.293–346.

Das, P., Xenopoulos, A.M., Williams, J.C., Hoque, M.E. and Metcalfe, D.C. 2012. Effects of silver nanoparticles on bacterial activity in natural waters. *Environmental Toxicology and Chemistry*. **31**(1), pp.122–130.

Davies, M.J. 2016. Protein oxidation and peroxidation. *Biochemical Journal*. **473**, pp.805–825.

Derby, H.A. and Hammer, B.W. 1931. Bacteriology of butter. IV. bacteriological studies on surface taint butter. *Iowa Agric Exp Stn Res Bull*. (145), pp.387–416.

Derfus, A.M., Chan, W.C.W. and Bhatia, S.N. 2004. Probing the Cytotoxicity of Semiconductor Quantum Dots. *Nano Letters*. **4**(1), pp.11–18.

Dhas, S.P., Shiny, P.J., Khan, S., Mukherjee, A. and Chandrasekaran, N. 2014. Toxic behavior of silver and zinc oxide nanoparticles on environmental microorganisms. *Journal of Basic Microbiology*. **54**(9), pp.916–927.

Domingos, R.F., Franco, C. and Pinheiro, J.P. 2013. Stability of core/shell quantum dots-role of pH and small organic ligands. *Environ Sci Pollut Res*. **20**, pp.4872–4880.

Dreyer, D.R., Miller, D.J., Freeman, B.D., Paul, D.R. and Bielawski, C.W. 2013. Perspectives on poly(dopamine). *Chemical Science*. **4**(10), pp.3796–3802.

Driscoll, M.E., Romine, F.E., Johun, F.S., Serres, M., McCue, L.A., Beliaev, A.S., Fredrickson, J.K. and Gradner, T.S. 2007. Identification of Diverse Carbon Utilization. *Genome Informatics*. **18**, pp.287–298.

Dubavik, A., Sezgin, E., Lesnyak, V., Gaponik, N., Schwille, P. and Eychmüller, A. 2012. Penetration of amphiphilic quantum dots through model and cellular plasma membranes. *ACS Nano*. **6**(3), pp.2150–2156.

Dumas, E.-M., Ozenne, V., Mielke, R.E. and Nadeau, J.L. 2009. Toxicity of CdTe Quantum Dots in Bacterial Strains. *IEEE Transactions on NanoBioscience*. **8**(1), pp.58–64.

Dumas, E., Gao, C., Suffern, D., Bradforth, S.E., Dimitrijevic, N.M. and Nadeau, J.L. 2010. Interfacial charge transfer between CdTe quantum dots and gram negative vs gram positive bacteria. *Environ Sci Technol*. **44**(4), pp.1464–1470.

Dworak, L., Matylitsky, V. V., Breus, V. V., Braun, M., Basché, T. and Wachtveitl, J. 2011. Ultrafast charge separation at the CdSe/CdS core/shell quantum dot/methylviologen interface: Implications for nanocrystal solar cells. *Journal of Physical Chemistry C*. **115**(10), pp.3949–3955.

Edwards, M.J., White, G.F., Lockwood, C.W., Lawes, M.C., Martel, A., Harris, G., Scott, D.J., Richardson, D.J., Butt, J.N. and Clarke, T.A. 2018. Structural modeling of an outer membrane electron conduit from a metal-reducing bacterium suggests electron transfer via periplasmic redox partners. *Journal of Biological Chemistry*. **293**(21), pp.8103–8112.

Erni, R., Rossell, M.D., Kisielowski, C. and Dahmen, U. 2009. Atomic-Resolution Imaging with a Sub-50-pm Electron Probe. *Physical Review Letters*. **096101**(March), pp.1–4.

Fadeel, B. and Garcia-Bennett, A.E. 2010. Better safe than sorry: Understanding the toxicological properties of inorganic nanoparticles manufactured for biomedical applications. *Advanced Drug Delivery Reviews*. **62**(3), pp.362–374.

Faraday, M. 1857. The Bakerian Lecture: Experimental Relations of Gold (and Other Metals) to Light. *Philosophical Transactions of the Royal Society of London*. **147**(0), pp.145–181.

Feng, H., Yang, Y., You, Y., Li, G., Guo, J., Yu, T., Shen, Z., Wu, T. and Xing, B. 2009. Simple and rapid synthesis of ultrathin gold nanowires, their self-assembly and application in surface-enhanced Raman scattering. *Chemical Communications*. (15), pp.1984–1986.

Finneran, K.T., Anderson, R.T., Nevin, K.P. and Lovley, D.R. 2002. Potential for Bioremediation of Uranium-Contaminated Aquifers with Microbial U(VI) Reduction. *Soil and Sediment Contamination: An International Journal*. **11**(3), pp.339–357.

Foley, J.M., Rozendal, R.A., Hertle, C.K., Lant, P.A. and Rabaey, K. 2010. Life cycle assessment of high-rate anaerobic treatment, microbial fuel cells, and microbial electrolysis cells. *Environmental Science and Technology*. **44**(9), pp.3629–3637.

Furukawa, Y. and Dale, J.R. 2013. The surface properties of Shewanella putrefaciens 200 and S. oneidensis MR-1: The effect of pH and terminal electron acceptors. *Geochemical Transactions*. **14**(3), pp.1–11.

Gao, L., Lu, X., Liu, H., Li, J., Li, W., Song, R. and Wang, R. 2019. Mediation of Extracellular Polymeric Substances in Microbial Reduction of Hematite by Shewanella oneidensis MR-1. *Frontiers in Microbiology*. **10**(March), pp.1–12.

Gaponik, N., Talapin, D. V., Rogach, A.L., Eychmuller, A. and Weller, H. 2002. Efficient Phase Transfer of Luminescent Thiol-Capped Nanocrystals: From Water to Nonpolar Organic Solvents. *Nano Letters*. **2**(8), pp.803–806.

Gaponik, N., Talapin, D. V., Rogach, A.L., Hoppe, K., Shevchenko, E. V., Kornowski, A., Eychmuller, A. and Weller, H. 2002. Thiol-Capping of CdTe Nanocrystals : An Alternative to Organometallic Synthetic Routes Thiol-Capping of CdTe Nanocrystals : An Alternative to Organometallic Synthetic Routes. *Journal of Physical Chemistry B*. **106**(29), pp.7177–7185.

Ghangrekar, M.M. and Shinde, V.B. 2007. Performance of membrane-less microbial fuel cell treating wastewater and effect of electrode distance and area on electricity production. *Bioresource Technology*. **98**(15), pp.2879–2885.

Gomes, S.A.O.O., Vieira, C.S., Almeida, D.B., Santos-Mallet, J.R., Menna-Barreto, R.F.S.S., Cesar, C.L. and Feder, D. 2011. CdTe and CdSe quantum dots cytotoxicity: A comparative study on microorganisms. *Sensors*. **11**(12), pp.11664–11678.

Grabarek, Z. and Gergely, J. 1990. Zero-length crosslinking procedure with the use of active esters. *Analytical Biochemistry*. **185**(1), pp.131–135.

Gralnick, J.A., Vali, H., Lies, D.P. and Newman, D.K. 2006. Extracellular

respiration of dimethyl sulfoxide by Shewanella oneidensis strain MR-1. *Proceedings of the National Academy of Sciences*. **103**(12), pp.4669–4674.

Green, M., Williamson, P., Samalova, M., Davis, J., Brovelli, S., Dobson, P. and Cacialli, F. 2009. Synthesis of type II/type I CdTe/CdS/ZnS quantum dots and their use in cellular imaging. *Journal of Materials Chemistry*. **19**(44), pp.8341–8346.

Gross, M.A., Reynal, A., Durrant, J.R. and Reisner, E. 2014. Versatile Photocatalytic Systems for H 2 Generation in Water Based on an Efficient DuBois-Type Nickel Catalyst. *Journal of the American Chemical Society*. **136**(1), pp.356–366.

Gruenwedel, D.W. 1968. Multidentate Coordination Compounds. Chelating Properties of Aliphatic Amines Containing α-Pyridyl Residues and Other Aromatic Ring Systems as Donor Groups. *Inorganic Chemistry*. **7**(3), pp.495–501.

Guan, Y.F., Zhang, F., Huang, B.C. and Yu, H.Q. 2019. Enhancing electricity generation of microbial fuel cell for wastewater treatment using nitrogen-doped carbon dots-supported carbon paper anode. *Journal of Cleaner Production*. **229**, pp.412–419.

Guo, J., Suástegui, M., Sakimoto, K.K., Moody, V.M., Xiao, G., Nocera, D.G. and Joshi, N.S. 2018. Light-driven fine chemical production in yeast biohybrids. *Science*. **362**(6416), pp.813–816.

Guttentag, M., Rodenberg, A., Kopelent, R., Probst, B., Buchwalder, C., Brandstätter, M., Hamm, P. and Alberto, R. 2012. Photocatalytic H2 production with a rhenium/cobalt system in water under acidic conditions. *European Journal of Inorganic Chemistry*. (1), pp.59–64.

Halder, S., Yadav, K.K., Sarkar, R., Mukherjee, S., Saha, P., Haldar, S., Karmakar, S. and Sen, T. 2015. Alteration of Zeta potential and membrane permeability in bacteria: a study with cationic agents. *SpringerPlus*. **4**(1), p.672.

Hasan, M., Bethell, D. and Brust, M. 2002. The Fate of Sulfur-Bound Hydrogen on Formation of Self-Assembled Thiol Monolayers on Gold. *J.*

Am. Chem. Soc. **142**(7), p.1132.

Hatakeyama, M., Kishi, H., Kita, Y., Imai, K., Nishio, K., Karasawa, S., Masaike, Y., Sakamoto, S., Sandhu, A., Tanimoto, A., Gomi, T., Kohda, E., Abe, M. and Handa, H. 2011. A two-step ligand exchange reaction generates highly water-dispersed magnetic nanoparticles for biomedical applications. *Journal of Materials Chemistry*. **21**(16), p.5959.

Hau, H.H. and Gralnick, J.A. 2007. Ecology and Biotechnology of the Genus *Shewanella*. *Annual Review of Microbiology*. **61**(1), pp.237–258.

He, L., Du, P., Chen, Y., Lu, H., Cheng, X., Chang, B. and Wang, Z. 2017. Advances in microbial fuel cells for wastewater treatment. *Renewable and Sustainable Energy Reviews*. **71**(May 2016), pp.388–403.

He, W., Yuan, S., Zhong, W. and Siddikee, A. 2016. Application of genetically engineered microbial whole-cell biosensors for combined chemosensing. *Applied Microbiology and Biotechnology*., pp.1109–1119.

Heath, G.R., Li, M., Polignano, I.L., Richens, J.L., Catucci, G., Shea, P.O., Sadeghi, S.J., Gilardi, G., Butt, J.N. and Jeuken, L.J.C. 2015. Layer-by-Layer Assembly of Supported Lipid Bilayer Poly -. *ACS Biomacromolecules*. (17), pp.324–335.

Heidelberg, J.F., Paulsen, I.T., Nelson, K.E., Gaidos, E.J., Nelson, W.C., Read, T.D., Eisen, J.A., Seshadri, R., Ward, N., Methe, B., Clayton, R.A., Meyer, T., Tsapin, A., Scott, J., Beanan, M., Brinkac, L., Daugherty, S., DeBoy, R.T., Dodson, R.J., Durkin, A.S., Haft, D.H., Kolonay, J.F., Madupu, R., Peterson, J.D., Umayam, L.A., White, O., Wolf, A.M., Vamathevan, J., Weidman, J., Impraim, M., Lee, K., Berry, K., Lee, C., Mueller, J., Khouri, H., Gill, J., Utterback, T.R., McDonald, L.A., Feldblyum, T. V., Smith, H.O., Venter, J.C., Nealson, K.H. and Fraser, C.M. 2002. Genome sequence of the dissimilatory metal ion–reducing bacterium Shewanella oneidensis. *Nature Biotechnology*. **20**(11), pp.1118–1123.

Hell, S.W. and Wichmann, J. 1994. Breaking the diffrection limit by stimulated emission: stimulated emission-depletion fluorescence microscopy. *Optics letters*. **19**(11), p.780.

Herschel, J.F. 1845. No. I.—on a case of superficial colour presented by a homogeneous liquid internally colourless. *Philos Trans R Soc London*. **135**, pp.143–145.

Higgins, S.R., Foerster, D., Cheung, A., Lau, C., Bretschger, O., Minteer, S.D., Nealson, K., Atanassov, P. and Cooney, M.J. 2011. Fabrication of macroporous chitosan scaffolds doped with carbon nanotubes and their characterization in microbial fuel cell operation. *Enzyme and Microbial Technology*. **48**(6–7), pp.458–465.

Holzinger, M., Goff, A. Le and Cosnier, S. 2014. Nanomaterials for biosensing applications : a review. *Frontiers in Chemistry*. **2**(August), pp.1–10.

Holzmeister, I., Schamel, M., Groll, J., Gbureck, U. and Vorndran, E. 2018. Artificial inorganic biohybrids: The functional combination of microorganisms and cells with inorganic materials. *Acta Biomaterialia*. **74**, pp.17–35.

Hostetler, M.J., Templeton, A.C. and Murray, R.W. 1999. Dynamics of place-exchange reactions on monolayer-protected gold cluster molecules. *Langmuir*. **15**(11), pp.3782–3789.

Huismant, O., Arit, R.D. and Gottesmant, S. 1984. Cell-division control in Escherichia coli : Specific induction of the SOS function SfiA protein is sufficient to block septation. *Proceedings of the National Academy of Sciences*. **81**(July), pp.4490–4494.

Huygens, C. 1622. Letter from Constatntijin Huygens, London, 30 March 1622, to his Parents in Netherlands.

Hwang, E.T., Sheikh, K., Orchard, K.L., Hojo, D., Radu, V., Lee, C.Y., Ainsworth, E., Lockwood, C., Gross, M.A., Adschiri, T., Reisner, E., Butt, J.N. and Jeuken, L.J.C. 2015. A decaheme cytochrome as a molecular electron conduit in dye-sensitized photoanodes. *Advanced Functional Materials*. **25**(15), pp.2308–2315.

Ipe, B.I., Shukla, A., Lu, H., Zou, B., Rehage, H. and Niemeyer, C.M. 2006. Dynamic light-scattering analysis of the electrostatic interaction of hexahistidine-tagged cytochrome P450 enzyme with semiconductor quantum dots. *ChemPhysChem*. **7**(5), pp.1112–1118.

Jamieson, T.T., Bakhshi, R., Petrova, D., Pocock, R., Imani, M. and Seifalian, A.M. 2007. Biological applications of quantum dots. *Biomaterials*. **28**(31), pp.4717–4732.

Janda, J.M. and Abbott, S.L. 2012. The genus Shewanella: From the briny depths below to human pathogen. *Critical Reviews in Microbiology*. **40**(4), pp.293–312.

Jordan, H.J., Wegner, M. and Tiziani, H. 1998. Highly accurate non-contact characterization of engineering surfaces using confocal microscopy. *Measurement Science and Technology*. **9**(7), pp.1142–1151.

Jung, R.K., Dec, J., Bruns, M.A. and Logan, B.E. 2008. Removal of odors from swine wastewater by using microbial fuel cells. *Applied and Environmental Microbiology*. **74**(8), pp.2540–2543.

Kalathil, S., Lee, J. and Cho, M.H. 2011. Granular activated carbon based microbial fuel cell for simultaneous decolorization of real dye wastewater and electricity generation. *New Biotechnology*. **29**(1), pp.32–37.

Kanellos, M. 2006. Cabon NT in tiur de france.pdf. *https://www.cnet.com/*. [Online]. Available from: https://www.cnet.com/news/carbon-nanotubes-enter-tour-de-france/.

Karakoti, A.S., Shukla, R., Shanker, R. and Singh, S. 2015. Surface functionalization of quantum dots for biological applications. *Advances in Colloid and Interface Science*. **215**, pp.28–45.

Keer, J.T. and Birch, L. 2003. Molecular methods for the assessment of bacterial viability. *Journal of Microbiological Methods*. **53**(2), pp.175–183.

Kelf, T.A., Sreenivasan, V.K.A., Sun, J., Kim, E.J., Goldys, E.M. and Zvyagin, A. V. 2010. Non-specific cellular uptake of surface-functionalized quantum dots. *Nanotechnology*. **21**(28).

Kern, M., Einsle, O. and Simon, J. 2008. Variants of the tetrahaem cytochrome c quinol dehydrogenase NrfH characterize the menaquinol-binding site, the haem c-binding motifs and the transmembrane segment. *Biochemical Journal*. **414**(1), pp.73–79.

Kisielowski, C., Freitag, B., Bischoff, M., Lin, H. Van, Lazar, S., Knippels, G.,

Tiemeijer, P., Stam, M. Van Der, Harrach, S. Von, Stekelenburg, M., Haider, M., Uhlemann, S., Müller, H., Hartel, P., Kabius, B., Miller, D., Petrov, I., Olson, E.A., Donchev, T., Kenik, E.A., Lupini, A.R., Bentley, J., Pennycook, S.J., Anderson, I.M., Minor, A.M., Schmid, A.K., Duden, T., Radmilovic, V., Ramasse, Q.M., Watanabe, M., Erni, R., Stach, E.A. and Denes, P. 2008. Detection of Single Atoms and Buried Defects in Three Dimensions by Aberration-Corrected Electron Microscope with 0 . 5-Å Information Limit. *Microscopy and Microanalysis*. **14**, pp.469–477.

Klar, T.A., Jakobs, S., Dyba, M., Egner, A. and Hell, S.W. 2000. Fluorescence microscopy with diffraction resolution barrier broken by stimulated emission. . **97**(15).

Kloepfer, J.A., Mielke, R.E. and Nadeau, J.L. 2005. Uptake of CdSe and CdSe / ZnS Quantum Dots into Bacteria via Purine-Dependent Mechanisms Uptake of CdSe and CdSe / ZnS Quantum Dots into Bacteria via Purine-Dependent Mechanisms. *Applied and environmental microbiology*. **71**(5), pp.2548–2557.

Korenevsky, A. and Beveridge, T.J. 2007. The surface physicochemistry and adhesiveness of Shewanella are affected by their surface polysaccharides. *Microbiology*. **153**(6), pp.1872–1883.

Korenevsky, A.A., Vinogradov, E., Gorby, Y. and Beveridge, T.J. 2002. Characterization of the lipopolysaccharides and capsules of Shewanella spp. *Applied and Environmental Microbiology*. **68**(9), pp.4653–4657.

Kornienko, N., Sakimoto, K.K., Herlihy, D.M., Nguyen, S.C., Alivisatos, A.P., Harris, C.B., Schwartzberg, A. and Yang, P. 2016. Spectroscopic elucidation of energy transfer in hybrid inorganic–biological organisms for solar-to-chemical production. *Proceedings of the National Academy of Sciences*. **113**(42), pp.11750–11755.

Kornienko, N., Zhang, J.Z., Sakimoto, K.K., Yang, P. and Reisner, E. 2018. Interfacing nature's catalytic machinery with synthetic materials for semi-artificial photosynthesis. *Nature Nanotechnology*. **13**(10), pp.890–899.

Kreuzer, H.W., Hill, E.A., Moran, J.J., Bartholomew, R.A., Yang, H. and Hegg, E.L. 2014. Contributions of the [NiFe]- and [FeFe]-hydrogenase to H 2

production in Shewanella oneidensis MR-1 as revealed by isotope ratio analysis of evolved H 2. *FEMS Microbiology Letters*. **352**(1), pp.18–24.

Kumar, G.G., Sarathi, V.G.S. and Nahm, K.S. 2013. Recent advances and challenges in the anode architecture and their modifications for the applications of microbial fuel cells. *Biosensors and Bioelectronics*. **43**(1), pp.461–475.

Kundu, S. and Patra, A. 2017. Nanoscale Strategies for Light Harvesting. *Chemical Reviews*. **117**, pp.712–757.

Lakshmi, C., Hanshaw, R.G. and Smith, B.D. 2004. Fluorophore-linked zinc(II)dipicolylamine coordination complexes as sensors for phosphatidylserine-containing membranes. *Tetrahedron*. **60**(49), pp.11307–11315.

Lawal, A.T. 2016. Synthesis and utilization of carbon nanotubes for fabrication of electrochemical biosensors. *Materials Research Bulletin*. **73**, pp.308–350.

Lee, H., Dellatore, S.M., Miller, W.M. and Messersmith, P.B. 2007. Mussel-inspired surface chemistry for multifunctional coatings. *Science*. **318**(5849), pp.426–430.

Leevy, W.M., Johnson, J.R., Lakshmi, C., Morris, J., Marquez, M. and Smith, B.D. 2006. Selective recognition of bacterial membranes by zinc(ii)-coordination complexes. *Chemical Communications*. **1**(15), p.1595.

Leigh, K., Bouldin, J. and Buchanan, R. 2012. Effects of Exposure to Semiconductor Nanoparticles on Aquatic Organisms. *Journal of Toxicology*. **2012**, pp.1–9.

Leong, J.X., Daud, W.R.W., Ghasemi, M., Liew, K. Ben and Ismail, M. 2013. Ion exchange membranes as separators in microbial fuel cells for bioenergy conversion: A comprehensive review. *Renewable and Sustainable Energy Reviews*. **28**, pp.575–587.

Leroy, P., Tournassat, C., Bernard, O., Devau, N. and Azaroual, M. 2015. The electrophoretic mobility of montmorillonite. Zeta potential and surface conductivity effects. *Journal of Colloid and Interface Science*. **451**, pp.21–

39.

Leuko, S., Legat, A., Fendrihan, S. and Stan-lotter, H. 2004. Evaluation of the LIVE/DEAD BacLight Kit for Detection of Extremophilic Archaea and Visualization of Microorganisms in Environmental Hypersaline Samples Stefan. *Applied and Environmental Microbiology*. **70**(11), pp.6884–6886.

Li, D.B., Cheng, Y.Y., Wu, C., Li, W.W., Li, N., Yang, Z.C., Tong, Z.H. and Yu, H.Q. 2014. Selenite reduction by Shewanella oneidensis MR-1 is mediated by fumarate reductase in periplasm. *Scientific Reports*. **4**(0), pp.1–7.

Li, M., Zhou, H., Zhang, H., Sun, P., Kuiyu, Y., Meng, W., Dong, Z. and Xu, S. 2010. Preparation and purification of l-cysteine capped CdTe quantum dots and its self-recovery of degenerate fluorescence. *Journal of Luminescence*. **130**, pp.1935–1940.

Li, Y., Yang, D., Wang, S., Li, C., Xue, B., Yang, L., Shen, Z., Jin, M., Wang, J. and Qiu, Z. 2018. The Detailed Bactericidal Process of Ferric Oxide. *Molecules*. **23**(606), pp.1–12.

Lies, D.P., Hernandez, M.E., Kappler, A., Mielke, R.E., Gralnick, J.A., Dianne, K. and Newman, D.K. 2005. Shewanella oneidensis MR-1 Uses Overlapping Pathways for Iron Reduction at a Distance and by Direct Contact under Conditions Relevant for Biofilm. *Applied and environmental microbiology*. **71**(8), pp.4414–4426.

Liu, C., Sakimoto, K.K., Colón, B.C., Silver, P.A. and Nocera, D.G. 2017. Ambient nitrogen reduction cycle using a hybrid inorganic–biological system. *Proceedings of the National Academy of Sciences*. **114**(25), pp.6450–6455.

Liu, H. and Logan, B.E. 2004. Electricity generation using an air-cathode single chamber microbial fuel cell in the presence and absence of a proton exchange membrane. *Environmental Science and Technology*. **38**(14), pp.4040–4046.

Liu, X., Tang, J., Wang, L. and Giesy, J.P. 2018. Ecotoxicology and Environmental Safety Mechanisms of oxidative stress caused by CuO nanoparticles to membranes of the bacterium Streptomyces coelicolor

M145. *Ecotoxicology and Environmental Safety*. **158**(February), pp.123–130.

Logan, B.E. 2008. Microbial fuels for the future A potter round Darwin ' s patch. *Nature opinions*. **454**(August).

Logan, B.E. and Elimelech, M. 2012. Membrane-based processes for sustainable power generation using water. *Nature*. **488**(7411), pp.313–319.

Logan, B.E., Hamelers, B., Rozendal, R., Schröder, U., Keller, J., Freguia, S., Aelterman, P., Verstraete, W. and Rabaey, K. 2006. Microbial fuel cells: Methodology and technology. *Environmental Science and Technology*. **40**(17), pp.5181–5192.

Logan, B.E. and Rabaey, K. 2012. Conversion of Wastes into Bioelectricity and Chemicals by Using Microbial Electrochemical Technologies. *Science*. **337**(August), pp.686–690.

Logan, B.E. and Regan, J.M. 2006. Electricity-producing bacterial communities in microbial fuel cells. *Trends in Microbiology*. **14**(12), pp.512–518.

Logan, B.E., Wallack, M.J., Kim, K.Y., He, W., Feng, Y. and Saikaly, P.E. 2015. Assessment of Microbial Fuel Cell Configurations and Power Densities. *Environmental Science and Technology Letters*. **2**(8), pp.206–214.

Long, H.F. and Hammer, B.W. 1941. Classification of the Organisms Important in Dairy Products. *Research Bulletin*. **285**, pp.176–195.

Loukanov, A.R., Dushkin, C.D., Papazova, K.I., Kirov, A. V., Abrashev, M. V. and Adachi, E. 2004. Photoluminescence depending on the ZnS shell thickness of CdS/ZnS core-shell semiconductor nanoparticles. *Colloids and Surfaces A: Physicochemical and Engineering Aspects*. **245**(1–3), pp.9–14.

Lovley, D. and Walker, D. 2019. Geobacter protein nanowires. *PeerJ Preprints*. **10**(September).

Lovley, D.R. 2006a. Bug juice: Harvesting electricity with microorganisms.

Nature Reviews Microbiology. **4**(7), pp.497–508.

Lovley, D.R. 2012. Long-range electron transport to Fe(III) oxide via pili with metallic-like conductivity. *Biochemical Society Transactions*. **40**(6), pp.1186–1190.

Lovley, D.R. 2006b. Microbial fuel cells: novel microbial physiologies and engineering approaches. *Current Opinion in Biotechnology*. **17**(3), pp.327–332.

Lovley, D.R. and Malvankar, N.S. 2015. Seeing is believing: Novel imaging techniques help clarify microbial nanowire structure and function. *Environmental Microbiology*. **17**(7), pp.2209–2215.

Lovley, D.R. and Nevin, K.P. 2018. Microbial production of multi-carbon chemicals and fuels from water and carbon dioxide using electrical current. . **US 9**, **856**.

Lovrić, J., Bazzi, H.S., Cuie, Y., Fortin, G.R.A., Winnik, F.M. and Maysinger, D. 2005. Differences in subcellular distribution and toxicity of green and red emitting CdTe quantum dots. *Journal of Molecular Medicine*. **83**(5), pp.377–385.

Luo, H., Guo, Q., Szilágyi, P.Á., Jorge, A.B. and Titirici, M.M. 2020. Carbon Dots in Solar-to-Hydrogen Conversion. *Trends in Chemistry*. **2**(7), pp.623–637.

Luo, Z., Manders, J. and Yurek, J. 2018. Your Guide to Television's Quantum-Dot Future. *Your Guide to Television's Quantum-Dot Future*. [Online]. Available from: https://spectrum.ieee.org/consumer-electronics/audiovideo/your-guide-to-televisions-quantumdot-future.

MacDonell, M.T. and Colwell, R.R. 1985. Phylogeny of the Vibrionaceae, and Recommendation for Two New Genera, Listonella and Shewanella. *Systematic and Applied Microbiology*. **6**(2), pp.171–182.

Madden, D.P., da Mota, M.M. and Nelson, S.M. 1970. Five-co-ordination in Molecular Complexes of Zinc, Cadmium, and Mercury(ii) with Potentially Ter- or Tetra-dendate Ligands with Nitrogen Donor Atoms. *J. Chem. Soc. A*. **0**, pp.790–794.

Maffre, P., Brandholt, S., Nienhaus, K., Shang, L., Parak, W.J. and Nienhaus, G.U. 2014. Effects of surface functionalization on the adsorption of human serum albumin onto nanoparticles - A fluorescence correlation spectroscopy study. *Beilstein Journal of Nanotechnology*. **5**(1), pp.2036–2047.

Maldonado, M.I., López-martín, A., Colón, G., Peral, J., Martínez-costa, J.I. and Malato, S. 2018. Applied Catalysis B : Environmental Solar pilot plant scale hydrogen generation by irradiation of Cu / TiO 2 composites in presence of sacri fi cial electron donors. *Applied Catalysis B: Environmental*. **229**(February), pp.15–23.

Malvankar, N.S., Vargas, M., Nevin, K.P., Franks, A.E., Leang, C., Kim, B.C., Inoue, K., Mester, T., Covalla, S.F., Johnson, J.P., Rotello, V.M., Tuominen, M.T. and Lovley, D.R. 2011. Tunable metallic-like conductivity in microbial nanowire networks. *Nature Nanotechnology*. **6**(9), pp.573–579.

Manke, A., Wang, L. and Rojanasakul, Y. 2013. Mechanisms of Nanoparticle-Induced Oxidative Stress and Toxicity. *BioMed Research International*. **2013**, pp.1–15.

Marshall, M.J., Plymale, A.E., Kennedy, D.W., Shi, L., Wang, Z., Reed, S.B., Dohnalkova, A.C., Simonson, C.J., Liu, C., Saffarini, D.A., Romine, M.F., Zachara, J.M., Beliaev, A.S. and Fredrickson, J.K. 2008. Hydrogenase- and outer membrane c-type cytochrome-facilitated reduction of technetium(VII) by Shewanella oneidensis MR-1. *Environmental Microbiology*. **10**(1), pp.125–136.

Marsili, E., Baron, D.B., Shikhare, I.D., Coursolle, D., Gralnick, J.A. and Bond, D.R. 2008. Shewanella secretes flavins that mediate extracellular electron transfer. *Proceedings of the National Academy of Sciences*. **105**(10), pp.3968–3973.

Mattera, L., Bhuckory, S., Wegner, K.D., Qiu, X., Agnese, F., Lincheneau, C., Senden, T., Djurado, D., Charbonnière, L.J., Hildebrandt, N. and Reiss, P. 2016. Compact quantum dot–antibody conjugates for FRET immunoassays with subnanomolar detection limits. *Nanoscale*. **8**(21),

pp.11275–11283.

Mazia, D., Schatten, G. and Sale, W. 1975. Adhesion of Cells to Surfaces Coated with Polylysine. Aoplications to Electron Microscopy. *Journal of Cell Biology*. **66**(3), pp.198–200.

McCormick, A.J., Bombelli, P., Bradley, R.W., Thorne, R., Wenzel, T. and Howe, C.J. 2015. Biophotovoltaics: Oxygenic photosynthetic organisms in the world of bioelectrochemical systems. *Energy and Environmental Science*. **8**(4), pp.1092–1109.

Mcmillan, D.G.G., Marritt, S.J., Firer-sherwood, M.A., Shi, L., Richardson, D.J., Evans, S.D., Elliott, S.J., Butt, J.N. and Jeuken, L.J.C. 2013. Protein–Protein Interaction Regulates the Direction of Catalysis and Electron Transfer in a Redox Enzyme Complex. *Journal of the American Chemical Society*. **135**(28), pp.10550–10556.

Medintz, I.L., Uyeda, H.T., Goldman, E.R. and Mattoussi, H. 2005. Quantum dot bioconjugates for imaging, labelling and sensing. *Nature Materials*. **4**(6), pp.435–446.

Melhuish, C., Ieropoulos, I., Greenman, J. and Horsfield, I. 2006. Energetically autonomous robots: Food for thought. *Autonomous Robots*. **21**(3), pp.187–198.

Meshulam-Simon, G., Behrens, S., Choo, A.D. and Spormann, A.M. 2007. Hydrogen metabolism in Shewanella oneidensis MR-1. *Applied and Environmental Microbiology*. **73**(4), pp.1153–1165.

Mikhailenko, S.D., Zaidi, S.M.J. and Kaliaguine, S. 2000. Sulfonated polyether ether ketone based composite polymer electrolyte membranes. *4th International Conference on Catalysis in Membrane Reactors (ICCMR-2000_)*. **67**, pp.225–236.

Min, B. and Logan, B.E. 2004. Continuous electricity generation from domestic wastewater and organic substrates in a flat plate microbial fuel cell. *Environmental Science and Technology*. **38**(21), pp.5809–5814.

Min, D., Cheng, L., Liu, D.F., Li, W.W. and Yu, H.Q. 2020. Electron transfer via the non-Mtr respiratory pathway from Shewanella putrefaciens CN-32

for methyl orange bioreduction. *Process Biochemistry*. **95**(March), pp.108–114.

Minsky, M. 1961. Microscopy Apparatus. , p.3013467.

Moos, N. von and Slaveykova, V.I. 2014. Oxidative stress induced by inorganic nanoparticles in bacteria and aquatic microalgae – state of the art and knowledge gaps aquatic microalgae – state of the art and knowledge gaps. *Nanotoxicology*. **8**(6), pp.605–630.

Mueller, N.C. and Nowack, B. 2008. Exposure modelling of engineered nanoparticles in the environment. *Environmental science & technology*. **42**(12), pp.44447–53.

Myers, C.R. and Myers, J.M. 1997. Cloning and sequence of cymA, a gene encoding a tetraheme cytochrome c required for reduction of iron(III), fumarate, and nitrate by Shewanella putrefaciens MR-1. *Journal of Bacteriology*. **179**(4), pp.1143–1152.

Myers, C.R.C., Nealson, K.H.K. and June, I. 1988. Bacterial Manganese Reduction and Growth with Manganese Oxide as the Sole Electron Acceptor. *Science*. **240**(4857), pp.1319–1321.

Nabiev, I., Rakovich, A., Sukhanova, A., Lukashev, E., Zagidullin, V., Pachenko, V., Rakovich, Y.P., Donegan, J.F., Rubin, A.B. and Govorov, A.O. 2010. Fluorescent quantum dots as artificial antennas for enhanced light harvesting and energy transfer to photosynthetic reaction centers. *Angewandte Chemie - International Edition*. **49**(40), pp.7217–7221.

Nangle, S.N., Sakimoto, K.K., Silver, P.A. and Nocera, D.G. 2017. Biological-inorganic hybrid systems as a generalized platform for chemical production. *Current Opinion in Chemical Biology*. **41**, pp.107–113.

Nealson, K.H. and Scott, J. 2006. Ecophysiology of the Genus Shewanella. *In*: *The Prokaryotes* [Online]. New York: Springer, New York, NY, pp.1133–1151. Available from: https://link.springer.com/referenceworkentry/10.1007/0-387-30746-X_45#citeas.

Ngo, H.T., Liu, X. and Jolliffe, K.A. 2012. Anion recognition and sensing with

Zn(ii)–dipicolylamine complexes. *Chemical Society Reviews*. **41**(14), p.4928.

Niidome, Y., Honda, K., Higashimoto, K., Kawazumi, H., Yamada, S., Nakashima, N., Sasaki, Y., Ishida, Y. and Kikuchi, J. 2007. Surface modification of gold nanorods with synthetic cationic lipids. *Chemical communications (Cambridge, England)*. (36), pp.3777–9.

Nocera, D.G. 2017. Solar fuels and solar chemicals industry. *Accounts of Chemical Research*. **50**(3), pp.616–619.

Oh, E., Liu, R., Nel, A., Gemill, K.B., Bilal, M., Cohen, Y. and Medintz, I.L. 2016. Meta-analysis of cellular toxicity for cadmium-containing quantum dots. *Nature Nanotechnology*. **11**(5), pp.479–486.

Oliveira, V.B., Simões, M., Melo, L.F. and Pinto, A.M.F.R. 2013. Overview on the developments of microbial fuel cells. *Biochemical Engineering Journal*. **73**, pp.53–64.

Pal, U., Ghosh, S. and Chatterjee, D. 2012. Effect of sacrificial electron donors on hydrogen generation over visible light – irradiated nonmetal-doped TiO 2 photocatalysts. *Transittion Met Chem*. **2**(37), pp.93–96.

Pant, D., Van Bogaert, G., Diels, L. and Vanbroekhoven, K. 2010. A review of the substrates used in microbial fuel cells (MFCs) for sustainable energy production. *Bioresource Technology*. **101**(6), pp.1533–1543.

Pellegrin, Y. and Odobel, F. 2017. Les donneurs d'électron sacrificiels pour la production de combustible solaire. *Comptes Rendus Chimie*. **20**(3), pp.283–295.

Pelletier, D.A., Suresh, A.K., Holton, G.A., Mckeown, C.K., Wang, W., Gu, B., Mortensen, N.P., Allison, D.P., Joy, D.C., Allison, M.R., Brown, S.D., Phelps, T.J. and Doktycz, M.J. 2010. Effects of Engineered Cerium Oxide Nanoparticles on Bacterial Growth and Viability □ †. *Applied and Enviromental Microbiology*. **76**(24), pp.7981–7989.

Pinchuk, G.E., Geydebrekht, O. V., Hill, E.A., Reed, J.L., Konopka, A.E., Beliaev, A.S. and Fredrickson, J.K. 2011. Pyruvate and Lactate Metabolism by Shewanella oneidensis MR-1 under Fermentation ,

Oxygen Limitation , and Fumarate Respiration Conditions □ †. *Applied and Enviromental Microbiology*. **77**(23), pp.8234–8240.

Pirbadian, S., Barchinger, S.E., Man Leung, K., Suk Byun, H., Jangir, Y., Bouhenni, R.A., Reed, S.B., Romine, M.F., Saffarini, D.A., Shi, L., Gorby, Y.A., Golbeck, J.H., El-Naggar, M.Y., Leung, K.M., Byun, H.S., Jangir, Y., Bouhenni, R.A., Reed, S.B., Romine, M.F., Saffarini, D.A., Shi, L., Gorby, Y.A., Golbeck, J.H. and El-Naggar, M.Y. 2014. Shewanella oneidensis MR-1 nanowires are outer membrane and periplasmic extensions of the extracellular electron transport components. *Proceedings of the National Academy of Sciences*. **111**(35), pp.12883–12888.

Pramanik, S., Hill, S.K.E., Zhi, B., Hudson-smith, N. V, Wu, J.J., White, J.N., Mcintire, E.A., Kondeti, V.S.S.K., Lee, A.L., Bruggeman, P.J., Kortshagen, U.R. and Haynes, C.L. 2018. Comparative toxicity assessment of novel Si quantum dots and their traditional Cd-based counterparts using bacteria models Shewanella oneidensis and Bacillus subtilis†. *Environmental Science Nano*. **5**, pp.1890–1901.

Prasher, D.C., Eckenrode, V.K., Ward, W.W., Prendergast, F.G. and Cormier, M.J. 1992. Aequorea victoria. *Gene*. **111**, pp.229–233.

Qiu, T.A., Meyer, B.M., Christenson, K.G., Klaper, R.D. and Haynes, C.L. 2017. A mechanistic study of TiO2nanoparticle toxicity on Shewanella oneidensis MR-1 with UV-containing simulated solar irradiation: Bacterial growth, riboflavin secretion, and gene expression. *Chemosphere*. **168**, pp.1158–1168.

Reguera, G., McCarthy, K.D., Mehta, T., Nicoll, J.S., Tuominen, M.T. and Lovley, D.R. 2005. Extracellular electron transfer via microbial nanowires. *Nature*. **435**(7045), pp.1098–1101.

Reiss, P., Protière, M. and Li, L. 2009. Core/shell semiconductor nanocrystals. *Small*. **5**(2), pp.154–168.

Rice, D.R., Gan, H. and Smith, B.D. 2015. Bacterial Imaging and Photodynamic Inactivation Using Zinc(II)-Dipicolylamine BODIPY Conjugates †. *Photochem Photobiol Sci.* **14**, pp.1271–1281.

Rodrigues, J.L.M., Serres, M.H. and Tiedje, J.M. 2011. Large-scale

comparative phenotypic and genomic analyses reveal ecological preferences of Shewanella species and identify metabolic pathways conserved at the genus level. *Applied and Environmental Microbiology*. **77**(15), pp.5352–5360.

Rogach, A.L., Franzl, T., Klar, T.A., Feldmann, J., Gaponik, N., Lesnyak, V., Shavel, A., Eychmüller, A., Rakovich, Y.P., Donegan, J.F., Rogavch, A.L., Franzi, T., Klar, T.A., Feldmann, J., Gaponik, N., Lesnyak, V., Shevei, A., Eychmuller, A., Rakovich, Y.P. and Donegan, J.F. 2007. Aqueous synthesis of thiol-capped CdTe nanocrystals: State-of-the-art. *Journal of Physical Chemistry C*. **111**(40), pp.14628–14637.

Roiter, Y., Ornatska, M., Rammohan, A.R., Balakrishnan, J., Heine, D.R. and Minko, S. 2008. Interaction of nanoparticles with lipid membrane. *Nano Letters*. **8**(3), pp.941–944.

Ross, D.E., Ruebush, S.S., Brantley, S.L., Hartshorne, R.S., Clarke, T.A., Richardson, D.J. and Tien, M. 2007. Characterization of protein-protein interactions involved in iron reduction by Shewanella oneidensis MR-1. *Applied and Environmental Microbiology*. **73**(18), pp.5797–5808.

Rowe, A.R., Rajeev, P., Jain, A., Pirbadian, S., Okamoto, A., Gralnick, J.A., El-Naggar, M.Y. and Nealson, K.H. 2018. Tracking Electron Uptake from a Cathode into Shewanella Cells: Implications for Energy Acquisition from Solid-Substrate Electron Donors. *mBio*. **9**(1), pp.1–19.

Rowe, S.F., Le Gall, G., Ainsworth, E. V., Davies, J.A., Lockwood, C.W.J., Shi, L., Elliston, A., Roberts, I.N., Waldron, K.W., Richardson, D.J., Clarke, T.A., Jeuken, L.J.C., Reisner, E. and Butt, J.N. 2017. Light-Driven H 2 Evolution and C═C or C═O Bond Hydrogenation by Shewanella oneidensis : A Versatile Strategy for Photocatalysis by Nonphotosynthetic Microorganisms. *ACS Catalysis*. **7**(11), pp.7558–7566.

Ruedas-Rama, M.J., Orte, A., Hall, E.A.H., Alvarez-Pez, J.M. and Talavera, E.M. 2011. Effect of surface modification on semiconductor nanocrystal fluorescence lifetime. *ChemPhysChem*. **12**(5), pp.919–929.

Ruska, E. 1987. Nobel Lecture The Development of the Electron Microscope and of Electron Microscopy. *Bioscience Reports*. **7**(8), pp.607–623.

Rzigalinski, B.A. and Strobl, J.S. 2009. Cadmium-containing nanoparticles : Perspectives on pharmacology and toxicology of quantum dots i. *Toxicology and Applied Pharmacology*. **238**(3), pp.280–288.

Saha, K., Agasti, S.S., Kim, C., Li, X. and Rotello, V.M. 2012. Gold Nanoparticles in Chemical and Biological Sensing. *Chemical Reviews*. **112**(5), pp.2739–2779.

Sakamoto, T., Ojida, A. and Hamachi, I. 2009. Molecular recognition, fluorescence sensing, and biological assay of phosphate anion derivatives using artificial Zn((II)–Dpa complexes. *Chem. Commun.* (2), pp.141–152.

Sakimoto, K.K., Kornienko, N., Cestellos-Blanco, S., Lim, J., Liu, C. and Yang, P. 2018. Physical Biology of the Materials-Microorganism Interface. *Journal of the American Chemical Society*. **140**(6), pp.1978–1985.

Sakimoto, K.K., Kornienko, N. and Yang, P. 2017. Cyborgian material design for solar fuel production: The emerging photosynthetic biohybrid systems. *Accounts of Chemical Research*. **50**(3), pp.476–481.

Sakimoto, K.K., Wong, A.B. and Yang, P. 2016. Self-photosensitization of nonphotosynthetic bacteria for solar-to-chemical production. *Science*. **351**(6268).

Santoro, C., Arbizzani, C., Erable, B. and Ieropoulos, I. 2017. Microbial fuel cells: From fundamentals to applications. A review. *Journal of Power Sources*. **356**, pp.225–244.

Santoro, C., Lei, Y., Li, B. and Cristiani, P. 2012. Power generation from wastewater using single chamber microbial fuel cells (MFCs) with platinum-free cathodes and pre-colonized anodes. *Biochemical Engineering Journal*. **62**, pp.8–16.

Dos Santos, J.P., Iobbi-Nivol, C., Couillault, C., Giordano, G. and Méjean, V. 1998. Molecular analysis of the trimethylamine N-oxide (TMAO) reductase respiratory system from a Shewanella species. *Journal of Molecular Biology*.

Schicklberger, M., Bücking, C., Schuetz, B., Heide, H. and Gescher, J. 2011.

Involvement of the Shewanella oneidensis Decaheme Cytochrome MtrA in the Periplasmic Stability of the β-Barrel Protein MtrB. *Applied and Environmental Microbiology*. **77**(4), pp.1520–1523.

Schneider, R., Wolpert, C., Guilloteau, H., Balan, L., Lambert, J. and Merlin, C. 2009. The exposure of bacteria to CdTe-core quantum dots: the importance of surface chemistry on cytotoxicity. *Nanotechnology*. **20**(22), p.225101.

Serrano, I.C., Ma, Q. and Palomares, E. 2011. QD-"Onion"-Multicode silica nanospheres with remarkable stability as pH sensors. *Journal of Materials Chemistry*. **21**(44), pp.17673–17679.

Serres, M.H. and Riley, M. 2006. Genomic Analysis of Carbon Source Metabolism of Shewanella oneidensis MR-1 : Predictions versus Experiments †. *Journal of Bacteriology*. **188**(13), pp.4601–4609.

Shi, L., Belchik, S.M., Plymale, A.E., Heald, S., Dohnalkova, A.C., Sybirna, K., Bottin, H., Squier, T.C., Zachara, J.M. and Fredrickson, J.K. 2011. Purification and characterization of the [NiFe]-Hydrogenase of Shewanella oneidensis MR-1. *Applied and Environmental Microbiology*. **77**(16), pp.5584–5590.

Smoluchowski, M. 1906. Zur kinetischen Theorik der Brownschen Molekularbewegung und der Suspetionen. *Annelen der Physik*. **17**, pp.756–780.

Spence, J.C.H. 1988. A scanning tunneling microscope in a side-entry holder for reflection electron microscopy in the Philips EM400. *Ultramicroscopy*. **25**, pp.165–169.

Stokes, G. 1852. On the change of refrangibility of light. *Philos Trans R Soc London*. **142**, pp.463–562.

Sturm, G., Richter, K., Doetsch, A., Heide, H., Louro, R.O. and Gescher, J. 2015. A dynamic periplasmic electron transfer network enables respiratory flexibility beyond a thermodynamic regulatory regime. *ISME Journal*. **9**(8), pp.1802–1811.

Sun, M., Yang, L., Jose, P., Wang, L. and Zweit, J. 2013. Functionalization of

quantum dots with multidentate zwitterionic ligands: impact on cellular interactions and cytotoxicity. *Journal of Materials Chemistry B*. **1**(44), p.6137.

Suresh, A.K., Pelletier, D.A. and Doktycz, M.J. 2013. Relating nanomaterial properties and microbial toxicity. *Nanoscale*. **5**(2), pp.463–474.

Tamang, S., Beaune, G., Texier, I. and Reiss, P. 2011. Aqueous phase transfer of InP/ZnS nanocrystals conserving fluorescence and high colloidal stability. *ACS Nano*. **5**(12), pp.9392–9402.

Tefft, N.M. and TerAvest, M.A. 2019. Reversing an extracellular electron transfer pathway for electrode-driven NADH generation. *ACS Synthetic Biology*. **8**(7), pp.1590–1600.

Thompson, D.T. 2008. Michael Faraday's recognition of Ruby Gold: The birth of modern nanotechnology. *Gold Bulletin*. **40**(4), pp.267–269.

Tian, L.-J.J., Li, W.-W.W., Zhu, T.-T.T., Chen, J.-J.J., Wang, W.-K.K., An, P.-F.F., Zhang, L., Dong, J.-C.C., Guan, Y., Liu, D.-F.F., Zhou, N.-Q.Q., Liu, G., Tian, Y.-C.C. and Yu, H.-Q.Q. 2017. Directed Biofabrication of Nanoparticles through Regulating Extracellular Electron Transfer. *Journal of the American Chemical Society*. **139**(35), pp.12149–12152.

Ting, C.H. and Lee, D.J. 2007. Production of hydrogen and methane from wastewater sludge using anaerobic fermentation. *International Journal of Hydrogen Energy*. **32**(6), pp.677–682.

Tsipotan, A.S., Gerasimova, M.A., Polyutov, S.P., Aleksandrovsky, A.S. and Slabko, V. V 2017. Comparative Analysis of Methods for Enhancement of the Photostability of CdTe@TGA QD Colloid Solutions. *The Journal of Physical Chemistry B*. **121**, pp.5876–5881.

Uyeda, T. and Dot, H.Q. 2005. Quantum Dot Bioconjugates for Imaging , Labelling and Sensing Quantum Dot Bioconjugates for Imaging , Labelling and Sensing What are Quantum Dots ? *Nature Materials*. **4**, pp.1–17.

Valentine, R.C. and Valentine, D.L. 2004. Omega-3 fatty acids in cellular membranes: A unified concept. *Progress in Lipid Research*. **43**(5),

pp.383–402.

Vargas, M., Malvankar, N.S., Tremblay, P., Amino, A., Required, A., Conductivity, P., Transport, L.E.E., This, S., Feeds, R.S.S. and Journal, A.S.M. 2013. Aromatic Amino Acids Required for Pili Conductivity and Long- Range Extracellular Electron Transport in Geobacter sulfurreducens. *mB*. **4**(2), pp.1–6.

Vaselbehagh, M., Karkhanechi, H., Mulyati, S., Takagi, R. and Matsuyama, H. 2014. Improved antifouling of anion-exchange membrane by polydopamine coating in electrodialysis process. *Desalination*. **332**(1), pp.126–133.

Venkateswaran, K., Dollhopf, M.E., Lies, D.P., Saffarini, D.A., Gregor, B.J.M., White, D.C., Ni, M., Ri, D.B., Stackebrandp, E. and Nealsonl, K.H. 1999. Polyphasic taxonomy of the genus Shewanella and description of Shewanella oneidensis sp . nov. *International Journal of Systematic Bacteriology*. (4), pp.705–724.

Vologni, V., Kakarla, R., Angelidaki, I. and Min, B. 2013. Increased power generation from primary sludge by a submersible microbial fuel cell and optimum operational conditions. *Bioprocess and Biosystems Engineering*. **36**(5), pp.635–642.

Vybrant Cell Metabolic Assay Kit 2001. Resazurin Molecular Probes Flier. Available from: https://www.thermofisher.com/document-connect/document-connect.html?url=https://assets.thermofisher.com/TFS-Assets/LSG/manuals/mp23110.pdf&title=Vybrant Cell Metabolic Assay Kit.

Walter, X.A., Merino-Jiménez, I., Greenman, J. and Ieropoulos, I. 2018. PEE POWER® urinal II - Urinal scale-up with microbial fuel cell scale-down for improved lighting. *Journal of Power Sources*. **392**(February), pp.150–158.

Wang, F., Gu, Y., O'Brien, J.P., Yi, S.M., Yalcin, S.E., Srikanth, V., Shen, C., Vu, D., Ing, N.L., Hochbaum, A.I., Egelman, E.H. and Malvankar, N.S. 2019. Structure of Microbial Nanowires Reveals Stacked Hemes that

Transport Electrons over Micrometers. *Cell*. **177**(2), p.361–369.e10.

Wang, S., Mamedova, N., Kotov, N. a, Chen, W. and Studer, J. 2002. Antigen / Antibody Immunocomplex from CdTe Nanoparticle Bioconjugates. *Nano Letters*. **2**(8), pp.817–822.

Wang, T. and Jiang, X. 2013. Size-dependent stability of water-solubilized CdTe quantum dots and their uptake mechanism by live HeLa cells. *ACS Applied Materials and Interfaces*. **5**(4), pp.1190–1196.

Wang, X., Feng, Y.J. and Lee, H. 2008. Electricity production from beer brewery wastewater using single chamber microbial fuel cell. *Water Science and Technology*. **57**(7), pp.1117–1121.

Wang, Y. and Hu, A. 2014. Carbon quantum dots: synthesis, properties and applications. *Journal of Materials Chemistry C*. **2**(34), p.6921.

Watanabe, T. and Honda, K. 1982. Measurement of the extinction coefficient of the methyl viologen cation radical and the efficiency of its formation by semiconductor photocatalysis. *The Journal of Physical Chemistry*. **86**(14), pp.2617–2619.

Wei, J., Liang, P. and Huang, X. 2011. Recent progress in electrodes for microbial fuel cells. *Bioresource Technology*. **102**(20), pp.9335–9344.

White, G.F., Edwards, M.J., Gomez-Perez, L., Richardson, D.J., Butt, J.N. and Clarke, T.A. 2016. Mechanisms of Bacterial Extracellular Electron Exchange. *Advances in microbial physiology*. **68**, pp.87–138.

Wick, P., Malek, A., Manser, P., Meili, D., Maeder-Althaus, X., Diener, L., Diener, P.A., Zisch, A., Krug, H.F. and Von Mandach, U. 2010. Barrier capacity of human placenta for nanosized materials. *Environmental Health Perspectives*. **118**(3), pp.432–436.

Williams, D.N., Pramanik, S., Brown, R.P., Zhi, B., McIntire, E., Hudson-Smith, N. V., Haynes, C.L. and Rosenzweig, Z. 2018. Adverse Interactions of Luminescent Semiconductor Quantum Dots with Liposomes and Shewanella oneidensis. *ACS Applied Nano Materials*. **1**, acsanm.8b01000.

Winterbourn, C.C. 2008. Reconciling the chemistry and biology of reactive

oxygen species. *Nature Chemical Biology*. **4**(5), pp.278–286.

Wong, B.A., Friedle, S. and Lippard, S.J. 2009. Solution and Fluorescence Properties of Symmetric Sensors. *Journal of Americaln Chemicall Society*. (23), pp.7142–7152.

Wu, X., Liu, H., Liu, J., Haley, K.N., Treadway, J.A., Larson, J.P., Ge, N., Peale, F. and Bruchez, M.P. 2003. Immunofluorescent labeling of cancer marker Her2 and other cellular targets with semiconductor quantum dots. *Nature Biotechnology*. **21**(1), pp.41–46.

Wu, X., Zou, L., Huang, Y., Qiao, Y., Long, Z. er, Liu, H. and Li, C.M. 2018. Shewanella putrefaciens CN32 outer membrane cytochromes MtrC and UndA reduce electron shuttles to produce electricity in microbial fuel cells. *Enzyme and Microbial Technology*. **115**(September 2017), pp.23–28.

Xiao, Q., Huang, S., Su, W., Li, P. and Liu, Y. 2013. Evaluate the potential toxicity of quantum dots on bacterial metabolism by microcalorimetry. *Thermochimica Acta*. **552**, pp.98–105.

Xiao, S., Turkyilmaz, S. and Smith, B.D. 2013. Convenient synthesis of multivalent zinc(II)-dipicolylamine complexes for molecular recognition. *Tetrahedron Letters*. **54**(8), pp.861–864.

Xu, H.S., Roberts, N., Singleton, F.L., Attwell, R.W., Grimes, D.J. and Colwell, R.R. 1982. Survival and viability of nonculturable Escherichia coli and Vibrio cholerae in the estuarine and marine environment. *Microbial Ecology*. **8**(4), pp.313–323.

Xu, L., Hao, J., Yi, T., Xu, Y., Niu, X., Ren, C., Chen, H. and Chen, X. 2015. Probing the mechanism of the interaction between l-cysteine-capped-CdTe quantum dots and Hg2+using capillary electrophoresis with ensemble techniques. *Electrophoresis*. **36**(6), pp.859–866.

Xu, Z. and Cotlet, M. 2011. Quantum dot-bridge-fullerene heterodimers with controlled photoinduced electron transfer. *Angewandte Chemie - International Edition*. **50**(27), pp.6079–6083.

Xue, L., Wang, H.H., Wang, X.J. and Jiang, H. 2008. Modulating affinities of di-2-picolylamine (DPA)-substituted quinoline sensors for zinc ions by

varying pendant ligands. *Inorganic Chemistry*. **47**(10), pp.4310–4318.

Yan, B.Y., Zheng, W., Su, L. and Mao, L. 2006. Carbon-Nanotube-Based Glucose / O 2 Biofuel Cells **. *Advanced Materials*. **18**, pp.2639–2643.

Yang, C., Aslan, H., Zhang, P., Zhu, S., Xiao, Y., Chen, L., Khan, N., Boesen, T., Wang, Y., Liu, Y., Wang, L., Sun, Y., Feng, Y., Besenbacher, F., Zhao, F. and Yu, M. 2020. Carbon dots-fed Shewanella oneidensis MR-1 for bioelectricity enhancement. *Nature Communications*. **11**(1), pp.1–11.

Yong, K.T., Law, W.C., Hu, R., Ye, L., Liu, L., Swihart, M.T. and Prasad, P.N. 2013. Nanotoxicity assessment of quantum dots: From cellular to primate studies. *Chemical Society Reviews*. **42**(3), pp.1236–1250.

Yu, W.W., Qu, L., Guo, W. and Peng, X. 2003. Experimental determination of the extinction coefficient of CdTe, CdSe, and CdS nanocrystals. *Chemistry of Materials*. **15**(14), pp.2854–2860.

Yuen, K.K.Y. and Jolliffe, K.A. 2013. Bis[zinc(ii)dipicolylamino]-functionalised peptides as high affinity receptors for pyrophosphate ions in water. *Chemical Communications*. **49**(42), p.4824.

Zeng, S., Yong, K.T., Roy, I., Dinh, X.Q., Yu, X. and Luan, F. 2011. A Review on Functionalized Gold Nanoparticles for Biosensing Applications. *Plasmonics*. **6**(3), pp.491–506.

Zhang, H., Tang, X., Munske, G.R., Zakharova, N., Yang, L., Zheng, C., Wolff, M.A., Tolic, N., Anderson, G.A., Shi, L., Marshal, M.J., Fredrickson, J.K. and Bruce, J.E. 2008. In Vivo Identification of the Outer Membrane Protein OmcA–MtrC Interaction Network in Shewanella oneidensis MR-1 Cells Using Novel Hydrophobic Chemical Cross-Linkers. *Journal of Proteome Research*. **7**(4), pp.1712–1720.

Zhao, S., Li, Y., Yin, H., Liu, Z., Luan, E., Zhao, F., Tang, Z. and Liu, S. 2015. Three-dimensional graphene/Pt nanoparticle composites as freestanding anode for enhancing performance of microbial fuel cells. *Science Advances*. **1**(10), pp.1–8.

Zhao, X., Zhong, J., Wei, C., Lin, C.W. and Ding, T. 2017. Current perspectives on viable but non-culturable state in foodborne pathogens.

Frontiers in Microbiology. **8**(570).